Biogenic-Volatile-Organic-Compound-Profiles in the Amazon Rainforest

Dissertation

zur Erlangung des Grades

„Doktorin der Naturwissenschaften“

Im Promotionsfach Chemie

Am Fachbereich Chemie, Pharmazie,

Geographie und Geowissenschaften

der Johannes Gutenberg-Universität Mainz

Monika Akima Ringsdorf

geb. in Weilburg

Mainz, 2024

Paul Crutzen
Graduate School

Dean:

1st examiner:

2nd examiner:

Date of oral exam: 03.05.2024

Declaration of authorship

I hereby declare that I wrote the dissertation submitted without any unauthorized external assistance and used only sources acknowledged in the work.
All textual passages that are appropriated verbatim or paraphrased from published and unpublished texts as well as all information obtained from oral sources are duly indicated and listed in accordance with bibliographical rules. In carrying out this research, I complied with the rules of standard scientific practice as formulated in the statutes of Johannes-Gutenberg-Universitat Mainz to ensure standard scientific practice.

Acknowledgment

I want to start by thanking Jonathan for his encouraging and motivating supervision and his trust. Thank you for giving me the opportunity to be part of so many amazing research projects. I also want to thank my university supervisor Thorsten for his commitment to always taking his time, in spite of many other duties.

With all my heart I want to thank the ORSUM group, all the great scientists and amazing colleagues that came and went in the past 5 years. It was a pleasure and inspiration to work with you! Achim, my informal third supervisor introduced me to the world of PTR-MS and to the ATTO site, together with Eva. I am very grateful for how well we worked together on many projects. Thomas, I am very thankful for all your support. Whenever there was a campaign to prepare, lab work to do, or issues to discuss, I could always rely on you and your experience. Special thanks also go to Lisa, I am glad that we shared the experience of a HALO campaign during lock down and however, still enjoyed our time at DLR. Christoph, thanks for being a great office mate, especially in the last weeks.

I also want to thank Jordi for his cooperation on my first paper. Our discussions were very supportive and motivating.

A big thank you goes to the team at ATTO, especially Sipko, for making research in the Amazon possible. I will never forget all the nice colleagues (and musicians) I met at ATTO.

I also want to express my gratitude to the team at DLR and all members of the CAFE campaigns, who made this challenging work a great experience.

At the end, I would like to thank Louis, my family, and friends for your support and everything else.

Contents

Acknowledgment i
Abstract vii
Zusammenfassung ix
1 Introduction – From leaf to global scales 3
1.1 Biogenic VOC from the Amazon rainforest 4
1.1.1 Bidirectional exchange of BVOC 4
1.1.2 Atmospheric chemistry of BVOC 7
1.2 BVOC distribution above the Amazon rainforest 8
1.2.1 Atmospheric boundary layer 8
1.2.2 Free troposphere 10
1.3 Instrumentation: PTR-ToF-MS 11
1.3.1 Line effects and ozone interference 13
1.4 Research objective and thesis outline 14
1.5 References 18
2 Inferring OH radical concentrations from BVOC measurements 27
2.1 Abstract 28
2.2 Introduction 28
2.3 Results and discussion 30
2.3.1 Mixing time in the low ABL 32
2.3.2 Sensitivity towards OH chemistry 34
2.3.3 Inferring OH 37
2.3.4 OH simulated using a hierarchy of models: turbulence-resolved, regional and global 41
2.4 Conclusion 44
2.5 Method 45
2.5.1 Observation 45
2.5.2 Atmospheric Models 46
2.5.3 Dynamical Time Warping 47
2.6 References 50
3 Investigating carbonyl compounds using PTR-ToF-MS with NO^+ chemical ionization 57
3.1 Abstract 58
3.2 Introduction 58

3.3 Experimental 60
3.3.1 Measurement site and instrumentation 60
3.3.2 NO^+ chemical ionisation 61
3.3.3 VOC data analysis 62
3.3.4 Validation of observations 63
3.4 Results 66
3.4.1 Atmospheric conditions and seasonality 66
3.4.2 Vertical distribution of carbonyls above canopy 67
3.4.3 Correlations at 80m and common sources 70
3.4.4 Nocturnal loss rates 74
3.5 Discussion 74
3.6 Conclusion 85
3.7 References 87
3.8 Supplementary material 98
4 Influence of ozone on VOC measurements 105
4.1 Abstract 106
4.2 Introduction 106
4.3 Materials and methods 107
4.3.1 Experimental setup 108
4.3.2 Instrumentation 109
4.3.3 Ozone scrubbing 111
4.3.4 Scrubber lifetime calculation 111
4.3.5 Potential effects causing interference 111
4.4 Results and discussion 112
4.4.1 Influence of ozone on VOC measurements 112
4.4.2 Scrubber endurance 119
4.4.3 Effect of humidity 123
4.5 Conclusions 124
4.6 References 127
5 Conclusions and future perspectives 131
5.1 Conclusions 132
5.2 Future perspectives 133
Appendices 137

List of figures 138
List of tables 141
Abbreviations and acronyms 142
CURRICULUM VITAE 144
List of publications 146

Abstract

Biogenic volatile organic compounds (BVOC) released from the Amazon rainforest play a key role in the local, regional, and global atmospheric chemistry. A huge variety of BVOC is emitted from the Amazonian biosphere into the atmosphere and even more are formed via subsequent oxidative reactions. This makes the canopy and adjacent atmospheric layers a chemically complex interface of great importance. BVOC observations at this interface link biological metabolic mechanisms and chemical communication to oxidative atmospheric chemistry, and to turbulent boundary layer dynamics. This doctoral thesis focuses on the vertical and temporal distribution of selected BVOC, measured from a tower at the heights of 80, 150, and 325 m with a proton transfer time-of-flight mass spectrometer (PTR-ToF-MS). With this in-situ measurement technique, many of the most atmospherically relevant BVOC can be detected with a high time resolution. It has been found that ozone, which is ubiquitous in the troposphere can cause interferences in the detection of some BVOC. The interfering signals can be generated within the inlet tubing or inside the instrument. A laboratory experiment to comprehensively investigate this effect and the influence of an ozone scrubber under varying humidity was performed with a PTR-ToF-MS and a gas chromatograph-mass spectrometer (GC-MS). It showed that ozone can induce a decrease in the signals of certain unsaturated species, including terpenes, but it can also artificially enhance the signals of most tested carbonyl compounds. A thiosulfate ozone scrubber was applied to reduce the interferences, which was found to not influence the detection of the tested VOC itself. It successfully inhibited the interference for all tested compounds, except for sesquiterpenes, and its performance and lifetime improved under humid conditions. It was also shown that the ozone levels in an unpolluted environment such as the remote parts of the Amazon (O_3 < 40 ppb) are not sufficient to induce significant interferences for all tested compounds except for sesqui- and to a smaller extent monoterpenes, due to their high ozone reactivity.

Measurement of the vertical distribution of BVOC led to two main studies that contribute to the characterization of the canopy-atmosphere interface region of the Amazon Forest. In the first, the vertical gradients of isoprene and its combined oxidation products methyl ethyl ketone, methacrolein, and isoprene hydroxy hydroperoxide were scrutinized. The observations were used to constrain the Dutch Large Eddy Simulation (DALES), which was applied to investigate the sensitivity of the isoprene gradient towards chemical loss, dominated by reaction with the OH radical, and turbulent transport leading to dilutive mixing. Moreover, the impact of segregation through inhomogeneous mixing, a small-scale phenomenon influencing the rate of atmospheric reactions was also considered. The simulation showed that more than 50 % of the decrease in isoprene over the first 325 m of the atmosphere was determined by dilutive mixing from above, while the residual loss was attributed to the reaction with OH. This relation was used to infer a concentration of the OH radical ranging from $0.2\ (0.1, 7.4) \times 10^5$ to $2.2\ (0.2, 3.8) \times 10^6$ molecules $cm^{-3}\ s^{-1}$, necessary to account for the observed residual loss. For the calculation of the OH concentration, an estimation of the mixing timescale between 80 and 325 m was crucial. Therefore a method from the field of speech recognition (Dynamical Time Warping) was utilized to determine a mixing timescale of 105 minutes in the morning which decreases to 15 minutes at 15:00 local time, based on the observed heating at two heights in the lowermost atmosphere. Those results were useful in examining the vertical distribution of carbonyl compounds at the same measurement site, which forms the second study of BVOC above the Amazon Forest. Usually, isomeric carbonyl compounds, i.e. aldehydes and ketones cannot be measured separately by conventional PTR-

ToF-MS using H_3O^+ as the reagent ion. Their distribution in the atmosphere is expected to be different though, since ketones have significantly longer atmospheric lifetimes (days to weeks) than aldehydes (hours to days). Biogenic emission ratios of these compounds are poorly known. To overcome this limitation for carbonyl compounds, NO^+ chemical ionization has been shown to be effective. The diel variability and vertical dispersion between 80 and 325 m of the ketones indicated a strong source close to the forest's canopy. The vertical distribution of aldehydes varied from compound to compound depending on their chemical precursors, direct emission sources, and atmospheric lifetimes. At nighttime, an overall loss of carbonyl species was found and mainly attributed to canopy deposition and uptake by leaves.

Zusammenfassung

Biogene flüchtige organische Spurengase (BVOC) aus dem Amazonas Regenwald spielen eine grundlegende Rolle in der lokalen, regionalen und globalen Atmosphärenchemie. Eine große Vielzahl von BVOC werden von der Biosphäre des Amazonas in die Atmosphäre emittiert oder in darauffolgenden oxidativen Reaktionen gebildet. Dies macht das Kronendach des Regenwaldes und die darüberliegende Schicht der Atmosphäre zu einer bedeutenden Grenzschicht. Beobachtungen von BVOC an dieser Grenzschicht verbinden biologische Stoffwechselmechanismen und chemische Kommunikation mit der oxidativen Atmosphärenchemie sowie mit turbulenter Grenzschichtdynamik. In diesem Projekt zur Erhaltung des Doktorgrades geht es im Fokus um die vertikale Verteilung von ausgewählten BVOC, welche entlang eines Turmes in den drei Höhen, 80, 150 und 325 m mit einem Proton Transfer Reaktions Time-of-Flight Massenspektrometer (PTR-ToF-MS) gemessen wurden. Mit dieser in-situ Messmethode können viele der atmosphärisch relevanten BVOC mit hoher Zeitauflösung detektiert werden. Es ist bereits bekannt, dass Ozon, welches in der Troposphäre allgegenwärtig ist, Interferenzen in den Signalen mancher BVOC auslösen kann. Die Interferenzen entstehen sowohl in der Einlassleitung als auch im Instrument selbst. Um diesen Effekt sowie den potentiellen Effekt eines Ozonfilters bei variabler Luftfeuchtigkeit umfassend zu untersuchen, wurde ein Laborexperiment durchgeführt. Gemessen wurde dabei mit einem PTR-ToF-MS und einem Gaschromatographen gekoppelt mit einem Quadrupol Massenspektrometer (GC-MS). Es zeigte, dass Ozon eine Verringerung des Signals bestimmter ungesättigten Stoffe, einschließlich Terpene hervorrufen kann. Für die meisten Carbonylverbindungen wurde allerdings eine künstliche Erhöhung ihres Signals festgestellt. Ein Thiosulfat-Ozonfilter wurde getestet um die Interferenz zu reduzieren, da er keinen eigenen Effekt auf die Messung von BVOC aufwies. Dieser verhinderte erfolgreich die Interferenz für alle getesteten Spurengase, mit Ausnahme von Sesquiterpenen. Es wurde außerdem gezeigt, dass die Lebensdauer und die Wirksamkeit des Filters mit höherer Luftfeuchtigkeit zunehmen. Des Weiteren wurde festgestellt, dass das Mischungsverhältnis von Ozon in der reinen, nicht verschmutzten Atmosphäre des Amazonas Regenwaldes (O_3 < 40 ppb) nicht ausreicht um signifikante Interferenzen zu verursachen, unter der Ausnahme von Sesqui- und in geringerem Ausmaß Monoterpenen, die sehr reaktiv gegenüber Ozon sind.

Messungen der vertikalen Verteilung von BVOC führte zu zwei Studien, welche der Charakterisierung der Grenzschicht zwischen Amazonas Regenwald und Atmosphäre dienen. Die erste Studie untersucht den vertikalen Gradienten von Isopren und der Summe dessen Oxidationsprodukten, Methylethylketon, Methacrolein und Isopren Hydroxyhydroperoxid. Diese Beobachtungen wurden genutzt um die „Dutch Large Eddy Simulation“ (DALES) zu initialisieren, welche dann angewandt wurde um die Sensitivität des Isopren Gradienten gegenüber chemischem Abbau und turbulenter Durchmischung zu ermitteln. Der chemische Abbau wurde dabei klar von der Reaktion mit dem OH Radikal dominiert. Darüber hinaus wurde auch der Effekt der Segregation in inhomogenen Gasgemischen berücksichtigt, ein kleinskaliges Phänomen das die Reaktionsraten von Spurengasen beeinflussen kann. Die LES zeigte, dass mehr als 50 % der beobachteten Abnahme von Isopren in den ersten 325 m der Atmosphäre durch Verdünnung mit darüberliegenden Luftschichten während turbulenter Durchmischung erklärt werden kann. Die restliche Abnahme von Isopren wird dementsprechend der Reaktion mit OH zugeordnet. Dieser Zusammenhang wurde genutzt um die OH Konzentrationen zwischen 0.2 (0.1, 7.4) × 10^5 und 2.2 (0.2, 3.8) × 10^6 Molekülen cm^{-3} s^{-1} zu berechnen, welche nötig sind um den beobachteten chemischen Abbau von Isopren zu erklären. Für diese Berechnung war es notwendig die

Zeitskala für die turbulente Mischung der Luftmassen zwischen 80 und 325 m abzuschätzen. Dafür wurde eine Technik aus dem Feld der Spracherkennung (Dynamical Time Warping) auf die beobachtete Erwärmung der unteren Troposphäre in zwei Höhen angewandt. Sie ergab eine Zeitskala von 105 Minuten am Morgen bis 15 Minuten um 15:00 lokale Zeit, welche benötigt wird um eine Größe durch konvektiv angetriebene turbulente Durchmischung von 80 auf 325 m zu transportieren. Die somit erhaltenen Ergebnisse waren auch nützlich für die zweite Studie von BVOC über dem Amazonas, genauer, der Erforschung der vertikalen Verteilung von Carbonylverbindungen. Ein herkömmliches PTR-ToF-MS mit H_3O^+ als Reagenzionen kann isomere Carbonylverbindungen, d.h. Aldehyde und Ketone nicht separat detektieren. Ihre Verteilung in der Atmosphäre unterscheidet sich jedoch stark, da Ketone wesentlich längere atmosphärische Lebenszeiten (Tage bis Wochen) aufweisen wie Aldehyde (Stunden bis Tage). Biogene Emissionsraten der Aldehyde und Ketone sind nur wenig bekannt. Um diese Limitierung für Carbonylverbindungen zu überwinden hat sich die chemische Ionisation durch NO^+ als geeignet erwiesen. Die Variabilität verteilt über den Tag und die vertikale Distribution der Ketone zwischen 80 und 325 m deuteten auf eine Quelle für eben diese in Nähe der Baumkronen hin. Die Verteilung der Aldehyde mit der Höhe variiert hingegen stark von Verbindung zu Verbindung, abhängig von dessen chemischen Vorläufern, den direkten Emissionen und dessen atmosphärischer Lebensdauer. In der Nacht wurden zeitlich abnehmende Mischungsverhältnisse für alle gemessenen Carbonylverbindungen festgestellt, was hauptsächlich der Deposition in den Baumkronen und der Aufnahme durch das Laub zugeordnet wurde.

Chapter 1

Introduction – From leaf to global scales

1.1 Biogenic VOC from the Amazon rainforest

Volatile organic compounds (VOC) form a class of molecules that includes almost all carbon containing gaseous trace compounds with vapor pressures greater than 0.01 hPa under atmospheric conditions. Usually carbon monoxide, carbon dioxide, and methane are excluded from this classification based on their higher atmospheric concentrations and lifetimes. The variety of presumable millions of VOC species is huge (Anon, 2007). These species have been detected at low mixing ratios in the range of ppm (1 in 10^6 air molecules) down to a few ppt (1 in 10^{12} air molecules), yet their effect on air quality and global climate is of great importance. Volatile organic molecules became first known during the investigation of the mechanisms leading to the formation of smog in urban areas in the early 1950s. Ongoing research and the combination of emission inventories and global climate models has revealed that the emission of biogenic VOC (BVOC) is an order of magnitude greater than anthropogenic VOC (Anon, 2007; Guenther et al., 1995). The total flux of BVOC into the atmosphere was estimated to account for 1150 Tg C yr^{-1} (Guenther et al., 1995), with about 40 % of the emissions originating from the Amazon rainforest in South America (Guenther et al., 2012). It is the largest rainforest worldwide, has developed over the last 55 million years, and domiciles a great biodiversity (Maslin et al., 2005). About 100 billion tons of carbon are stored in the forest's biomass, which accounts for 15 % of the global terrestrial biomass. This is comparable to the amount of global fossil fuel carbon emissions over the past 10 years (Davidson et al., 2012; Houghton et al., 2001). In terms of carbon, energy, and water cycles, which involve the emission and atmospheric chemistry of BVOC, the Amazon rainforest is of great importance (Davidson et al., 2012; Andreae et al., 2002; Gloor et al., 2012; Xu et al., 2022).

The most strongly emitted and abundant BVOC, isoprene (C_5H_8), accounts for almost half of the total BVOC emissions (Guenther et al., 1995; Kesselmeier and Staudt, 2000) and was accordingly also the first BVOC that was identified as such in 1970 (Rasmussen, 1970). Together, hemi-(C_5H_8), mono- ($C_{10}H_{18}$), sesqui-($C_{15}H_{24}$), and even diterpenes ($C_{20}H_{32}$) form the diverse class of isoprenoids, some 80 % of which originate from tropical forests (Guenther et al., 2012; Kesselmeier and Staudt, 2000). Isoprenoids are emitted directly from the forest, while other BVOC are formed following reactions involving the most important atmospheric oxidants, namely the OH radical (OH), ozone (O_3), and the nitrate radical (NO_3) or upon photolysis and subsequent reactions in the atmosphere. Many oxygenated BVOC (OVOC) have primary and secondary sources. The dominant OVOC detected in forested environments are formaldehyde, methanol, acetone, acetaldehyde, formic acid, acetic acid, and the oxidation products of isoprene, methyl vinyl ketone, and methacrolein (Seco et al., 2007; Kesselmeier et al., 2000). Altogether BVOC from forests comprise isoprenoids, carbonyls, alkenes, alcohols, acids, esters, halocarbons, and some alkanes (Kesselmeier and Staudt, 2000). This large and diverse group is often organized according to their reactivity, which also mainly determines the atmospheric lifetimes of BVOC. The diversity is also reflected in the range of those lifetimes, from reactive isoprenoids that exist minutes to hours in the atmosphere to some OVOC like acetone with lifetimes of days to weeks to finally certain halocarbons with lifetimes of centuries (Williams, 2004).

1.1.1 Bidirectional exchange of BVOC

BVOC synthesized within plants are key products in the fundamental processes of plant growth, reproduction, and defense (Laothawornkitkul et al., 2009). The subsequent release of BVOC to the

atmosphere has been found to constitute up to 10 % of the carbon that is fixed by plants through photosynthesis (Seco et al., 2007; Peñuelas and Llusià, 2001). Emissions have been found to be either beneficial for the plant in some way or just not avoidable (Peñuelas and Llusià, 2004). BVOC emissions can benefit the plant through protection against biotic or abiotic threats and communication (Fig. 1.1). Biotic stresses include infestation by fungi, viruses, and different kinds of herbivores, which plants counteract by producing repellent, intoxicating, antimicrobial, and/or antifungal BVOC to protect damaged tissues. A well-known group of C_6 compounds with antimicrobial properties released immediately upon herbivore infestation are the green leaf volatiles (Scala et al., 2013), however the emitted BVOC blend is specific to plant and herbivore species. The same BVOC family is also emitted due to mechanical wounding of plants, e.g. after treefall or storm damages (Sarang et al., 2021). Abiotic stresses comprise meteorological and climatic conditions, such as extreme temperatures, limitation of water, storms, oxidative stress by high ozone levels, and human activities related to damage to plants. The synthesis and emission of isoprene has been proven to benefit the plant as an antioxidant by reacting with ozone and strengthening cell membranes to protect chloroplasts (Laothawornkitkul et al., 2009). BVOC serve as signaling compounds in communication within a plant, among multiple plants as well as among plants and insects and even birds (Holopainen et al., 2018). Certain BVOC attract specific pollinators to ensure the plant's reproduction, but there exist more reasons for plant-insect communication. The so-called tritrophic communication involves an infested plant that emits a complex, specific BVOC mixture that can comprise hundreds of compounds to attract a predator of the infesting species (Mumm and Dicke, 2010). Signaling among different plants, or different branches of the same plant can serve as a warning to prime defense mechanisms prior to the actual infestation. Plant communication implies that plants can not only emit but also receive BVOC signals, thus that a bidirectional exchange of BVOC exists. Niinemets et al. (2014) concluded from experimental and modeling work that most BVOC fluxes from leaves are bidirectional.

The bidirectional exchange of BVOC occurs mainly in the vegetative parts of plants (Laothawornkitkul et al., 2009). In their global model, Guenther et al. (1995) state that over 90 % of BVOC emissions escape via the foliage. However, it is important to note that bidirectional exchange of BVOC also takes place between the atmosphere and soils (Bourtsoukidis et al., 2018), cryptogams such as mosses and lichen (Edtbauer et al., 2021), and living beings such as mammals and insects. Those routes have been often overlooked in the past. Most of the exchange from plants happens via the leaf's stomata, which are in simplified form, small openings in the outer leaf's tissue that represent the transition between the ambient air and the mesophyll and are necessary for carbon fixation during photosynthesis. To prevent dehydration, the stomata aperture can be regulated, which was also observed as a drop in the emission flux of some BVOC e.g. linalool during high insolation at noon (Niinemets et al., 2002). Exchange between the leaf and the atmosphere is also possible by diffusion through the leaf's cuticle following deposition. This process is limited by low diffusion rates and is thus thought to be much less effective (Koppmann, 2008). Factors that determine the exchange rate are the compound specific Henry's law constant expressing the water-solubility or volatility, and the gradient in concentration between the inside of the leaf and the ambient atmosphere (Niinemets and Reichstein, 2003; Seco et al., 2007). Emission of a particular BVOC is thus only feasible if the concentration in the intercellular air space exceeds the ambient concentration, while high volatility promotes a fast transition from liquid phases to the intercellular air space and vice versa. The uptake of a certain VOC is accordingly much more effective if the leaf-atmosphere concentration gradient is maintained by a metabolism that processes the uptaken BVOC or by storage in a liquid or lipid storage pool, which holds for most OVOC (Niinemets et al., 2014). For certain plant species and BVOC, a

compensation point has been observed, representing an ambient concentration threshold above which the BVOC is uptaken and below which it is emitted (Kuhn et al., 2002). Compensation points are also driven by the capacity of the plant to process the BVOC and thus alter the concentration gradient. The conductance of the stomata is an additional factor that determines the BVOC exchange. Only the emission of highly volatile BVOC is not sensitive towards stomatal conductance since their partial pressures in the leaf's intercellular air space increase immediately upon stomatal closure (Niinemets et al., 2014).

Synthesis and exchange rates of BVOC have been shown to be affected dominantly by light and temperature (Guenther et al., 1995). To understand their influence on BVOC exchange it has to be considered that some BVOC are stored in specialized or temporarily in unspecialized tissues whereas others are produced de novo from products of metabolic processes like photosynthesis. The temperature dependency of enzymatic synthesis of BVOC is characterized by an optimum temperature with the highest enzymatic activity (Anon, 1990). Additionally, the partial pressure of BVOC in the intercellular air space increases with increasing leaf temperature, leading to enhanced BVOC emission. The stomatal conductance is affected by temperature variabilities as well. Altogether the BVOC emission is found to depend exponentially on temperature, with an emission maximum for compounds that are not stored (Laothawornkitkul et al., 2009; Guenther et al., 1995). Sunlight, as the main driver for photosynthesis strongly influences the production of non-stored BVOC and thus their emission (Laothawornkitkul et al., 2009). Isoprene is the most prominent BVOC that is produced de novo and emitted in a light and temperature dependent manner, whereas some but not all monoterpenes are stored in specialized compartments and therefore exhibit only a temperature sensitive emission rate (Peñuelas and Llusià, 2001; Kesselmeier et al., 1996).

The phenology of plants differs among tropical plant species, but leaf flush events (simultaneous growth of new leaves) were found to peak in the dry season at different sites across the Amazon forest in conjunction with high insolation (Restrepo-Coupe et al., 2013). Insolation in the wet season is reduced by more frequent cloud shading. The composition and magnitude of the BVOC mixture from young leaves differ from aged leaves (Kuhn et al., 2004; Bracho-Nunez et al., 2011) and floral scents to attract pollinators comprise many specific BVOC, as well.

Plants react to the limitation of water, especially in combination with high temperatures during a drought by closing the leaf's stomata which suppresses the exchange of BVOC and limits the emission of less volatile BVOC. Also, the synthesis of certain BVOC is largely reduced due to missing water availability (Peñuelas and Llusià, 2001; Bertin and Staudt, 1996), leading to altered composition of the emitted BVOC mixture (Byron et al., 2022). The bidirectional exchange is affected by changes in relative humidity and thus in foliar moisture and diffusion rates through the leaf's cuticle (Peñuelas and Llusià, 2001). Water limitations were so far irrelevant in tropical rainforest (Restrepo-Coupe et al., 2013), but future scenarios of the changing climate predict more extreme events, such as droughts, storms, and flooding as well as a temperature increase between 1.4 K and 4.4 K for the end of the 21st century compared to 1986-2005 (Calvin et al., 2023; Ometto, et al., 2022). The overall effect of climate change based on a temperature change of 2-3 K was estimated to cause a 30-45 % increase in atmospheric BVOC concentrations with severe impacts on the OH budget and therefore on the lifetime of many greenhouse gases (GHG), as well as on ozone and secondary aerosol formation (Peñuelas and Staudt, 2010). Long established ways for plant and tritrophic communication are also expected to be disturbed and phenological cycles might adapt to the new conditions (Peñuelas and Staudt, 2010; Holopainen et al., 2018).

1.1.2 Atmospheric chemistry of BVOC

BVOC in the atmosphere are generally subject to oxidative degradation, through reactions with OH, O_3, NO_3, or loss mechanisms like photolysis or deposited to surfaces via dry or wet deposition (Fig. 1.1). The extent of the respective mechanism depends on location, time of day, and properties of the BVOC, solubility in water and chemical structure such as possession of one or more double bonds. A high aqueous solubility increases the deposition rate and unsaturated BVOC have higher reaction rates since the oxidant can be added to the double bond (Atkinson and Arey, 2003). By far the most important oxidant in daytime is the OH radical, which is primarily formed upon photolysis of O_3 (Levy, 1971).

$$O_3 \xrightarrow{h\nu} O_2 + O(^1D) \quad (1.1)$$

$$O(^1D) + H_2O \longrightarrow 2OH^{\bullet} \quad (1.2)$$

The OH radicals react with BVOC within less than a second to most commonly form alkyl radicals ($R^{\bullet}$), which combine with O_2 to organic peroxy radicals ($RO_2^{\bullet}$) as shown in reaction 1.3-1.4 (Atkinson and Arey, 2003). During the absence of solar radiation at night, the NO_3 radical gains importance, as formation of OH ceases.

$$RH + OH \longrightarrow R^{\bullet} + H_2O \quad (1.3)$$

$$R^{\bullet} + O_2 \xrightarrow{M} RO_2^{\bullet} \quad (1.4)$$

$$NO + RO_2^{\bullet} \longrightarrow NO_2 + RO^{\bullet} \quad (1.5)$$

$$RO^{\bullet} + O_2 \longrightarrow R'CHO + HO_2^{\bullet} \quad (1.6)$$

$$NO + HO_2^{\bullet} \longrightarrow NO_2 + OH^{\bullet} \quad (1.7)$$

$$NO_2 \xrightarrow{h\nu} NO + O(^3P) \quad (1.8)$$

$$O(^3P) + O_2 \longrightarrow O_3 \quad (1.9)$$

$$RH + 3O_2 + NO \longrightarrow R'CHO + O_3 + NO_2 + H_2O \quad (1.10)$$

The oxidized products (R'CHO, e.g. carbonyls) that emerge from the chemical transformation of BVOC have different properties than their precursors in terms of volatility, water solubility, chemical reactivity, and contributions to radiative forcing. The decomposition of R'CHO generates the ultimate products CO_2 and H_2O. Further oxidation of R'CHO leads to highly oxidized BVOC with low volatilities which can condense on existing particles or accumulate to form new particles, thus affecting the formation of clouds and their albedo (Mahilang et al., 2021; Pöschl, 2005). In general, BVOC have the ability to absorb infrared radiation and act as GHG themselves, but the indirect contribution to the radiative budget of the atmosphere and thus climate change through promoting the growth of aerosol particles is more significant (Mellouki et al., 2015). Several more aspects add to the indirect climate effects of BVOC, firstly the net production of tropospheric O_3 (Reaction 1.10), an effective GHG and pollutant with negative impacts on plant tissues, human health, and ecosystems (Mellouki et al., 2015). Its formation involves the OH initiated oxidation of VOC in the presence of NO_x (NO + NO_2), whereas in the relatively unpolluted

rainforest atmosphere, NO mainly originates from the emission by soils or lightning strikes. There is a rapid interconversion between NO and NO_2 leading to a steady state including O_3. The availability of NO_x determines whether the oxidation of BVOC is a source (Reaction 1.7-1.9) or sink for O_3 (Reaction 1.11).

$$O_3 + HO_2^{\bullet} \longrightarrow OH^{\bullet} + 2O_2 \qquad (1.11)$$

In the rainforest, where NO_x is a limiting factor, the production of O_3 depends on NO_x concentrations (Seinfeld and Pandis, 2016; Pike et al., 2010) or a degradation of O_3 is favored. Secondly, the oxidative reaction sequence described in equation 1.3-1.4 leads to the generation of reservoir species for NO_x, also referred to as peroxycarboxylic nitric anhydrides (PANs), if followed by the reaction with NO_2 (Reaction 1.12). Most BVOC are suited to generate PANs but the yields are only significant for the oxidation of aldehydes or the photolysis of ketones and dicarbonyls (Koppmann, 2008; Fischer et al., 2014).

$$RO_2^{\bullet} + NO_2 \xrightarrow{M} RO_2NO_2 \qquad (1.12)$$

Those reservoir species are typically thermally instable near the warm surface, but in the colder free troposphere, they can be transported over large distances. Thus they can represent a source of NOx in the remote troposphere where it efficiently produces O_3 and OH radicals with implications on oxidative chemistry and the radiative budget (Koppmann, 2008). Thirdly, BVOC are the dominant reactive compounds in the atmosphere (largest sources of OH reactivity) and their oxidation is the strongest sink for OH. By implication the lifetime of pollutants and effective GHG as carbon monoxide and methane increase with decreasing oxidative capacity of the atmosphere (Koppmann, 2008; Mellouki et al., 2015; Pfannerstill et al., 2021).

Another atmospherically relevant oxidative reaction is the ozonolysis of unsaturated BVOC, most importantly by terpenes. The addition of O_3 to the double bond between two carbon atoms and following degradation and isomerization steps generate oxygenated products, including carbonyls and are a source of OH radicals (Atkinson and Arey, 2003).

In conclusion, the chemistry of BVOC impacts the immediate atmospheric composition on a local scale but also more distant from their source, via various direct and indirect physical and chemical processes.

1.2 BVOC distribution above the Amazon rainforest

1.2.1 Atmospheric boundary layer

BVOC exchange between the rainforest and the atmosphere has a turbulent nature and is not only governed by the bidirectional BVOC exchange of plants but also by coherent turbulent structures within and above the canopy (Fuentes et al., 2022; Parrish et al., 2007; Ganzeveld et al., 2008). Generally, the part of the atmosphere where the dispersion of BVOC emissions is regulated is the atmospheric boundary layer (ABL) that spans from the canopy top to about 0.1-2 km. It is defined as the layer that is directly impacted by surface forces and processes, such as heat and moisture transfer and frictional drag. Those forces can be seen as distinct diurnal cycles in sensible and latent heat or BVOC time series in the ABL, whereas a less variable general trend is observed in the free troposphere. In the ABL turbulence leads to the distribution of those quantities, whereas in the free troposphere, turbulence does not occur so frequently (Stull, 1988).

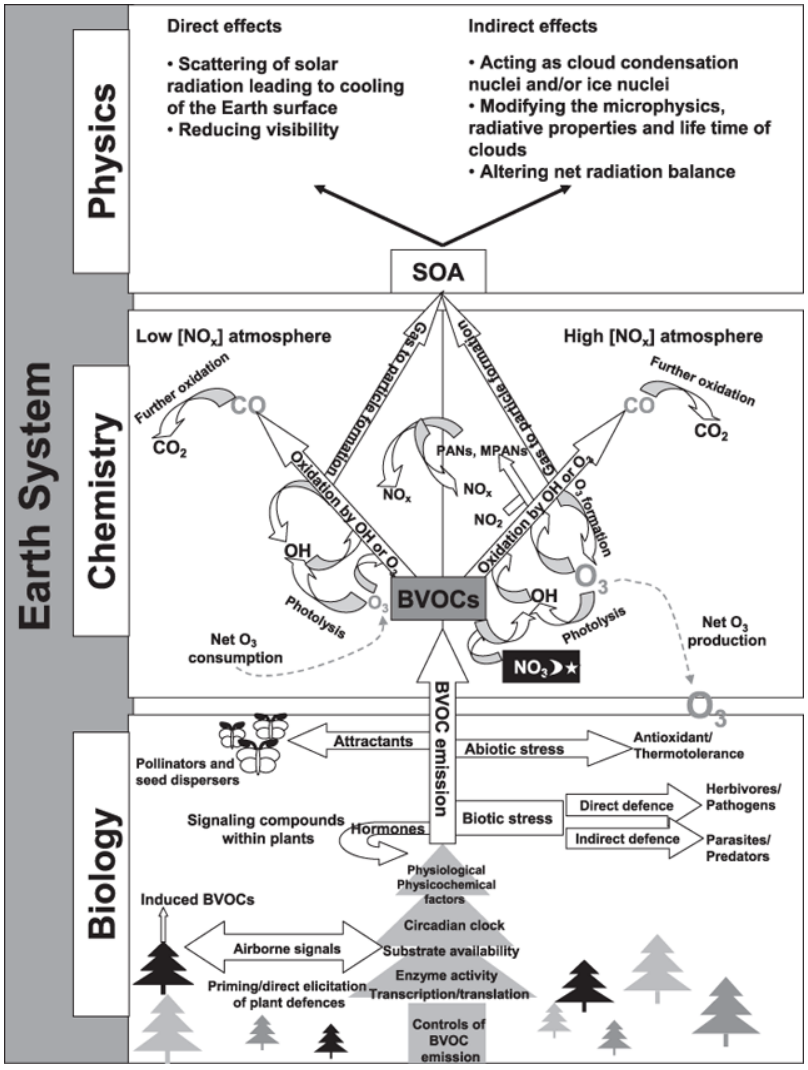

Figure 1.1: *Overview of biological and atmospheric processes that involve BVOC. BVOC released to the atmosphere imply feedback to the biosphere by direct (e.g. generation of Ozone) and indirect (e.g. cloud formation) effects. This schematic drawing is taken from Laothawarnkitkull et al., 2009 with permission from the publisher "John Wiley and Sons".*

Turbulence is a vague term, here it describes swirling motions of air on different size scales, so-called eddies, which transport and mix quantities at scales from 10^{-3} to $3x10^{3}$ m (Stull, 1988). There are two ways how turbulence is generated: mechanically and thermally. Instabilities in air flows that mechanically cause turbulence are created when the wind speed differs vertically, e.g. due to the rough canopy imposing resistance to surface winds or when the wind encounters an obstacle. Turbulence is imposed thermally due to the positive buoyancy of heated air at ground level, which leads to the formation of large eddies since rising air (convection) at one site causes a subsident downward transport at a nearby site (Jordi Vilà-Guerau de Arellano, et al., 2015).

Above the canopy turbulent structures are organized in cycles of coherent ejections and sweeps, which penetrate the upper part of the canopy, imposed by mechanical turbulence. Those structures exchange BVOC-rich air from inside the canopy with outside canopy air that contains more oxidants. The layer that is influenced by these induced ejections and sweeps through the canopy is called the roughness sublayer

(typically 2-3 times the canopy height) (Fuentes et al., 2022; Cava et al., 2022). During thermally unstable and thus convective conditions, those mechanically induced motions are influenced by coherent thermal plumes (Cava et al., 2022). BVOC transport at the top of the canopy is thus regulated by the interplay of mechanically and thermally imposed turbulence, the bidirectional exchange of BVOC at leaf level, and chemistry within and above the canopy. The roughness sublayer is part of the mixing layer, where strong thermally induced turbulent eddies mix the quantities well. Only at its upper part, air entrainment from the free troposphere causes inhomogenities (Jordi Vilà-Guerau de Arellano, et al., 2015; Dias-Júnior et al., 2019). The mixed layer is typically confined by a stable layer, also referred to as the entrainment zone. The whole boundary layer undergoes a diurnal evolution, with extension and vertical growth after sunrise when the heated surface causes convection and collapse after sunset. The stable boundary layer at nighttime reaches only a few hundred meters in height, while the height of the convective boundary layer is around 2 km (Stull, 1988).

The degree or timescale of simultaneous mixing and chemistry drive the vertical distribution of BVOC within the ABL. Therefore vertical gradient measurements reveal information on emission, chemical formation, and loss under consideration of turbulent mixing at daytime (Holzinger et al., 2005; Yáñez-Serrano et al., 2016; Karl et al., 2009). Since BVOC emission and turbulence generally depend on solar radiation, the formation of clouds can alter the distribution of BVOC and sensible and latent heat fluxes, which in turn influence particle growth and cloud properties. This demonstrates the interconnectedness of the rainforest atmosphere (Vilà-Guerau de Arellano et al., 2020). During night the BVOC exchange between canopy and atmosphere is most often still driven by turbulence (Oliveira et al., 2017), but vertical mixing is much slower due to the decay of thermally driven turbulence (Stull, 1988). The vertical distribution in the lower part of the nocturnal atmosphere thus strongly depends on the height of the boundary layer, with nighttime chemistry, emission, and deposition as the main drivers.

1.2.2 Free troposphere

BVOC observed in the free troposphere or their chemical precursors must have passed through the ABL, either slowly through mixing or via strong convection. Average transport times of properties out of the boundary layer into the free troposphere via mixing are 1-2 days while vertical mixing within the free troposphere happens on timescales of month (Koppmann, 2008). The atmospheric lifetime of BVOC and other constituents is therefore strongly linked to their occurrence and distribution in the troposphere. Without the phenomenon of deep convection, only long-lived species such as some alkanes or halocarbons and potentially some oxidized VOC, that are formed en route could reach the upper troposphere. As the name implies, deep convection transports chemicals from the ABL to the upper troposphere (12-16 km), whereas shallow convection reaches up to the lower free troposphere. However, both shallow and deep convection occurs frequently in the Amazon, due to the combination of strong insolation generating thermals and high latent heat fluxes from evapotranspiration in the canopy. The Amazon rainforest has been described as a global convective center (Zhuang et al., 2017). Deep convection is additionally initiated by other thermodynamic processes, e.g. mesoscale circulations or wave activity (Gentine et al., 2019).

The chemical composition in the free and upper troposphere is significantly different from that of the ABL. Due to cold temperatures (210-235 K), the mixing ratio of water is low (10-300 ppm). The reaction to

generate OH described in equation 1.1-1.2 is thus less efficient in producing HO_x (OH + HO_2) radicals. Aircraft based studies conducted in the late 1990s found 2-4 times higher HO_x concentrations than expected from this source (Jaeglé et al., 2001). Additionally, unexpectedly high concentrations of OVOC were observed in the remote upper troposphere over the Pacific (Singh et al., 2001). The observed OVOC were short-chained molecules such as methanol, acetone, formaldehyde, acetaldehyde, and acetic acid, which can be photolyzed and thus serve as HO_x precursors. Depending on the available NO_x mainly from lightning, stratospheric downdrafts, or PAN species, the OVOC can frequently also react to generate or destroy O_3. Convection transporting air from the ABL to the the mid- or upper troposphere has been shown to also deliver also highly reactive VOC like isoprene to the high altitudes, impacting the composition and photochemical chemistry and thus the formation of particles (Colomb et al., 2006; Scheeren et al., 2003; Singh et al., 2004; Warneke et al., 2001). Aircraft based measurement campaigns enable observation of vertical concentration profiles throughout the troposphere, promoting the understanding of HO_x-NO_x-VOC chemistry and particle formation.

1.3 Instrumentation: PTR-ToF-MS

The measurements on which this work is based were primarily conducted using a proton transfer reaction time-of-flight mass spectrometer (PTR-ToF-MS). This method was developed in the 1990s by Lindinger et al. to sensitively quantify VOC in the air matrix with a high time resolution. It is a chemical ionization technique that is rather soft (low energy) with less fragmentation of the analytes compared to electron ionization (Lindinger et al., 1998).

In the hollow cathode ion source (Fig. 1.2), the reagent ions are generated. Typically an adjustable flow of water vapor from a liquid reservoir is introduced into an electrical discharge to obtain H_3O^+ ions. H_3O^+ can donate a proton (H^+) to all molecules in the air matrix with a proton affinity greater than water (691 kJ mol^{-1}), which includes most BVOC, unlike nitrogen and oxygen, the main constituents of air. By introducing synthetic air instead of water vapor into the ion source, NO^+ reagent ions are generated, which undergo a set of ionization reactions, that are described in Chapter 3. Briefly summarized, the important reaction pathways are charge transfer, hydrogen abstraction, and association reactions (Koss et al., 2016). Other reagent ions that were tested and applied are O^+ and less frequently NH_4^+, Xe^+, and Kr^+ for specialized targeted analysis (Müller et al., 2020; Edtbauer et al., 2014; Norman et al., 2007). The advantage of utilizing H_3O^+ ions is the relatively simple obtained mass spectra, whereas for the detection of certain molecules, other reagent ions provide benefits, e.g. the isomerically resolved detection of carbonyls with NO^+ as applied in Chapter 3. The development of an ion source that allows for fast switching between H_3O^+, $NO^{+,}$ and O_2^+ was therefore helpful (Jordan et al., 2009).

The ionization of the air sample occurs in the drift tube (Fig. 1.2). Ions move through the drift tube with a velocity determined by the applied electrical field strength (E) and the number density of the neutral molecules in the sample (N). The applied electrical field in combination with the pressure in the drift tube thus regulate how much fragmentation occurs upon a collision between molecules. The parameter E/N is usually in the range of 60-120 Townsend at drift pressures between 2-4 mbar and field strengths of 500-800 V. The drift parameters are tuned to achieve the lowest possible impurities of the reagent ions (< 5 %) and a high signal of the analyte with minimum fragmentation. The abundance of the reagent ions

strongly exceeds the concentration of the analytes in the drift tube, so that the reagent ion concentration can be assumed unchanged upon ionization reactions (Lindinger et al., 1998).

The drift tube is connected with an intermediate space where most of the air is pumped out by a vacuum pump so that only a fraction of the ionized molecules passes through a nose cone to the mass spectrometer (Fig. 1.2). The pressure in the time-of-flight mass spectrometer is kept as low as possible, typically in the range of 10^{-7} mbar to avoid collisions among the ions. This is realized by another vacuum pump connected to the mass spectrometer. A pulser orthogonally accelerates the ions at a rate of ca. 125 kHz into an electrical field. There the ions are reflected to fly along a path in a “V”- or “W”-shape. During the pulsing, the same amount of kinetic energy is transferred to each ion, but the mass-to-charge ratio (m/z) determines how much time the ion needs to reach the detector. The light ions have a shorter “time of flight” than heavier ions. A multichannel plate multiplies the signal which is processed by an ultra-fast data acquisition board, since each pulse yields one mass spectrum with a mass range of 500 m/z (Jordan et al., 2009; de Gouw and Warneke, 2007). The ToF-MS is able to separate most nominally isobaric ions, unlike a quadrupole mass spectrometer that is still applied as a detector in some PTR-MS instruments. In this study, two commercially available instruments from Ionicon Analytics in Innsbruck (Austria) were used to measure BVOC, the PTR-ToF-MS 4000 and the PTR-ToF-MS 8000. The PTR-ToF-MS 8000 was modified and built into a flight rack so that it can be integrated in an aircraft. The names of the instruments indicate their optimal mass resolution, on average the mass resolution m/Δm was around 3000 and 4000-5000 respectively.

The signal for each m/z is normalized with respect to the concentration of the reagent ions the drift parameters length, temperature, and pressure to account for possible changes in the ionization or transmission through the instrument. The software for peak integration and mass scale calibration “IDA” also applies certain necessary corrections, such as baseline subtraction and duty-cycle correction which are explained in detail in Müller et al. (2013). Mixing ratios (ppb_v) are obtained by calibration of a gas standard with the same humidity range that was observed during the measurement. The so-called k-rate, which is the proton transfer rate coefficient together with the transmission efficiency through the instrument can be used to calculate the mixing ratio (Cappellin et al., 2012).

Besides PTR-MS also gas chromatographic analyses of BVOC are widely applied. The advantage of GC-MS is the resolution of isomeric compounds prior to detection by the mass spectrometer and thus a much more specific identification of BVOC. However, the time resolution is usually much lower (< 3 minutes to hours) since a preconcentration and separation of the sample is required. The combination of both methods is in most cases the most promising strategy to observe BVOC (de Gouw and Warneke, 2007).

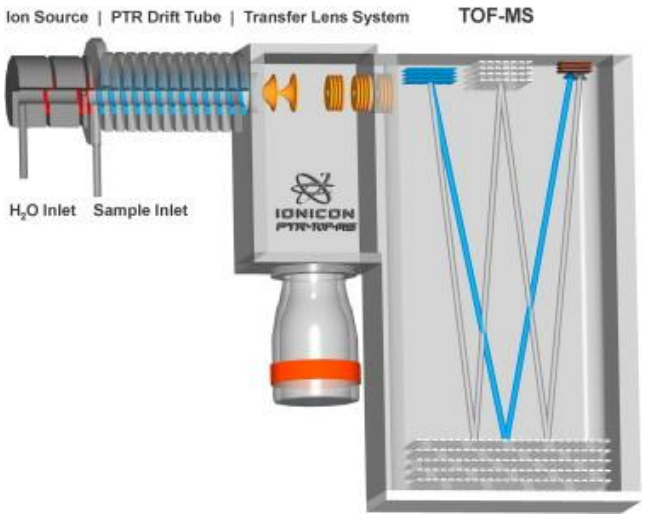

Figure 1.2: *A schematic setup showing the main components of a PTR-ToF-MS. The two different flight paths towards the detector are indicated by blue and gray beams in the ToF-MS. This figure is taken from Jordan et al. 2009, with permission from the publisher "Elsevier".*

1.3.1 Line effects and ozone interference

The measurement of BVOC usually requires an inlet line of some length to sample the airmasses of interest. In this entire work the inlet tubing was made of fluorinated ethylene propylene (FEP) and tubing inside the PTR-ToF-MS includes mainly FEP or polyetheretherketone (PEEK). FEP and perfluoroalkoxy alkanes (PFA) were recommended from an intercomparison of different tubing materials for VOC sampling. Interactions of the BVOC by absorptive partitioning to the inner walls of the polymer tubing cause measurement delays (Deming et al., 2019). Pagonis et al. described the absorptive behavior by the principles of gas chromatography, with the stationary phase being the tubing walls and chromatographic retention times were compared to tubing delay. The affinity for a BVOC to partition to the tubing walls is determined by their volatility, in most studies expressed by the saturation concentration (C*) in µg/m^3. Less volatile compounds with saturation concentrations in the range of $1 < C^* < 10^4$ µg/m^3 thus have longer tubing delays than highly volatile BVOC with $C^* > 10^6$ µg/m^3 at similar tubing length and flow rate (Pagonis et al., 2017). Absorption partitioning in polymer tubing was found to be not dependent on humidity or the concentration of other VOC in the sampled air matrix (Deming et al., 2019). The longest line utilized in this work for vertical profile measurements above the Amazon rainforest had a length of about 330 m and was made of FEP, which led to an observed delay of about 90 seconds at the applied flow of 10 L/min for volatile BVOCs in the gas standard ($C^* > 10^7$ µg/m^3). All tubing (inside and outside the instruments) is usually insulated to avoid light effects and heated to minimize wall effects and to prevent condensation of water vapor. Li et al. conducted a study with a similar long inlet line (400 m, PFA) and found tubing delays at comparable flow to be < 200 seconds for compounds with $C^* > 10^7$ µg/m^3 (Li et al., 2023).

Another measurement artifact can occur when atmospheric oxidants enter the insulated sampling line and react with BVOC in the gas phase or on the tubing surface. Photochemical reactions or reactions involving the OH radical can be excluded since the tubing is insulated and the OH lifetime in air very short. In the dark environment inside the tubing, reactions with sampled O_3 and NO_3 are, however, still possible

(Northway et al., 2004; Apel et al., 2003; Li et al., 2023). In the ABL above the Amazon rainforest, O_3 is present at mixing ratios below 40 ppb, but throughout the troposphere concentrations between 10 and 200 ppb are typical (Seinfeld and Pandis, 2016; Gerken et al., 2016). The NO_3 radical is only of importance during the night since fast photolysis leads to its destruction during daylight. Potentially the NO_3 radical might be formed in the dark tubing during the limited residence time of the air sample as suggested by Li et al. (2023). Both oxidants react rather slowly with saturated BVOC whereas the ozonolysis of unsaturated BVOC such as terpenes is efficient and can lead to the loss of those BVOC in the inlet line. Some monoterpenes and sesquiterpenes, are thus not detected via the 330 m sampling line due to an expected combination of ongoing ozonolysis or reaction with NO_3 and long delay times due to a low volatility of those BVOC. A positive interference from the formation of oxygenated BVOC upon ozonolysis or reaction with NO_3 at tubing walls and the gas phase can also occur. In chapter 4 the effect of ozone on BVOC sampling under varying humidity is investigated in detail.

1.4 Research objective and thesis outline

Biogenic volatile organic compounds are major reactive species in the global atmosphere (Koppmann, 2008). Thus BVOC, as a sink for the hydroxyl radical, play an important role in modulating the oxidation capacity of the atmosphere (Williams, 2004). Vast amounts of BVOC are emitted from the largest rainforest worldwide, the Amazon rainforest. Their transformations in the atmosphere have implications for local physical and chemical processes and global climate (Guenther et al., 1995; Vilà-Guerau de Arellano et al., 2020). The rainforest canopy and the adjacent lowermost atmosphere represent an important, complex interface region, where chemistry and turbulence determine the dispersion and transformations of the emitted BVOC (Fuentes et al., 2022). Moreover, strong tropical convection has the potential to transport BVOC-rich, moist air from this region into the mid and upper troposphere. The accurate measurement of BVOC to characterize their concentrations and distribution within this interface region is thus essential for the understanding and model simulation of canopy exchange, atmospheric transport, and chemistry. BVOC observations are part of the Amazon Tall Tower Observatory (ATTO) which was founded to study the connections between the Amazon Forest, carbon-, water-, and other important cycles and global climate (https://www.attoproject.org). The 325 m tall tower allows measurements throughout the rainforest boundary layer. The findings presented in this thesis were mostly conducted at this measurement site using a PTR-ToF-MS. With this technique a wide range of BVOC, including terpenes, alkenes, and many oxygenated compounds can be measured continuously with a temporal resolution of seconds, although not all are isomerically resolved. The continuous long-term measurement of BVOC in conjunction with multidisciplinary observations of forest and atmosphere as implemented at ATTO enables investigation of seasonal and longer timescale changes. Deforestation and anthropogenically induced climate change promote extreme conditions in the Amazon, leaving many open questions on the future role of the rainforest. While the long-term characterization of BVOC will be presented elsewhere, the focus of this thesis is on the vertical distribution and temporal variability of atmospherically relevant species, namely isoprene and carbonyl compounds.

Chapter 2 investigates the vertical profile of isoprene concentration and that of its oxidation products to infer the OH radical concentration from those observations conducted at ATTO. So far there have been only a few direct measurements of OH radical concentrations in the Amazon, also due to instrumental difficulties in BVOC-rich environments (Jeong et al., 2022). The OH radical determines the lifetimes of all

BVOC to a great extent, thus there is a great interest in knowing its concentration close to the major emission source of BVOC, the rainforest canopy. The BVOC profile data was also used to constrain a turbulence resolving large eddy simulation (LES) to gain insights into the transport and dilutive mixing of isoprene. Moreover, an estimation of the mixing time between 80 and 325 m above ground was necessary for the calculation of OH concentrations, which can serve as a basis for future studies on vertical profiles. This was achieved by using a method from the field of speech recognition, called dynamical time warping. Finally, we compared the results to the Dutch Atmospheric LES (DALES), to a regional-scale model (WRF-chem), and to a global-scale model (EMAC).

In **Chapter 3** the adaptation of the PTR-ToF-MS to NO^+ chemical ionization allowed measurement of aldehydes and ketones separately, for the first time above the Amazon rainforest. Thereby we overcame one of the limitations of conventional PTR-MS using H_3O^+, which is the common detection of carbonyl isomers (Koss et al., 2016). Carbonyl compounds are key to oxidative atmospheric chemistry (Koppmann, 2008; Singh et al., 2001) and their individual detection is particularly important since ketones have considerably longer lifetimes than aldehydes. The observed temporal and vertical distribution above the Amazon rainforest indicated a strong source of ketones in proximity to the canopy. The vertical distribution in combination with correlation analysis is studied for carbonyl compounds and related to existing literature to constrain their sources and sinks.

To measure BVOC distributions throughout the troposphere and to observe the effects of convective outflow, aircraft-based measurements are required. In the course of the CAFE (Chemistry of the Atmosphere Field Experiment) Campaigns over Africa, Europe, Brazil, and currently the Pacific Ocean, BVOC are measured in very different air masses. During the flight campaign in Europe (Voigt et al., 2022), an interference in the detection of several BVOC compounds during the sampling of ozone-rich airmasses became obvious for the PTR-ToF-MS and a GC-MS. It could be related to ozone reactions occurring in the inlet tubings (Northway et al., 2004; Apel et al., 2003). As a consequence, a comprehensive laboratory experiment on the measurement artifacts due to ozone and humidity as well as on the use of a thiosulfate ozone scrubber for both instruments was performed. **Chapter 4** presents this experiment and the resulting implications for VOC measurements. The aim was to ascertain at which atmospheric concentrations of ozone the interference becomes relevant and how the thiosulfate scrubber performs to prevent it.

Chapter 2

Inferring OH radical concentrations from BVOC measurements

Published in Scientific Repors, 2023

Capter 3

Investigating carbonyl compounds using PTR-ToF-MS with NO^+ chemical ionization

Chapter 4

Influence of ozone on VOC measurements

Published in Atmospheric Measurement Techniques, 2023

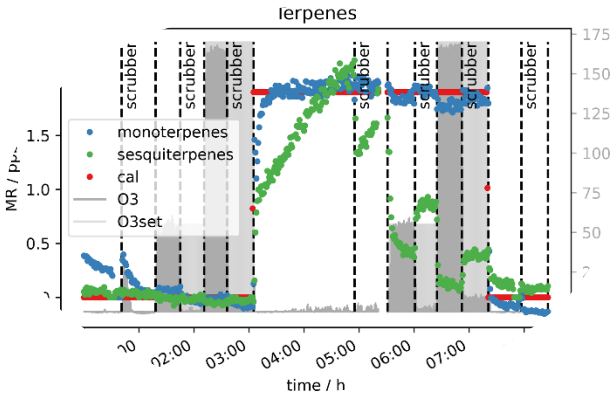

Chapter 5

Conclusions and future perspectives

1.5 References

Andreae, M. O., Artaxo, P., Brandão, C., Carswell, F. E., Ciccioli, P., da Costa, A. L., Culf, A. D., Esteves, J. L., Gash, J. H. C., Grace, J., Kabat, P., Lelieveld, J., Malhi, Y., Manzi, A. O., Meixner, F. X., Nobre, A. D., Nobre, C., Ruivo, M. d. L. P., Silva-Dias, M. A., Stefani, P., Valentini, R., von Jouanne, J., and Waterloo, M. J.: Biogeochemical cycling of carbon, water, energy, trace gases, and aerosols in Amazonia: The LBA-EUSTACH experiments, J. Geophys. Res. Atmospheres, 107, LBA 33-1-LBA 33-25, https://doi.org/10.1029/2001JD000524, 2002.

Anon: FACTORS CONTROLLING THE EMISSIONS OF MONOTERPENES AND OTHER VOLATILE ORGANIC COMPOUNDS, U.S. Environmental Protection Agency, Washington, D.C, 1990.

Anon: Known and Unexplored Organic Constituents in the Earth's Atmosphere, Environ. Sci. Technol., 41, 1514–1521, https://doi.org/10.1021/es072476p, 2007.

Apel, E. C., Hills, A. J., Lueb, R., Zindel, S., Eisele, S., and Riemer, D. D.: A fast-GC/MS system to measure C 2 to C 4 carbonyls and methanol aboard aircraft, J. Geophys. Res. Atmospheres, 108, 2002JD003199, https://doi.org/10.1029/2002JD003199, 2003.

Atkinson, R. and Arey, J.: Atmospheric Degradation of Volatile Organic Compounds, Chem. Rev., 103, 4605–4638, https://doi.org/10.1021/cr0206420, 2003.

Bertin, N. and Staudt, M.: Effect of water stress on monoterpene emissions from young potted holm oak (Quercus ilex L.) trees, Oecologia, 107, 456–462, https://doi.org/10.1007/BF00333935, 1996.

Bourtsoukidis, E., Behrendt, T., Yañez-Serrano, A. M., Hellén, H., Diamantopoulos, E., Catão, E., Ashworth, K., Pozzer, A., Quesada, C. A., Martins, D. L., Sá, M., Araujo, A., Brito, J., Artaxo, P., Kesselmeier, J., Lelieveld, J., and Williams, J.: Strong sesquiterpene emissions from Amazonian soils, Nat. Commun., 9, 2226, https://doi.org/10.1038/s41467-018-04658-y, 2018.

Bracho-Nunez, A., Welter, S., Staudt, M., and Kesselmeier, J.: Plant-specific volatile organic compound emission rates from young and mature leaves of Mediterranean vegetation, J. Geophys. Res. Atmospheres, 116, https://doi.org/10.1029/2010JD015521, 2011.

Byron, J., Kreuzwieser, J., Purser, G., van Haren, J., Ladd, S. N., Meredith, L. K., Werner, C., and Williams, J.: Chiral monoterpenes reveal forest emission mechanisms and drought responses, Nature, 609, 307–312, https://doi.org/10.1038/s41586-022-05020-5, 2022.

Calvin, K., Dasgupta, D., Krinner, G., Mukherji, A., Thorne, P. W., Trisos, C., Romero, J., Aldunce, P., Barrett, K., Blanco, G., Cheung, W. W. L., Connors, S., Denton, F., Diongue-Niang, A., Dodman, D., Garschagen, M., Geden, O., Hayward, B., Jones, C., Jotzo, F., Krug, T., Lasco, R., Lee, Y.-Y., Masson-Delmotte, V., Meinshausen, M., Mintenbeck, K., Mokssit, A., Otto, F. E. L., Pathak, M., Pirani, A., Poloczanska, E., Pörtner, H.-O., Revi, A., Roberts, D. C., Roy, J., Ruane, A. C., Skea, J., Shukla, P. R., Slade, R., Slangen, A., Sokona, Y., Sörensson, A. A., Tignor, M., van Vuuren, D., Wei, Y.-M., Winkler, H., Zhai, P., Zommers, Z., Hourcade, J.-C., Johnson, F. X., Pachauri, S., Simpson, N. P., Singh, C., Thomas, A., Totin, E., Arias, P., Bustamante, M., Elgizouli, I., Flato, G., Howden, M., Méndez-Vallejo, C., Pereira, J. J., Pichs-Madruga, R., Rose, S. K., Saheb, Y., Sánchez Rodríguez, R., Ürge-Vorsatz, D., Xiao, C., Yassaa, N., Alegría, A., Armour, K., Bednar-Friedl, B., Blok, K., Cissé, G., Dentener, F., Eriksen, S., Fischer, E., Garner, G., Guivarch, C., Haasnoot, M., Hansen, G., Hauser, M., Hawkins, E., Hermans, T., Kopp, R., Leprince-Ringuet, N., Lewis, J., Ley, D., Ludden, C., Niamir, L., Nicholls, Z., Some, S., Szopa, S., Trewin, B., van der Wijst, K.-I., Winter, G., Witting, M., Birt, A., Ha, M., et al.: IPCC, 2023: Climate Change 2023: Synthesis Report. Contribution of Working Groups I, II and III to the Sixth Assessment Report of the Intergovernmental Panel on Climate Change [Core Writing Team, H. Lee and J. Romero (eds.)]. IPCC, Geneva, Switzerland., Intergovernmental Panel on Climate Change (IPCC), https://doi.org/10.59327/IPCC/AR6-9789291691647, 2023.

Cappellin, L., Karl, T., Probst, M., Ismailova, O., Winkler, P. M., Soukoulis, C., Aprea, E., Märk, T. D., Gasperi, F., and Biasioli, F.: On Quantitative Determination of Volatile Organic Compound Concentrations Using Proton Transfer Reaction Time-of-Flight Mass Spectrometry, Environ. Sci. Technol., 46, 2283–2290, https://doi.org/10.1021/es203985t, 2012.

Cava, D., Dias-Júnior, C. Q., Acevedo, O., Oliveira, P. E. S., Tsokankunku, A., Sörgel, M., Manzi, A. O., de Araújo, A. C., Brondani, D. V., Toro, I. M. C., and Mortarini, L.: Vertical propagation of submeso and coherent structure in a tall and dense Amazon Forest in different stability conditions PART I: Flow structure within and above the roughness sublayer, Agric. For. Meteorol., 322, 108983, https://doi.org/10.1016/j.agrformet.2022.108983, 2022.

Colomb, A., Williams, J., Crowley, J., Gros, V., Hofmann, R., Salisbury, G., Klüpfel, T., Kormann, R., Stickler, A., Forster, C., and Lelieveld, J.: Airborne Measurements of Trace Organic Species in the Upper Troposphere Over Europe: the Impact of Deep Convection, Environ. Chem., 3, 244–259, https://doi.org/10.1071/EN06020, 2006.

Davidson, E. A., de Araújo, A. C., Artaxo, P., Balch, J. K., Brown, I. F., C. Bustamante, M. M., Coe, M. T., DeFries, R. S., Keller, M., Longo, M., Munger, J. W., Schroeder, W., Soares-Filho, B. S., Souza, C. M., and Wofsy, S. C.: The Amazon basin in transition, Nature, 481, 321–328, https://doi.org/10.1038/nature10717, 2012.

Deming, B. L., Pagonis, D., Liu, X., Day, D. A., Talukdar, R., Krechmer, J. E., de Gouw, J. A., Jimenez, J. L., and Ziemann, P. J.: Measurements of delays of gas-phase compounds in a wide variety of tubing materials due to gas–wall interactions, Atmospheric Meas. Tech., 12, 3453–3461, https://doi.org/10.5194/amt-12-3453-2019, 2019.

Dias-Júnior, C. Q., Dias, N. L., dos Santos, R. M. N., Sörgel, M., Araújo, A., Tsokankunku, A., Ditas, F., de Santana, R. A., von Randow, C., Sá, M., Pöhlker, C., Toledo Machado, L. A., de Sá, L. D., Moran-Zuloaga, D., Janssen, R., Acevedo, O., Oliveira, P., Fisch, G., Chor, T., and Manzi, A.: Is There a Classical Inertial Sublayer Over the Amazon Forest?, Geophys. Res. Lett., 46, 5614–5622, https://doi.org/10.1029/2019GL083237, 2019.

Edtbauer, A., Hartungen, E., Jordan, A., Hanel, G., Herbig, J., Jürschik, S., Lanza, M., Breiev, K., Märk, L., and Sulzer, P.: Theory and practical examples of the quantification of CH4, CO, O2, and CO2 with an advanced proton-transfer-reaction/selective-reagent-ionization instrument (PTR/SRI-MS), Int. J. Mass Spectrom., 365–366, 10–14, https://doi.org/10.1016/j.ijms.2013.11.014, 2014.

Edtbauer, A., Pfannerstill, E. Y., Pires Florentino, A. P., Barbosa, C. G. G., Rodriguez-Caballero, E., Zannoni, N., Alves, R. P., Wolff, S., Tsokankunku, A., Aptroot, A., de Oliveira Sá, M., de Araújo, A. C., Sörgel, M., de Oliveira, S. M., Weber, B., and Williams, J.: Cryptogamic organisms are a substantial source and sink for volatile organic compounds in the Amazon region, Commun. Earth Environ., 2, 1–14, https://doi.org/10.1038/s43247-021-00328-y, 2021.

Fischer, E. V., Jacob, D. J., Yantosca, R. M., Sulprizio, M. P., Millet, D. B., Mao, J., Paulot, F., Singh, H. B., Roiger, A., Ries, L., Talbot, R. W., Dzepina, K., and Pandey Deolal, S.: Atmospheric peroxyacetyl nitrate (PAN): a global budget and source attribution, Atmospheric Chem. Phys., 14, 2679–2698, https://doi.org/10.5194/acp-14-2679-2014, 2014.

Fuentes, J. D., Gerken, T., Chamecki, M., Stoy, P., Freire, L., and Ruiz-Plancarte, J.: Turbulent transport and reactions of plant-emitted hydrocarbons in an Amazonian rain forest, Atmos. Environ., 279, 119094, https://doi.org/10.1016/j.atmosenv.2022.119094, 2022.

Ganzeveld, L., Eerdekens, G., Feig, G., Fischer, H., Harder, H., Konigstedt, R., Kubistin, D., Martinez, M., Meixner, F. X., Scheeren, H. A., Sinha, V., Taraborrelli, D., Williams, J., de Arellano, J. V.-G., and Lelieveld, J.: Surface and boundary layer exchanges of volatile organic compounds, nitrogen oxides and ozone during the GABRIEL campaign, Atmos Chem Phys, 2008.

Gentine, P., Massmann, A., Lintner, B. R., Hamed Alemohammad, S., Fu, R., Green, J. K., Kennedy, D., and Vilà-Guerau de Arellano, J.: Land–atmosphere interactions in the tropics – a review, Hydrol. Earth Syst. Sci., 23, 4171–4197, https://doi.org/10.5194/hess-23-4171-2019, 2019.

Gerken, T., Wei, D., Chase, R. J., Fuentes, J. D., Schumacher, C., Machado, L. A. T., Andreoli, R. V., Chamecki, M., Ferreira de Souza, R. A., Freire, L. S., Jardine, A. B., Manzi, A. O., Nascimento dos Santos, R. M., von Randow, C., dos Santos Costa, P., Stoy, P. C., Tóta, J., and Trowbridge, A. M.: Downward transport of ozone rich air and implications for atmospheric chemistry in the Amazon rainforest, Atmos. Environ., 124, 64–76, https://doi.org/10.1016/j.atmosenv.2015.11.014, 2016.

Gloor, M., Gatti, L., Brienen, R., Feldpausch, T. R., Phillips, O. L., Miller, J., Ometto, J. P., Rocha, H., Baker, T., de Jong, B., Houghton, R. A., Malhi, Y., Aragão, L. E. O. C., Guyot, J.-L., Zhao, K., Jackson, R., Peylin, P., Sitch, S., Poulter, B., Lomas, M., Zaehle, S., Huntingford, C., Levy, P., and Lloyd, J.: The carbon balance of South America: a review of the status, decadal trends and main determinants, Biogeosciences, 9, 5407–5430, https://doi.org/10.5194/bg-9-5407-2012, 2012.

de Gouw, J. and Warneke, C.: Measurements of volatile organic compounds in the earth's atmosphere using proton-transfer-reaction mass spectrometry, Mass Spectrom. Rev., 26, 223–257, https://doi.org/10.1002/mas.20119, 2007.

Guenther, A., Hewitt, C. N., Erickson, D., Fall, R., Geron, C., Graedel, T., Harley, P., Klinger, L., Lerdau, M., Mckay, W. A., Pierce, T., Scholes, B., Steinbrecher, R., Tallamraju, R., Taylor, J., and Zimmerman, P.: A global model of natural volatile organic compound emissions, J. Geophys. Res. Atmospheres, 100, 8873–8892, https://doi.org/10.1029/94JD02950, 1995.

Guenther, A. B., Jiang, X., Heald, C. L., Sakulyanontvittaya, T., Duhl, T., Emmons, L. K., and Wang, X.: The Model of Emissions of Gases and Aerosols from Nature version 2.1 (MEGAN2.1): an extended and updated framework for modeling biogenic emissions, Geosci. Model Dev., 5, 1471–1492, https://doi.org/10.5194/gmd-5-1471-2012, 2012.

Holopainen, J. K., Virjamo, V., Ghimire, R. P., Blande, J. D., Julkunen-Tiitto, R., and Kivimäenpää, M.: Climate Change Effects on Secondary Compounds of Forest Trees in the Northern Hemisphere, Front. Plant Sci., 9, 2018.

Holzinger, R., Lee, A., Paw, K. T., and Goldstein, U. a. H.: Observations of oxidation products above a forest imply biogenic emissions of very reactive compounds, Atmospheric Chem. Phys., 5, 67–75, https://doi.org/10.5194/acp-5-67-2005, 2005.

Houghton, R. A., Lawrence, K. T., Hackler, J. L., and Brown, S.: The spatial distribution of forest biomass in the Brazilian Amazon: a comparison of estimates, Glob. Change Biol., 7, 731–746, https://doi.org/10.1111/j.1365-2486.2001.00426.x, 2001.

Jaeglé, L., Jacob, D. J., Brune, W. H., and Wennberg, P. O.: Chemistry of HOx radicals in the upper troposphere, Atmos. Environ., 35, 469–489, https://doi.org/10.1016/S1352-2310(00)00376-9, 2001.

Jeong, D., Seco, R., Emmons, L., Schwantes, R., Liu, Y., McKinney, K. A., Martin, S. T., Keutsch, F. N., Gu, D., Guenther, A. B., Vega, O., Tota, J., Souza, R. A. F., Springston, S. R., Watson, T. B., and Kim, S.: Reconciling Observed and Predicted Tropical Rainforest OH Concentrations, J. Geophys. Res. Atmospheres, 127, https://doi.org/10.1029/2020JD032901, 2022.

Jordan, A., Haidacher, S., Hanel, G., Hartungen, E., Herbig, J., Märk, L., Schottkowsky, R., Seehauser, H., Sulzer, P., and Märk, T. D.: An online ultra-high sensitivity Proton-transfer-reaction mass-spectrometer combined with switchable reagent ion capability (PTR+SRI–MS), Int. J. Mass Spectrom., 286, 32–38, https://doi.org/10.1016/j.ijms.2009.06.006, 2009.

Jordi Vilà-Guerau de Arellano, C. C. van H., Bart J. H. van Stratum, and Kees van den Dries: Atmospheric Boundary Layer, Cambridge University Press, 2015.

Karl, T., Guenther, A., Turnipseed, A., Tyndall, G., Artaxo, P., and Martin, S.: Rapid formation of isoprene photo-oxidation products observed in Amazonia, Atmos Chem Phys, 2009.

Kesselmeier, J. and Staudt, M.: Biogenic volatile organic compounds (VOC): An overview on emission, physiology and ecology, Environ. Pollut., 109, 175, 2000.

Kesselmeier, J., Schäfer, L., Ciccioli, P., Brancaleoni, E., Cecinato, A., Frattoni, M., Foster, P., Jacob, V., Denis, J., Fugit, J. L., Dutaur, L., and Torres, L.: Emission of monoterpenes and isoprene from a Mediterranean oak species Quercus ilex L. measured within the BEMA (Biogenic Emissions in the Mediterranean Area) project, Atmos. Environ., 30, 1841–1850, https://doi.org/10.1016/1352-2310(95)00376-2, 1996.

Kesselmeier, J., Kuhn, U., Wolf, A., Andreae, M. O., Ciccioli, P., Brancaleoni, E., Frattoni, M., Guenther, A., Greenberg, J., De Castro Vasconcellos, P., de Oliva, T., Tavares, T., and Artaxo, P.: Atmospheric volatile organic compounds (VOC) at a remote tropical forest site in central Amazonia, Atmos. Environ., 34, 4063–4072, https://doi.org/10.1016/S1352-2310(00)00186-2, 2000.

Koppmann, R.: Volatile Organic Compounds in the Atmosphere, John Wiley & Sons, 523 pp., 2008.

Koss, A. R., Warneke, C., Yuan, B., Coggon, M. M., Veres, P. R., and de Gouw, J. A.: Evaluation of NO⁺ reagent ion chemistry for online measurements ofatmospheric volatile organic compounds, Atmospheric Meas. Tech., 9, 2909–2925, https://doi.org/10.5194/amt-9-2909-2016, 2016.

Kuhn, U., Rottenberger, S., Biesenthal, T., Ammann, C., Wolf, A., Schebeske, G., Oliva, S. T., Tavares, T. M., and Kesselmeier, J.: Exchange of short-chain monocarboxylic acids by vegetation at a remote tropical forest site in Amazonia, J. Geophys. Res. Atmospheres, 107, LBA 36-1-LBA 36-18, https://doi.org/10.1029/2000JD000303, 2002.

Kuhn, U., Rottenberger, S., Biesenthal, T., Wolf, A., Schebeske, G., Ciccioli, P., Brancaleoni, E., Frattoni, M., Tavares, T. M., and Kesselmeier, J.: Seasonal differences in isoprene and light-dependent monoterpene emission by Amazonian tree species, Glob. Change Biol., 10, 663–682, https://doi.org/10.1111/j.1529-8817.2003.00771.x, 2004.

Laothawornkitkul, J., Taylor, J. E., Paul, N. D., and Hewitt, C. N.: Biogenic volatile organic compounds in the Earth system, New Phytol., 183, 27–51, https://doi.org/10.1111/j.1469-8137.2009.02859.x, 2009.

Levy, H.: Normal Atmosphere: Large Radical and Formaldehyde Concentrations Predicted, Science, 173, 141–143, https://doi.org/10.1126/science.173.3992.141, 1971.

Li, X.-B., Zhang, C., Liu, A., Yuan, B., Yang, H., Liu, C., Wang, S., Huangfu, Y., Qi, J., Liu, Z., He, X., Song, X., Chen, Y., Peng, Y., Zhang, X., Zheng, E., Yang, L., Yang, Q., Qin, G., Zhou, J., and Shao, M.: Assessment of long tubing in measuring atmospheric trace gases: applications on tall towers, Environ. Sci. Atmospheres, 3, 506–520, https://doi.org/10.1039/D2EA00110A, 2023.

Lindinger, W., Hansel, A., and Jordan, A.: On-line monitoring of volatile organic compounds at pptv levels by means of proton-transfer-reaction mass spectrometry (PTR-MS) medical applications, food control and environmental research, Int. J. Mass Spectrom. Ion Process., 173, 191–241, https://doi.org/10.1016/S0168-1176(97)00281-4, 1998.

Mahilang, M., Deb, M. K., and Pervez, S.: Biogenic secondary organic aerosols: A review on formation mechanism, analytical challenges and environmental impacts, Chemosphere, 262, 127771, https://doi.org/10.1016/j.chemosphere.2020.127771, 2021.

Maslin, M., Malhi, Y., Phillips, O., and Cowling, S.: New views on an old forest: assessing the longevity, resilience and future of the Amazon rainforest, Trans. Inst. Br. Geogr., 30, 477–499, https://doi.org/10.1111/j.1475-5661.2005.00181.x, 2005.

Mellouki, A., Wallington, T. J., and Chen, J.: Atmospheric Chemistry of Oxygenated Volatile Organic Compounds: Impacts on Air Quality and Climate, Chem. Rev., 115, 3984–4014, https://doi.org/10.1021/cr500549n, 2015.

Müller, M., Mikoviny, T., Jud, W., D'Anna, B., and Wisthaler, A.: A new software tool for the analysis of high resolution PTR-TOF mass spectra, Chemom. Intell. Lab. Syst., 127, 158–165, https://doi.org/10.1016/j.chemolab.2013.06.011, 2013.

Müller, M., Piel, F., Gutmann, R., Sulzer, P., Hartungen, E., and Wisthaler, A.: A novel method for producing NH4+ reagent ions in the hollow cathode glow discharge ion source of PTR-MS instruments, Int. J. Mass Spectrom., 447, 116254, https://doi.org/10.1016/j.ijms.2019.116254, 2020.

Mumm, R. and Dicke, M.: Variation in natural plant products and the attraction of bodyguards involved in indirect plant defense, Can. J. Zool., 88, 628–667, https://doi.org/10.1139/Z10-032, 2010.

Niinemets, Ü. and Reichstein, M.: Controls on the emission of plant volatiles through stomata: A sensitivity analysis, J. Geophys. Res. Atmospheres, 108, https://doi.org/10.1029/2002JD002626, 2003.

Niinemets, Ü., Reichstein, M., Staudt, M., Seufert, G., and Tenhunen, J. D.: Stomatal Constraints May Affect Emission of Oxygenated Monoterpenoids from the Foliage of Pinus pinea , Plant Physiol., 130, 1371–1385, https://doi.org/10.1104/pp.009670, 2002.

Niinemets, Ü., Fares, S., Harley, P., and Jardine, K. J.: Bidirectional exchange of biogenic volatiles with vegetation: emission sources, reactions, breakdown and deposition, Plant Cell Environ., 37, 1790–1809, https://doi.org/10.1111/pce.12322, 2014.

Norman, M., Hansel, A., and Wisthaler, A.: O2+ as reagent ion in the PTR-MS instrument: Detection of gas-phase ammonia, Int. J. Mass Spectrom., 265, 382–387, https://doi.org/10.1016/j.ijms.2007.06.010, 2007.

Northway, M. J., de Gouw, J. A., Fahey, D. W., Gao, R. S., Warneke, C., Roberts, J. M., and Flocke, F.: Evaluation of the role of heterogeneous oxidation of alkenes in the detection of atmospheric acetaldehyde, Atmos. Environ., 38, 6017–6028, https://doi.org/10.1016/j.atmosenv.2004.06.039, 2004.

Oliveira, P. E. S., Acevedo, O. C., Sörgel, M., Tsokankunku, A., Wolff, S., Araújo, A. C., Sá, M. O., Manzi, A. O., and Andreae, M. O.: Turbulent and non-turbulent exchange of scalars between the forest and the atmosphere at night in Amazonia, Biosphere Interactions/Field Measurements/Troposphere/Physics (physical properties and processes), https://doi.org/10.5194/acp-2017-638, 2017.

Ometto, J.P., K. Kalaba, G.Z. Anshari, N. Chacón, A. Farrell, S.A. Halim, H. Neufeldt, and R. Sukumar, 2022: Cross-Chapter Paper 7: Tropical Forests. In: *Climate Change 2022: Impacts, Adaptation and Vulnerability.* Contribution of Working Group II to the Sixth Assessment Report of the Intergovernmental Panel on Climate Change [H.-O. Pörtner, D.C. Roberts, M. Tignor, E.S. Poloczanska, K. Mintenbeck, A. Alegría, M. Craig, S. Langsdorf, S. Löschke, V. Möller, A. Okem, B. Rama (eds.)]. Cambridge University Press, Cambridge, UK and New York, NY, USA, pp. 2369–2410, doi:10.1017/9781009325844.024.

Pagonis, D., Krechmer, J. E., de Gouw, J., Jimenez, J. L., and Ziemann, P. J.: Effects of gas–wall partitioning in Teflon tubing and instrumentation on time-resolved measurements of gas-phase organic compounds, Atmospheric Meas. Tech., 10, 4687–4696, https://doi.org/10.5194/amt-10-4687-2017, 2017.

Parrish, D. D., Stohl, A., Forster, C., Atlas, E. L., Blake, D. R., Goldan, P. D., Kuster, W. C., and de Gouw, J. A.: Effects of mixing on evolution of hydrocarbon ratios in the troposphere, J. Geophys. Res. Atmospheres, 112, 2006JD007583, https://doi.org/10.1029/2006JD007583, 2007.

Peñuelas, J. and Llusià, J.: The Complexity of Factors Driving Volatile Organic Compound Emissions by Plants, Biol. Plant., 44, 481–487, https://doi.org/10.1023/A:1013797129428, 2001.

Peñuelas, J. and Llusià, J.: Plant VOC emissions: making use of the unavoidable, Trends Ecol. Evol., 19, 402–404, https://doi.org/10.1016/j.tree.2004.06.002, 2004.

Peñuelas, J. and Staudt, M.: BVOCs and global change, Trends Plant Sci., 15, 133–144, https://doi.org/10.1016/j.tplants.2009.12.005, 2010.

Pfannerstill, E. Y., Reijrink, N. G., Edtbauer, A., Ringsdorf, A., Zannoni, N., Araújo, A., Ditas, F., Holanda, B. A., Sá, M. O., Tsokankunku, A., Walter, D., Wolff, S., Lavrič, J. V., Pöhlker, C., Sörgel, M., and Williams, J.: Total OH reactivity over the Amazon rainforest: variability with temperature, wind, rain, altitude, time of day, season, and an overall budget closure, Atmospheric Chem. Phys., 21, 6231–6256, https://doi.org/10.5194/acp-21-6231-2021, 2021.

Pike, R. C., Lee, J. D., Young, P. J., Carver, G. D., Yang, X., Warwick, N., Moller, S., Misztal, P., Langford, B., Stewart, D., Reeves, C. E., Hewitt, C. N., and Pyle, J. A.: NO_x and O_3 above a tropical rainforest: an analysis with a global and box model, Atmospheric Chem. Phys., 10, 10607–10620, https://doi.org/10.5194/acp-10-10607-2010, 2010.

Pöschl, U.: Atmospheric Aerosols: Composition, Transformation, Climate and Health Effects, Angew. Chem. Int. Ed., 44, 7520–7540, https://doi.org/10.1002/anie.200501122, 2005.

Rasmussen, R. A.: Isoprene: identified as a forest-type emission to the atmosphere, Environ. Sci. Technol., 4, 667–671, https://doi.org/10.1021/es60043a008, 1970.

Restrepo-Coupe, N., da Rocha, H. R., Hutyra, L. R., da Araujo, A. C., Borma, L. S., Christoffersen, B., Cabral, O. M. R., de Camargo, P. B., Cardoso, F. L., da Costa, A. C. L., Fitzjarrald, D. R., Goulden, M. L., Kruijt, B., Maia, J. M. F., Malhi, Y. S., Manzi, A. O., Miller, S. D., Nobre, A. D., von Randow, C., Sá, L. D. A., Sakai, R. K., Tota, J., Wofsy, S. C., Zanchi, F. B., and Saleska, S. R.: What drives the seasonality of photosynthesis across the Amazon basin? A cross-site analysis of eddy flux tower measurements from the Brasil flux network, Agric. For. Meteorol., 182–183, 128–144, https://doi.org/10.1016/j.agrformet.2013.04.031, 2013.

Sarang, K., Rudziński, K. J., and Szmigielski, R.: Green Leaf Volatiles in the Atmosphere—Properties, Transformation, and Significance, Atmosphere, 12, 1655, https://doi.org/10.3390/atmos12121655, 2021.

Scala, A., Allmann, S., Mirabella, R., Haring, M. A., and Schuurink, R. C.: Green Leaf Volatiles: A Plant's Multifunctional Weapon against Herbivores and Pathogens, Int. J. Mol. Sci., 14, 17781–17811, https://doi.org/10.3390/ijms140917781, 2013.

Scheeren, H. A., Lelieveld, J., Roelofs, G. J., Williams, J., Fischer, H., de Reus, M., de Gouw, J. A., Warneke, C., Holzinger, R., Schlager, H., Klüpfel, T., Bolder, M., van der Veen, C., and Lawrence, M.: The impact of monsoon outflow from India and Southeast Asia in the upper troposphere over the eastern Mediterranean, Atmospheric Chem. Phys., 3, 1589–1608, https://doi.org/10.5194/acp-3-1589-2003, 2003.

Seco, R., Peñuelas, J., and Filella, I.: Short-chain oxygenated VOCs: Emission and uptake by plants and atmospheric sources, sinks, and concentrations, Atmos. Environ., 41, 2477–2499, https://doi.org/10.1016/j.atmosenv.2006.11.029, 2007.

Seinfeld, J. H. and Pandis, S. N.: Atmospheric Chemistry and Physics: From Air Pollution to Climate Change, John Wiley & Sons, 1146 pp., 2016.

Singh, H., Chen, Y., Staudt, A., Jacob, D., Blake, D., Heikes, B., and Snow, J.: Evidence from the Pacific troposphere for large global sources of oxygenated organic compounds, Nature, 410, 1078–1081, https://doi.org/10.1038/35074067, 2001.

Singh, H. B., Salas, L. J., Chatfield, R. B., Czech, E., Fried, A., Walega, J., Evans, M. J., Field, B. D., Jacob, D. J., Blake, D., Heikes, B., Talbot, R., Sachse, G., Crawford, J. H., Avery, M. A., Sandholm, S., and Fuelberg, H.: Analysis of the atmospheric distribution, sources, and sinks of oxygenated volatile organic chemicals based on measurements over the Pacific during TRACE-P, J. Geophys. Res. Atmospheres, 109, https://doi.org/10.1029/2003JD003883, 2004.

Stull, R. B.: Mean Boundary Layer Characteristics, in: An Introduction to Boundary Layer Meteorology, edited by: Stull, R. B., Springer Netherlands, Dordrecht, 1–27, https://doi.org/10.1007/978-94-009-3027-8_1, 1988.

Vilà-Guerau de Arellano, J., Wang, X., Pedruzo-Bagazgoitia, X., Sikma, M., Agustí-Panareda, A., Boussetta, S., Balsamo, G., Machado, L. a. T., Biscaro, T., Gentine, P., Martin, S. T., Fuentes, J. D., and Gerken, T.: Interactions Between the Amazonian Rainforest and Cumuli Clouds: A Large-Eddy Simulation, High-Resolution ECMWF, and Observational Intercomparison Study, J. Adv. Model. Earth Syst., 12, e2019MS001828, https://doi.org/10.1029/2019MS001828, 2020.

Voigt, C., Lelieveld, J., Schlager, H., Schneider, J., Curtius, J., Meerkötter, R., Sauer, D., Bugliaro, L., Bohn, B., Crowley, J. N., Erbertseder, T., Groß, S., Hahn, V., Li, Q., Mertens, M., Pöhlker, M. L., Pozzer, A., Schumann, U., Tomsche, L., Williams, J., Zahn, A., Andreae, M., Borrmann, S., Bräuer, T., Dörich, R., Dörnbrack, A., Edtbauer, A., Ernle, L., Fischer, H., Giez, A., Granzin, M., Grewe, V., Harder, H., Heinritzi, M., Holanda, B. A., Jöckel, P., Kaiser, K., Krüger, O. O., Lucke, J., Marsing, A., Martin, A., Matthes, S., Pöhlker, C., Pöschl, U., Reifenberg, S., Ringsdorf, A., Scheibe, M., Tadic, I., Zauner-Wieczorek, M., Henke, R., and Rapp, M.: Cleaner Skies during the COVID-19 Lockdown, Bull. Am. Meteorol. Soc., 103, E1796–E1827, https://doi.org/10.1175/BAMS-D-21-0012.1, 2022.

Warneke, C., Holzinger, R., Hansel, A., Jordan, A., Lindinger, W., Pöschl, U., Williams, J., Hoor, P., Fischer, H., Crutzen, P. J., Scheeren, H. A., and Lelieveld, J.: Isoprene and Its Oxidation Products Methyl Vinyl Ketone, Methacrolein, and Isoprene Related Peroxides Measured Online over the Tropical Rain Forest of Surinam in March 1998, 2001.

Williams, J.: Organic Trace Gases in the Atmosphere: An Overview, Environ. Chem., 1, 125, https://doi.org/10.1071/EN04057, 2004.

Xu, X., Zhang, X., Riley, W. J., Xue, Y., Nobre, C. A., Lovejoy, T. E., and Jia, G.: Deforestation triggering irreversible transition in Amazon hydrological cycle, Environ. Res. Lett., 17, 034037, https://doi.org/10.1088/1748-9326/ac4c1d, 2022.

Yáñez-Serrano, A. M., Nölscher, A. C., Bourtsoukidis, E., Derstroff, B., Zannoni, N., Gros, V., Lanza, M., Brito, J., Noe, S. M., House, E., Hewitt, C. N., Langford, B., Nemitz, E., Behrendt, T., Williams, J., Artaxo, P., Andreae, M. O., and Kesselmeier, J.: Atmospheric mixing ratios of methyl ethyl ketone (2-butanone) in tropical, boreal, temperate and marine environments, Atmospheric Chem. Phys., 16, 10965–10984, https://doi.org/10.5194/acp-16-10965-2016, 2016.

Zhuang, Y., Fu, R., Marengo, J. A., and Wang, H.: Seasonal variation of shallow-to-deep convection transition and its link to the environmental conditions over the Central Amazon, J. Geophys. Res. Atmospheres, 122, 2649–2666, https://doi.org/10.1002/2016JD025993, 2017.

Chapter 2

This chapter has been published as: Ringsdorf, A., Edtbauer, A., Vilà-Guerau de Arellano, J., Pfannerstill, E. Y., Gromov, S., Kumar, V., Pozzer, A., Wolff, S., Tsokankunku, A., Soergel, M., Sá, M. O., Araújo, A., Ditas, F., Poehlker, C., Lelieveld, J., and Williams, J.: Inferring the diurnal variability of OH radical concentrations over the Amazon from BVOC measurements, Sci. Rep., 13, 14900, https://doi.org/10.1038/s41598-023-41748-4, 2023.

Contribution to this paper: Akima Ringsdorf performed the BVOC measurements, analyzed the data, developed the method to estimate the mixing timescale, and drafted the manuscript.

Inferring OH radical concentrations from BVOC measurements

2.1 Abstract

The atmospheric oxidation of biogenic volatile organic compounds (BVOC) by OH radicals over tropical rainforests impacts local particle production and the lifetime of globally distributed chemically and radiatively active gases. For the pristine Amazon rainforest during the dry season, we empirically determined the diurnal OH radical variability at the forest-atmosphere interface region between 80 and 325m from 07:00 to 15:00 LT using BVOC measurements. A dynamic time warping approach was applied showing that median averaged mixing times between 80 m to 325 m decrease from 105 to 15 minutes over this time period. The inferred OH concentrations show evidence for an early morning OH peak (07:00-08:00 LT) and an OH maximum (14:00 LT) reaching 2.2 (0.2, 3.8) $x10^6$ molecules cm^{-3} controlled by the coupling between BVOC emission fluxes, nocturnal NO_x accumulation, convective turbulence, air chemistry and photolysis rates. The results were evaluated with a turbulence resolving transport (DALES), a regional scale (WRF-Chem) and a global (EMAC) atmospheric chemistry model.

2.2 Introduction

The hydroxyl radical (OH) is the main atmospheric oxidant for trace gases in the global atmosphere (Lelieveld et al., 2016). By initializing the removal of natural and anthropogenic hazardous and radiatively active gases (e.g. CH_4) it is an important factor for human health and global climate (Montzka et al., 2011). The primary atmospheric source of OH is a pathway of ozone photolysis which forms $O(^1D)$ atoms, that can react rapidly with water to produce two OH radicals (Levy, 1971). As a result most OH initiated atmospheric oxidation occurs in the tropical lower troposphere where high insolation and water vapor combine with ubiquitous ozone to generate high OH production rates (Lelieveld et al., 2016). However, in the same regions, tropical forests provide the largest global emission source of biogenic volatile organic compounds (BVOC) which react readily with OH (Guenther, 2013; Kesselmeier and Staudt, 2000). Therefore, a critical interface region exists directly above tropical forests where strong sources and sinks of OH are co-located, the net result being key to the lifetime of many gases (Lelieveld et al., 2008, 2016). Due to their coarse resolution (typical grid cell sizes > 25 km with about 10 horizontal layers in the atmospheric boundary layer (ABL)), global atmospheric models are known to experience problems in this region as the strong VOC emissions suppress OH and cause overestimates of BVOC mixing ratios relative to measurements (Carslaw et al., 2001; Pugh et al., 2010; Stone et al., 2010; Hofzumahaus et al., 2009; Tan et al., 2001).

Simultaneous airborne measurements of OH, hydroperoxyl radicals (HO_2) and BVOC over a tropical rainforest in 2005 led to the closer scrutiny of isoprene oxidation chemistry, for additional OH sources and recycling routes (Lelieveld et al., 2008). Although the OH measurements reported were subsequently found to be artificially high due to an instrumental interference (Mao et al., 2012), theoretical studies (Peeters et al., 2014), mechanistic and modelling investigations (Taraborrelli et al., 2012; Lelieveld et al., 2008), laboratory chamber-based oxidation studies (Nölscher et al., 2014) and kinetic experiments (Dillon and Crowley, 2008) revealed underestimated or even overlooked routes through which OH was recycled during the oxidation of isoprene.

In this paper we present a new empirical derivation of the OH abundance and diurnal variation above a largely pristine part of the Amazonian rainforest (Andreae et al., 2015) characterized by low nitrogen

oxides (NO_x) conditions (NO < 150 ppt at 80 m). To infer an OH radical abundance, other than by direct measurement, requires measurement of a change in concentration of one or more BVOCs with a known OH reaction rate coefficient, and to accurately know the reaction time (period during which reactive molecules are exposed to OH oxidation). Here a change of the BVOC concentration with height above a rainforest is studied. We have measured BVOC concentrations on a tall tower at two heights (80 and 325 m) and investigate to which extent the concentration gradients are influenced by oxidation chemistry, turbulent mixing, emission and dilution due to transport from above (Fig. 2.1). Several indirect estimates of OH have been made in the past using BVOC concentrations and fluxes acquired from towers and aircraft in conjunction with models (Kuhn et al., 2007; Karl et al., 2007). However, all have approximated the reaction time in the vertical direction through use of the convective velocity (w_*) of the ABL. In order to better ascertain the timescale, in this study we approach the vertical reaction time by applying the Dynamic Time Warping (DTW) analysis alignment method (Rabiner and Juang, 2016) to simultaneously observed meteorological data (see method for details).

'Dynamical Time Warping' (DTW) in conjunction with a chemically inert tracer like the potential temperature (ϑ), which varies with time, allows quantification of the time offset between the timeseries at two reference heights (Fig. 2.2) under diurnal turbulent convective conditions. Air heated at the top of the canopy by conduction is transported vertically via turbulent convection, creating turbulent buoyant plumes that are organized in warm upward and cold downward motions. At the interfaces of these plumes lateral mixing occurs between the motions, resulting in a warming of the boundary layer. This heating is observed in the time offset of ϑ between 80 and 325 m. After normalizing the observed daily cycles of ϑ according to their magnitude, the time offset is extracted by DTW as it projects one timeseries onto another (using a cost minimization matrix). Thus, the DTW method provides a mixing timescale that approaches the time that air is exposed to oxidation. Mixing of airmasses containing isoprene and OH also result from the ensemble of the upward and downward turbulent motions. We exploit the daily time differences observed in ϑ at each height under diurnal convective conditions averaged over 23 days to extract a statistically robust, continuous and representative vertical mixing time as a function of time-of-day. Combining the extracted time with isoprene concentrations at 80 and 325 m and the corresponding formation of its oxidation products (IsoO, here: Methyl Vinyl Ketone (MVK) + Methacrolein (MACR) + Isoprene Hydroxyhydroperoxides (ISOPOOH)) allows calculation of the OH concentration between 80 and 325 m and from 07:00-15:00 LT with two different methods. The empirically derived OH concentrations were then evaluated against those simulated by three different atmospheric chemistry models: the turbulence resolving Dutch Atmospheric Large-Eddy Simulation (DALES) (Ouwersloot et al., 2017) the regional scale forecasting model WRF-Chem (Grell et al., 2005) and the atmospheric chemistry general circulation model EMAC (Jöckel et al., 2010, 2006). Since DALES is able to calculate the most energetic turbulent eddies in the roughness sublayer, we use it to independently test the uncertainties of the empirical methods using control numerical experiments.

OH concentrations are derived between 80 and 325 m in the ABL, which extends from just above the canopy at about 37 m (Kuhn et al., 2007) to about 2 km between sunrise at 06:00 and 14:00 local time (UTC - 4 h) (Fig. 2.1a). During the night the lower atmosphere is stably stratified with positive vertical gradients of ϑ. After sunrise, the positive sensible and latent heat fluxes lead to the formation of the convective boundary layer via thermal expansion of air that triggers buoyancy, i.e. density instabilities that lead to convective turbulence. Turbulent eddies that form coherent structures characterized by upward thermal and downward subsidence motions are induced(Stull, 1988; Vilà-Guerau De Arellano et

al., 2015). During the transport and mixing chemical reactions take place (Fuentes et al., 2022). Strong insulation and rising surface temperature throughout the day lead to increasing buoyancy and turbulence until the afternoon transition (Vilà-Guerau De Arellano et al., 2015). The warming and growth of the ABL have implications for the derived mixing timescale. When considering the free convective scaling velocity of single updrafts, w*, an increase with increasing buoyancy is observed (Stull, 1988). Direct comparison between w* and the mixing timescale derived here is however not possible. The DTW-derived timescale considers the heating of the boundary layer, which represents the ensemble of thermal upwards and subsiding transport. Further, the measurements taken at around 80 m are likely to be inside the roughness-sublayer that spans within the ABL from the ground to 2-3 times the canopy height (37 m) (Dias-júnior et al., 2019; Chamecki et al., 2020). Turbulence there differs from the layers aloft with strongly inhomogeneous flows of sweeping and ejection motions induced by deceleration of wind at the rough canopy surface (Finnigan, 2000; Cava et al., 2022). The timescale of w* represents that of individual large eddies in reaching the top of the ABL.

2.3 Results and discussion

The BVOC measurements reported here were taken at 80, 150 and 325 m from the ATTO tower sited amidst the pristine Amazon rainforest. Isoprene and its combined oxidation products IsoO were measured using PTR-ToF-MS at m/z 69.069 and 71.049. In order to investigate the vertical evolution of BVOC above the forest canopy, air from 80, 150 and 325 m was measured sequentially for five minutes at each height generating four datapoints per hour at each level. Isoprene was chosen for the OH radical concentration determination as it is an abundant, primary emitted BVOC without secondary sources and predominantly oxidized by OH (Pfannerstill et al., 2021). Meteorological variables were observed on the ATTO tower at 321 m and the 80 m tall walk-up tower on the same site at 81 m. BVOC and meteorological variables were measured continuously but the method to infer OH concentrations is restricted to convective periods which are defined by $\vartheta_{325m} < \vartheta_{80m}$. This condition ensures a net-upward propagation of thermal energy that can be converted into a mixing time. The maximum of ϑ at 80 m serves as an upper limit after noon. By then the declining insolation and concomitant decreasing buoyancy force leads to stabilization rendering the method inoperable. The vertical distribution of BVOC at ATTO is affected by the complex dynamic regime at the atmosphere-canopy interface (Chamecki et al., 2020) as well as by chemical processing. Measured dry season vertical mixing ratio profiles of isoprene, IsoO, specific humidity (q) and ϑ are shown at noon in Figure 2.1b. Isoprene, q and ϑ show the largest values at the canopy level, where their source is located, decreasing with altitude due to multiple processes, including emission strength changes, mixing and chemical reactions. The highly reactive isoprene decreases by 14.4 % from 80 m to 150 m and 24.3 % up to 325 m. Conversely IsoO, the OH photochemical product slightly increases with height in the measurements, due to the interplay of isoprene oxidation and turbulent mixing, that implies up- and downwards movement and mixing of more or less aged emissions. Observations reported by Rinne et al. (2012) indicated little chemical degradation of isoprene above the boreal forest up to 22 m, however, OH production rates there and turbulence intensity are expected to be substantially lower than in the tropics. Rinne et al. (2012) also noted that highly reactive sesquiterpene emissions from a boreal forest would be chemically oxidized faster than they can be transported aloft. This is also in agreement with this study as although sesquiterpenes have been measured previously at ground level at the ATTO site (Bourtsoukidis et al., 2018; Edtbauer et al., 2021), these species were not quantifiable at 325m. The

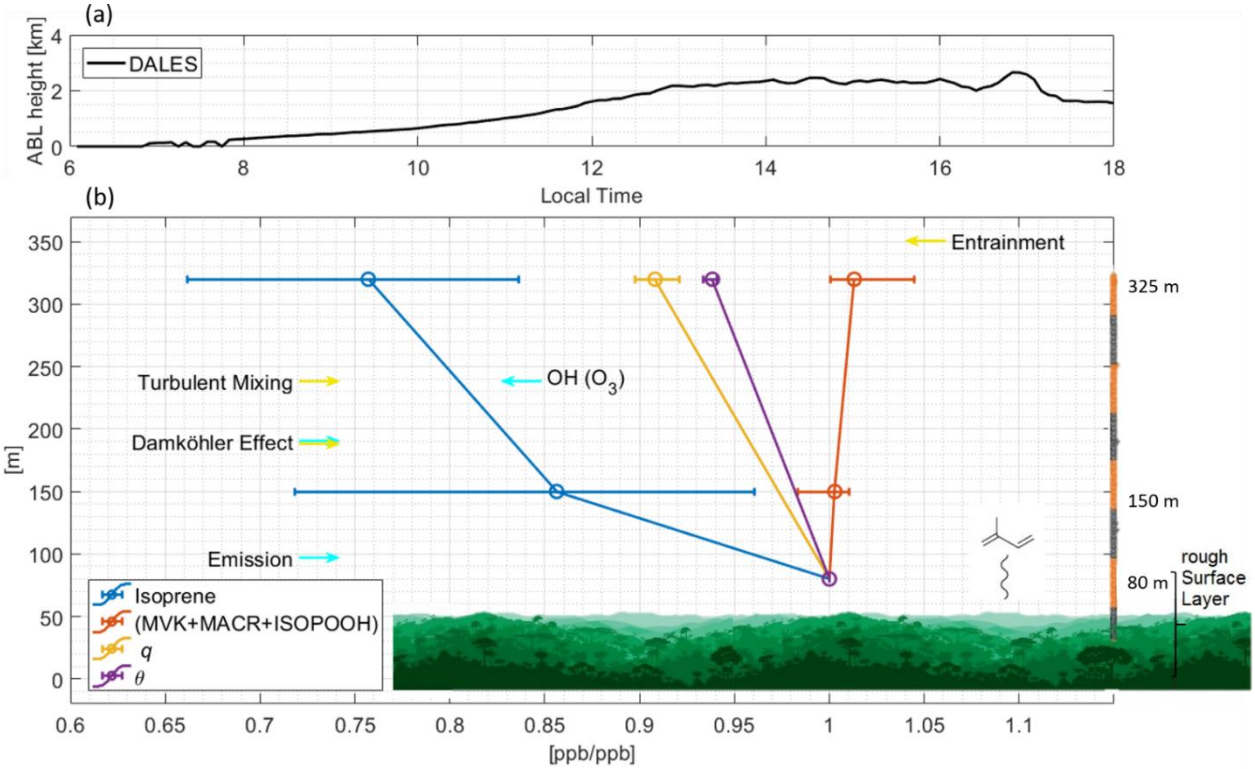

Figure 2.1: *Overview of the processes that govern the vertical distribution of variables observed at ATTO a) Time series of the boundary layer height simulated by DALES b) Schematic sketch of the processes governing the vertical gradient of reactive trace gases, here isoprene, emitted from the Amazon forest. Dynamic processes are marked with yellow arrows while blue arrows indicate chemistry related processes. The Damköhler effect has two arrows since it quantifies the relation between the turbulent and chemistry time scales. The relative vertical gradients of isoprene, the isoprene oxidation products Methyl Vinyl Ketone + Methacrolein + Isoprene Hydroxyhydroperoxides (ISOPOOH), specific humidity q and potential temperature ϑ observed at ATTO are median averages at 12:00-14:00. The error bars indicate the (0.15, 0.85) quantiles.*

sensitivity of the vertical isoprene gradient to OH oxidation chemistry and mixing is investigated with the use of the turbulent-resolved simulation technique DALES later in this study.

The vertical concentration gradient of isoprene, observed over 80-325 m becomes steeper with height (i.e. large concentration differences between top and bottom) due to three processes: surface emission, entrainment of isoprene-free air from above and OH oxidation (Vilà Guerau De Arellano et al., 2011; Krol et al., 2000). In contrast turbulent mixing causes two effects that both act to weaken the vertical gradient. Firstly, the establishment of the concentration gradient is counteracted by the mixing of isoprene rich upward motions with isoprene poor air transported from the downward subsident motions. This asymmetry in the transport also leads to segregation due to the inhomogeneous mixing (Ouwersloot et al., 2011; Krol et al., 2000). The segregation of isoprene lowers the effective reaction rate ($k_{\mathrm{iso+OH}}$), and as a result, the impact of OH oxidation on the vertical gradient in isoprene is weakened (Clifton et al., 2022; Ouwersloot et al., 2011).

In order to quantify the competition and relative dominance of dynamical processes and chemical processes over the whole day the Damköhler number (Da) is introduced. This term is defined as:

$$\mathrm{Da} = \frac{\tau_\mathrm{D}}{\tau_\mathrm{C}} = \frac{\text{mixing time (s)}}{([\mathrm{OH}]\, k_{\mathrm{iso+OH}})^{-1}\ (\mathrm{s})} \quad \text{(E2.1)}$$

It is a dimensionless number that compares the timescale of dynamics τ_D to that of chemistry τ_C, with values of unity indicative of a competitive regime and a maximum intensity of segregation (Ouwersloot et al., 2011). Within equation E2.1 the timescale of dynamics is typically represented by the convection timescale *t*

$$t = \frac{h}{w_*} \quad \text{(E2.2)}$$

where h is the boundary layer height and w_*. As the aim is to investigate the conditions over the vertical extent of the ATTO tower, the DTW derived mixing time is introduced in the following section (Figs. 2.2 and 2.3) and used instead. It is shown that ensemble turbulent motions in the atmosphere canopy interface region happen on longer timescales than estimated by *t* which is critically important for the OH estimation.

2.3.1 Mixing time in the low ABL

The DTW technique as described within the methods section was applied to the observed time-series of potential temperature ϑ for a total of 23 dry season days from October 2018 and September 2019 between 6:00 – 18:00 LT. This is shown for one example day in Figure 2.2 where normalized ϑ values at 80 and 325 m are allocated to find the time index difference corresponding to warming at both heights. The warming is a result of lateral mixing induced by turbulent buoyant plumes.

As precipitation events interfere with the vertical distribution of ϑ a filter is applied to remove such periods (30.8 % of data). To infer OH concentrations from the oxidative change of isoprene concentrations with height and DTW derived mixing times requires convective conditions. Periods with a stable stratification ($\vartheta_{325\mathrm{m}} > \vartheta_{80\mathrm{m}}$) were therefore excluded. This affects the morning transition from the stable nocturnal ABL to the convectively mixed ABL. The daily maximum of ϑ at 80 m was taken as the later limit for the calculation of OH, which occurred at the latest by 15:00 LT. The time restriction was also supported by the sign of the non-dimensional z/L number (sampling height *z* divided by the Obukhov length *L*) observed at ATTO (Supplementary Fig. 1). It indicates the stability of the ABL with positive values representing a stable stratification (Stull, 1988). The Obukhov length was estimated from the meteorological flux measurements at 81 m.

Median averaged mixing times from 80 m to 325 m ranged from 15 to 105 minutes (Fig. 2.3). Large mixing timescales are found in the morning when thermal and shear driven motions are slow due to the sensible and latent heat fluxes being still small. Throughout the day the values of the mixing timescale decrease as turbulent convection becomes more dominant. To further complete the assessment of the DTW method, it was also applied to the observed timeseries of specific humidity *q* at the sampling heights. Despite ϑ being related to the sensible heat flux and therefore to the active part of turbulence, and *q* in contrast being transported by this turbulence, the time scale derived with *q* has similar values. It varies around 45 minutes and is comprised within the 75$^{\mathrm{th}}$ percentile of the timescale derived with ϑ after 10:00 LT. Before

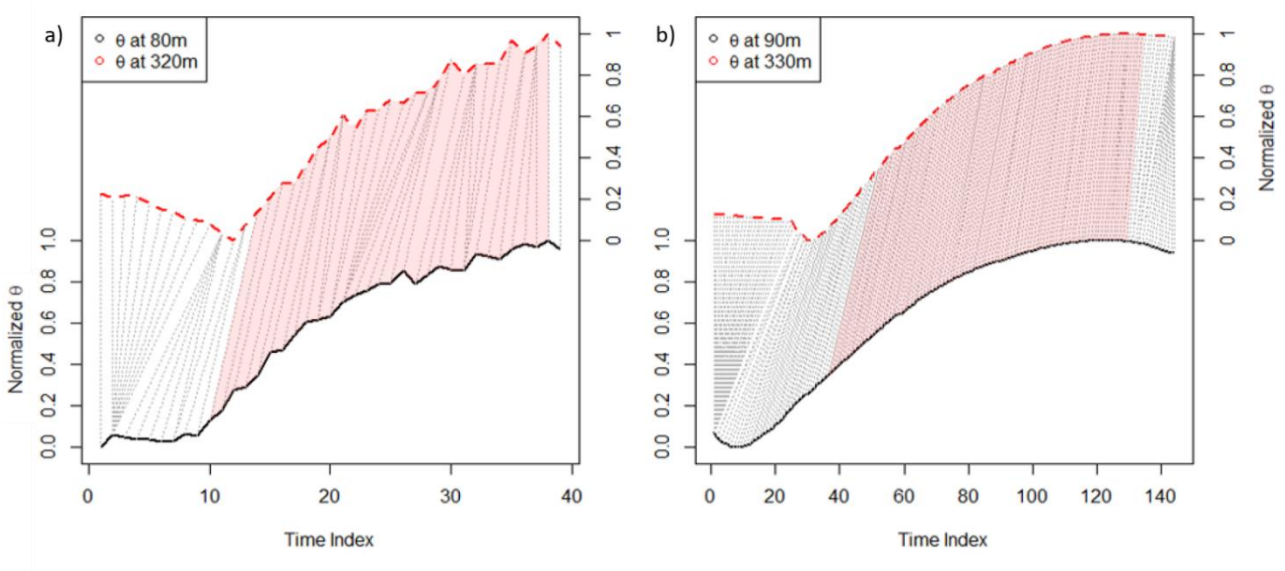

Figure 2.2: *Example of Dynamical Time Warping alignment of the normalized time series of potential temperature ϑ between zero and one over the course of one day. The dotted lines visualize their alignment pointwise. Convective ABL conditions apply only for the marked alignments, thus the mixing timescale is derived only from this period. This precludes edge effects. The index represents the time steps depending on their resolution. a) ϑ observed at the measurement heights. The period under analysis includes 23 dry season days. b) ϑ at two corresponding levels simulated for a representative day with DALES.*

that time both timescales show considerable differences, likely because the timeseries of q are altered due to condensation and evaporation in low level clouds that are often observed visually in the morning over the rainforest.

The DTW-derived mixing times between the two equivalent ϑ levels of DALES (90 m to 330 m) from 9:00 to 15:00 LT are slightly higher than derived for ATTO but comprised within the day to day variation. DALES is constrained to the isoprene observed at ATTO and explicitly resolves turbulence above the canopy, without resolving explicitly the interactions between the tall canopy and the above layer. As a result, the characteristic motions of ejection and sweeping at the interface are not resolved. The canopy is represented by a bulk layer with a high roughness length to account for changes in turbulence just above the canopy top (Vilà-Guerau de Arellano et al., 2020). Thus, using DALES, the influence of the tall canopy on turbulent transport above cannot be disentangled. Friction velocity however, simulated by DALES agrees well with observations above the Amazon forest (Vilà-Guerau de Arellano et al., 2020).

For comparison the timescale t calculated from the convective velocity (E2.2) is shown in Figure 2.3a. The vertical timescale as applied in previous studies (Kuhn et al., 2007; Karl et al., 2007), calculated from E2.2 using w_*, is presented too; here the sampling height z (here: 240 m) instead of the boundary layer height h is used. The magnitudes of the convective timescale t and DTW derived timescales are not expected to match, as both timescales consider convective transport differently. The DTW derived time represents mixing within up and subsident downdraft transport in the first 325 m of the ABL. Conversely, t represents the timescale of individual convective updrafts within the entire ABL.

It should be noted that the extracted vertical timescale varies in the vertical and is correlated with the turbulent kinetic energy (TKE) timescale shown in Figure 2.3b. The timescale of the TKE, obtained from

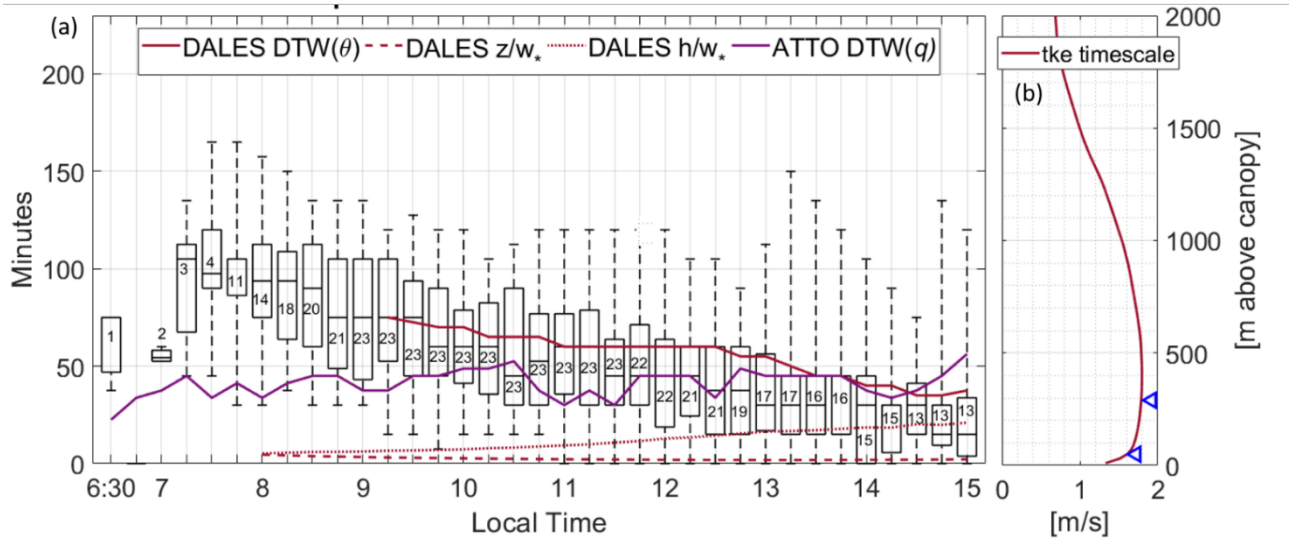

Figure 2.3: *Variations of the mixing time with time of day and height a) The box-whisker plots shows the median and the range of the 75th percentile of the Dynamical Time Warping derived mixing time from ATTO observations. Whiskers include all datapoints. The numbers in the boxes describe the numbers of days used to generate the box and whiskers. The dark red line is the DTW derived mixing time with potential temperature simulated at the corresponding altitude levels of DALES. Timescales calculated from the convective velocity with the ABL height (h) and sampling height (z) are included as dashed lines. The purple line shows the DTW derived mixing time from observed timeseries of q. b) The distribution of the vertical velocity timescale based on turbulent kinetic energy (TKE) by DALES at 12:00 LT. Blue arrows point at the ATTO sampling heights.*

DALES, has a maximum at around half the height of the ABL (Stull, 1988). The observed layer marked with blue arrows thus comprises the transition to maximum vertical velocity indicating that the mixing time based on DTW has a non-linear dependency on height.

2.3.2 Sensitivity towards OH chemistry

To better understand the sensitivity of the isoprene concentration gradient in the vertical to OH radical abundance, a suite of systematic experiments that vary OH recycling efficiencies were performed by DALES (Fig. 2.4). The OH radical recycling efficiency, namely the extent to which OH is regenerated during the oxidative degradation of organic molecules, is a current topic of research especially in low NO_x – high isoprene regions (Wells et al., 2020). Within the BVOC-NO_x-O_3-mechanism for gas phase chemistry in DALES (Supplementary Table 1), OH recycling takes place via the reactions of OH + Isoprene → RO_2 and RO_2 + HO_2 → n·OH + product, where n is a tunable parameter. Figure 2.4 shows that the best fit to the ATTO isoprene observation was obtained for the DALES model with recycling efficiencies around n = 0.8-1, but all cases of recycling are incorporated within the day to day variation of the measurement. The presented simulated vertical isoprene gradients are significantly larger for conditions with increased OH recycling; a one percent increase in OH decreases isoprene by about 0.7 - 1.2 % at 330 m between 12:00 and 14:00 LT. This sensitivity varies throughout the day, and isoprene is less sensitive to a change in OH

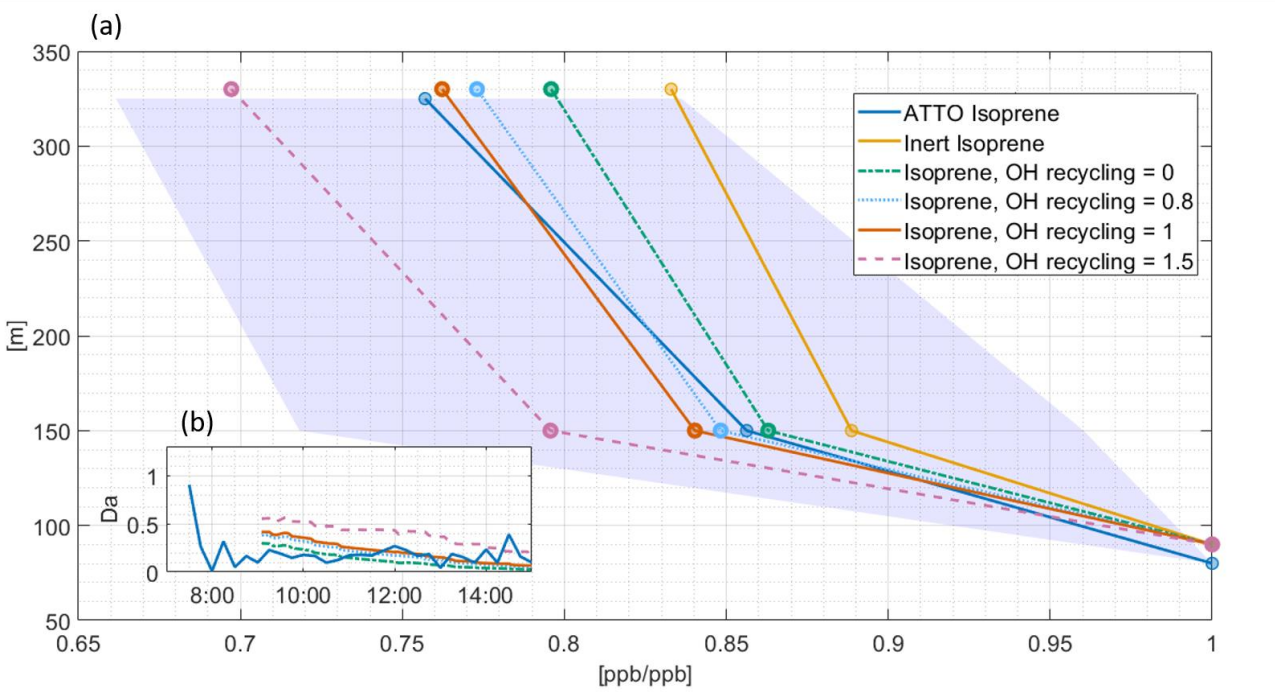

Figure 2.4: *Isoprene profiles above the rainforest canopy under varying OH concentrations simulated with DALES and compared to ATTO observations and the resulting Damköhler Number (Da) a) Relative vertical gradients, median averaged between 12:00-14:00 of isoprene under increasing OH recycling efficiencies calculated with DALES. Inert isoprene represents a non reactive tracer with identical initial profile and emission flux as isoprene. The shadings of the measured isoprene gradient indicate the (0.15, 0.85) quantiles. b) In the box insert the variation of Da for the different recycling efficiencies and over the course of one day is shown. The Dynamical Time Warping based mixing time of DALES is used here. For the Da at ATTO isoprene observations, the mixing time at ATTO (Fig. 2.3) and final OH concentrations (Fig. 2.5) are applied.*

concentration in the morning. Investigations with DALES reveal that the oxidation of isoprene is likely limited by the availability of isoprene itself, suggesting a higher intensity of segregation occurs in the morning.

To further elucidate the effect of chemistry, a chemically inert analogue of isoprene was also simulated in the DALES model. Diurnal emissions were set to be the same as for isoprene (Supplementary Fig. 2.2). The resulting residual gradient of the inert isoprene analogue provides evidence for dilution of isoprene emissions by entrainment of isoprene free air from above. The ensemble of up- and downward motions that tend to mix isoprene concentrations and thus counteract the establishment of a vertical gradient also effects the inert analogue of isoprene. Together, this constitutes a relative decrease of the inert isoprene tracer of 16.8 %, which is more than half of the total isoprene decrease. A tracer that can be considered here as chemically inert and that is also measured at ATTO is the conserved variable q. It is defined as the mass of water vapor in 1 kg of moist air (Stull, 1988). The annual mean lifetime of water vapor from evaporation to precipitation in the Amazon region is about 3-6 days (Sodemann, 2020) so that it can be classified in this context as practically inert. Isoprene and water vapor originate from the canopy or below, and both are diluted with drier and isoprene poorer air from the above layers. Noontime (12:00 – 14:00 LT) relative decrease of q representing the loss due to turbulent mixing was 9.2 % (Supplementary Fig. 3a).

The (0.15, 0.85) quantiles for the gradient of *q* is 7.9 % and 10.2 % respectively. Subtracting either the loss of *q* or the simulated inert isoprene from the total decrease in isoprene yields its oxidation driven decrease.

It should be noted that a local effect of cloud shading is that the isoprene emissions can drop abruptly. As a result, there can be momentarily more isoprene aloft than lower down. Combined with inert isoprene or *q*, which are not or less sensitive towards a change in local irradiation, the corrected isoprene gradient can turn positive for short periods, which are not representative for the convective ABL. Those cases result in negative OH concentrations (Supplementary Fig. 4) and are filtered out for both methods. The opposite, an enhanced negative isoprene gradient due to reduced irradiation of the 320 m footprint area is less probable as it covers a much larger area and is therefore less susceptible to complete shading.

Subtracting the gradient of q or of the simulated inert isoprene thus implies an oxidation driven decrease of 18.5 % or 15.3 % in isoprene at noon, that is used to infer the OH concentration. There is a large difference between the gradients of *q* and inert isoprene which most likely results from different emission and entrainment strengths of H_2O and isoprene. The emission flux of H_2O relative to its mixing ratio above, at 90 m, is calculated using DALES and reveals a smaller emission and dilution velocity for *q* compared to inert isoprene (Supplementary Fig. 3b). This can explain the larger gradient of inert isoprene in the investigated layer. Choosing *q* enables correction for each day individually, which is an advantage as the observed gradients of *q* and isoprene show variability between days, whereas the inert isoprene tracer shows one representative day. Also, *q* at 80 m is, like isoprene, influenced by the complex turbulence within the roughness sublayer above the tall canopy. For comprehensiveness and as combining simulated and observed parameters creates additional uncertainty, both ways are applied to infer OH in the following section. However, using simulated inert isoprene is expected to obtain better results as the strength of emission, which is the same for isoprene and inert isoprene, is very relevant in the first 325 meters of the ABL.

The diurnal evolution of Da, calculated from E2.1 for the five DALES experiments and for ATTO data is presented in Figure 2.4b. Values between 0.01 and 0.6 decreasing between 8:00 to 16:00 LT for all OH recycling efficiencies were obtained from DALES. Those values indicate a regime with competing dynamics and chemistry as shown already by the sensitivity of the isoprene gradients towards OH chemistry. At ATTO, the mixing time (Fig. 2.3) is somewhat faster than the isoprene-OH chemistry lifetime, which ranges from one hour to one day. This is indicated by Da < 1, except for the period in the morning where high OH concentrations lead to fast oxidation chemistry and a Damköhler number of 1.7. The origin of elevated OH concentrations before 8:00 LT is discussed later in the Results and Discussion section. Besides the timescale comparison over the course of one day, a Damköhler number of around one (Da ≈ 1) indicates maximum intensity of isoprene segregation (I_s) (Ouwersloot et al., 2011; Krol et al., 2000). The derived values for Da are below one, with a tendency to be closer to one in the morning. To derive I_s, measurements with a higher time resolution than used in this study are necessary. For completeness in the following section a control case with no reduction of the reaction rate constant between isoprene, IsoO and OH is compared to a case with 30 % reduction as deduced maximally from a previous study (Butler et al., 2008; Krol et al., 2000). In that study, the deviations from chemical equilibrium were investigated by comparing a turbulence resolving large eddy simulation to a chemistry box model. Recently, Clifton et al. (2022) found a maximum I_s of 9 % for the reaction of isoprene and OH at canopy height that decreases with altitude. They combined a multilayer model for vegetation canopy coupled with in- and above-canopy chemistry and a fine scale large eddy simulation to obtain I_s. Assuming an

intensity of segregation of 30 % thus represents an extreme case that provides an upper limit for resulting OH concentrations.

2.3.3 Inferring OH

Two methods were applied to estimate OH. Both are based on the removal of isoprene by OH only (E2.3), as its reaction rate coefficient with the second most potent oxidant, O_3, is about seven orders of magnitude slower and O_3 levels are below 20 ppb. (Kuhn et al., 2007) found a contribution of O_3 to the depletion of isoprene of 1 %. The formula of the first method reads:

$$\frac{\partial\,[\mathrm{Iso}]}{\partial\,t} = -k_{\mathrm{Iso,OH}}\,[\mathrm{OH}]\,[\mathrm{Iso}] \qquad \text{(E2.3)}$$

Where $k_{\mathrm{Iso,OH}}$ = 1x10^{-10} cm molecules^{-1} s^{-1} (IUPAC) is the rate coefficient of the reaction of isoprene and OH. Solving E2.3 for OH is a simple but effective way to estimate its concentrations with the observed gradient of isoprene and the estimated reaction time. Effectively air parcels containing isoprene follow the ensemble of up- and downward motions between 80 m and 325 m for the duration approached by the derived mixing time. The isoprene concentrations at both heights were detected sequentially, but within a 15 minutes period. As the transport between the heights is expected to happen on longer timescales, the measurements conducted at 325 m have to be shifted by the respective mixing time to account for turbulent transport and mixing between the heights. This also holds for the observed *q* at 80 and 325m.

In the previous section the necessity to avoid the erroneous attribution of the dynamical driven reduction of isoprene to OH was demonstrated. Therefore, its partitioning to the isoprene gradient is considered by subtracting the relative decline of *q* or the simulated inert isoprene tracer (9.0 % or 15.4% on daily average) from the isoprene gradient. Hereafter this is referred to as the gradient method.

The second method includes the formation as well as further oxidation of IsoO (E2.4). Combining and integrating E2.3 and E2.4 gives a time dependent relation for the ratio of isoprene and IsoO that represents the progress of oxidation (Kuhn et al., 2007; Karl et al., 2007; Eerdekens et al., 2009).

$$\frac{\partial\,[\mathrm{IsoO}]}{\partial\,t} = y_{\mathrm{IsoO,OH}}\,\frac{\partial\,[\mathrm{Iso}]}{\partial\,t} - k_{\mathrm{IsoO,OH}}[\mathrm{OH}]\,[\mathrm{IsoO}] \qquad \text{(E2.4)}$$

$$\frac{[\mathrm{IsoO}]}{[\mathrm{Iso}]} = y_{\mathrm{IsoO,OH}}\,\frac{k_{\mathrm{Iso,OH}}}{k_{\mathrm{IsoO,OH}}-k_{\mathrm{Iso,OH}}}\left(1-e^{\left(k_{\mathrm{Iso,OH}}-k_{\mathrm{IsoO,OH}}\right)[\mathrm{OH}]\,t}\right) \qquad \text{(E2.5)}$$

Where $y_{\mathrm{IsoO,OH}}$ is the total yield of MVK, MACR and ISOPOOH from the oxidation of isoprene (Rivera-Rios et al., 2014) and $k_{\mathrm{IsoO,OH}}$ is the rate coefficient of IsoO + OH. The chemical partitioning of IsoO strongly depends on the availability of NO_x as MVK and MACR are formed in a second step via NO while ISOPOOH emerges from the reaction of RO_2 and HO_2 (Liu et al., 2016). At ATTO the portion of ISOPOOH depends not only on the abundance of NO but also possibly on wall exchange effects of the sticky ISOPOOH in the inlet line (< 330m) (Pagonis et al., 2017). As this potentially generates considerable uncertainty the effect of a varying ISOPOOH proportion on the resulting OH was considered by two cases of 100 % and no line loss for ISOPOOH. Assuming no line loss the proportion of ISOPOOH constitutes 50 % of the IsoO signal in accordance with (Rivera-Rios et al., 2014) for NO concentrations of 50 ppt, whereby MVK + MACR both contribute 25 %. Consequently, the weighted yield is $y_{\mathrm{IsoO,OH}}$ = 0.7 and the weighted reaction rate is

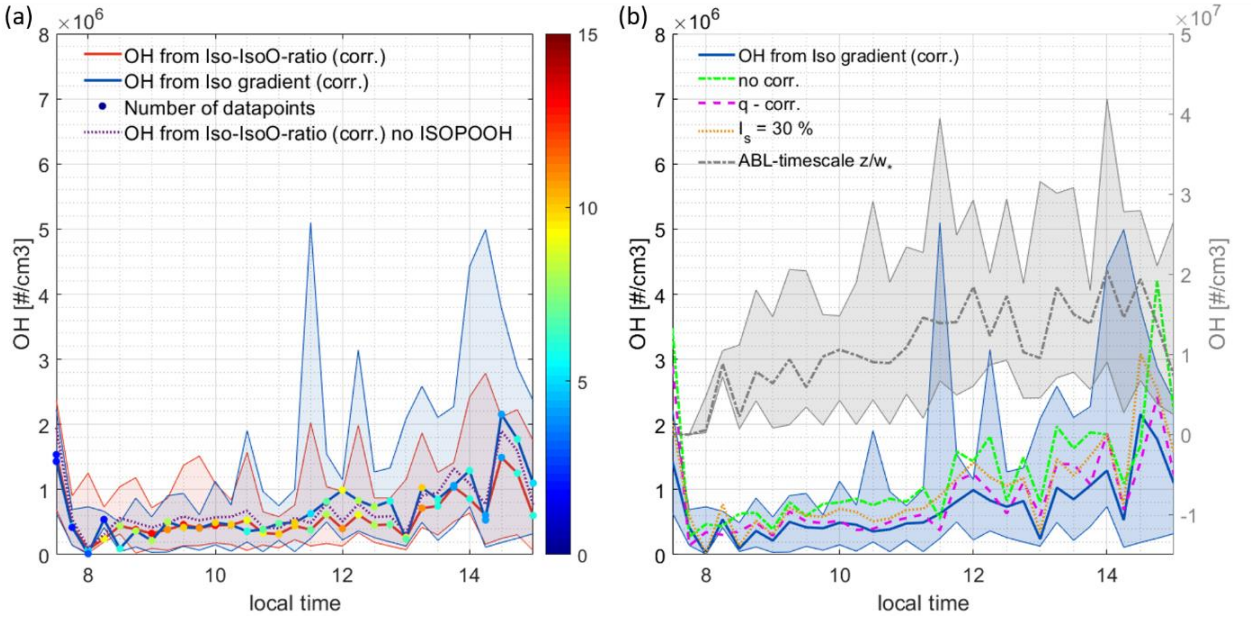

Figure 2.5: *OH concentrations inferred over the course of one day from ATTO observations. The shadings indicate the (0.15, 0.85) quantiles. a) The daily evolution of estimated OH using the gradient and ratio based method corrected for the impact of dynamics on the isoprene gradient using the inert isoprene simulated by DALES. The color code represents the number of median averaged days. The sensitivity of OH towards the composition of IsoO without ISOPOOH is shown in purple.* ***b)*** *The plot includes sensitivity of OH from the gradient method towards the Damköhler effect, the reaction time used and the correction for the effect of dynamics with inert isoprene (blue) and q (pink). OH concentrations inferred with the ABL-timescale (grey) have units on the right axis.*

$k_{\mathrm{IsoO,OH}}$ = 5.6x10^{-11} cm molecules^{-1} s^{-1}. Without considering ISOPOOH the weighted yield is $y_{\mathrm{IsoO,OH}}$ = 0.55 and $k_{\mathrm{IsoO,OH}}$ = 2.35x10^{-11} cm molecules^{-1} s^{-1}. E2.5 was then discretized and integrated with a time resolution of 1 s. By comparing the evolved time with the derived mixing time, the height can be allocated and OH is adjusted to fit the observed ratio of isoprene and IsoO at 325 m. This method is referred to as the ratio method. Here again, the isoprene concentration gradient is corrected for its reduction due to dynamical processes by subtracting the gradient of *q* or inert isoprene. A limitation of the ratio method is that dynamic processes affecting the IsoO gradient and its simultaneous formation via isoprene oxidation cannot be separated, thus cannot be corrected for. IsoO is formed most effectively when isoprene concentrations are highest, above the canopy, but mixing of IsoO in the up- and downdrafts and further formation modify the resulting gradient. Also, possible entrainment of IsoO poor air during the ABL growth may influence its gradient. In that respect it would be ideal to have observations available above the ATTO tower to account for this. Thus, it is possible that the IsoO gradient due to chemistry only may be stronger than the observed gradient, especially when turbulent mixing is strong. In conclusion, OH calculated with the ratio method can be expected to be an underestimate.

Uncertainty in both methods is implied by further factors, such as the composition of IsoO, the segregation of isoprene, turbulent transport and the reaction time in the vertical. These are addressed in Figure 2.5. The measurement uncertainty is estimated and provided in the methods section.

The OH concentrations thus derived (Fig. 2.5a) yield median average values ((0.15, 0.85) quantiles) between 8:00 and 15:00 LT of 5.3 (2.0, 12.7) x10^5 molecules cm^{-3} and 4.5 (1.6, 11.8) x10^5 molecules cm^{-3}

for the isoprene gradient-based method and the ratio-based method respectively. The enhanced OH concentrations before 8:00 LT are not considered in the average as they represent very few observations, but are discussed separately in the next section. OH derived with the first method ranges from 0.2 (0.1, 7.4) x10^5 to 2.2 (0.2, 3.8) x10^6 molecules cm^{-3} at around 14:00 LT. Here, the simulated inert isoprene was used to correct for dynamics affecting the isoprene gradient. After 11:30 the Iso-IsoO-ratio method indicates lower OH concentrations than the isoprene gradient method likely due to the limitation of the IsoO gradient with respect to mixing and entrainment. We therefore conclude that the isoprene gradient method gives more realistic OH concentrations as dynamic processes are considered for the isoprene gradient. Both methods have a large day-to-day variation due to the limited numbers of observations. It should be noted that fewer data are available in the early morning and late afternoon due to the application of the filters to ensure convective conditions.

The importance of applying the mixing time, derived by DTW, rather than the convective velocity w_* of individual updrafts becomes clear when comparing the resulting OH estimates, see Figure 2.5b. OH concentrations from the latter method exceed the OH estimate of this study 19-fold on average throughout the day with values around 1.0 (0.4, 2.0) x10^7 molecules cm^{-3}. The correction for dynamic processes with inert isoprene simulated by DALES, as described above, is greatest after 12:00 when turbulent transport is very efficient. Its OH concentrations yield 54 % of the uncorrected OH concentrations averaged over one day. Compared to the correction using q it yields 79 % of the OH throughout the day. However, OH concentrations using q or no correction are mainly found within the (0.15, 0.85) quantiles of the OH values using the inert isoprene tracer. Next, the isoprene and IsoO segregation effect on OH, when assumed to be at the upper limit of I_s = 30 %, leads to 42 % higher OH concentrations than derived with no effect of segregation but still lies within its day-to-day variation. Finally, the IsoO composition that encompasses between 0 % and 50 % ISOPOOH has a non-negligible impact on the ratio method, with OH concentrations for the case with 50 % ISOPOOH reaching 79 % of OH inferred for 0 % ISOPOOH (IsoO = 50 % MACR + 50 % MVK) (Fig. 2.5a). When taking into account all uncertainties of the gradient method, using an average correction for dynamic processes of 16.8 % derived from the inert isoprene tracer, the upper limit of the method is achieved by assuming I_s = 30 % which constitutes a rather extreme case. The upper limit of the inferred OH concentrations ranges from 0.2 (0.1, 1.1) x10^5 to 3.1 (0.3, 5.4) x10^6 molecules cm^{-3} (Fig. 2.5b).

Previous OH measurements conducted in the atmosphere-canopy interface region of forested sites or at the forest edge with little anthropogenic influence are presented in Table 2.1. They are in general agreement with the OH concentrations estimated here when considering the high isoprene and low NO conditions observed at ATTO. The OH reactivity measured at ATTO corresponds most closely with the SOAS campaign in the southeastern US, although the SOAS site had lower isoprene and higher NO abundance (Sanchez et al., 2018). SOAS reported a reactivity of up to 35 s^{-1} about 5 m above the canopy while Pfannerstill et al. (2021) measured up to 40 s^{-1} at 50 m above canopy at the ATTO site during the dry season of 2019 parallel to the observations used in this study. OH concentrations up to 2x10^6 molecules cm^{-3} measured during SOAS also agree well within the variability of the OH inferred in this study. Both the lower isoprene and higher NO is expected to enhance SOAS OH relative to ATTO, however, photolysis rates at the tropical ATTO site are higher. Another OH measurement was made in the Amazon rainforest during GoAmazon, with OH concentrations in the same range although the simulated OH reactivity was substantially smaller and the measurements were performed at ground level next to the forest (Jeong et al., 2021). Conversely, during GoAmazon concentrations of O_3, which

Table 2.1: *Overview of OH observations conducted in largely remote, forested sites. a) values taken from averaged daily cycles, b) daily mean values, c) box model simulations with MCM v3.3.1, d) mean values 10:00 – 15:00 LT, e) simulated mean values 10:00 – 15:00*

Project	Year	site	Height above ground [m]	OH measured [#/cm^3]	NO [ppt]	O_3 [ppb]	Isoprene [ppb]	OH [s^{-1}]	
PROPHET	1998/ 2008	Michigan, USA	31	1.9-3.9x10^6/ 0-3E6[a] (FAGE)	< 150[a]	30-47[a]/ 22-35[a]	1-2.5/ 0.2-2.5[a]	-	(Griffith et al., 2013; Tan et al., 2001)
GABRIEL	2005	Surinam	< 1000 (ABL)	5.6x10^6 ±1.9[b] (FAGE)	20 ±20[b]	18.5 ±4.6	2.00 ±0.76[b]	-	(Lelieveld et al., 2008)
OP3	2008	Borneo	6 (forest edge, canopy height 10m)	0-2.5x10^6 [a] (FAGE)	20-200[a]	5-15[a]	0-3[a]	5-30[a]	(Whalley et al., 2011)
CABINEX	2009	Michigan, USA	31	0-1.5 x10^6 [a] (FAGE)	< 150 [a]	22-35[a]	0.1-2[a]	2-14[a]	(Griffith et al., 2013)
SOAS	2013	Alabama, USA	15 (canopy height 9-12m)	0.2-2 x10^6 [a] (LIF) /0-2 x10^6 [a] (CIMS)	< 300[a]	15-40[a]	1-7[a]	15-33[a] (LIF) / 18-35[a] (CIMS)	(Sanchez et al., 2018)
GoAmazon	2014/ 2015	Amazonia, Brazil (T3)	2 (forest edge)	0.2-1.5 x10^6 [a] (CIMS)	0-150[a,c]	21[d]	0.5-3[a]	8.5[e]	(Jeong et al., 2021; Vilà-Guerau de Arellano et al., 2020)

is involved in OH recycling under low NO_x conditions (Lelieveld et al., 2016), exceeded the concentrations detected at ATTO, being below 0.15 ppb on average at 38 m height just above the canopy. Similar levels of OH have been observed at midlatitudes where production rates and BVOC fluxes are both lower (Rohrer and Berresheim, 2006). In the boreal forest where insolation is lower and BVOC fluxes are high the OH concentrations are correspondingly lower, but still 3-6×10^5 molecules cm^{-3} (Petäjä et al., 2009). All OH concentrations detected in forested, remote sites in the interface region of the canopy and the atmosphere would be overestimated using w_* to approximate the reaction time, whereas the mixing timescale yields comparable results. A separate study using a variability-lifetime based method to indirectly estimate OH from airborne measurements of nonmethane hydrocarbons in the first km of the ABL in Surinam reported average OH concentrations of 2x10^5 molecules cm^{-3} (Williams et al., 2000).

All previous measurements tabulated above show a diel cycle in the averaged OH concentrations with a maximum around solar noon, driven by its photolytic source. This is also observed in this study with maximum OH occurring around 14:00 LT. For the studies presented in Table 2.1 the maximum OH concentration ranges from 11:00 - 15:00 LT. Interestingly none of the previous observations reported a second OH maximum (1.4 x10^6 molecules cm^{-3}) in the morning as was the case from both methods applied in this study.

2.3.4 OH simulated using a hierarchy of models: turbulence-resolved, regional and global

Three different models were used to simulate OH radical concentrations as a function of time-of-day and height above forest, and these were compared to the OH inferred in this study. Results from the turbulence-resolving transport model DALES (50x50x20 m), a nested regional atmospheric chemistry model WRF-Chem (3x3 km, 7 layers in the first 500 m), and a global atmospheric chemistry model EMAC (208x208 km, 3 layers in the first 500 m) are shown for the dry season in Figure 2.6. In the case of DALES one typical day is simulated whereas EMAC and WRF-Chem present median average time series of the dry season in 2010 and 2018 respectively, with precipitation events being as well excluded.

Model simulations were matched with the estimated OH from the isoprene gradient method, which was deemed to be most reliable (see section "Inferring OH"). Large differences in the predicted OH concentration and its daily variability are found between models. The highest OH concentration up to $2x10^6 \pm 0.3x10^6$ molecules cm^{-3} is predicted by the global model EMAC which shows a classical diurnal evolution following the intensity of solar irradiation and photochemistry. The diurnal cycle of WRF-Chem has a similar shape exhibiting a second early morning maximum on some days at 380 m, but relatively low concentrations up to $3.6x10^5 \pm 1.8x10^5$ molecules cm^{-3} around noon. Up until about 11:30 LT WRF-Chem produces OH concentrations similar to those of the gradient method. Simulated OH by DALES shows highest values in the morning at 90 m and 330 m depending on the OH recycling efficiency. Choosing n = 1.5 from the DALES runs that were performed to test the sensitivity of the isoprene gradients towards OH, fits best the averaged empirically estimated concentrations. Though it overestimates concentrations derived before 11:30 LT and underestimates the values thereafter as it shows decreasing OH concentrations throughout the day. Looking at higher altitudes in DALES reveals a shift of the daily maximum towards noon. The two major differences between the models is the spatial resolution around the location of ATTO and the complexity of chemistry. DALES is equipped with a modest chemistry scheme (Supplementary Table 1) but high-resolution simulation (20m) of vertical turbulence; WRF-Chem uses the larger MOZART-4 gas phase chemical mechanism scheme (Emmons et al., 2010) and a medium spatial resolution, while EMAC involves the very detailed MECCA (Sander et al., 2005) chemistry scheme but has a coarse vertical and horizontal resolution.

Due to a highly parameterized vertical exchange in EMAC, local issues occur, e.g. the temperature at the canopy interface is too high so that a large amount of isoprene and other BVOC with temperature dependent emission parameterizations is emitted from surface vegetation (Guenther et al., 2006) (Supplementary Fig. 5). To overcome the mismatch, the EMAC isoprene emissions are arbitrarily reduced by about half, to avoid passing the issue on to all mechanisms involving isoprene (Pozzer et al., 2007). Figure 2.6 also includes the case of full isoprene emissions which depress the OH concentration substantially. Nevertheless, the reduced isoprene emissions are still higher compared to DALES and WRF-Chem. In Figure 2.7 the isoprene mixing ratios of the three models are compared, as well as dominant driving factors for OH like O_3 and NO. Taking them into account, high OH concentrations in EMAC are a result of high O_3 and recycling within the MECCA chemistry scheme. Elevated O_3 concentrations in EMAC are suspected to arise from a strong entrainment from above layers due to the highly parameterized vertical transport.

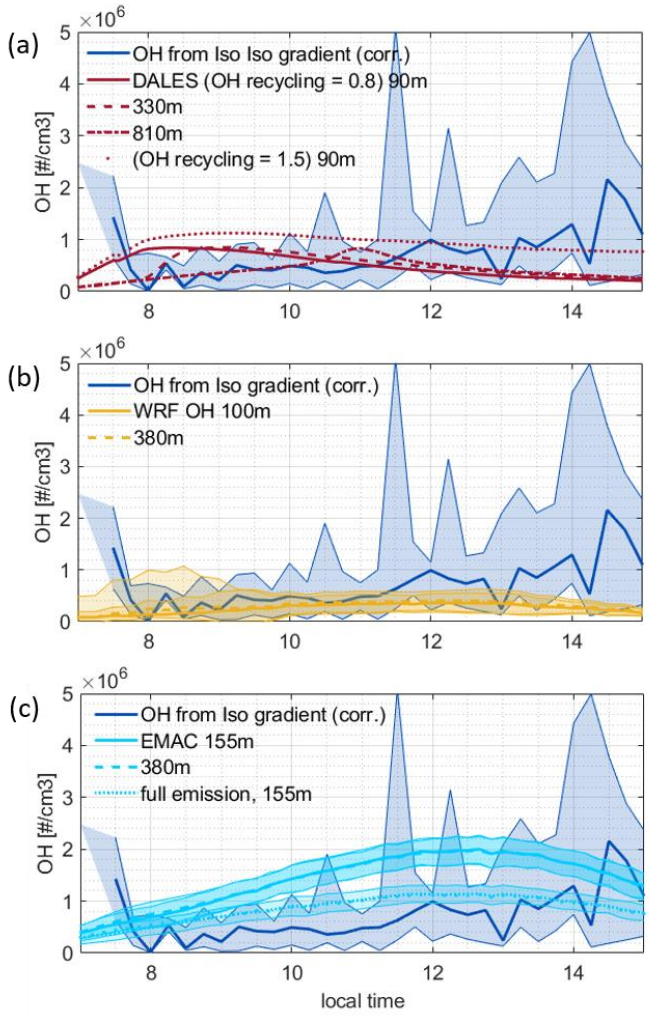

Figure 2.6: *Diurnal variability of OH time series at different heights compared to OH estimate in this study (80 – 325 m) with the gradient method. The shadings indicate the (0.15, 0.85) quantiles for inferred OH and 1 sigma for modeled concentrations. a) DALES results are obtained by including the sensitivity towards OH recycling efficiencies of 0.8 and 1.5 b) WRF-Chem c) EMAC run with halved biogenic emissions at different heights and the full emission for comparison.*

The O_3 concentrations of WRF-Chem and DALES are closer to mixing ratios observed at ATTO, but in WRF-Chem average NO is additionally very low. The standard deviation of NO from WRF-Chem is enhanced in the morning between 6:00 and 9:00 LT though, when also DALES and ATTO measurements show peaking NO from nocturnal accumulation of soil emission and subsequent ejection into the ABL during its transition to a convective layer. The reaction of HO_2 with NO to form OH (Peeters et al., 2014) leads to temporally enhanced OH concentrations between 6:00 and 9:00 LT which can be seen in the empirically inferred OH and for DALES as well as for WRF-Chem on some days. In the case of DALES this is the only maximum during the day, as the production of OH via NO is the largest source of OH over the day (Supplementary Fig. 6). The chemistry scheme of DALES does for example not include terpenes other than isoprene which are considered in the detailed chemistry schemes of WRF-Chem and EMAC, so differences in sources and sinks for OH are generated (Supplementary Fig. 7). Further investigation of the DALES

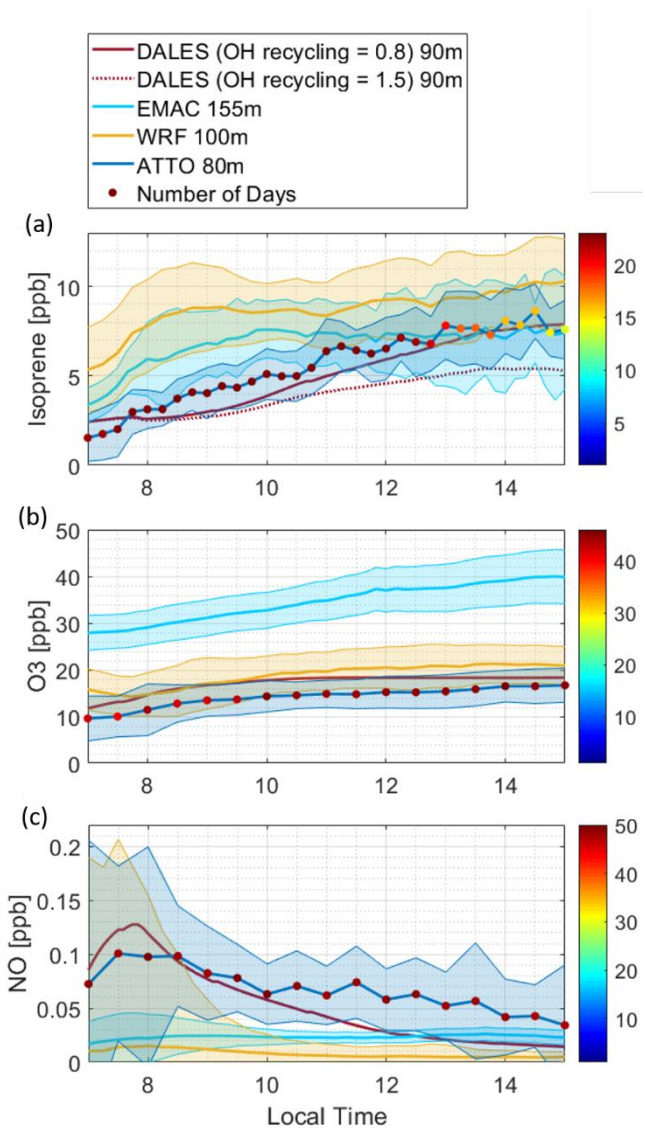

Figure 2.7: *Diurnal variability of simulated Isoprene, O_3 and NO concentration time series compared to ATTO observations under no-rain conditions. The shadings indicate the (0.15, 0.85) quantiles for observations and 1 sigma for modeled data. a) Isoprene mixing ratio measured at ATTO compared to model results. The number of days with isoprene data presented as colored marks decreases after noon as precipitation events are excluded. For DALES simulations with two different recycling efficiencies are included. b) O_3 observed and simulated c) NO observed and simulated*

simulated OH showed that the diurnal evolution and the morning peak in particular depends strongly on the initial boundary conditions of NO_x. These initial profiles depend on the chemistry and the emissions occurring in the nocturnal boundary layer and in the residual layer before sunrise. The empirical method has the advantage that entrainment of NO_x from the residual layer and formation of OH is inherently considered. Therefore, it can act to guide the large eddy simulation along with additional observations.

DALES and WRF-Chem produce elevated OH concentrations due to NO between 8:00 and 9:00, but at ATTO the OH peaks before 8:00 LT reaching 1.4 x10^6 molecules cm^{-3}. On average observations of NO in

the 2018 dry season peak at 7:00 - 9:00. However, data coverage is limited to only four days of overlapping inferred OH and NO data. These days all show enhanced NO before 8:00 LT (Supplementary Fig. 8). The elevated OH concentrations at ATTO shortly after sunrise are found on two days, which stand out because the temperature profiles indicate unstable conditions before 8:00 LT, earlier than usual, connected with long mixing times and high isoprene gradients observed (Supplementary Fig. 9). Thus, the elevated OH concentrations between 7:00 and 8:00 LT could be strongly influenced by the morning transition and the boundary layer growth if air at 325 m is still affected by the isoprene poor nocturnal stable boundary layer. This is prevented by regarding the same airmass at 80 and 325 m, ensured by the shift of 325 m isoprene concentrations according to the mixing time. High OH concentrations derived with the ratio method might also be caused by an enhanced increase of IsoO with height. Entrainment of IsoO rich air from above the ATTO tower, accumulated in the nocturnal boundary layer can not be ruled out without further measurements at higher levels. Another possible explanation is that the accumulated NO ascends together with the emitted isoprene earlier than on the other considered 21 days. To evaluate the ratio- and gradient-method during the boundary layer transition in closer detail more parallel measurements of NO and VOC will need to be acquired.

2.4 Conclusion

A novel and measurement-constrained method for the empirical estimation of the diurnal variability of OH radical abundances has been developed and applied to data obtained from the 325 m ATTO tower in the remote Amazon rainforest. In this region, high fluxes of BVOC coincide with high primary production rates of OH (Lelieveld et al., 2016), highly variable vertical mixing and low NO concentrations. Under these conditions, uncertainties regarding OH recycling mechanisms have been reported to be significant (Jeong et al., 2021; Novelli et al., 2020). Our findings show that the resulting daytime median averaged OH concentrations are characterized by peaks in the morning (short) and after solar noon (main), varying between 8:00 – 15:00 LT from 0.2 (0.1, 7.4) $x10^5$ to 2.2 (0.2, 3.8) $x10^6$ molecules cm^{-3}. OH concentrations within that part of the day are consistent with observations previously conducted at rainforest sites. The peak in the morning needs to be verified by additional simultaneous observation of NO and isoprene to infer OH concentrations during the nocturnal-diurnal transition over of a tall rainforest canopy. Furthermore, the reaction of isoprene and OH under different mixing conditions with regard to the intensity of segregation needs to be known to reduce the OH variability uncertainty in the morning.

To infer accurate OH variations over the day, we show the need to consider emission, turbulent mixing and dilution of the isoprene by entrainment to adequately quantify the partitioning of these dynamic processes and the oxidative chemistry taking place simultaneously. By introducing the DTW-derived mixing time (105 to 15 minutes) based on observations of the warming of the lower ABL, we find that the timescales of mixing are faster than isoprene chemistry but within a similar range throughout the day. The choice of the reaction time estimation has a large impact on the resulting OH concentration. Here, the assumption of using a timescale based on the convective velocity w_* inferred from individual convective updrafts needs to be revisited. The DTW derived mixing time represents the time shift due to the observed warming between two levels, driven by vertical motions and lateral mixing. The plumes of air containing isoprene and OH also undergo lateral mixing and the ensemble of turbulent motions. Accounting for these turbulent motions as a whole is crucial when analyzing measurements in the roughness sublayer or lower boundary layer. This is substantiated by the agreement of observed and

estimated OH concentrations under similar environmental conditions when applying the mixing time, whereas applying w_* yields concentrations one order of magnitude higher.

Comparing the diurnal variability of OH inferred in this study against a hierarchy of models, all characterized by different assumptions in resolving turbulent transport (explicit or parameterized), vertical and horizontal resolution and in chemical mechanisms, we find that all applied models provided very different OH concentrations and temporal patterns in the first 380 m. Greater agreement of the diurnal variability between the models was achieved above 500 m. We therefore conclude that the lower interface region characterized by a tall canopy is still difficult to model accurately, being complex in both chemistry and dynamics. The dynamical time warping method presented here has been shown to be suitable for calculating mixing times and hence OH concentrations and it can be applied when direct OH observations are lacking. In future it will be of great interest to compare our estimates to in-situ OH measurements if they can be realized at the site. Since this region governs emission export to, and oxidant levels in, the free troposphere, further measurements and numerical models that explicitly account for the canopy-atmosphere interactions are recommended to examine OH characteristics in other seasons and ecosystems.

2.5 Method

2.5.1 Observation

The observations presented here were made at the Amazon Tall Tower Observatory (ATTO), a collaborative Brazilian-German project, located 135 km north-east of Manaus (02.14°S,58.99°W, 120 m above sea level). A detailed description of the observatory including a map is published in (Andreae et al., 2015). A detailed map of the ATTO site can be found in the supplementary (Supplementary Fig. 15). The site provides close to pristine conditions with low levels of NO_x in the absence of nearby anthropogenic sources (Yáñez-Serrano et al., 2015). A Proton Transfer Reaction Time of Flight Mass Spectrometer (PTR-TOF-MS; Ionicon Analytik, Innsbruck, Austria) (Jordan et al., 2009) was installed within an air-conditioned laboratory container at the foot of the ATTO tower. Sample inlets (3/8”OD insulated Teflon) are installed from the container to 80m, 150m and 325m, so that semi-continuous measurements can be made at three heights by sequentially sampling at each height for 5 minutes. Each height is therefore sampled for 5 minutes every 15 minutes. The time resolution was 20 seconds averaged to 1 minute. The PTR-TOF-MS was operated with hydronium ions (H3O+) at a pressure of 3.5mbar and an E/N of 120 Td. VOC mixing ratios were obtained by calibrating to a VOC gas-standard (Apel-Riemer Environmental Inc., Colorado, USA). Isoprene (m/z 69.069) can be detected as low as 40 ppt, with an uncertainty of 11.6 % and a precision of 3.2 %. The oxidation products of isoprene, measured as their sum at m/z 71.049, MVK, MACR and ISOPOOH can be detected with a total uncertainty of 12.3% and 2.3 % precision down to 21 ppt. The total uncertainty includes the precision and the calibration error. Possible line loss of those compounds is in experience neglected. In this study, 23 days of data from the dry season (September and October) of 2018/2019 is used under exclusion of periods with precipitation for the use of DTW (in 2018: 10/21/2018 – 10/24/2018 and in 2019: 09/01 - 09/06, 09/08 – 09/16, 09/18, 09/19, 09/21 and 09/26). Median mixing ratios for isoprene were found to vary from 1.48 ± 0.35 ppb after sunrise up to 8.12 ± 1.92 ppb at 14:30 at 80m height averaged over the considered period. IsoO follows the daily evolution of isoprene with

median values of 1.05 ± 0.21 ppb to 4.00 ± 0.80 ppb at 80m. The mixing ratios measured represent the integrated emission of the forest biosphere, which is assumed to be uniform over the whole catchment area of ATTO (Andreae et al., 2015). Meteorological and flux data up to 80m is measured at 80 m on the Instant tower, a walk-up-tower in 1 km distance from ATTO (Andreae et al., 2015) (LI7500A, LI-COR Biotechnology, Lincoln,USA) and at a weather station at 325m installed directly on the ATTO tower (Lufft, WS600-LMB, G. Lufft Mess- und Regeltechnik GmbH, Fellbach, Germany). Both meteorological datasets are available with a 1 minute time resolution. The potential temperature has a measurement uncertainty of less than 1 % at 80m and 325m. For the period studies here, there was no meteorological data available for the altitudes in between 80m and 320m. To estimate the uncertainty of OH due to the precision of the measurement of isoprene, IsoO and ϑ, a Monte Carlo simulation is performed for the gradient and the ratio method. Samples with 10,000 normally distributed random values for each variable (isoprene, IsoO, mixing time) constrained by the median and the precision of measurement are used to calculate OH and its distribution. The uncertainty of the mixing time related to the DTW method is small, but uncertainty may arise from local anomalies that alter ϑ only on one of the two sample heights. For the purpose of demonstration, it is assumed to be 0, 5 and 10 %. We report uncertainty factors relative to the median, derived from the 15 % and 85 % quantiles since the distribution of OH concentrations is not normal. For the gradient method uncertainties of $OH_{0.59}^{0.88}$ assuming no uncertainty of the mixing time, $OH_{0.59}^{0.90}$ for 5 % uncertainty of the mixing time and $OH_{0.59}^{0.91}$ for 10 % uncertainty of the mixing time are estimated. The calculation of OH with the ratio method is computationally more demanding, thus a sample number of 2,000 is applied for the Monte Carlo simulation. It yields $OH_{0.41}^{0.50}$ for 10 % uncertainty on the mixing timescale. The OH variability with measurement uncertainty is shown in the supplementary Fig 16.

2.5.2 Atmospheric Models

The model applied is the numerical experiment, described by Vilà-Guerau de Arellano et al. (2020) based on the **Dutch Atmospheric Large-Eddy Simulation (DALES)** (Ouwersloot et al., 2017) with an integrated O_3-NO_x-VOC-HO_x chemical system. The numerical experiment is designed according to observations made during the GoAmazon campaign in September 2014 (dry season), that took place in Amazonia (Martin et al., 2016). The initial profiles of isoprene and its oxidation products are constrained by the observation regarded in this study, therefore they are set to 2 ppb and 0.2 ppb for all altitude levels respectively. Wind is calculated explicitly using Navier-Stokes simulations. Surface winds that induce mechanical turbulence and wind profiles are compared to sounding observations with good agreement (Vilà-Guerau de Arellano et al., 2020). DALES has a vertical resolution of 20 m and a horizontal resolution of 50 m so that the dimension of the ATTO tower is well represented in the model. The forest canopy is treated as a single layer. At the high of the measurements 80 m and 325 m, the coupling of vegetation and atmosphere processes, including the interaction with clouds, vegetation responses to radiation and meteorological conditions and turbulent transport during the course of the day is explicitly (not parameterized) reproduced by DALES. The large eddy simulation code and the numerical experiment settings can be accessed here: http://doi.org/10.5281/zenodo.3759193.

The Weather Research and Forecasting coupled with chemistry (WRF-Chem) (Grell et al., 2005) is a regional atmospheric chemistry model which has been extensively used in the past for several regions of the world for a variety of studies requiring high spatial and vertical resolution (Kuik et al., 2018; Teixeira et al., 2016). By setting up nested domains such that the outer-most (parent) domain is driven by a

chemical and meteorological boundary conditions of a global model or global reanalysis dataset, one can achieve spatial resolutions of up to a few km.

For the current study, WRF-Chem was set up in a nested configuration such that spatial resolution of the parent domain (d01) is 15×15 km^2 and that of the inner domain (d02) is 3×3 km^2. Vertically the setup has 42 terrain following layers from surface until 50 hPa with 3 and 10 layers in the bottom 80m and 1km, respectively. The simulation was performed for a period between 01/09/2018 and 20/10/2018. The meteorological boundary conditions were prescribed by the ERA5 reanalysis dataset (Hersbach et al., 2020) updated every 3 hours. Similarly, the chemical conditions were prescribed from the archived model output of CAM-Chem every 6 hours available from https://www.acom.ucar.edu/cam-chem/cam-chem.shtml. We also employed spectral nudging of geopotential height (ph) and U and V components of wind from ERA5 above the boundary layer height to make sure that the large scale features of the simulations don't drift away from the reanalysis dataset while allowing it to resolve the fine scale meteorological features (Gómez and Miguez-Macho, 2017).

Biogenic and soil NO_x emissions in WRF-Chem are calculated online using the MEGAN version 2.0, while the anthropogenic and fire emissions are prescribed from the EDGAR v5.0 inventory (Crippa et al., 2019) and GFAS (Kaiser et al., 2012) respectively. We used the HERMESv3 tool (Guevara et al., 2019) for mapping of the emissions inventories on the WRF-Chem horizontal grid.

The **ECHAM/MESSy Atmospheric Chemistry** (**EMAC**) is the Earth System Model with core atmospheric general circulation model ECHAM5 (Roeckner et al., 2006) coupled with the Modular Earth Submodel System (MESSy) implementing relevant (sub)grid processes (trace gas/aerosol chemistry, emission, dry/wet removal of species, etc.) in one consistent modelling framework (Jöckel et al., 2010, 2006). In the current study we use the output of the MESSy v2.54 evaluation study (Pozzer et al., 2007) performed with a model resolution T63L31 (equivalent to 1.88° or about 208 km at the ATTO location in horizontal, model top at 10 hPa or approx. 31 km). In comparison to DALES and WRF-Chem, EMAC has coarser spatial resolution (three lowermost layers span approximately 500 m with interfaces at about 70 and 250 m) and more parameterized representation of the BL dynamics and tracer transport (Ouwersloot et al., 2015), yet being equipped with the most comprehensive kinetic chemistry mechanism MOM (Lelieveld et al., 2016; Sander et al., 2019). The latter intrinsically reproduces high OH reactivities over the Amazon (Lelieveld et al., 2016) however isoprene emissions reduced by 50% of their nominal strength (calculated by the MEGAN v2.1 model (Guenther et al., 2012)) yield best agreement with the observed OH and isoprene surface concentrations globally and at ATTO (Pozzer et al., 2007). Similar to WRF-Chem, EMAC atmospheric dynamics are nudged towards the ERA5 [ref.above] reanalysis fields, the anthropogenic and fire emissions of NO_X and BVOC are calculated based on the EDGAR v4.3.2 and GFAS v1.0 inventories, respectively. Model output (grid column encircling ATTO location, no interpolation used) for September 2010 from the simulated 2008−2017 period is analysed here.

2.5.3 Dynamical Time Warping

DTW is a method to allocate common points of two differently stretched curves in order to warp one of the curves into the other (Rabiner and Juang, 2016). It was developed within the field of speech recognition in order to identify words that are the same but pronounced differently. It is, however, applicable to many forms of time-series. In a first step the daily time-series are normalized to values

between zero and one. Then a two-dimensional cross-distance-matrix $D = d(x, y)$ containing the Euclidean distance between every pair of elements is created (Supplementary Fig. 10). x and y are the time indices of each time series respectively. The goal of DTW is to find the best allocation, that is the path through the cross-distance-matrix that yields a minimal distance between elements of the time-series. The so-called warping path defines possible allocations and underlies certain constraints (Keogh and Pazzani, 2001):

1. The boundary conditions can force the warping path to start or end in the opposite diagonal corners of the cross-distance-matrix.
2. To ensure continuity the warping path must proceed continuous through the cross-distance-matrix
3. The warping path must be monotonic to avoid pointless detours and loops
4. A user defined windowing function forbids the warping path to cross the window (S9) that prevents negative mixing times $(x(i) - y(i) \geq 0)$
5. User defined step patterns can constrain the steps taken by the warping path, e.g. it must not move straight upwards, leading to a warping path with unique indices y. In this study the 'symmetric2' step pattern is used, that allows all steps that fulfil the points 1-4.

The warping path reallocates the time indices x and y according to the minimalized warping path. The result is an allocation of the data points of two timeseries, which is presented in Figure 2.2. The warping yields the relative temporal variabilities between both curves, which shows in this application how one curve is followed by the other. The last step is to calculate this time shift, here the mixing time, from the obtained allocation. The time indices correspond to the temporal resolution of the time-series, so E2.6 results in the time shift for every element of the time-series.

$$t_{mixing} = (x(i) - y(i)) * res_t \quad , i = 1 \dots n \qquad \text{(E2.6)}$$

n is the length of the array of indices. With the applied settings is possible that multiple indices $x(i)$ are allocated to one index of $y(i)$, if this is the case the average of the distances $x(i) - y(i)$ give the mixing time. The property used to derive the mixing time needs to fulfill two requirements: It must have primary (emission) source located at the level of the rainforest, and its chemical lifetime must strongly exceed the mixing time. We chose the potential temperature (ϑ) to be used to obtain the mixing time because conductive heating takes place at the ground and at canopy level leading to lateral mixing of up and downdraft turbulent motions and thus to heating of the ABL during convective conditions at daytime. ϑ is also indifferent towards chemical processing. The resulting time shift is the consequence of boundary layer warming through the mixing of heat fluxes.

Data Availability

Profile data of VOC [ppb] that support the findings of this study will be available in the ATTO Data Portal via https://doi.org/10.17871/atto.300.3.1213.

Meteorological data and products, pressure, temperature, relative humidity and z/L conducted at the Instant tower (80 m) that support the findings of this study have been deposited in the ATTO Data Portal and are accessible upon request at http://attodata.org/.

Meteorological data, pressure, temperature and relative humidity conducted at the ATTO tower (320 m) in 2019 that support the findings of this study are available via https://doi.org/10.17871/atto.95.12.742. For the year 2018 this data is deposited in the ATTO Data Portal and accessible upon request at http://attodata.org/.

Profile data of NO and O_3 [ppb] that support the findings of this study have been deposited in the ATTO Data Portal and are accessible upon request at http://attodata.org/.

Outputs from DALES, WRF-chem and EMAC that support the findings of this study are available from J. Vilà-Guerau de Arellano, V. Kumar and S. Gromov respectively upon reasonable request.

Code availability

Dynamical Time Warping (version 1.22-3) is a freely available package for R (version 3.6.1). Commented R code is attached.

Supplement

The supplementary material related to this article can be found online at https://www.nature.com/articles/s41598-023-41748-4#Sec12

Competing interests

The authors declare no competing interests.

Acknowledgements

We acknowledge the support by the German Federal Ministry of Education and Research (BMBF contract 01LB1001A and 01LK1602B) and the Brazilian Ministério da Ciência, Tecnologia e Inovação (MCTI/FINEP contract 01.11.01248.00) as well as the Amazon State University (UEA), FAPESP, CNPq, FAPEAM, LBA/INPA, and SDS/CEUC/RDS-Uatumã. We thank Thomas Klüpfel for help with VOC measurements. Especially acknowledged are the contributions for technical and logistical support by the ATTO team (in particular Reiner Ditz and Hermes Braga Xavier). We also thank Andrew Crozier for creating and providing a detailed map of the ATTO site.

Funding

Open Access funding enabled and organized by Projekt DEAL.

2.6 References

Andreae, M. O., Acevedo, O. C., Artaxo, P., Barbosa, C. G. G., Barbosa, H. M. J., Brito, J., Carbone, S., Chi, X., Cintra, B. B. L., Dias, N. L., Ditas, F., Ditz, R., Godoi, A. F. L., Godoi, R. H. M., Heimann, M., Hoffmann, T., Kesselmeier, J., Lavric, J. V, Manzi, A. O., Lopes, A. P., Martins, D. L., Mikhailov, E. F., Nelson, B. W., Nogueira, D. S., Piedade, M. T. F., Quesada, C. A., Rizzo, L. V, Ruckteschler, N., Sales, C. B., Saturno, J., Souza, C. M. De, Souza, R. A. F. De, Su, H., Targhetta, N., Trebs, I., Trumbore, S., Eijck, A. Van, Walter, D., Wang, Z., Weber, B., Williams, J., Winderlich, J., Wittmann, F., and Wolff, S.: The Amazon Tall Tower Observatory (ATTO): overview of pilot measurements on ecosystem ecology , meteorology , trace gases , and aerosols, 10723–10776, https://doi.org/10.5194/acp-15-10723-2015, 2015.

Bourtsoukidis, E., Behrendt, T., Yañez-Serrano, A. M., Hellén, H., Diamantopoulos, E., Catão, E., Ashworth, K., Pozzer, A., Quesada, C. A., Martins, D. L., Sá, M., Araujo, A., Brito, J., Artaxo, P., Kesselmeier, J., Lelieveld, J., and Williams, J.: Strong sesquiterpene emissions from Amazonian soils, Nat. Commun., 9, 1–11, https://doi.org/10.1038/s41467-018-04658-y, 2018.

Butler, T. M., Taraborrelli, D., Brühl, C., Fischer, H., Harder, H., Martinez, M., Williams, J., Lawrence, M. G., and Lelieveld, J.: Improved simulation of isoprene oxidation chemistry with the ECHAM5/MESSy chemistry-climate model: Lessons from the GABRIEL airborne field campaign, Atmospheric Chem. Phys., 8, 4529–4546, https://doi.org/10.5194/acp-8-4529-2008, 2008.

Carslaw, N., Creasey, D. J., Harrison, D., Heard, D. E., Hunter, M. C., Jacobs, P. J., Jenkin, M. E., Lee, J. D., Lewis, A. C., Pilling, M. J., Saunders, S. M., and Seakins, P. W.: OH and HO2 radical chemistry in a forested region of north-western Greece, Atmos. Environ., 35, 4725–4737, https://doi.org/10.1016/S1352-2310(01)00089-9, 2001.

Cava, D., Dias-Júnior, C. Q., Acevedo, O., Oliveira, P. E. S., Manzi, O., Araújo, A. C. De, Tsokankunku, A., Matthias, S., Brondani, D. V, Mauricio, I., Toro, C., and Mortarini, L.: Agricultural and Forest Meteorology Vertical propagation of submeso and coherent structure in a tall and dense Amazon Forest in different stability conditions PART I : Flow structure within and above the roughness sublayer, 322, https://doi.org/10.1016/j.agrformet.2022.108983, 2022.

Chamecki, M., Freire, L. S., Dias, N. L., Chen, B., Dias-Júnior, C. Q., Machado, L. A. T., Sörgel, M., Tsokankunku, A., and De Araujo, A. C.: Effects of Vegetation and Topography on the Boundary Layer Structure above the Amazon Forest, 2941–2957, https://doi.org/10.1175/JAS-D-20-0063.1, 2020.

Clifton, O. E., Patton, E. G., Wang, S., Barth, M., Orlando, J., and Schwantes, R. H.: Large Eddy Simulation for Investigating Coupled Forest Canopy and Turbulence Influences on Atmospheric Chemistry, J. Adv. Model. Earth Syst., 14, e2022MS003078, https://doi.org/10.1029/2022MS003078, 2022.

Crippa, M., Oreggioni, G., D, G., Muntean, M., Schaaf, E., Lo Vullo, E., Solazzo, E., Monforti-Ferrario, F., Olivier, J. G. J., and Vignati, E.: Fossil CO2 and GHG emissions of all world countries - 2019 Report Publications Office of the EU, JRC Science for Policy Report, 251 pp., https://doi.org/10.2760/687800, 2019.

Dias-júnior, C. Q., Dias, N. L., Maria, R., Santos, N., Sörgel, M., Araújo, A., Tsokankunku, A., Ditas, F., Santana, R. A. De, Randow, C. Von, Sá, M., and Pöhlker, C.: Is There a Classical Inertial Sublayer Over the Amazon Forest ?, 1–9, https://doi.org/10.1029/2019GL083237, 2019.

Dillon, T. J. and Crowley, J. N.: Direct detection of OH formation in the reactions of HO2 with CH3C(O)O2 and other substituted peroxy radicals, Atmospheric Chem. Phys., 8, 4877–4889, https://doi.org/10.5194/acp-8-4877-2008, 2008.

Edtbauer, A., Pfannerstill, E. Y., Pires Florentino, A. P., Barbosa, C. G. G., Rodriguez-Caballero, E., Zannoni, N., Alves, R. P., Wolff, S., Tsokankunku, A., Aptroot, A., de Oliveira Sá, M., de Araújo, A. C., Sörgel, M., de Oliveira, S. M., Weber, B., and Williams, J.: Cryptogamic organisms are a substantial source and sink for volatile organic compounds in the Amazon region, Commun. Earth Environ., 2, https://doi.org/10.1038/s43247-021-00328-y, 2021.

Eerdekens, G., Ganzefeld, L., Vilà-Guerau de Arellano, J., Klüpfel, T., Sinha, V., Yassaa, N., and Williams, J.: Physics Flux estimates of isoprene , methanol and acetone from airborne PTR-MS measurements over the tropical rainforest during the GABRIEL 2005 campaign, 4207–4227, 2009.

Emmons, L. K., Walters, S., Hess, P. G., Lamarque, J. F., Pfister, G. G., Fillmore, D., Granier, C., Guenther, A., Kinnison, D., Laepple, T., Orlando, J., Tie, X., Tyndall, G., Wiedinmyer, C., Baughcum, S. L., and Kloster, S.: Description and evaluation of the Model for Ozone and Related chemical Tracers, version 4 (MOZART-4), Geosci. Model Dev., 3, 43–67, https://doi.org/10.5194/gmd-3-43-2010, 2010.

Finnigan, J. J.: TURBULENCE IN PLANT CANOPIES, Annu Rev Fluid Mech 200032519-571, 519–571, 2000.

Fuentes, J. D., Gerken, T., Chamecki, M., Stoy, P., Freire, L., and Ruiz-Plancarte, J.: Turbulent transport and reactions of plant-emitted hydrocarbons in an Amazonian rain forest, Atmos. Environ., 279, 119094, https://doi.org/10.1016/j.atmosenv.2022.119094, 2022.

Gómez, B. and Miguez-Macho, G.: The impact of wave number selection and spin-up time in spectral nudging, Q. J. R. Meteorol. Soc., 143, 1772–1786, https://doi.org/10.1002/qj.3032, 2017.

Grell, G. A., Peckham, S. E., Schmitz, R., McKeen, S. A., Frost, G., Skamarock, W. C., and Eder, B.: Fully coupled “online” chemistry within the WRF model, Atmos. Environ., 39, 6957–6975, https://doi.org/10.1016/j.atmosenv.2005.04.027, 2005.

Griffith, S. M., Hansen, R. F., Dusanter, P. S., Alaghmand, M., B, B. S., Carroll, M. A., Galloway, M., Grossberg, N., Hottle, J., Hou, J., Jobson, B. T., Kammrath, A., Keutsch, F. N., Lefer, B. L., Mielke, L. H., O’Brian, A., Shepson, P. B., Thurlow, M., Wallace, W., Zhang, N., and Zhou, X. L.: OH and HO 2 radical chemistry during PROPHET 2008 and CABINEX 2009 – Part 1 : Measurements and model comparison, 5403–5423, https://doi.org/10.5194/acp-13-5403-2013, 2013.

Guenther, A.: Biological and Chemical Diversity of Biogenic Volatile Organic Emissions into the Atmosphere, ISRN Atmospheric Sci., 2013, 1–27, https://doi.org/10.1155/2013/786290, 2013.

Guenther, A., Karl, T., Harley, P., Wiedinmyer, C., Palmer, P. I., and Geron, C.: Estimates of global terrestrial isoprene emissions using MEGAN (Model of Emissions of Gases and Aerosols from Nature), Atmospheric Chem. Phys., 6, 3181–3210, https://doi.org/10.5194/acp-6-3181-2006, 2006.

Guenther, A. B., Jiang, X., Heald, C. L., Sakulyanontvittaya, T., Duhl, T., Emmons, L. K., and Wang, X.: The model of emissions of gases and aerosols from nature version 2.1 (MEGAN2.1): An extended and updated framework for modeling biogenic emissions, Geosci. Model Dev., 5, 1471–1492, https://doi.org/10.5194/gmd-5-1471-2012, 2012.

Guevara, M., Tena, C., Porquet, M., Jorba, O., and Pérez García-Pando, C.: HERMESv3, a stand-alone multi-scale atmospheric emission modelling framework-Part 1: Global and regional module, Geosci. Model Dev., 12, 1885–1907, https://doi.org/10.5194/gmd-12-1885-2019, 2019.

Hersbach, H., Bell, B., Berrisford, P., Hirahara, S., Horányi, A., Muñoz-Sabater, J., Nicolas, J., Peubey, C., Radu, R., Schepers, D., Simmons, A., Soci, C., Abdalla, S., Abellan, X., Balsamo, G., Bechtold, P., Biavati, G., Bidlot, J., Bonavita, M., De Chiara, G., Dahlgren, P., Dee, D., Diamantakis, M., Dragani, R., Flemming, J., Forbes, R., Fuentes, M., Geer, A., Haimberger, L., Healy, S., Hogan, R. J., Hólm, E., Janisková, M., Keeley, S., Laloyaux, P., Lopez, P., Lupu, C., Radnoti, G., de Rosnay, P., Rozum, I., Vamborg, F., Villaume, S., and Thépaut, J. N.: The ERA5 global reanalysis, Q. J. R. Meteorol. Soc., 146, 1999–2049, https://doi.org/10.1002/qj.3803, 2020.

Hofzumahaus, A., Rohrer, F., Lu, K., Bohn, B., Brauers, T., Chang, C. C., Fuchs, H., Holland, F., Kita, K., Kondo, Y., Li, X., Lou, S., Shao, M., Zeng, L., Wahner, A., and Zhang, Y.: Amplified trace gas removal in the troposphere, Science, 324, 1702–1704, https://doi.org/10.1126/science.1164566, 2009.

Jeong, D., Seco, R., Emmons, L., Schwantes, R., Liu, Y., McKinney, K. A., Martin, S. T., Keutsch, F. N., Gu, D., Guenther, A. B., Vega, O., Tota, J., Souza, R. A. F., Springston, S. R., Watson, T. B., and Kim, S.: Reconciling Observed and Predicted Tropical Rainforest OH Concentrations, J. Geophys. Res. Atmospheres, https://doi.org/10.1029/2020jd032901, 2021.

Jöckel, P., Tost, H., Pozzer, A., Brühl, C., Buchholz, J., Ganzeveld, L., Hoor, P., Kerkweg, A., and Lawrence, M. G.: and Physics The atmospheric chemistry general circulation model ECHAM5 / MESSy1 : consistent simulation of ozone from the surface to the mesosphere, 5067–5104, 2006.

Jöckel, P., Kerkweg, A., Pozzer, A., Sander, R., Tost, H., Riede, H., Baumgaertner, A., Gromov, S., and Kern, B.: Model Development Development cycle 2 of the Modular Earth Submodel System, 717–752, https://doi.org/10.5194/gmd-3-717-2010, 2010.

Jordan, A., Haidacher, S., Hanel, G., Hartungen, E., Märk, L., Seehauser, H., Schottkowsky, R., Sulzer, P., and Märk, T. D.: A high resolution and high sensitivity proton-transfer-reaction time-of-flight mass spectrometer (PTR-TOF-MS), Int. J. Mass Spectrom., 286, 122–128, https://doi.org/10.1016/j.ijms.2009.07.005, 2009.

Kaiser, J. W., Heil, A., Andreae, M. O., Benedetti, A., Chubarova, N., Jones, L., Morcrette, J. J., Razinger, M., Schultz, M. G., Suttie, M., and Van Der Werf, G. R.: Biomass burning emissions estimated with a global fire assimilation system based on observed fire radiative power, Biogeosciences, 9, 527–554, https://doi.org/10.5194/bg-9-527-2012, 2012.

Karl, T., Guenther, A., Yokelson, R. J., Greenberg, J., Potosnak, M., Blake, D. R., and Artaxo, P.: The tropical forest and fire emissions experiment : Emission , chemistry , and transport of biogenic volatile organic compounds in the lower atmosphere over Amazonia, 112, 1–17, https://doi.org/10.1029/2007JD008539, 2007.

Keogh, E. J. and Pazzani, M. J.: Derivative Dynamic Time Warping, 1–11, https://doi.org/10.1137/1.9781611972719.1, 2001.

Kesselmeier, J. and Staudt, M.: Biogenic volatile organic compounds (VOC): An overview on emission, physiology and ecology, Environ. Pollut., 109, 175, 2000.

Krol, C., Molemaker, M. J., Guerau, J. V., and Arellano, D.: photochemically active species in the convective - k2 (CO + / RH) + k • NO2, 105, 6871–6884, 2000.

Kuhn, U., Andreae, M., Ammann, C., Araujo, A., Brancaleoni, E., Ciccioli, P., Dindorf, T., and Frattoni, M.: Isoprene and monoterpene fluxes from Central Amazonian rainforest inferred from tower-based and …, Atmospheric Chem. Phys., 2855–2879, 2007.

Kuik, F., Kerschbaumer, A., Lauer, A., Lupascu, A., Von Schneidemesser, E., and Butler, T. M.: Top-down quantification of NOx emissions from traffic in an urban area using a high-resolution regional atmospheric chemistry model, Atmospheric Chem. Phys., 18, 8203–8225, https://doi.org/10.5194/acp-18-8203-2018, 2018.

Lelieveld, J., Butler, T. M., Crowley, J. N., Dillon, T. J., Fischer, H., Ganzeveld, L., Harder, H., Lawrence, M. G., Martinez, M., Taraborrelli, D., and Williams, J.: Atmospheric oxidation capacity sustained by a tropical forest, Nature, 452, 737–740, https://doi.org/10.1038/nature06870, 2008.

Lelieveld, J., Gromov, S., Pozzer, A., and Taraborrelli, D.: Global tropospheric hydroxyl distribution, budget and reactivity, Atmospheric Chem. Phys., 16, 12477–12493, https://doi.org/10.5194/acp-16-12477-2016, 2016.

Levy, H.: Normal atmosphere: Large radical and formaldehyde concentrations predicted, Science, 173, 141–143, https://doi.org/10.1126/science.173.3992.141, 1971.

Liu, Y., Brito, J., Dorris, M. R., Rivera-Rios, J. C., Seco, R., Bates, K. H., Artaxo, P., Duvoisin, S., Keutsch, F. N., Kim, S., Goldstein, A. H., Guenther, A. B., Manzi, A. O., Souza, R. A. F., Springston, S. R., Watson, T. B., McKinney, K. A., and

Martin, S. T.: Isoprene photochemistry over the Amazon rainforest, Proc. Natl. Acad. Sci. U. S. A., 113, 6125–6130, https://doi.org/10.1073/pnas.1524136113, 2016.

Mao, J., Ren, X., Zhang, L., Van Duin, D. M., Cohen, R. C., Park, J. H., Goldstein, A. H., Paulot, F., Beaver, M. R., Crounse, J. D., Wennberg, P. O., Digangi, J. P., Henry, S. B., Keutsch, F. N., Park, C., Schade, G. W., Wolfe, G. M., Thornton, J. A., and Brune, W. H.: Insights into hydroxyl measurements and atmospheric oxidation in a California forest, Atmospheric Chem. Phys., 12, 8009–8020, https://doi.org/10.5194/acp-12-8009-2012, 2012.

Martin, S. T., Artaxo, P., MacHado, L. A. T., Manzi, A. O., Souza, R. A. F., Schumacher, C., Wang, J., Andreae, M. O., Barbosa, H. M. J., Fan, J., Fisch, G., Goldstein, A. H., Guenther, A., Jimenez, J. L., Pöschl, U., Silva Dias, M. A., Smith, J. N., and Wendisch, M.: Introduction: Observations and Modeling of the Green Ocean Amazon (GoAmazon2014/5), Atmospheric Chem. Phys., 16, 4785–4797, https://doi.org/10.5194/acp-16-4785-2016, 2016.

Montzka, S. A., Krol, M., Dlugokencky, E., Hall, B., and Jo, P.: Small Interannual Variability of, Science, 331, 67–69, 2011.

Nölscher, A. C., Butler, T., Auld, J., Veres, P., Muñoz, A., Taraborrelli, D., Vereecken, L., Lelieveld, J., and Williams, J.: Using total OH reactivity to assess isoprene photooxidation via measurement and model, Atmos. Environ., 89, 453–463, https://doi.org/10.1016/j.atmosenv.2014.02.024, 2014.

Novelli, A., Vereecken, L., Bohn, B., Dorn, H., Gkatzelis, G. I., Hofzumahaus, A., Holland, F., Reimer, D., Rohrer, F., Rosanka, S., Taraborrelli, D., Tillmann, R., Wegener, R., Yu, Z., Kiendler-scharr, A., Wahner, A., and Fuchs, H.: Importance of isomerization reactions for OH radical regeneration from the photo-oxidation of isoprene investigated in the atmospheric simulation chamber SAPHIR, 3333–3355, 2020.

Ouwersloot, H. G., Vilà-Guerau De Arellano, J., Van Heerwaarden, C. C., Ganzeveld, L. N., Krol, M. C., and Lelieveld, J.: On the segregation of chemical species in a clear boundary layer over heterogeneous land surfaces, Atmospheric Chem. Phys., 11, 10681–10704, https://doi.org/10.5194/acp-11-10681-2011, 2011.

Ouwersloot, H. G., Pozzer, A., Steil, B., Tost, H., and Lelieveld, J.: Revision of the convective transport module CVTRANS 2.4 in the EMAC atmospheric chemistry-climate model, Geosci. Model Dev., 8, 2435–2445, https://doi.org/10.5194/gmd-8-2435-2015, 2015.

Ouwersloot, H. G., Moene, A. F., Attema, J. J., and Vilà-Guerau de Arellano, J.: Large-Eddy Simulation Comparison of Neutral Flow Over a Canopy : Sensitivities to Physical and Numerical Conditions , and Similarity to Other Representations, Bound.-Layer Meteorol., 162, 71–89, https://doi.org/10.1007/s10546-016-0182-5, 2017.

Pagonis, D., Krechmer, J. E., De Gouw, J., Jimenez, J. L., and Ziemann, P. J.: Effects of gas-wall partitioning in Teflon tubing and instrumentation on time-resolved measurements of gas-phase organic compounds, Atmospheric Meas. Tech., 10, 4687–4696, https://doi.org/10.5194/amt-10-4687-2017, 2017.

Peeters, J., Müller, J. F., Stavrakou, T., and Nguyen, V. S.: Hydroxyl radical recycling in isoprene oxidation driven by hydrogen bonding and hydrogen tunneling: The upgraded LIM1 mechanism, J. Phys. Chem. A, 118, 8625–8643, https://doi.org/10.1021/jp5033146, 2014.

Petäjä, T., Mauldin, R. L., Kosciuch, E., McGrath, J., Nieminen, T., Paasonen, P., Boy, M., Adamov, A., Kotiaho, T., and Kulmala, M.: Sulfuric acid and OH concentrations in a boreal forest site, Atmospheric Chem. Phys., 9, 7435–7448, https://doi.org/10.5194/acp-9-7435-2009, 2009.

Pfannerstill, E. Y., Reijrink, N. G., Edtbauer, A., Ringsdorf, A., Zannoni, N., Araújo, A., Ditas, F., Holanda, B. A., Sá, M. O., Tsokankunku, A., Walter, D., Wolff, S., Lavri, J. V., Pöhlker, C., Sörgel, M., and Williams, J.: Total OH reactivity over the

Amazon rainforest: Variability with temperature, wind, rain, altitude, time of day, season, and an overall budget closure, Atmospheric Chem. Phys., 21, 6231–6256, https://doi.org/10.5194/acp-21-6231-2021, 2021.

Pozzer, A., Jöckel, P., Tost, H., Sander, R., Ganzeveld, L., Kerkweg, A., and Lelieveld, J.: Simulating organic species with the global atmospheric chemistry general circulation model ECHAM5/MESSy1: A comparison of model results with observations, Atmospheric Chem. Phys., 7, 2527–2550, https://doi.org/10.5194/acp-7-2527-2007, 2007.

Pugh, T. A. M., MacKenzie, A. R., Hewitt, C. N., Langford, B., Edwards, P. M., Furneaux, K. L., Heard, D. E., Hopkins, J. R., Jones, C. E., Karunaharan, A., Lee, J., Mills, G., Misztal, P., Moller, S., Monks, P. S., and Whalley, L. K.: Simulating atmospheric composition over a South-East Asian tropical rainforest: Performance of a chemistry box model, Atmospheric Chem. Phys., 10, 279–298, https://doi.org/10.5194/acp-10-279-2010, 2010.

Rabiner, L. and Juang, B.-H.: Fundamentals of speech recognition, https://doi.org/10.1016/b978-0-12-802398-3.00002-7, 2016.

Rinne, J., Markkanen, T., Ruuskanen, T. M., Petäjä, T., Keronen, P., Tang, M. J., Crowley, J. N., Rannik, Ü., and Vesala, T.: Effect of chemical degradation on fluxes of reactive compounds - A study with a stochastic Lagrangian transport model, Atmospheric Chem. Phys., 12, 4843–4854, https://doi.org/10.5194/acp-12-4843-2012, 2012.

Rivera-Rios, J. C., Nguyen, T. B., Crounse, J. D., Jud, W., St. Clair, J. M., Mikoviny, T., Gilman, J. B., Lerner, B. M., Kaiser, J. B., De Gouw, J., Wisthaler, A., Hansel, A., Wennberg, P. O., Seinfeld, J. H., and Keutsch, F. N.: Conversion of hydroperoxides to carbonyls in field and laboratory instrumentation: Observational bias in diagnosing pristine versus anthropogenically controlled atmospheric chemistry, Geophys. Res. Lett., 41, 8645–8651, https://doi.org/10.1002/2014GL061919, 2014.

Roeckner, E., Brokopf, R., Esch, M., Giorgetta, M. A., Hagemann, S., Kornblueh, L., Manzini, E., Schlese, U., and Schulzweida, U.: Sensitivity of simulated climate to horizontal and vertical resolution in the ECHAM5 atmosphere model, J. Clim., 19, 3771–3791, https://doi.org/10.1175/JCLI3824.1, 2006.

Rohrer, F. and Berresheim, H.: Strong correlation between levels of tropospheric hydroxyl radicals and solar ultraviolet radiation, 442, 1–4, https://doi.org/10.1038/nature04924, 2006.

Sanchez, D., Jeong, D., Seco, R., Wrangham, I., Park, J. H., Brune, W. H., Koss, A., Gilman, J., de Gouw, J., Misztal, P., Goldstein, A., Baumann, K., Wennberg, P. O., Keutsch, F. N., Guenther, A., and Kim, S.: Intercomparison of OH and OH reactivity measurements in a high isoprene and low NO environment during the Southern Oxidant and Aerosol Study (SOAS), Atmos. Environ., 174, 227–236, https://doi.org/10.1016/j.atmosenv.2017.10.056, 2018.

Sander, R., Kerkweg, A., Jöckel, P., and Lelieveld, J.: Technical note: The new comprehensive atmospheric chemistry module MECCA, Atmospheric Chem. Phys., 5, 445–450, https://doi.org/10.5194/acp-5-445-2005, 2005.

Sander, R., Baumgaertner, A., Cabrera-perez, D., Frank, F., Gromov, S., Grooß, J. U., Harder, H., Huijen, V., Jöckel, P., Karydis, V. A., Niemeyer, K. E., Pozzer, A., Riede, H., Schultz, M. G., Taraborrelli, D., and Tauer, S.: The community atmospheric chemistry box model, 1365–1385, 2019.

Sodemann, H.: Beyond turnover time: Constraining the lifetime distribution of water vapor from simple and complex approaches, J. Atmospheric Sci., 77, 413–433, https://doi.org/10.1175/JAS-D-18-0336.1, 2020.

Stone, D., Evans, M. J., Commane, R., Ingham, T., Floquet, C. F. A., McQuaid, J. B., Brookes, D. M., Monks, P. S., Purvis, R., Hamilton, J. F., Hopkins, J., Lee, J., Lewis, A. C., Stewart, D., Murphy, J. G., Mills, G., Oram, D., Reeves, C. E., and Heard, D. E.: HOx observations over West Africa during AMMA: Impact of isoprene and NOx, Atmospheric Chem. Phys., 10, 9415–9429, https://doi.org/10.5194/acp-10-9415-2010, 2010.

Stull, R. B.: An Introduction to Boundary Layer Meteorology, Springer Science & Business Media, 692 pp., 1988.

Tan, D., Faloona, I., Simpas, J. B., Brune, W., Shepson, P. B., Couch, T. L., Sumner, A. L., Carroll, M. A., Thornberry, T., Apel, E., Riemer, D., and Stockwell, W.: HOx budgets in a deciduous forest: Results from the PROPHET summer 1998 campaign, J. Geophys. Res. Atmospheres, 106, 24407–24427, https://doi.org/10.1029/2001JD900016, 2001.

Taraborrelli, D., Lawrence, M. G., Crowley, J. N., Dillon, T. J., Gromov, S., Groß, C. B. M., Vereecken, L., and Lelieveld, J.: Hydroxyl radical buffered by isoprene oxidation over tropical forests, Nat. Geosci., 5, 190–193, https://doi.org/10.1038/ngeo1405, 2012.

Teixeira, J. C., Carvalho, A. C., Tuccella, P., Curci, G., and Rocha, A.: WRF-chem sensitivity to vertical resolution during a saharan dust event, Phys. Chem. Earth, 94, 188–195, https://doi.org/10.1016/j.pce.2015.04.002, 2016.

Vilà Guerau De Arellano, J., Patton, E. G., Karl, T., Van Den Dries, K., Barth, M. C., and Orlando, J. J.: The role of boundary layer dynamics on the diurnal evolution of isoprene and the hydroxyl radical over tropical forests, J. Geophys. Res. Atmospheres, 116, 1–16, https://doi.org/10.1029/2010JD014857, 2011.

Vilà-Guerau De Arellano, J., Van Heerwaarden, C. C., Van Stratum, B. J. H., and Van Den Dries, K.: Atmospheric boundary layer: Integrating air chemistry and land interactions, 1–265 pp., 2015.

Vilà-Guerau de Arellano, J., Wang, X., Pedruzo-Bagazgoitia, X., Sikma, M., Agustí-Panareda, A., Boussetta, S., Balsamo, G., Machado, L. A. T., Biscaro, T., Gentine, P., Martin, S. T., Fuentes, J. D., and Gerken, T.: Interactions Between the Amazonian Rainforest and Cumuli Clouds: A Large-Eddy Simulation, High-Resolution ECMWF, and Observational Intercomparison Study, J. Adv. Model. Earth Syst., 12, 1–33, https://doi.org/10.1029/2019MS001828, 2020.

Wells, K. C., Millet, D. B., Payne, V. H., Deventer, M. J., Bates, K. H., de Gouw, J. A., Graus, M., Warneke, C., Wisthaler, A., and Fuentes, J. D.: Satellite isoprene retrievals constrain emissions and atmospheric oxidation, Nature, 585, 225–233, https://doi.org/10.1038/s41586-020-2664-3, 2020.

Whalley, L. K., Edwards, P. M., Furneaux, K. L., Goddard, A., Ingham, T., Evans, M. J., Stone, D., Hopkins, J. R., Jones, C. E., Karunaharan, A., Lee, J. D., Lewis, A. C., Monks, P. S., Moller, S. J., and Heard, D. E.: Quantifying the magnitude of a missing hydroxyl radical source in a tropical rainforest, Atmospheric Chem. Phys., 11, 7223–7233, https://doi.org/10.5194/acp-11-7223-2011, 2011.

Williams, J., Fischer, H., Harris, G. W., Crutzen, P. J., Hoor, P., Hansel, A., Holzingcr, R., Lindinger, W., Scheeren, B., and Lelieveld, J.: Variability-lifetime relationship for organic trace gases: A novel aid to compound identification and estimation of HO concentrations, 105, 2000.

Yáñez-Serrano, A. M., Nölscher, A. C., Williams, J., Wolff, S., Alves, E., Martins, G. A., and Bourtsoukidis, E.: Diel and seasonal changes of biogenic volatile organic compounds within and above an Amazonian rainforest, 3359–3378, https://doi.org/10.5194/acp-15-3359-2015, 2015.

Chapter 3

Investigating carbonyl compounds using PTR-ToF-MS with NO^+ chemical ionization

3.1 Abstract

The photochemistry of carbonyl compounds significantly affects tropospheric chemical composition by altering the local oxidative capacity, free radical abundance in the upper troposphere, and formation of ozone, PAN and secondary organic aerosol particles. Carbonyl compounds can be emitted directly from the biosphere into the atmosphere or formed through photochemical degradation of a variety of precursor compounds. Aldehydes have atmospheric lifetimes of hours to days, in contrast to ketones, which linger for days to several weeks. While standard operating conditions for proton transfer time-of-flight mass spectrometer (PTR-ToF-MS) using H_3O^+ ions are unable to separate aldehydes and ketones, the operation using NO^+ reagent ions allows for the differential detection of isomeric carbonyl compounds with a high time resolution. Here we study the temporal (24 h) and vertical (80-325 m) variability of individual carbonyl compounds in the Amazon rainforest atmosphere with respect to their rainforest-specific sources and sinks. Strong sources within or just above the rainforest canopy were found for the ketones (acetone, MEK, and C_5-ketones). A common feature of the carbonyls was nocturnal deposition observed by loss rates, most likely since oxidized volatile organic compounds are rapidly metabolized and utilized by the biosphere. With NO^+ chemical ionization we show that the dominant carbonyl species include acetone and propanal, which are present at a ratio of 1:10 in the wet-to-dry transition and 1:20 in the dry season.

3.2 Introduction

On a global scale, tropical forests are regarded as the largest source of biogenic volatile organic compounds (BVOC) to the atmosphere (Guenther, 2013). However, in view of the high biodiversity and plant species related emission quality, the ecosystem composition and development needs to be considered as clearly demonstrated by Ciccioli et al. (2023). BVOC comprises multiple compound classes including terpenes, alkenes, alkanes, alcohols, acids, esters, halocarbons, and carbonyls, all emitted due to various physiological processes and as a function of environmental conditions. Most of the carbon released as BVOC from the tropical rainforest is in the form of terpenes, including the hemiterpene isoprene (C_5H_8) (Yáñez-Serrano et al., 2015), monoterpenes such as alpha-pinene ($C_{10}H_{16}$) (Zannoni et al., 2020b), and sesquiterpenes such as copaene ($C_{15}H_{24}$) (Yee et al., 2020). In addition, considerable amounts of oxygenated VOC (OVOC) are known to be present in rainforest air, with carbonyl compounds, namely aldehydes and ketones containing the C=O functional group, as an important subset of the atmospheric OVOC (Kesselmeier and Staudt, 1999). Direct biogenic emission, biomass burning, and secondary formation, mainly from the oxidation of the aforementioned terpene precursors and photolysis of larger carbonyls, all contribute to the cocktail of carbonyl compounds in the atmosphere (Guenther, 2013; Mellouki et al., 2015; Liu et al., 2022). To understand such a cocktail, deposition and uptake by vegetation i.e. bidirectional exchange, should always be considered as potential players (Kesselmeier, 2001; Kesselmeier et al., 1997; Villanueva et al., 2014). Carbonyl species form after VOC oxidation is initiated by hydroxyl radical (OH), ozone (O_3), or at nighttime by the nitrate radical (NO_3), and the resulting peroxy radicals (RO_2) react either with NO (when present) or with other ambient RO_2 radicals. Under the presence of NO this oxidation chain results in a net production of O_3, an important radiatively active oxidant in the Amazon and worldwide (Mellouki et al., 2015; Trebs et al., 2012).

The main atmospheric carbonyl sinks are photolysis and oxidation by OH (Atkinson and Arey, 2003). As a consequence, the reactions with carbonyls combined with those of other BVOC control the availability of OH and thus the oxidative capacity of the atmosphere (Lelieveld et al., 2016). In Amazon rainforest air, OVOC contribute 22-40 % to the OH reactivity, namely the overall loss frequency of OH radicals (Pfannerstill et al., 2021). For unsaturated carbonyls, like the isoprene oxidation products methacrolein (MACR) and methyl vinyl ketone (MVK) oxidation by O_3 is also possible. Ketones, such as acetone, react much less readily with OH than aldehydes and have accordingly longer atmospheric lifetimes. Thus they are sustained during long-range transport and convective lifting to high altitudes, whereas more reactive aldehydes impact the chemistry more locally. However, through rapid, deep convection, a frequent phenomenon in the humid and hot tropics, carbonyls can be transported to altitudes between 10 and 17 km (Prather and Jacob, 1997).

Oxidation of aldehydes and photolysis of ketones and dicarbonyls and further reaction with NO_x (NO + NO_2) yields peroxycarboxylic nitric anhydride (PAN). PAN and other peroxynitrates are thermally unstable near the surface but in the cooler mid and upper troposphere PAN is the most abundant reservoir for nitrogen oxides, being transported over long distances (Mellouki et al., 2015; Fischer et al., 2014; Singh et al., 1990; Roberts, J. M, 2007). The main precursors of PAN are acetaldehyde, followed by more minor contributions from methylglyoxal (not reported here) and acetone (Fischer et al., 2014). Sources of NO_x in the tropical atmosphere are a composite of several processes, starting with microbial activities in soils and the release of NO, which is rapidly oxidized to NO_2, a large fraction even before it escapes the canopy. NO_2 can be taken up by the vegetation, and here again only a part of this molecule is passing the canopy to the atmosphere above (Breuninger et al., 2013; Rummel et al., 2002; Chaparro-Suarez et al., 2011). Further sources are lightning discharges, and biomass burning, the latter having the strongest seasonal variability (Bond et al., 2002). The photochemical degradation of carbonyls in the atmosphere is also a source of HO_x (HO_2 + OH) radicals, particularly important in the upper troposphere where OH radical production from carbonyls can exceed primary production in areas impacted by convection (Liu et al., 2022; Lary and Shallcross, 2000; Prather and Jacob, 1997). Furthermore, the abundance of radicals and oxidation products of carbonyls and dicarbonyls can promote the formation and growth of secondary organic aerosols (Liu et al., 2022).

In this study, the observed diel and vertical (80-325 m) variability of 15 carbonyl species (C_2-C_9) was investigated. They were detected online with a PTR-ToF-MS using NO^+ as a reagent ion. This technique enables the separation of isomeric aldehydes and ketones to identify their partitioning in the Amazonian atmospheric boundary layer (ABL) at the ATTO site. Previous measurements of carbonyls have been conducted over the rainforest using PTR-MS with H_3O^+ as the reagent ion. With this method, both, aldehyde and ketone carbonyl forms are detected at the same mass. Usually, for airborne measurements, atmospheric chemists have argued that the m/z used for the detection of C_3 carbonyls can be interpreted as predominantly acetone since its atmospheric lifetime is relatively long (Williams et al., 2001). However, if the data is used to extract further information about the environment, such as OH concentrations (Williams et al., 2000), the validity of this assumption should be verified.

The dataset presented here is the first online measurement of speciated individual aldehydes and ketones in the Amazon. This rainforest environment is characterized by high solar insolation and vigorous vertical transport by deep convection. We aim to quantify the relative abundance of carbonyl species and to

improve the understanding of their emissions, secondary formation in the atmosphere, transformation, and deposition.

3.3 Experimental

3.3.1 Measurement site and instrumentation

All measurements were conducted at the Amazon Tall Tower Observatory (ATTO) within the primary tropical rainforest of Brazil. The site is located at 135 km NE of Manaus (02.14°S,58.99°W, 120 m above sea level) with the main wind direction being NE to SE (Fig. S 3.1 at the end of this chapter). In the wet season (February-May) the air is typically nearly pristine since the airmasses pass over more than 1000 km of mostly untouched rainforest before being sampled. This is reflected by low concentrations of NO_x of less than 150 ppt in the ABL. In the dry season (August-November), however, biomass burning influenced air caused by human activities was sampled at the site, and enhanced black carbon concentrations were observed due to the hemispheric wide summer maximum in biomass burning. The site is equipped with a 325 m tall tower and an 80 m walk-up tower, among other measurement and accommodation facilities. A detailed map can be found in the supplement (Fig. S 3.2 at the end of this chapter). The canopy height of the surrounding forest is about 35 m (Kuhn et al., 2007). A comprehensive description of the site is provided by Andreae et al. (2015). The measurements were conducted from 23 June until 8 July and from 27 September until 14 October 2019.

The sampling inlets for the BVOC measurements are located at 80, 150, and 325 m on the tall tower. Air is drawn by high-volume pumps down to the instrumentation that is stored in an airconditioned container at the foot of the tower. By sequentially sampling each height for 5 minutes, a semi-continuous measurement can be achieved, so that each height is sampled four times per hour. The flow in the insulated and heated (40°C) Teflon sampling lines (3/8”OD) is about 10 l min^{-1}. A long inlet line can be compared to a gas chromatographic column, which retains the sampled VOC depending on their volatility and polarity, expressed by a wall saturation concentration (Pagonis et al., 2017). Adsorption to the inner walls of the Teflon line caused a response time of 90 seconds at ATTO using a VOC gas standard. Before the actual sampling of each height, the line was therefore flushed with ambient air to achieve saturation. Some less volatile molecules, like sesquiterpenes never reached equilibrium and were potentially degraded by O_3, thus they were not detected. Tests with a 400 m inlet line in China have also shown that the carbonyl compounds investigated in this study have high saturation concentrations (C*, which is inversely proportional to the wall partitioning) and are not affected by line loss (Li et al., 2023; Deming et al., 2019), but line effects such as a broadening of initially sharp concentration peaks cannot be excluded. It has to be noted that sharp concentration peaks or spikes of short duration (< 90 s) were not expected high above the homogenous vegetation of the rainforest. VOC were measured by a Proton Transfer Reaction Time of Flight Mass Spectrometer (PTR-ToF-MS 4000, Ionicon Analytik, Innsbruck, Austria) (Jordan et al., 2009) with a time resolution of 20 seconds.

Meteorological data was measured at the walk-up tower at multiple heights up to 80 m (LI7500A, LI-COR Biotechnology, Lincoln, USA) and at the tall tower at 325 m (Lufft, WS600-LMB, G. Lufft Mess- und Regeltechnik GmbH, Fellbach, Germany) with a time resolution of 1 minute.

3.3.2 NO^+ chemical ionisation

PTR-ToF-MS in general is a form of chemical ion mass spectrometry (CIMS) commonly operated with hydronium ions (H_3O^+) to chemically ionize VOC in air samples. This is a well-established and sensitive technique that is able to detect most of the prominent VOC in ambient air with a high time resolution of Fseconds (de Gouw and Warneke, 2007). The proton transfer reaction that lends its name to the instrument occurs between H_3O^+ ions and the molecules R with a higher proton affinity than water (> 691 kJ mol^{-1}) (Hunter and Lias, 1998).

$$R + H_3O^+ \longrightarrow RH^+ + H_2O \qquad (3.1)$$

Thus, isomeric molecules (such as acetone and propanal) form the same product ion RH^+ and cannot be distinguished. For the purpose of investigating the atmospheric chemistry of carbonyl compounds, this is a major disadvantage since the distribution between short-lived aldehydes and longer-lived ketones with the same carbon number remains unclear. However, it has been shown that by using an alternative reagent ion (i.e. NO^+), aldehydes and ketones can be distinguished. NO^+ ionizes aldehydes mainly via hydride abstraction (Reaction 3.2) whereas ketones and NO+ tend to form a cluster (Reaction 3.3) leading to different product ions (Koss et al., 2016; Španěl et al., 1997).

$$R + NO^+ \longrightarrow (R\text{-}H)^+ + HNO \qquad (3.2)$$

$$R + NO^+ \longrightarrow (RNO)^+ \qquad (3.3)$$

To implement the NO^+ chemical ionization mass spectrometer (NO^+ CIMS) synthetic air instead of water vapor was introduced in the ion source and the source parameters were tuned to achieve a low contribution of impurity ions (H_3O^+, O_2^+, NO_2^+) and high counts of NO^+. Which reaction occurs to ionize the target compound depends on the thermodynamical properties of the molecule. The hydride ion affinity of aldehydes is less than that of NO^+, so reaction 3.2 is exothermic and favored (Karl et al., 2012; Španěl et al., 1997). Ketones do not show the same tendency to donate a hydrogen atom and the ionization energies of most, especially small ketones is slightly higher than that of NO (> 9.26 eV) (Smith et al., 2003). Thus, an association reaction, reaction 3.3, primarily occurs for the ketones in this study. Due to the humid conditions in the rainforest, $NO^+(H_2O)$-clusters were also available to react with ketones via ligand switching, producing the same products as the association reaction 3.3 (Smith et al., 2003). The ionization energies of 3-hexanone, 2-heptanone, and 2-nonanone are smaller or equal than that of NO, nevertheless the association reaction has been shown to be favored by selected ion flow tube (SIFT) studies (Španěl et al., 1997). Those compounds were, however, not detected in the mass spectra obtained in the rainforest environment examined in this study.

Besides the most favored reaction, other ionization channels can also produce product ions. This and partial fragmentation in the drift tube can lead to additional complications of the mass spectra. To test the distribution of product ions and fragments for the carbonyls for the type of instrument used in this study, a single-compound headspace analysis was performed in the laboratory using a PTR-ToF-MS 8000. The basic components of the instrument, mainly the ion source, drift tube, and detector are similar to a PTR-ToF-MS 4000 so that the relative transmission can be assumed identical. The instrument was tuned to have the same E/N (electric field intensity divided by gas number density) in the drift tube and similar impurities (≤ 5 %) as the instrument in the field. In both, field and laboratory, two different settings for the E/N values were applied. One setting had a relatively low E/N of 70 Td, recommended by previous

studies to minimize fragmentation (Koss et al., 2016; Romano and Hanna, 2018), the other was operated with 120 Td for comparison. The results of the single-compound headspace analysis can be found at the end of this chapter (Table S 3.1).

The complexity of the mass spectra measured with a NO^+ CIMS is a disadvantage if one aims for a non-targeted analysis of VOC present in a certain environment, such as the rainforest. Long-term VOC observations at ATTO are therefore conducted with a PTR-ToF-MS using H_3O^+ ions. However, for a targeted analysis, specifically for separating carbonyl compounds, the NO^+ CIMS is a convenient method (Koss et al., 2016; Karl et al., 2012; Ernle et al., 2023). Another advantage of the NO^+ chemistry is the ability to detect certain alkanes, as their proton affinity is too low to be detected by a PTR-MS (Koss et al., 2016). This has been widely used in urban or rural areas to quantify vehicle emissions but such species have not yet been investigated at the ATTO rainforest site (Wang et al., 2020a; Chen et al., 2022).

3.3.3 VOC data analysis

Integration of the mass spectra, baseline, and duty-cycle correction were performed using the IDA software (Ionicon Analytik). In a subsequent step, the obtained signals were normalized to NO^+ and H_2ONO^+ and drift parameters like pressure and temperature, to account for fluctuations.

Table 3.1 shows the sensitivities and limits of detection (LoD) for all target molecules with E/N values of 70 and 120 Td applied. It is obvious that the sensitivity of ketones decreases dramatically with high E/N conditions, most probably due to enhanced fragmentation caused by more collisions in the drift tube.

Compounds displayed in bold in Table 3.1 were quantified using a primary VOC gas-standard (Apel-Riemer Environmental Inc., Colorado, USA). Unfortunately, this did not comprise all target carbonyls, and for those compounds not in the standard, a theoretical method was applied to obtain concentrations, albeit with a higher uncertainty. The relative distribution of the product ions obtained from the single-compound headspace analysis was used to correct for the fragmentation of carbonyl compounds with higher m/z-ratios on the parent m/z-ratio of other target compounds.

For those compounds not included in the gas-standard, mixing ratios were obtained by calculating the ionization efficiency with a previously determined reaction rate of NO^+ and the target compound under the current conditions in the drift tube (k-rate analysis) (Cappellin et al., 2012). The reaction rates (k-rates), also presented in Table 3.1, were derived for the sum of all product ions. Thus, a weighting factor for the relative production of the target ion needed to be applied, which was also obtained by the single-compound headspace analysis by the slope of the signals of the target ion vs. other product ions. The mixing ratios of both E/N settings, obtained by applying the respective product ion distributions, agree well for most compounds (except for n-hexanal and ketones, which have a low sensitivity at 120 Td). This conformance supports the assumption that product ion distributions were valid for both instruments. To calculate propanal, the calibration factor of methacrolein was used since the previous calibrations measured with the PTR-ToF-MS 8000 both had similar sensitivities (methacrolein: 0.13 ppb $ncps^{-1}$, propanal: 0.17 ppb $ncps^{-1}$).

The measurement uncertainty in the mixing ratios of standard calibrated VOC was less than 25 %. It was derived from the accuracy of the VOC gas-standard (± 5 %), the flow meter used for the calibration (± 1 %), the accuracy of the least square fit of the calibration curve (molecule dependent, circa ± 10 %) and the

uncertainty of the relative distribution of product ions, which was expected to be below 20 %. The uncertainty of the product ion distribution was estimated from the purity of the liquid carbonyls tested (> 95%) as well as possible contamination during the headspace sampling. In the case of theoretically calculated mixing ratios using k-rates the accuracy was accordingly higher. The accuracy of the k-rate (± 20 %) (Španěl et al., 1997) and the accuracy of the distribution of product ions give the absolute accuracy for k-rate calibrated mixing ratios which was thus estimated to be below 30 %.

Detection limits were defined as three times the standard deviation of the background noise at the specified mass. Those are also displayed in Figure 3.1-3.2. Negative values arising from the subtraction of the background were set to zero to account for a slightly too high background measurement of some compounds during calibration.

3.3.4 Validation of observations

Preseparation of the VOC with a GC column prior to detection with the NO^+ CIMS can indicate the pureness or compound specificity of an m/z ratio. Koss et al. reported such data for urban ambient air and concluded that certain masses can be seen as unambiguous in that environment. The E/N field used in that study, which strongly impacts the fragmentation patterns on different m/z ratios, was similar to this study (60 Td), but the measurement site was a parking lot in an urban area (Koss et al., 2016). Uncontaminated m/z ratios assigned to carbonyl compounds were found for acetaldehyde, propanal, methacrolein, and crotonaldehyde, the sum of C_5-aldehydes, acetone, hexanal, MVK, methyl ethyl ketone (MEK), benzaldehyde, heptanal, the sum of C_5-ketones and octanal. Nevertheless, biogenic compounds that may not be present in an urban environment were, therefore, not part of the GC method applied in Koss et al. and remained as potential interferents for the carbonyl m/z ratios.

Allyl ethyl ether, an isomer of C_5-aldehydes that also undergoes hydride transfer, was potentially such a candidate (Smith et al., 2011; Španěl and Smith, 1998). The m/z ratio of C_5-aldehydes might have also been affected by 1-5 pentanediol if present at significant concentrations (Španěl et al., 2002). Some carboxylic acids react with NO^+ under the drift tube conditions to form $R - OH + HNO_2$ and thus make isomers to the ionized carbonyl species. Trimethylacetic acid was reported to mainly form $C_5H_9O^+$ and thus also potentially interfered with C_5-aldehydes (Ŝpaněl and Smith, 1998).

N-butyric acid is part of the glucose metabolism in plants and, upon ionization, partly makes $C_4H_7O^+$ ions (m/z 71.0491) thus it potentially interfered with butanal (Smith et al., 2011). The same holds for isobutyric acid. Also valeric acid has been shown to fragment into $C_4H_7O^+$ to a great extent (Ŝpaněl and Smith, 1998). For the alcohols 2-butanol, 1,4-butanediol, and the ester methyl butyrate, fragmentation into $C_4H_7O^+$ has been shown to occur (Koss et al., 2016; Španěl et al., 2002; Ŝpaněl and Smith, 1998). Tetrahydrofuran, an ether isomeric with butanal is ionized via hydride transfer and also forms $C_4H_7O^+$ (Španěl and Smith, 1998). Contamination from 2-butanol was shown to contribute around 50 % to $C_4H_7O^+$ at the urban site in Boulder, USA (Koss et al., 2016). Since 2-butanol has been previously found in emissions from vegetation (Kesselmeier and Staudt, 1999) and the mixing ratios of $C_4H_7O^+$ were close to the detection limit, butanal could not be investigated without suspecting bias from other oxygenated VOC. With another measurement technique (sampling to adsorbent tubes and measurement with a GC-ToF-MS) applied at ATTO also no significant butanal peak was found. Though, butanal has been identified in the Amazonian atmosphere during the dry and wet season at another site in 1999 (Andreae et al., 2002).

Table 3.1: *List of identified carbonyl compounds and other hydrocarbons and their properties for the detection with NO^+ CIMS (PTR-ToF-MS 4000). The sensitivities are compared to the classical PTR-MS method using H_3O^+ reagent ions. The "product factor" represents the weighting factor for the k-rate obtained from the distribution of product ions as described in section 3.3.3. Compounds given in bold were quantified using a primary standard.*

				NO^+						H_3O^+
				E/N = 70 Td			E/N = 120 Td			E/N = 120 Td
Carbonyl species	Ion formula	Exact m/z	k-rate 10^{-9} cm^3 s^{-1}	Prod. factor	Sensitivity ppb $ncps^{-1}$	LoD ppb	Prod. factor	Sensitivity ppb $ncps^{-1}$	LoD ppb	Sensitivity ppb $ncps^{-1}$
Acetaldehyde	$C_2H_3O^+$	43.01784	0.6(Španěl et al., 1997)	-	0.155	0.112	-	0.431	0.160	0.025
Acetone	$C_3H_6NO_2^+$	88.0393	1.2(Španěl et al., 1997)	(0.43)	0.078	0.06	0.27	4.803	0.705	0.031
Propanal	$C_3H_5O^+$	57.0335	2.5(Španěl et al., 1997)	(0.79)	*0.046*	0.053	0.82	*0.256*	0.049	-
MEK	$C_4H_8NO_2^+$	102.055	2.8(Španěl et al., 1997)	(0.84)	0.049	0.008	0.61	1.027	0.111	0.028
MVK	$C_4H_6NO_2^+$	100.039	2.4(Michel et al., 2005)	0.86	-	0.004	0.67	-	0.012	-
MACR	$C_4H_5O^+$	69.03349	2.6(Michel et al., 2005)	(0.54)	0.046	0.021	0.42	0.256	0.093	0.028
n-pentanone	$C_5H_{10}NO_2^+$	116.0706	3.4(Španěl et al., 1997)	0.85	-	0.005	0.56	-	0.007	-
n-pentanal	$C_5H_9O^+$	85.0648	3.2(Španěl et al., 1997)	0.79	-	0.003	0.28	-	0.011	
n-hexanone	$C_6H_{12}NO_2^+$	130.0863	3.3(Španěl et al., 1997)	-	-	0.002	-	-	-	-
Hexanal	$C_6H_{11}O^+$	99.0804	2.5(Španěl et al., 1997)	0.75	-	0.006	0.4	-	0.016	-
Trans-2-hexenal	$C_6H_9O^+$	97.0672	2.8(Roberts et al., 2022)	0.68	-	0.006	0.82	-	0.005	-
Benzaldehyde	$C_7H_5O^+$	105.033	2.8(Španěl et al., 1997)	0.96	-	0.005	0.97	-	0.003	-
Heptanal	$C_7H_{13}O^+$	113.0961	2	-	-	0.004	-	-	0.007	-
Octanal	$C_8H_{15}O^+$	127.1117	2.7(Romano and Hanna, 2018)	0.81	-	0.004	0.61	-	0.004	-
Nonanal	$C_9H_{17}O^+$	141.1274	1.1(Roberts et al., 2022)	0.04	-	0.145	0.1	-	0.078	-
Nopinone	$C_9H_{14}O^+$	138.1039	2	-	-	0.019	-	-	0.002	-
Alkanes										
Isopentane	$C_5H_{11}^+$	71.086	2	-	-	0.013	-	-	0.027	-
Methyl-cyclopentane	$C_6H_{11}^+$	83.086	2	-	-	0.005	-	-	0.008	-
2-, 3-methyl-pentane	$C_6H_{13}^+$	85.101	2	-	-	0.007	-	-	0.006	-
C_7 cyclic alkanes	$C_7H_{13}^+$	97.101	2	-	-	0.004	-	-	0.003	-

Table 3.1 *continued.*

				NO^+						H_3O^+
				E/N = 70 Td			E/N = 120 Td			E/N = 120 Td
VOC species	Ion formula	Exact m/z	k-rate 10^{-9} cm^3 s^{-1}	Prod. factor	Sensitivity ppb $ncps^{-1}$	LoD ppb	Prod. factor	Sensitivity ppb $ncps^{-1}$	LoD ppb	Sensitivity ppb $ncps^{-1}$
C2-alkyl-cyclohexanes	$C_8H_{15}^+$	111.117	2	-	-	0.004	-	-	0.005	-
Alkenes										
C_5-alkene (2-pentenes)	$C_5H_{10}^+$	70.0777	2	-	-	-	-	-	0.009	-
C_5-alkene (a-olefin)	$C_5H_{10}NO^+$	100.076	2	-	-	0.006	-	-	0.003	-
C_6H_{10}	$C_6H_{10}^+$	82.0777	2	-	-	0.006	-	-	0.01	
Alcohols										
Ethanol	$C_2H_5O^+$	45.0335	2	-	-	0.050	-	-	0.019	-
Alkyne										
Propyne	$C_4H_6^+$	54.046	2	-	-	0.026	-	-	0.011	-
Aromatic										
Benzene	$C_6H_6^+$	78.046	-	-	0.101	0.020	-	0.071	0.009	0.063
Terpenes										
Isoprene	$C_5H_8^+$	68.0621	-	-	0.078	0.018	-	0.068	0.023	0.045
Sum of mono-terpenes	$C_{10}H_{16}^+$	136.125	-	-	0.067	0.004	-	0.554	0.039	0.103
Other										
Furan	$C_4H_4O^+$	68.0258	2	-	-	0.008	-	-	-	-
$C_5H_4O_3$	$C_5H_4NO_4^+$	142.014	2	-	-	0.005	-	-	0.003	-

Propionic acid is a potential contaminant for propanal on m/z of C_3H_5O+, but only a fraction of the acid was found to land on the propanal m/z (Ŝpaněl and Smith, 1998). A higher fraction of the fragments of methyl and ethyl propionate were detected as isomers to ionized propanal, but have not been found to be present in biogenic emissions so far (Ŝpaněl and Smith, 1998; Kesselmeier and Staudt, 1999).

It can also not be excluded that fragmentation to $C_2H_3O^+$ of several species, in particular acetic acid, methyl formate, methyl acetate, and ethyl acetate contributes to the m/z ratio of acetaldehyde ($C_2H_3O^+$). Experimental evidence for the contamination has been found only for a small contribution of methyl and ethyl acetate of less than 20% (Ŝpaněl and Smith, 1998).

The isomers hexanal and z-3-hexenol are known to be emitted together by damaged green leaves (Langford et al., 2010; Jardine et al., 2012a). A possible detection of both compounds on m/z of $C_6H_{11}O^+$ could not be excluded, since alcohols also undergo hydride abstraction during the reaction with NO^+ (Koss et al., 2016).

To our knowledge, none of the species that were demonstrated to fragment on the same m/z ratios like carbonyls have been reported to be abundant in forested environments or even biogenically emitted, except z-3-hexenol, 2-butanol, n- and isobutyric acid, acetic acid, and propionic acid. In general, acids have primary sources, including biogenic emissions and biomass burning but also photochemical sources including the ozonolysis of alkenes (Orzechowska et al., 2005). The dataset from this study and a comparison to the corresponding m/z of acids under H_3O^+ ionization that have been measured previously at the ATTO site, suggested that carboxylic acids undergo an association reaction with NO^+. A headspace analysis with acetic acid also revealed no significant contributions to any other m/z except the association product $C_2H_4NO_3^+$.

Fragmentation from higher carbonyls to m/z ratios attributed to lower carbonyls was observed in the single compound headspace analysis, conducted with aldehydes and ketones up to nonanal. The m/z of acetaldehyde ($C_2H_3O^+$, 43.0178) saw small contributions from acetone and pentanone, which were subtracted from the acetaldehyde signal. For this correction, the relative contribution of the fragments from their parent mass, which was determined by the headspace analysis, was used. A list of the single compounds and their product ions formed in the drift tube can be found in the supplementary Table S 3.1 at the end of this chapter. Contributions from higher carbonyls in the NO^+ CIMS were not probable since they were not observed or below the detection limit.

3.4 Results

3.4.1 Atmospheric conditions and seasonality

Seasonality in the central Amazon is characterized by a comparatively clean wet season (February – May) and a dry season (August – November) (Pöhlker et al., 2019). The NO^+ CIMS measurements took place from 23 June until 8 July and from 27 September until 14 October 2019. This section outlines the meteorological conditions of both measurement periods as they influenced seasonal variations in observed VOC mixing ratios and correlations. It is important to consider that the photochemical loss of VOC and reactions involving OH depend on the availability of photons, which also affects the secondary formation of OVOC from the oxidation of different hydrocarbons. VOC emissions from vegetation are driven by light (photosynthetically active radiation, PAR), temperature, water availability, air pollution and biotic factors, such as herbivore infestation, pathogenic infections, or the developmental stage of a plant. However, at heights above 80 m integrated VOC emissions from a whole forested area domiciled by various plant and herbivorous species at all developmental stages were sampled. As has been reported previously, inter-seasonal growth variations may even induce the plant to switch from isoprene emission to monoterpene emission and back (Kuhn et al., 2004a, b). The growing of new leaves (leaf flush), which are photosynthetically more effective than mature leaves peaks in the dry season, aligned with the availability of light (Restrepo-Coupe et al., 2013), which causes an inter-seasonal gradient possibly observed by the presented BVOC emissions.

On average, daytime temperatures differed by only 0.4 °C between the transition (June – July) and the dry season (Fig. S 3.3 at the end of this chapter). Maximum temperatures in the canopy (at 26 m) were reached at 12:00 local time (LT), with 30.5 °C in the transition season and 31.2 °C in the dry season on average. The diurnal evolution of temperature closely followed the incoming solar radiation, here represented by PAR. Dry season observations of PAR were higher by about 9 % compared to the transition

season. Precipitation in the month before the NO^+ CIMS measurements took place totaled 157 mm in June and 119 in September 2019 (Fig. S 3.4 at the end of this chapter). The water level measured in the Rio Negro close to Manaus in 2019, however, had maximum values in June and minimum values in October, with a difference of about 10 m (Chevuturi et al., 2022).

The sampled air originated predominantly from SE to NE, thus an influence from the city of Manaus could be excluded (Fig. S 3.1 at the end of this chapter). However, for long-lived anthropogenic alkanes, influence from populated areas along the Amazonas and smaller side rivers was conceivable. The detected alkanes (Table 3.1) had low mixing ratios below the detection limit, indicating no significant influence from industries based on fossil fuel combustion.

Black carbon (BC) was used as a marker of biomass burning emissions. BC sampled at ATTO has been shown to originate from biomass burning in South America and Africa (Holanda et al., 2020). Enhanced concentrations of 0.42 and 0.54 µg m^{-3} (80, 325 m) were found on average in the dry season 2019. Maximum concentrations reached 0.93 and 1.17 µg m^{-3}. Average concentrations of 0.18 and 0.21 BC (80, 325 m) in the transition season indicated less polluted conditions. A large number of VOC, including certain carbonyl compounds, are usually co-emitted during biomass burning at various emission factors and rates (Andreae and Merlet, 2001; Andreae, 2019). Therefore, the carbonyls detected with the NO^+ CIMS during this study and their precursors potentially had both biogenic and biomass burning sources. Correlations of carbonyls with BC at 325 m are shown in the supplementary for both seasons (Fig. S 3.5 at the end of this chapter) to find possible influence from advected, fresh, or aged biomass burning plumes. In the cases of acetaldehyde, acetone, methacrolein, MVK, and benzaldehyde, a Pearson coefficient of $p > 0.55$ was retrieved at day and nighttime so that an influence of biomass burning through co-advection or in plume production was feasible.

3.4.2 Vertical distribution of carbonyls above canopy

The distribution of carbonyls with height above the uniform rainforest-covered landscape provides information on the nature of emission sources, oxidative transformations, and sinks of the carbonyls under consideration of dynamic processes in the atmospheric mixed layer. Vertical gradients were governed by the strength and temporal variance of the respective source, the atmospheric lifetime of the species considered, and dilution through turbulent mixing or entrainment from the free troposphere during mixed layer growth. An earlier work investigated the chemical and dilutive loss of isoprene with height using observations at ATTO and a turbulence-resolving large eddy simulation (DALES). It demonstrated that slightly more than 50 % of the isoprene loss in the vertical (80-325 m) at noon occurred due to dilutive turbulent mixing (Ringsdorf et al., 2023). It is important to note that the lowest sampling height at 80 m was within the roughness sublayer. This is a layer within the mixed ABL of about 2-3 times the canopy height (≈ 35 m), which is strongly affected by the tall canopy with respect to wind fields and, thus, turbulence. Within this layer, the exchange between the canopy and atmosphere occurs by inhomogeneous flows into and out of the canopy (Chamecki et al., 2020). An important process influencing the ambient concentration of the compounds presented at all sampling heights was the growth of the ABL (up to 2 km height) after sunrise due to the strengthening of turbulences from thermal expansion of the heated air masses near the ground. During the growth, air from higher altitudes (residual

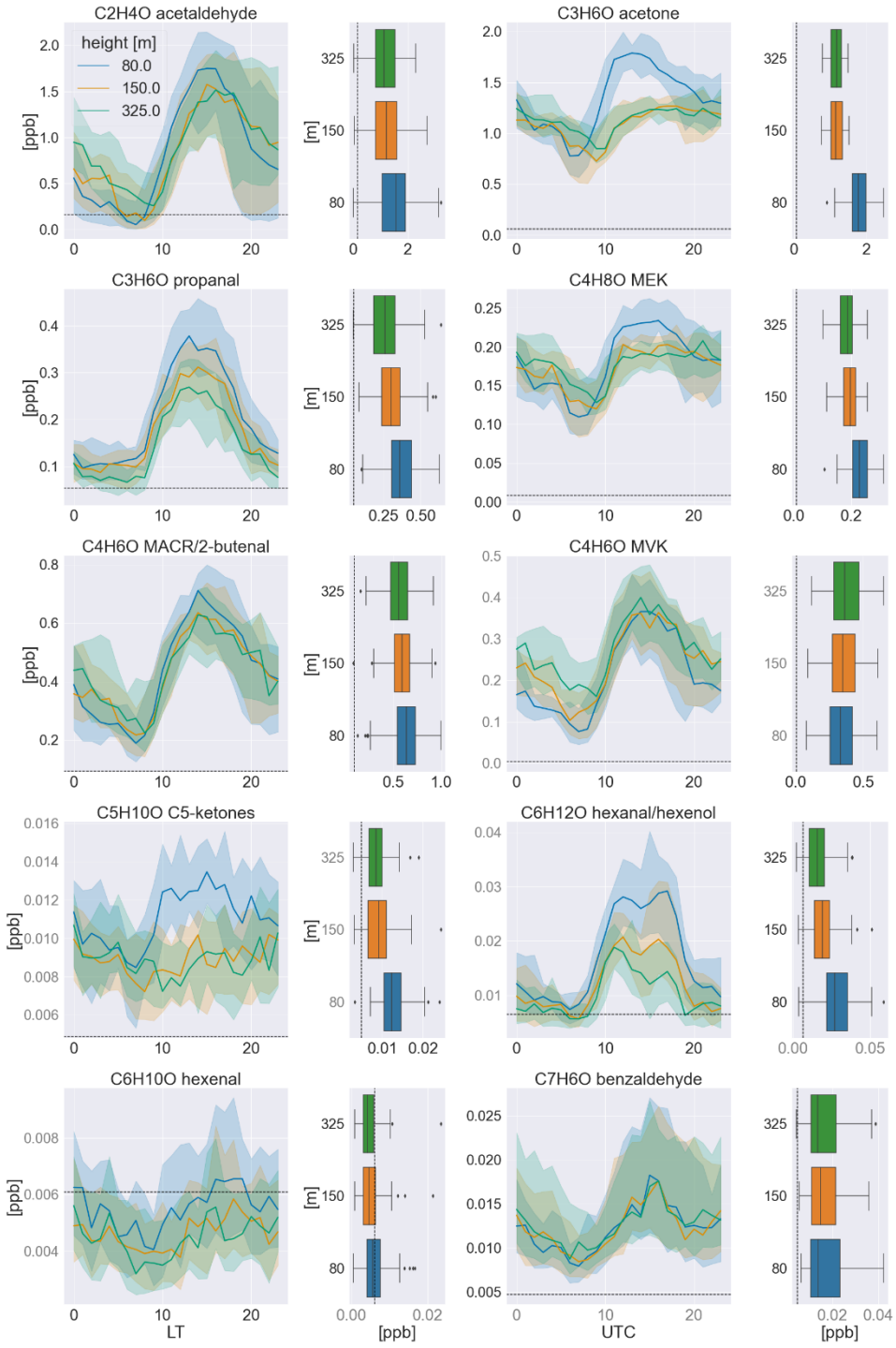

Figure 3.1: *Median averaged timeseries in the wet-to-dry transition season (June/July) of 2019 measured at all sampling heights for each carbonyl compound and its respective vertical profile at noon (12:00-15:00 LT) to the right. The shadings indicate the quartiles (25th and 75th). In the box-and-whisker plots, the boxes also represent the quartiles, while the residual data except outliers are included in the whiskers. The mixing ratios stated in black font were calibrated to standard, while those in gray font were calculated based on k-rate.*

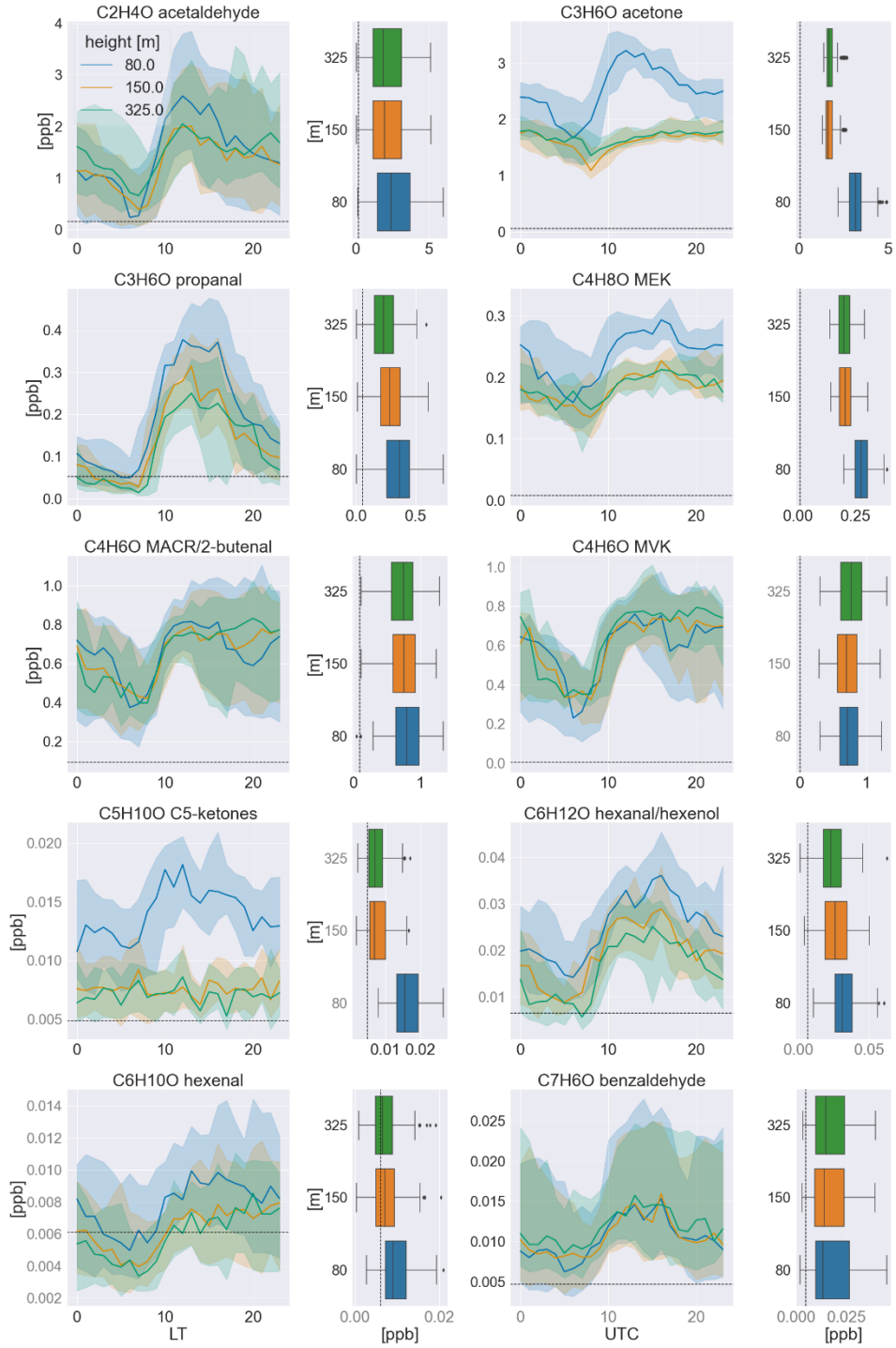

Figure 3.2: *Median averaged timeseries in the dry season (September/October) of 2019 measured at all sampling heights for each carbonyl compound and its respective vertical profile at noon (12:00-15:00 LT) to the right. The shadings indicate the quartiles (25th and 75th). In the box-and-whisker plots, the boxes also represent the quartiles, while the residual data except outliers are included in the whiskers. The mixing ratios stated in black font were calibrated to standard, while those in gray font were calculated based on k-rate.*

layer containing more aged air) is entrained, leading to the minimum mixing ratios observed after 06:00 LT at all three heights. During the day, the turbulent mixing via convection and associated downward motions is strongest until convection eases with decreasing insolation. At night, a stable stratification associated with low vertical mixing is formed (Jordi Vilà-Guerau de Arellano, et al., 2015).

Under the reasonable assumption of a carbonyl source at canopy level, the long-lived ketones were expected to have a certain background concentration in the convective mixing layer but also above, while short-lived aldehydes will be zero at higher altitudes, like isoprene. Consequently, the aldehydes should show a stronger decrease in their vertical profiles than the ketones, which were expected to be well mixed at a certain height above the canopy. Nonetheless, one has to also take the secondary chemical formation of carbonyls into account which can influence the vertical gradients depending on the emission source and atmospheric lifetime of the precursors.

Figures 3.1 and 3.2 present the diurnal variability observed at the three sampling heights for all carbonyls measured in the wet-to-dry-transition and in the dry season respectively. Some compounds were measured in very low concentrations, below the detection limit in one or both seasons, namely the sum of C_5-aldehydes, C_6-ketones, heptanal, octanal, and nonanal. All other carbonyls showed distinct diurnal variabilities with increasing concentrations after sunrise (06:00 LT) and decreasing concentrations at nighttime. Their diurnal cycle followed the evolution of PAR and temperature with a slight delay throughout the day, reflecting the expected biogenic emission and photochemical production. As hypothesized above, no significant vertical variability was found for ketones, though only at 150 and 325 m, whereas a strong decrease in mixing ratio with height was observed between 80 and 150 m. This distribution indicates that mixing ratios of ketones were only well mixed above 150 m, while the measurements at 80 m were influenced by a strong source of ketones, which is discussed compound-wise below. The observed aldehydes exhibited different vertical distributions, some showed increasing mixing ratios with height, others were rather steadily decreasing as it was hypothesized, and some showed very small variabilities throughout the lowermost 325 m of the atmosphere. The different sources and sinks leading to the observed vertical gradients are also discussed individually for each aldehyde or family of aldehydes.

3.4.3 Correlations at 80m and common sources

The chemical composition of airmasses measured at 80 m was governed by various processes occurring from the leaf level up to mixing scales of the lower atmosphere. At the leaf level, BVOC are formed by plant metabolic pathways or possibly in the case of OVOC including carbonyls via within-leaf reactions. Epicuticular waxes, also called leaf waxes consist of long-chained hydrocarbons, e.g. the triterpene squalene, which yield volatile compounds during ozonolysis. Depending on the position of the double bond of the long-chained molecule and its functional groups, aldehydes or ketones are formed, whereby the chances for the formation of short-chained carbonyls like acetone are highest (Fruekilde et al., 1998). Following their emission a fraction is deposited on surfaces, which is most of the time reversible, or uptaken by stomata, which represents a potential sink (Niinemets et al., 2014). Depending on their atmospheric lifetime, BVOC undergo within-canopy oxidation; in the case of reactive isoprene and monoterpenes, this was found to be not more than 10 % of their initial emission flux (Karl et al., 2004; Fuentes et al., 2022) before being ejected from the canopy. Within and above the canopy they are mixed

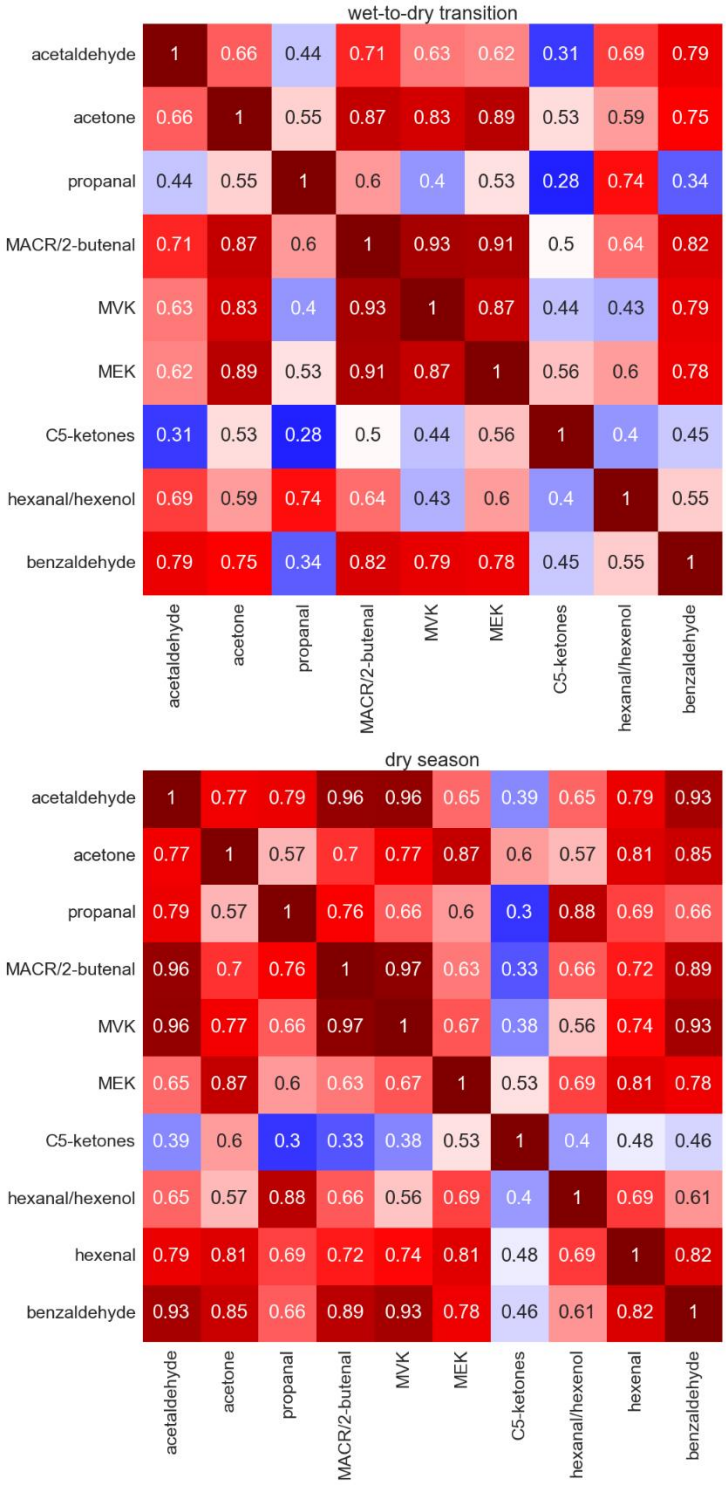

Figure 3.3: *Pearson correlation coefficients from the intercorrelation of the carbonyl species in the wet-to-dry transition season (upper) and in the dry season (lower).*

with more or less aged air masses and secondary production and depletion take place simultaneously. When correlating two timeseries of BVOC measured at that height, a high correlation coefficient can indicate similar production and loss or possibly a precursor-product relation. Here it is very important to consider the timescales of production and loss versus vertical transport since the residence time of airmasses in the first 80 m is limited during daytime convective conditions. In a previous study the mixing timescale, which accounted for turbulent up and downward motions, between 80 and 325 m at ATTO, was determined to range on average from 60 minutes at 10:00 LT to 15 min at 15:00 LT (Ringsdorf et al., 2023). Based on that study, we assumed the mean residence time between canopy and 80 m to be in the same time range of minutes to 1 hour. Carbonyl precursors including alkenes, isoprene, higher terpenes and alkanes have atmospheric lifetimes with respect to oxidation by OH radicals of $\tau > 2$ hours, $\tau \approx 3$ hours, minutes to hours and days to weeks for the much less reactive alkanes (Altshuller, 1991; Wolfe et al., 2011). The lifetimes with respect to OH of carbonyl compounds themselves range from 12 hours (trans-3-hexenal) (Jiménez et al., 2007) to 119 days (acetone) and are even shorter when considering photolysis, which is a significant sink for carbonyls (Mellouki et al., 2015). In Table 3.2 the lifetimes of carbonyls with respect to an average OH concentration of $1x10^6$ molecules cm^{-3} based on a previous study at the ATTO site are presented. This is the average over roughly the same time of day that was considered for carbonyl correlations (10:00 – 15:00) (Ringsdorf et al., 2023). However, isoprene oxidation was observed by the daily increase of the product MVK between 80 and 325 m.

Thus, correlations at 80 m will reflect only the processes that occur on a comparable or faster timescale than mixing. This is primary emission, product formation in the atmosphere from short-lived precursors like alkenes and terpenes, and progressive photochemical degradation/photolysis of short-lived carbonyls as well as loss via deposition.

Figures 3.3-3.4 show the Pearson correlation coefficients (p) for both seasons divided into day (10:00-17:00 LT) and nighttime (22:00-05:00 LT) between the carbonyl compounds and between carbonyls and other selected VOC, including terpenes (isoprene, sum of monoterpenes), alkenes (C_5-alkenes, benzene) and oxygenated compounds (ethanol, furan, acetic acid, $C_5H_4O_3$). Their diel and vertical distributions are presented in the supplementary Figures S 3.6-S 3.7 (at the end of this chapter). $C_5H_4O_3$ is a highly oxygenated compound, which was classified to be exclusively an oxidation product of very reactive BVOC in a previous study conducted within and above a pine forest. Therein, emission rates of very reactive BVOC were estimated to reach 6-30 times the emission rates of monoterpenes (Holzinger et al., 2005). In this study, the highest mixing ratios were found at 325 m, suggesting that besides being formed as a first order oxidation product close to the canopy it was also an oxidation product of higher order which therefore emerges at longer timescales. Very reactive BVOC presumably also represent precursors for Carbonyl compounds. Periods with precipitation were excluded from the correlations to avoid the effects of downbursts and washout. As expected, good correlations were found between isoprene and the sum of monoterpenes, which are all primary emissions that depend strongly on light and temperature. Correlation of carbonyl compounds with isoprene and monoterpenes was preferred over PAR and temperature to identify light and temperature dependent direct emission, due to the temporal delay between emission and detection. However, it is striking that most carbonyls showed good correlations with all other carbonyls with Pearson coefficients greater than 0.7. This likely resulted from the common driving variables, namely light and temperature for emission, as well as similar photochemical production rates.

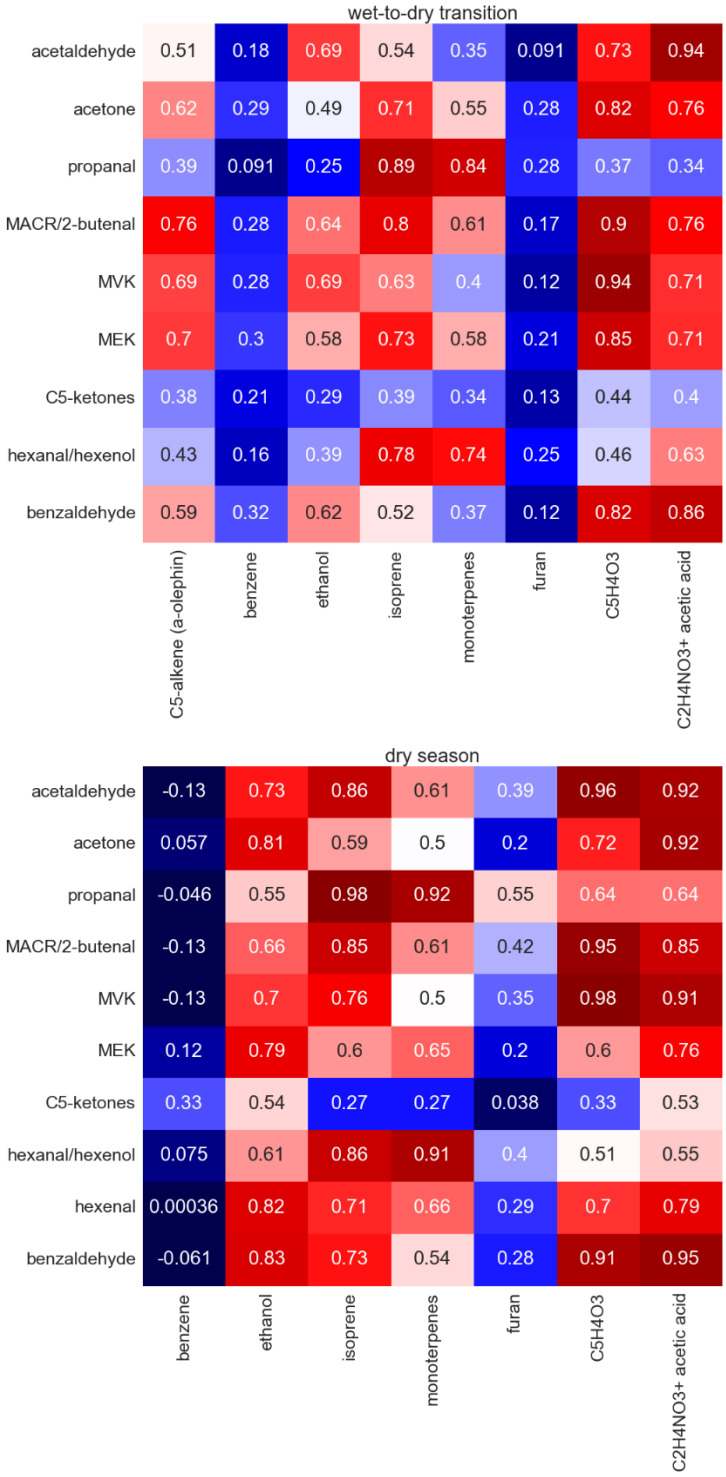

Figure 3.4: *Pearson correlation coefficients from the correlation of the carbonyl species with selected hydrocarbons in the wet-to-dry transition season (upper) and the dry season (lower).*

The highest correlations with the primary emitted isoprene and monoterpenes were obtained for propanal and n-hexanal. Other compounds that were found to correlate very well were acetaldehyde,

methacrolein, MVK, and $C_5H_4O_3$ as well as acetone and MEK. In the following section, implications drawn from different gradients are discussed in detail.

3.4.4 Nocturnal loss rates

Biogenic emissions, not related to photosynthesis, might have continued during night whereas oxidative chemistry and thus secondary production of carbonyls was limited to reactions with O_3 and NO_3, which were found in low levels in the remote forested atmosphere. Important loss mechanisms at night are deposition to surfaces and reaction with NO_3 (Brown and Stutz, 2012). Deposition at night is thought to happen via adsorption to the cuticle of the leaves since stomata are closed in the absence of light. However, there is evidence that the stomatal conductance is maintained at night by many woody species, implying an irreversible uptake for BVOCs that are further processed and converted to other metabolites(Niinemets et al., 2014). Reaction with NO_3 at nighttime is limited to unsaturated BVOC but is also efficient for some saturated aldehydes. A rather high assumed mixing ratio of 10 ppt NO_3 (Brown and Stutz, 2012; Khan et al., 2015) yields nighttime atmospheric lifetimes of 8 days for n-hexanal, the most reactive observed aldehyde with respect to NO_3. Ozone is circa a thousand times more abundant than NO_3, but the reaction rates with carbonyls are even slower. Therefore, deposition is expected to be the dominant loss mechanism for carbonyls at night. Table 3.2 summarizes properties of the observed carbonyl compounds that are important driving variables of deposition on surfaces together with their observed loss rates during the night. They were obtained by linear regression of the observed nocturnal timeseries at 80 m between 22:00 and 04:00 LT. Since the uptake of BVOC by leaves occurs only when the ambient concentration exceeds the concentration in the inter-leaf space, high loss rates were observed for BVOC with high ambient mixing ratios. However, the concentration gradient can be maintained by a metabolic transformation of the BVOC in the leaf. Table 3.2 also includes their reactivity towards the OH radical, O_3, and NO_3.

3.5 Discussion

In the following sections, the diel variability, vertical distribution (80-325 m) (Table 3.3), and correlations between all measured BVOC are considered in a compound-wise manner. The measurements presented here are related to previous studies related to the emission, formation, and loss of the carbonyl species.

Acetaldehyde

Acetaldehyde (ethanal), is known to be an important contributor to the total ambient carbonyl concentration levels in the atmosphere. Various sources of acetaldehyde have been characterized previously, including direct emissions from vegetation and the ocean, and secondary production from the OH, NO_3, and O_3 initiated photooxidation of hydrocarbons (Rottenberger et al., 2004; Wang et al., 2020b). Direct biogenic emissions may be of special importance for the Amazonian rainforest, as acetaldehyde and ethanol release have been reported to result from root anoxia (Bracho-Nunez et al., 2012; Holzinger et al., 2000; Rottenberger et al., 2008). This may occur in large areas caused by seasonal flooding (Parolin

Table 3.2: *Rate coefficients for the reaction with OH, NO_3, and O_3 and the atmospheric lifetime considering an OH radical concentration of 1x10^6 molecules cm^{-1}. The rate coefficients and boiling point temperature were taken from the NIST database. Water solubility has been reported by Sander et al.(Sander, 2023).The loss rate is calculated based on the median averaged slopes of the nocturnal (22:00-04:00) carbonyl timeseries.*

VOC species	k_{OH} [cm^3 #$^{-1}$ s^{-1}]	Estimated lifetime Amazon [days]	k_{NO3-} [cm^3 #$^{-1}$ s^{-1}]	k_{O3} [cm^3 #$^{-1}$ s^{-1}]	Volatility (T_{boil} [K])	Water-solubility (H_s^{cp}) [mol m^{-3} Pa^{-1}]	Loss rate [ppb min^{-1}] (transition, dry season)
Acetaldehyde	1.6E-11	1.4	2.4E-15	3.4E-20	294	1.3E-1	-6.7E-4, -1E-3
Acetone	1.9E-13	119.3	8.5E-18	8.5E-18	329	2.7E-1	-7.8E-4, -9.5E-4
Propanal	2E-11	1.2	6.2E-15	-	322	9.9E-2	-8.9E-5, -1.4E-4
MEK	1.2E-12	19.3	-	2.06E-16	353	1.8E-1	-8.4E-5, -7.4E-5
MVK	1.9E-11	1.25	1.2E-16	4.48E-18	354	4.0E-1	-1.1E-4, -4.8E-4
MACR 2-Butenal	3E-11 3.6E-11	0.75 0.64	3.3E-15 5.1E-15	1.09E-18 1.58E-18	341 375.5	4.5E-2 5.9E-1	-2.1E-4, -2.1E-4
2-pentanone (C_5-ketones)	4.6E-12	5.08	-	-	375	1.3E-1	-
n-hexanal Z-3-hexenol	2.8E-11 1E-10	0.83 0.21	1.1E-14 2.7E-13	- 6.4E-17	402 427.7	4.5E-2 -	-2E-6 -
z-2-hexenal	4.4E-11	0.52	1.2E-14	2.0E-18	419.7	1.4E-1	-
Benzaldehyde	1.3E-11	1.78	2.01E-15	2.0E-19	452	4.0E-1	-7.9E-6, -8E-6
Isoprene	1E-10	0.23	6.7E-13	1.28E-17	307	1.3E-4	-1.5E-3, -2.6E-3
α-pinene	5.3E-11	0.43	6.2E-12	9.6E-17	430	7E-4	1.7E-4, -3.2E-4

et al., 2004). At 80, 150, and 325 m in the wet-to-dry transition season of 2019, observed mean diurnal concentrations were 642, 702, 852 ppt and 1.38, 1.25, 1.47 ppb in the dry season of 2019.

Metabolic production pathways of acetaldehyde within plants and subsequent emission have been found to occur not only during root-flooding but also during fast light-dark transitions (Fall, 2003; Holzinger et al., 2000). The anaerobic conditions at the root's surface during flooding cause the ethanolic fermentation pathway to form ethanol that is transported to the leaves of the plant to provide an energy source.

Acetaldehyde is an intermediate of this pathway which tends to leak out to the atmosphere due to its high volatility (Kreuzwieser et al., 2000). Some Amazonian tree species can switch to the fermentative metabolism (Bracho-Nunez et al., 2012), but concentration or flux measurements during the dry-to-wet transition in Amazonia under field conditions are missing. In this study, a strong correlation was found for ethanol and acetaldehyde in the nighttime of the transition season ($p = 0.92$). Ethanol mixing ratios were ten times higher in the transition season and showed a diel maximum at nighttime. Since river levels were maximum in the transition season, root flooding may be responsible for the seasonal variability of ethanol

Table 3.3: *Median averaged mixing ratios of the observed carbonyl compounds for the measurement periods in the dry-to-wet transition and the dry season 2019. The range presents the lowest mixing ratio included in the 25th and the highest mixing ratio included in the 75th quantile of the median averaged diurnal cycle. Numbers in italics represent the limit of detection.*

Carbonyl species	Height [m]	Wet-to-dry transition – Jun-Jul 2019		Dry season 2019 – Sep-Oct 2019	
		Median [ppt]	Range [ppt]	Median [ppt]	Range [ppt]
Acetaldehyde	80	642	24 - 2043	1380	*160* - 3179
	150	702	24 - 1801	1252	239 - 3134
	325	852	59 - 1883	1472	256 - 3716
Acetone	80	1333	559 - 2083	2546	1155 - 3812
	150	1124	494 - 1509	1657	918 - 2105
	325	1146	661 - 1545	1707	1087 - 2115
Propanal	80	176	71 - 438	165	*53* - 410
	150	150	58 - 365	115	*53* - 349
	325	119	*53*- 348	85	*53* - 305
MEK	80	177	82 - 267	249	116 - 348
	150	175	81 - 229	188	98 - 259
	325	177	105 - 240	185	75 - 247
MVK	80	184	45 - 483	607	100 - 994
	150	229	53 - 481	599	164 - 967
	325	265	93 - 499	659	239 - 1014
MACR/2-Butenal	80	415	149 - 755	679	250 - 1026
	150	425	149 - 697	644	307 - 1010
	325	439	181 - 694	644	281 - 996
C_5-ketones	80	11	*7* - 18	14	*7* - 23
	150	9	*7* - 15	8	*7* - 13
	325	9	*7* - 15	*7*	*7* - 12
n-hexanal/ hexenols	80	15	*6* - 50	26	*6* - 53
	150	11	*6* - 33	19	*6* - 42
	325	9	*6* - 30	16	*6* - 43
Z-2-hexenal	80	-	< 11	8	*6* - 14
	150	-	< 9	-	< 12
	325	-	< 9	-	< 12
Benzaldehyde	80	12	*6* - 27	11	*6* - 26
	150	12	*6* - 24	10	*6* - 26
	325	12	*6* - 24	11	*6* - 25

(Kirstine and Galbally, 2012). However, acetaldehyde showed a different seasonal variability, indicating other sources were dominant. It is important to keep in mind, that the ATTO site is a Terra firme region with rare inundation events. Field measurements of roots under anoxia are still missing. Fast light-dark transitions occur all the time inside the forest canopy and are suspected to lead to an overproduction of cytosolic pyruvic acid in the leaves that is converted to acetaldehyde as a safety mechanism against acidification (Fall, 2003). The wounding of a plant through cutting or drying out plant tissues also releases acetaldehyde (Guenther, 2000). It is also found in emissions from leaf litter presumably as a byproduct of biomass degradation (Schade and Goldstein, 2001; Karl et al., 2003). Furthermore, the oxidation of polyunsaturated fatty acids in leaves leads to the formation of reactive aldehydes, which can represent a primary source for many aldehydes, including acetaldehyde (Niinemets et al., 2014; Matsui et al., 2010).

Once released, the atmospheric lifetime of acetaldehyde is in the range of 1.4 days with respect to OH (Table 3.2).

Tree branch enclosures and vertical gradient measurements at another Amazonian measurement site (Rondônia) in 1999 have revealed that the canopy's role as a sink can even dominate the emissions. Uptake to leaves mainly occurred via the leaf stomata and has been reported to be governed by a compensation point that varies between canopy and understory species. The authors concluded that the observed ambient concentrations were generated mainly by the secondary photochemical production of acetaldehyde (Rottenberger et al., 2004). In 2013, measurements of acetaldehyde vertical gradients below 80 m at ATTO conformingly showed increasing acetaldehyde between 24 m (inside the canopy, high influence by surrounding trees) and 79 m. However, interestingly, this has only been observed in the dry season (Sep), whereas during the wet season of 2013 (Feb/Mar), a dominance of primary emission over secondary production was indicated by decreasing concentrations directly above the canopy (Yáñez-Serrano et al., 2015). We observed decreasing mixing ratios at altitudes above 80 m under dry season or close to dry season conditions in 2019. At noon the acetaldehyde mixing ratios were peaking in the first 150 m above the canopy, consistent with a fast secondary production and a possible contribution from direct emission. Primary emission might vary in strength and dominance with season due to the variability of light, temperature, precipitation, and soil moisture and due to plant phenology. At 150 and 325 m, similar mixing ratios were measured, suggesting well mixed conditions and ongoing secondary formation between those heights, due to the many routes of acetaldehyde photochemical generation.

In the rainforest environment, the photochemical precursor hydrocarbons of acetaldehyde are most likely natural emissions or longer-lived emissions from distant biomass burning. Aldehydes are a common product of any hydrocarbons that are oxidized in the atmosphere (Mellouki et al., 2015; Calogirou et al., 1999). Laboratory experiments showed that acetaldehyde emerges from the oxidation of alkanes and alkenes, with ethane and propene having the largest emission fluxes globally (Singh et al., 2004). Ethane is globally distributed thus background concentrations of acetaldehyde are generated by this route, which are however low due to the rapid transformation via reaction with OH. Biogenically emitted compounds with high molar yields for the formation of acetaldehyde are > C_2 alkenes (0.85) and ethanol (0.95). Additionally, isoprene and terpenes have a low molar yield (0.019, 0.025), but the strongest emissions measured from the forest (Fischer et al., 2014). The reaction of other aldehydes, butanal, 2-pentanone, and 2-heptanone with OH and NO_3 also leads to the formation of acetaldehyde, sometimes with high yields (Atkinson et al., 2000). In the data presented here, acetaldehyde at 80 m correlated best with photolytically generated species like MVK, methacrolein, $C_5H_4O_3$ ($p = 0.96$) and with benzaldehyde ($p = 0.93$) in the dry season and well with acetic acid ($p > 0.92$) in both seasons. In the transition season correlations were weaker overall (Fig. 3.3-3.4), which could hint at varying primary and secondary acetaldehyde sources. Correlation coefficients of acetaldehyde and BC at 325 m lie below 0.6 at daytime but at nighttime, in the transition season, a rather high correlation with $p = 0.82$ is observed (Fig. S 3.6).

From about 16:00 LT onwards until the next day the vertical gradient is reversed with the lowest concentrations at 80 m. This likely reflects the uptake to plant tissues regulated by compensation points since the NO_3 and O_3 reactivity is rather low. Acetaldehyde exhibits the strongest observed loss rate at nighttime among all the carbonyl compounds in the dry season and it had the highest Henry's law constant (Table 3.2).

Acetone

Acetone (propanone) is the simplest ketone and the most abundant and widespread OVOC in the atmosphere due to its relatively long atmospheric lifetime of 15 days (Singh et al., 2004) (primarily driven by photolysis in the upper troposphere, 119 days with respect to OH). The variation of acetone mixing ratios throughout the day above the roughness sublayer at 150 and 325 m was small compared to the other carbonyls. However, mixing ratios at 80 m increased substantially with light and temperature during the day. In the wet-to-dry transition season mixing ratios reached 1.33, 1.12, 1.15 ppb on average, while in the dry season, 2.55, 1.66, 1.71 ppb (80, 150, 325 m) were measured.

The vertical distribution of acetone showed clearly enhanced mixing ratios at 80 m during daytime compared to well mixed conditions at higher altitudes. The strong gradient in the first 150 m above the canopy indicated a large positive flux above the canopy. Possible reasons for this strong gradient include primary biogenic emission, biomass burning, production from leaf wax, or efficient secondary formation from very short-lived precursors that exceed deposition and stomatal uptake. Flux measurements in a tropical forest in Costa Rica in the drier season have found a bidirectional but net positive canopy flux of acetone (Karl et al., 2004). Additionally in 2013, when several carbonyls have been measured at ATTO below 80 m, the acetone mixing ratios inside the canopy (influenced by surrounding trees) were lower than the values measured at 79 m in the dry season. Just as for acetaldehyde, this indicated a dominance of photolytically secondary formation over direct emission. In the wet season in 2013 however, mixing ratios measured in the canopy and at 79 m were of similar magnitude and compared to the dry season much lower on both heights. In conclusion, no clear dominance of secondary formation or direct emission was found in the wet season (Yáñez-Serrano et al., 2015). In this study, seasonal differences were also observed at all three heights, with lower mixing ratios in the transition compared to the dry season. While we cannot report acetone observations from the wet season, we did observe higher correlations of acetone with non-primary emitted OVOC methacrolein, MVK, and $C_5H_4O_3$ in the transition season ($p > 0.82$) compared to the dry season suggesting that in 2019 secondary formation contributed more acetone to observed mixing ratios in the transition season than in the dry season. In light of the widely differing atmospheric lifetimes of acetone and those OVOC, the most likely explanation for the high transition season correlations is a dominating secondary acetone source at a similar rate. Contributions from aged biomass burning plumes containing acetone in the dry season, when enhanced BC concentrations were observed, could also be the reason for a weaker correlation of $C_5H_4O_3$, methacrolein, and MVK with acetone in the dry season. By combining the information obtained in 2013 and from this study, the secondary production in the dry and transition season appears to be peaking somewhere between the canopy and 150 m above ground and added up to a varying contribution of direct emission from vegetation. Concludingly, the most relevant precursors were very reactive biogenic compounds. The best correlations were found with MEK ($p > 0.87$) in both seasons, another long-lived ketone that is known to be directly emitted from the Amazon rainforest and produced in the atmosphere above (Yáñez-Serrano et al., 2015, 2016).

Primary sources identified are direct emission from vegetation and to a smaller extent also from dead plant matter. Acetone is released during cyanogenesis, which repels herbivores eating the plant's leaves. During the production and release of volatile hydrogen cyanide, which deters the feeding herbivore, acetone is formed as a byproduct. Cyanogenesis occurs in many plant species though some employ different mechanisms for the production of hydrogen cyanide so that other carbonyl byproducts can be released (Fall, 2003). Another known biogenic pathway for acetone formation is acetoacetate

decarboxylation in soil bacteria and humans (Fall, 2003). Both light and temperature have been suspected to drive acetone emissions, as shown for some pine and spruce trees (Seco et al., 2007).

The secondary formation is known to occur from anthropogenically emitted C_3-C_5 isoalkanes (propane, isobutane, isopentane) and biogenic emitted methyl butenol and certain terpenes (Seco et al., 2007; Fischer et al., 2014; Jacob et al., 2002). We found mixing ratios of isopentane to be below the detection limit (13 ppt), and the vertical distribution and correlations reported for acetone indicated a fast formation in the first 150 m above ground by much more short-lived hydrocarbons than alkanes.

At night, deposition could be observed at the fastly decreasing mixing ratios at 80 m, compared to its slowly occurring reactions with NO_3 and O_3. Similar effects have been reported in flux measurements performed by Karl et al. (2004).

Propanal

Propanal is an isomer of acetone and is not distinguishable from acetone by classical PTR-MS type instruments using H_3O^+. In this study, the first high temporal resolution measurements of propanal in a tropical forest are presented, and the vertical distribution above the canopy was found to differ markedly from acetone. In general, in the remote atmosphere, we may expect the more reactive propanal to be at lower mixing ratios than acetone, although this needs not to be true close to sources. We measured average concentrations of 176, 150, and 119 ppt in the wet-to-dry transition and 165, 115, and 85 ppt in the dry season (80, 150, 325 m). The ratio of propanal to acetone in the roughness sublayer of the tropical forest and above yields 1:7.6, 1:9.6 (transition season) and 1:15.4, 1:20 (dry season) at 80 and 325 m. Globally, the mixing ratio of propanal has been estimated to be about one-third of acetaldehyde (Singh et al., 2004), while at ATTO a ratio of 1:4.2, 1:8.1 (transition season) and 1:7.2, 1:14 (dry season) was measured at 80 and 325 m, respectively. However, it should be noted that globally, a large source of propanal is the oxidation of propane, which is predominantly emitted from anthropogenic activities associated with the use of oil and gas. Acetaldehyde sources in the rainforest thus far exceed propanal sources compared to the global budget (Warneck, P.; Williams, J., 2012).

Propanal emission from vegetation has been reported for non-tropical forests (Guenther, 2000; Villanueva-Fierro et al., 2004), although without specifying its metabolic pathway. Wang et al. (2019) demonstrated the biosynthesis of acetaldehyde and propanal during fruit ripening. It was also noted that propanal emission occurs from fern (Isidorov et al., 1985), which is important since fern species are common in the understory of tropical forests.

Throughout the day, propanal exhibited a negative vertical gradient (i.e. decreasing mixing ratio with increasing height). This occurs most likely due to dilution and photochemical loss of propanal generated in, or emitted from the canopy. A similar distribution was also observed for monoterpenes and isoprene, which are primarily emitted VOC. Accordingly, propanal observed at 80 m also correlates best with isoprene in both seasons ($0.89 > p > 0.98$) followed by monoterpenes ($0.84 > p > 0.92$). The estimated atmospheric lifetime of propanal of about 1 day (Guimbaud et al., 2007) (1.2 days for the oxidation by OH, Table 3.2) is similar to that of acetaldehyde, but the vertical profiles revealed different distributions in the first 325 m above ground (Figures 3.1 and 3.2). The weak gradient of acetaldehyde between 150 and 325 m at daytime in contrast to the steadily decreasing vertical profile of propanal can thus only be explained by a higher yield of acetaldehyde from secondary production above 150 m. This is not surprising since acetaldehyde is produced during oxidative degradation of many hydrocarbons. The secondary

production of propanal is known to occur via the photochemical oxidation of C_3 and larger hyrocarbons (Singh et al., 2004) and propane (Altshuller, 1991). Their lifetimes range from 5 days to a few hours (Altshuller, 1991). However, due to the high correlation of propanal and isoprene, which is even higher than the correlation of isoprene and its oxidation products MVK and methacrolein, a primary and mainly light dependent source is surmised.

Nighttime mixing ratios of propanal were decreasing at 80 m (Table 3.2). Since the reaction rate of propanal with NO_3 is faster and the water solubility lower in comparison to the other carbonyl compounds, more propanal could potentially react in the atmosphere. While stomatal uptake for the terpenes might be driven by the concentration gradient between leaf and atmosphere, the same might hold for propanal.

Methyl ethyl ketone

Mixing ratios of MEK in the wet-to-dry transition were 177, 175, and 177 ppt on average, compared to 249, 188, and 185 ppb in the dry season (80, 150, 325 m). With a conventional PTR-MS, butanal and MEK are detected at the same exact mass, whereas in this study using NO^+ reagent ions solely MEK was measured. Butanal mixing ratios were determined to be below the detection limit (20 ppt), thus the contribution of butanal to MEK for PTR-MS can be assumed to be very low. The mixing ratios obtained in this study agree well with previous studies conducted with a PTR-quadrupole-MS at the ATTO site in 2013 and close to Manaus (Amazonia) in 2014, which could not completely exclude possible interferences of the nominal mass of MEK (Yáñez-Serrano et al., 2015, 2016). The vertical distribution of MEK throughout the day resembles that of acetone in both seasons. Mixing ratios above the roughness layer (at 150 and 325 m) were almost uniform, while those at 80 m showed a more pronounced diurnal cycle with strongly increasing values in the day and decreasing values at night. Not only structurally similar to acetone, MEK also has a long lifetime of 4.3 days (Fischer et al., 2014) (19.3 with respect to OH oxidation alone) relative to mixing timescales. It is also known to have primary and secondary sources (Yáñez-Serrano et al., 2016). Therefore, it is not surprising that MEK correlated best with acetone at 80 m ($p = 0.87$ in the dry season), but in the transition season, also with $C_5H_4O_3$, methacrolein, and MVK. This suggests secondary sources from biogenically emitted precursors were more dominant during the transition season than in the dry season, similar to acetone.

MEK emissions have been reported for rainforest canopies (Yáñez-Serrano et al., 2015) and fern (Isidorov et al., 1985), decaying plant matter (Warneke et al., 1999), fungi, and bacteria (Yáñez-Serrano et al., 2016). The metabolic pathways of production and the release mechanisms are poorly understood, but it has been suggested that it is related to plant signaling, injured leaves, and root-aphid interactions (Yáñez-Serrano et al., 2016). Within plant conversion of the cytotoxic 1,2-ISOPOOH, which deposited on poplar leaves, to first MVK and subsequently MEK has been reported to represent a large biogenic source for MEK. The responsible enzyme for the conversion of MVK to MEK is widespread among plants (Canaval et al., 2020).

The secondary formation of MEK occurs via the oxidation of n-butane with a yield of 80 % (Singh et al., 2004) and via oxidation of 2-butanol, 3-methyl pentane, and 2-methyl-1-butene (Yáñez-Serrano et al., 2016). Additionally, all alkenes with a methyl/ethyl group on the same side of the olefin bond are possible precursors of MEK (Singh et al., 2004). Butane was not expected to be abundant in the rainforest environment, due to its anthropogenic sources, and butane oxidation would also yield butanal, which was only detected below the LOD. As for acetone, the vertical distribution and correlations discussed above suggest more short-lived precursors of MEK than alkanes.

Rapidly decreasing concentrations at 80 m at night support earlier studies, that report deposition to the canopy due to its high water solubility (Yáñez-Serrano et al., 2016) (Table 3.2).

Methyl vinyl ketone and methacrolein/2-butenal

The main source of both carbonyls, MVK, and methacrolein is the oxidation of isoprene by OH. Thus, they are summarized in one section. It has been shown previously that methacrolein is detected together with 2-butenal (Koss et al., 2016), which is also found in vegetation emission studies, albeit in small concentrations (Isidorov et al., 1985; Hellén et al., 2004). (E)-2-butenal is a signaling compound within the plant to induce a response to abiotic stress (Yamauchi et al., 2015). Its atmospheric lifetime is around 20 hours, slightly longer than the lifetimes of methacrolein and MVK of 10 and 14 hours respectively (Hellén et al., 2004; Liu et al., 2016). It is also known that MVK and methacrolein cannot be detected separately from isoprene hydroxyhydroperoxides (ISOPOOH) without using a scrubber since the hydroperoxides decompose onto that m/z. With NO^+ CIMS the fragment of 1,2-ISOPOOH and methacrolein share one m/z-ratio, while 4,3-ISOPOOH is detected together with MVK (Rivera-Rios et al., 2014). Wall exchange effects in the inlet line might have led to the removal of ISOPOOH from the sampled air due to their reduced volatility, but a contribution to the signals of MVK and methacrolein must be considered. ISOPOOH also originate from the oxidation of isoprene and are very reactive, reflected by lifetimes of 3 and 2 hours. After the initial reaction of OH and isoprene, the subsequently formed peroxy radical (RO_2) can react with NO to form MVK and methacrolein, but it can also react with HO_2 to form ISOPOOH (Liu et al., 2016). At close to pristine conditions at ATTO, NO mixing ratios are low, and the yield distribution between ISOPOOH, MVK, and methacrolein was estimated to be 50, 25, and 25 %, respectively (Rivera-Rios et al., 2014; Ringsdorf et al., 2023). It has been shown that the oxidation of isoprene can proceed already within plant tissues, by reaction with accumulated reactive oxygen species. The accumulation of reactive oxygen species, including OH, is a reaction to biotic and abiotic stresses and can exceed the antioxidant defense capacities in the tissue. The oxidation of isoprene within the tissue reduces the amount of reactive oxidized species and leads to the direct emission of its products MVK and methacrolein, especially under stress (Jardine et al., 2012b, 2013).

Another secondary source for MVK has been found in the oxidation of the monoterpene ocimene (Calogirou et al., 1999). To our knowledge, there are no other significant direct or secondary sources of MVK, methacrolein, and ISOPOOH other than the oxidation of isoprene. This explains the observed diurnal cycle with an afternoon maximum due to the light dependent emission of isoprene and the photochemical production of OH. Since isoprene is present at relatively high mixing ratios at all tree sampling heights (3.69, 3.33, 3.0 ppb at 80, 150, and 325 m in the dry season), the oxidative formation of MVK, methacrolein, and ISOPOOH takes place throughout the mixed layer. The observed slightly increasing mixing ratios of MVK with height are consistent with fast isoprene oxidation above the canopy, slower removal of MVK itself, and turbulent in-mixing of cleaner air from above. Isoprene has an estimated atmospheric lifetime of about 3 hours, and it was previously reported that only circa 10 % of emitted isoprene was oxidized within the canopy (Karl et al., 2004). Unlike MVK, methacrolein and 2-butenal show a slightly decreasing vertical gradient. Sources and sinks of MVK and methacrolein are very closely related, even considering a contribution of ISOPOOH, so the presence of significant quantities of 2-butanal is the most likely explanation for that difference.

Dry deposition to leaf surfaces has been observed in a previous study for the sum of MVK and methacrolein, and individually during daytime (Nguyen et al., 2015; Tani et al., 2010). The uptake by leaves

represents a significant sink that exceeds loss via OH oxidation near leaves (Tani et al., 2010). In this study, the fast decrease of nocturnal concentrations at 80 m indicated also deposition at night.

MVK and methacrolein + 2-butenal showed similar mixing ratios in the dry season of 607, 599, 659 ppt MVK and 679, 644, 644 ppt methacrolein + 2-butenal. It has to be considered that the uncertainty of MVK mixing ratios is higher due to their k-rate based calculation rather than calibration to a gas standard. In the transition season, methacrolein + 2-butenal (415, 425, 439 ppt) exceeded the mixing ratios of MVK (184, 229, 265 ppt). Whether that resulted from a high seasonal variability of 2-butanal or from the contribution of ISOPOOH, unfortunately, remains unclear. Lower levels of all isoprene oxidation products were expected as a result of lower isoprene mixing ratios and photo-oxidation rates in the transition season.

Sum of C_5 ketones

The mixing ratios obtained for the sum of C_5 ketones were 11, 9, and 9 ppt in the transition season and slightly higher 14, 8, and 7 ppt (80, 150, 325 m) in the dry season. A diurnal cycle was observed at 80 m only, whereas levels at 150 and 325 m were similar and showed no trend throughout day and night. C_5 ketones were 2- and 3- pentanone as well as 3-methyl-2-butanone. The atmospheric lifetime of 2-pentanone is in the range of 5 days. All three ketones have been measured in emission inventories from plants (Isidorov et al., 1985; König et al., 1995; Kesselmeier and Staudt, 1999), but there is little information on metabolic pathways or mechanisms. 2-pentanone has been identified as a marker for fungal activity in indoor environments (Kalalian et al., 2020) since it is produced in the hyphae of Aspergillus niger (Lewis, 1970), a fungi that was also found to degrade biomass in the Amazon. 3-pentanone is one of the C_5 green leaf volatiles (GLV), emitted at lower rates than C_6 GLV, which are described in the next section (Jardine et al., 2012a). An increase of 3-pentanone coincident with high temperatures after noon was observed at another measurement station in the Amazon rainforest, with a simultaneous decrease of terpenoid emissions (Jardine et al., 2015). Consistent with this observation, in this study, the correlation of C_5 ketones with isoprene or monoterpenes was low in the transition and the dry season during daytime ($p < 0.39$). The best correlations for C_5-ketones were obtained with acetone and MEK of $0.53 < p < 0.6$. This was most likely a consequence of common sources, including primary emission and formation from rather short-lived hydrocarbons, and of the long atmospheric lifetimes relative to mixing timescales, which the observed ketones have in common. Above the height of 150 m, no diurnal variability was observed, also in agreement with the other ketones, suggesting they were well mixed above the Amazonian roughness sublayer.

Fumigation experiments with different VOC have shown a loss of all three C_5-ketones on leaf surfaces (Tani and Hewitt, 2009). A decrease of the mixing ratios at 80 m could be observed at nighttime and a high water solubility of the ketones indicated a high loss rate, but the signal was too noisy to draw loss rates from the data.

C_5-aldehydes, which were usually detected together with the C_5-ketones exhibited lower mixing ratios, especially in the dry season. Overall, the mixing ratios were below their LOD and thus not investigated in detail. However, a diurnal and vertical pattern of C_5-aldehydes with different vertical and diurnal variabilities to that of the C_5-ketones was still apparent.

n-hexanal/hexenols and hexenals

C_6-aldehydes, namely n-hexanal, Z-2-hexenal, Z-3-hexenal, E-2-hexenal, and E-3-hexenal, together with C_6-alcolhols and esters form the group that is often termed green leaf volatiles (GLV). Although different temporal variabilities were observed for n-hexanal/hexenols and hexenals, they are discussed in one section due to their common sources.

In the chloroplasts of almost all green plants, GLV are synthesized from fatty acids as part of the oxylipin pathway. Their emission results from wounding or mechanical damage, from abiotic factors (such as winds) or herbivore and pathogen attack (Scala et al., 2013). The amount of GLV emitted from corn plants has been shown to depend on soil water content, temperature, light, and fertilization, with a stronger emission response at higher temperatures (Gouinguené and Turlings, 2002). Furthermore, emission as a response to abiotic stress from light-dark transitions has been reported (Jardine et al., 2012a). Their production and release can be very fast, in the case of Z-3-hexenal emission begins only 1 or 2 seconds after damage (Fall et al., 1999). On one hand, GLV have antibiotic properties and protect the wounded tissue from the invasion of bacteria or other microorganisms. On the other hand, their fast production and release make them useful for intra and inter-chemical communication in plants to prime defense mechanisms. It has been found that a herbivore infested plant releases signaling compounds, like GLV to attract the predator (insects, beetles, birds, etc.) of the herbivore (Scala et al., 2013; Mumm and Dicke, 2010; Zannoni et al., 2020a). The release of GLV can happen on short timescales of minutes to hours but in case of repetitive wounding or drying of leaves, the emission can be continuous over days (Scala et al., 2013; Fall et al., 1999). The release of GLV is also caused by drought stress and GLV have been observed to increase during noon as a result of high temperatures in the Amazon forest (Jardine et al., 2015; Kesselmeier and Staudt, 1999).

It remains unclear if leaf alcohol, Z-3-hexanol, contributed to the hexanal signal. Z-3-hexanol is also a GLV and has been reported to represent a major part of the emission of many studied plants (Kesselmeier and Staudt, 1999). Its atmospheric lifetime was calculated to be 5 hours with respect to OH. Also, the less abundant isomers, such as Z-4-hexenol or E-2-hexenol, are also likely to contribute to the hexanal signal. The lifetime of n-hexanal due to photolysis and reaction with OH is about 4 hours (12 hours for oxidation by OH only), which also holds for E-2-hexenal (Jiménez et al., 2007). Z-3-hexenal has a shorter atmospheric lifetime of 3 hours (Xing et al., 2012).

At ATTO, the integrated emissions from a large uniform area were measured, which made it impossible to detect single wounding events, except for large-scale storm damage or human activities such as forest clearing. Measured mixing ratios were 15, 11, and 9 ppt in n-hexanal in the transition season and 26, 19, and 16 ppt in the dry season. Hexenals were detected at mixing ratios below LOD (6 ppt) for most parts of the day in the transition season, and 8 ppt were measured at 80 m in the dry season. Nighttime mixing ratios of hexenals at 150 and 325 m were, however, also below the LOD (6 ppt). During both measurement phases, n-hexanal was continuously present, exhibiting a distinct diurnal cycle with maximum mixing ratios in the afternoon and higher values in the dry season. Since the emission rate of damaged leaves of hexenals was found to be higher compared to n-hexanal (Fall et al., 1999), the contribution of hexanols to the signal of n-hexanal was very likely. Average daytime mixing ratios between 40 and 70 ppt have also been observed for hexanal and/or hexenols in an elevated position above the rainforest of Malaysia (Langford et al., 2010). To investigate whether the diurnal cycle results from temperature dependent emission of GLV or additional secondary formation, measurements inside the canopy are required.

Considering both, n-hexanal and hexenols, it was not surprising that a continuous decrease with height was observed throughout the day, similar to propanal and other reactive primary emissions like isoprene and monoterpenes. Correlations at 80 m with isoprene ($0.78 < p < 0.86$), monoterpenes ($0.74 < p < 0.91$), and propanal ($p = 0.88$, dry season) indicated a light or temperature driven emission or fast secondary formation close to the canopy. This correlation is interesting since GLV emissions upon biotic induced stresses such as herbivory do not necessarily follow a diel cycle. However, boundary layer dynamics might have modulated the diel cycle since mixing between the canopy and atmosphere is most efficient during daytime convective conditions. Additionally, temperature related drying of leaves could have led to the observed diel variability.

In contrast, hexenals exhibit a more pronounced seasonal variability, with very low mixing ratios, mostly below LOD, in the transition season. The correlation with isoprene and monoterpenes, in the dry season at daytime was rather low ($p = 0.71$), but highest with acetone, MEK, benzaldehyde, and ethanol ($p > 0.8$), suggesting primary and secondary sources of hexenals.

For all C_6-aldehydes investigated in this section, decreasing concentrations during nighttime on all three heights were observed in the dry season, when C_6-aldehydes mixing ratios were in general higher than in the transition season. A slightly slower decrease of 80 m mixing ratios compared to higher levels in the dry season, may indicate a continued nocturnal emission of GLV, which is plausible since production and release from mechanical wounding, stress or herbivory is possible without light (He et al., 2021).

Benzaldehyde

Average mixing ratios of benzaldehyde measured in this study are 12, 12, 12 ppt in the transition season and 11, 10, 11 ppt (80, 150, 325 m) in the dry season. No seasonal variability or vertical gradient was observed between the measurement periods.

Benzaldehyde is the lightest monoaromatic aldehyde and is formed via the oxidation of other aromatic compounds. It is a major intermediate product of the oxidation of benzyl radicals via OH and thereby of all alkyl substituted aromatic hydrocarbons (Sebbar et al., 2011). Biogenic aromatics, such as volatile benzenoids or larger molecules like lignols, are produced via the shikimate pathway by plants, an important metabolic process, but it can also be emitted by microorganisms (Ladino-Orjuela et al., 2016; Laothawornkitkul et al., 2009). The oxidation of toluene, which has been observed previously as emission from forested environments and from farm crops (Heiden et al., 1999), yields benzaldehyde as a product (6 %) (Atkinson and Arey, 2003). It is also a benzyl alcohol oxidation product, which has been reported previously to be emitted from biogenic sources (Bernard et al., 2013). Benzaldehyde is very reactive with a calculated atmospheric lifetime primarily determined by photolysis of 2.4 hours (Cabrera-Perez et al., 2016) (1.7 days with respect to OH).

Primary emission of benzaldehyde from vegetation has been reported for grass (Kirstine et al., 1998) and elevated concentrations under and within the canopy of the Amazon rainforest were measured (Kesselmeier et al., 2000). The high mixing ratios (about 300 ppt) found at the ground were suspected to result from the decomposition of biomass, specifically the decomposition of lignols within the litter. In that particular study, the mixing ratios above the canopy were much lower than those measured at ground level.

The apparent light or temperature driven diurnal cycle of benzaldehyde suggests secondary photochemical production from aromatic hydrocarbons, as the shikimate pathway is independent of light (Jan et al., 2021). The atmospheric lifetime of precursor aromatics is in the range of days to weeks (Altshuller, 1991). Secondary production from long-lived precursors is a feasible explanation for the missing vertical variability of the very reactive benzaldehyde in the first 325 m of the mixed layer. The rather slow secondary production throughout the mixed layer possibly compensated for the expected loss through oxidation and dilutive mixing. Mixing ratios observed at 80 m were only slightly more abundant in the dry season compared to higher altitudes, which could mean a stronger contribution of benzaldehyde emissions. However, the narrow vertical benzaldehyde distribution points towards well mixed conditions of aromatic precursor hydrocarbons. Daytime mixing ratios of carbonyls that are suspected to be formed predominantly due to photochemical formation, namely acetic acid, $C_5H_4O_3$, methacrolein, MVK but also acetaldehyde and acetone correlate very well with benzaldehyde in the dry season ($0.85 > p > 0.95$). In the transition season, the correlation with the same compounds is smaller ($0.75 > p > 0.86$). Possible explanations for this difference are most likely attributed to altered sources of precursors or benzaldehyde itself due to differences in e.g. litter decomposing activities. It is important to note that the missing vertical variability could also be a sign of contamination from the measurement tower itself, e.g. through temperature dependent outgassing of its coating. However, the measurement of the fresh paint did not show elevated benzaldehyde, while the fresh anticorrosion agent emits some benzaldehyde, but at much lower rates than other VOC, e.g. toluene or xylene.

Globally, dry deposition constitutes a small sink of benzaldehyde, in the same range as oxidation by NO_3 (Cabrera-Perez et al., 2016). We observed decreasing mixing ratios at all three heights throughout the night (Table 3.2). Wet deposition and uptake to leaves might have been the dominant sink.

There is evidence that a benzaldehyde PAN can emerge when transported to high NOx regions (Caralp et al., 1999). Mixing ratios of PAN are quite high so this must be considered, but photochemical PAN creation potential is the lowest of the whole compilation (Derwent et al., 1998).

3.6 Conclusion

In this study, a PTR-ToF-MS was operated using NO^+ as the reagent ion to measure specific carbonyl compounds at three heights (80, 150, 325 m), in two seasons, and over 24 hour cycles, on the ATTO tower located in the Brazilian Amazon rainforest. With the more commonly used ionization method for PTR-MS involving H_3O^+ ions, aldehyde and ketone isomers were detected together at the same exact mass. This precludes the investigation of the individual species. For the first time, mixing ratios of biogenic aldehydes and ketones measured at high frequency are reported for a rainforest ecosystem. Generally, higher mixing ratios were found in the dry season. To some extent, this can be attributed to higher levels of temperature and light, which drive emissions and photochemical activity. However, since temperature and PAR were only slightly enhanced in the dry season compared to wet-to-dry transition, other aspects such as phenology (gross ecosystem productivity peaking in the dry season) and contribution of long-lived species from aged biomass burning plumes are of importance. Ketones have atmospheric lifetimes (days to weeks) that are much longer than the vertical mixing times (15-60 min) (Ringsdorf et al., 2023). Such compounds can be therefore expected to be also present above the lowermost mixing layer (ABL) in the residual layer and free troposphere. Interestingly, elevated mixing ratios of ketones in the roughness

sublayer observed at 80 m by day suggest a large source at canopy level or just above. At night, the loss of these species indicates a rapid deposition to the canopy. The correlations shown in Figures 3.3-3.4 reveal seasonal differences in the partitioning of primary emission from the canopy and the rate of fast secondary production above the canopy. The most abundant individually measured carbonyls in this study were acetaldehyde and acetone, both effective PAN precursors, followed by isoprene oxidation products and propanal. Note that formaldehyde was not detected by the applied method. The shorter-lived, longer-chain aldehydes observed in this study showed great variation; exhibiting both increasing and decreasing vertical gradients, that vary considerably in strength. All carbonyl compounds showed a distinct diurnal cycle which followed the evolution of light and temperature during the day and for most compounds a decrease during the night driven in part by reaction with NO_3 but more importantly by deposition to plant tissues, as it has been shown by flux measurements for some few oxygenated species before (Karl et al., 2004). The nocturnal uptake of these carbonyl compounds is an important aspect of their local to regional scale budget. Based on this data, we hypothesize that the ecosystem can more efficiently produce reduced species such as isoprene and monoterpenes, but more efficiently utilize the oxygenated products of these precursors. The importance of uptake followed by metabolization or storage, especially for oxygenated BVOC has been stressed already in the context of bidirectional exchange of BVOC by Niinemets et al. (2014). This would imply that the rainforest exploits the atmospheric oxidation to convert products into more useful, metabolizable forms. Similar preferences of the uptake of oxygenated species over terpenes have been reported for epiphytes such as lichen and moss (Edtbauer et al., 2021). This idea can serve as the basis hypothesis for future plant experiments and the observed loss rates of carbonyl species can help to constrain turbulence resolving canopy exchange models. Overall, we need to improve our understanding of the complexity of biological production and consumption and invest into investigations of primary emissions on a leaf or branch level.

Butanal, and carbonyls higher than C_7 were found to be minor components of the rainforest atmosphere, as well as the alkanes isopentane, methylcyclopentane, sum of 2- and 3-methylpentane and C_7 cyclic alkanes. The ratio of the aldehydes propanal and acetaldehyde, which have comparable atmospheric lifetimes and were shown to correlate very well in previous studies, was found to be much higher with 1:4.2 and 1:7.2 in the transition and dry season at 80 m compared to the global average ratio of 1:3 (Singh et al., 2004), due to the overwhelming predominance of biogenic sources and precursors in the rainforest.

This application of the NO^+ CIMS method has enabled the study of the individual carbonyls not accessible by the H_3O^+ based method. We, therefore, recommend periodic switching of the reagents used in order to track biogenic emissions more specifically. This would complement long term measurements conducted using the H_3O^+ ionization method.

3.7 References

Altshuller, A. P.: Chemical reactions and transport of alkanes and their products in the troposphere, J. Atmospheric Chem., 12, 19–61, https://doi.org/10.1007/BF00053933, 1991.

Andreae, M. O.: Emission of trace gases and aerosols from biomass burning – an updated assessment, Atmospheric Chem. Phys., 19, 8523–8546, https://doi.org/10.5194/acp-19-8523-2019, 2019.

Andreae, M. O. and Merlet, P.: Emission of trace gases and aerosols from biomass burning, Glob. Biogeochem. Cycles, 15, 955–966, https://doi.org/10.1029/2000GB001382, 2001.

Andreae, M. O., Artaxo, P., Brandão, C., Carswell, F. E., Ciccioli, P., da Costa, A. L., Culf, A. D., Esteves, J. L., Gash, J. H. C., Grace, J., Kabat, P., Lelieveld, J., Malhi, Y., Manzi, A. O., Meixner, F. X., Nobre, A. D., Nobre, C., Ruivo, M. d. L. P., Silva-Dias, M. A., Stefani, P., Valentini, R., von Jouanne, J., and Waterloo, M. J.: Biogeochemical cycling of carbon, water, energy, trace gases, and aerosols in Amazonia: The LBA-EUSTACH experiments, J. Geophys. Res. Atmospheres, 107, LBA 33-1-LBA 33-25, https://doi.org/10.1029/2001JD000524, 2002.

Andreae, M. O., Acevedo, O. C., Araùjo, A., Artaxo, P., Barbosa, C. G. G., Barbosa, H. M. J., Brito, J., Carbone, S., Chi, X., Cintra, B. B. L., da Silva, N. F., Dias, N. L., Dias-Júnior, C. Q., Ditas, F., Ditz, R., Godoi, A. F. L., Godoi, R. H. M., Heimann, M., Hoffmann, T., Kesselmeier, J., Könemann, T., Krüger, M. L., Lavric, J. V., Manzi, A. O., Lopes, A. P., Martins, D. L., Mikhailov, E. F., Moran-Zuloaga, D., Nelson, B. W., Nölscher, A. C., Santos Nogueira, D., Piedade, M. T. F., Pöhlker, C., Pöschl, U., Quesada, C. A., Rizzo, L. V., Ro, C.-U., Ruckteschler, N., Sá, L. D. A., de Oliveira Sá, M., Sales, C. B., dos Santos, R. M. N., Saturno, J., Schöngart, J., Sörgel, M., de Souza, C. M., de Souza, R. A. F., Su, H., Targhetta, N., Tóta, J., Trebs, I., Trumbore, S., van Eijck, A., Walter, D., Wang, Z., Weber, B., Williams, J., Winderlich, J., Wittmann, F., Wolff, S., and Yáñez-Serrano, A. M.: The Amazon Tall Tower Observatory (ATTO): overview of pilot measurements on ecosystem ecology, meteorology, trace gases, and aerosols, Atmospheric Chem. Phys., 15, 10723–10776, https://doi.org/10.5194/acp-15-10723-2015, 2015.

Atkinson, R. and Arey, J.: Atmospheric Degradation of Volatile Organic Compounds, Chem. Rev., 103, 4605–4638, https://doi.org/10.1021/cr0206420, 2003.

Atkinson, R., Tuazon, E. C., and Aschmann, S. M.: Atmospheric Chemistry of 2-Pentanone and 2-Heptanone, Environ. Sci. Technol., 34, 623–631, https://doi.org/10.1021/es9909374, 2000.

Bernard, F., Magneron, I., Eyglunent, G., Daële, V., Wallington, T. J., Hurley, M. D., and Mellouki, A.: Atmospheric Chemistry of Benzyl Alcohol: Kinetics and Mechanism of Reaction with OH Radicals, Environ. Sci. Technol., 47, 3182–3189, https://doi.org/10.1021/es304600z, 2013.

Bond, D. W., Steiger, S., Zhang, R., Tie, X., and Orville, R. E.: The importance of NOx production by lightning in the tropics, Atmos. Environ., 36, 1509–1519, https://doi.org/10.1016/S1352-2310(01)00553-2, 2002.

Bracho-Nunez, A., Knothe, N. M., Costa, W. R., Maria Astrid, L. R., Kleiss, B., Rottenberger, S., Piedade, M. T. F., and Kesselmeier, J.: Root anoxia effects on physiology and emissions of volatile organic compounds (VOC) under short- and long-term inundation of trees from Amazonian floodplains, SpringerPlus, 1, 9, https://doi.org/10.1186/2193-1801-1-9, 2012.

Breuninger, C., Meixner, F. X., and Kesselmeier, J.: Field investigations of nitrogen dioxide (NO_2) exchange between plants and the atmosphere, Atmospheric Chem. Phys., 13, 773–790, https://doi.org/10.5194/acp-13-773-2013, 2013.

Brown, S. S. and Stutz, J.: Nighttime radical observations and chemistry, Chem. Soc. Rev., 41, 6405, https://doi.org/10.1039/c2cs35181a, 2012.

Cabrera-Perez, D., Taraborrelli, D., Sander, R., and Pozzer, A.: Global atmospheric budget of simple monocyclic aromatic compounds, Atmospheric Chem. Phys., 16, 6931–6947, https://doi.org/10.5194/acp-16-6931-2016, 2016.

Calogirou, A., Larsen, B. R., and Kotzias, D.: Gas-phase terpene oxidation products: a review, Atmos. Environ., 33, 1423–1439, https://doi.org/10.1016/S1352-2310(98)00277-5, 1999.

Canaval, E., Millet, D. B., Zimmer, I., Nosenko, T., Georgii, E., Partoll, E. M., Fischer, L., Alwe, H. D., Kulmala, M., Karl, T., Schnitzler, J.-P., and Hansel, A.: Rapid conversion of isoprene photooxidation products in terrestrial plants, Commun. Earth Environ., 1, 1–9, https://doi.org/10.1038/s43247-020-00041-2, 2020.

Cappellin, L., Karl, T., Probst, M., Ismailova, O., Winkler, P. M., Soukoulis, C., Aprea, E., Märk, T. D., Gasperi, F., and Biasioli, F.: On Quantitative Determination of Volatile Organic Compound Concentrations Using Proton Transfer Reaction Time-of-Flight Mass Spectrometry, Environ. Sci. Technol., 46, 2283–2290, https://doi.org/10.1021/es203985t, 2012.

Caralp, F., Foucher, V., Lesclaux, R., Wallington, T. J., and Hurley, M. D.: Atmospheric chemistry of benzaldehyde: UV absorption spectrum and reaction kinetics and mechanisms of the C6H5C(O)O2 radical, Phys. Chem. Chem. Phys., 1, 3509–3517, https://doi.org/10.1039/a903088c, 1999.

Chamecki, M., Freire, L. S., Dias, N. L., Chen, B., Dias-Junior, C. Q., Machado, L. A. T., Sörgel, M., Tsokankunku, A., and Araújo, A. C. de: Effects of Vegetation and Topography on the Boundary Layer Structure above the Amazon Forest, J. Atmospheric Sci., 77, 2941–2957, https://doi.org/10.1175/JAS-D-20-0063.1, 2020.

Chaparro-Suarez, I. G., Meixner, F. X., and Kesselmeier, J.: Nitrogen dioxide (NO2) uptake by vegetation controlled by atmospheric concentrations and plant stomatal aperture, Atmos. Environ., 45, 5742–5750, https://doi.org/10.1016/j.atmosenv.2011.07.021, 2011.

Chen, Y., Yuan, B., Wang, C., Wang, S., He, X., Wu, C., Song, X., Huangfu, Y., Li, X.-B., Liao, Y., and Shao, M.: Online measurements of cycloalkanes based on NO^+ chemical ionization in proton transfer reaction time-of-flight mass spectrometry (PTR-ToF-MS), Atmospheric Meas. Tech., 15, 6935–6947, https://doi.org/10.5194/amt-15-6935-2022, 2022.

Chevuturi, A., Klingaman, N. P., Rudorff, C. M., Coelho, C. A. S., and Schöngart, J.: Forecasting annual maximum water level for the Negro River at Manaus, Clim. Resil. Sustain., 1, e18, https://doi.org/10.1002/cli2.18, 2022.

Ciccioli, P., Silibello, C., Finardi, S., Pepe, N., Ciccioli, P., Rapparini, F., Neri, L., Fares, S., Brilli, F., Mircea, M., Magliulo, E., and Baraldi, R.: The potential impact of biogenic volatile organic compounds (BVOCs) from terrestrial vegetation on a Mediterranean area using two different emission models, Agric. For. Meteorol., 328, 109255, https://doi.org/10.1016/j.agrformet.2022.109255, 2023.

Deming, B. L., Pagonis, D., Liu, X., Day, D. A., Talukdar, R., Krechmer, J. E., de Gouw, J. A., Jimenez, J. L., and Ziemann, P. J.: Measurements of delays of gas-phase compounds in a wide variety of tubing materials due to gas–wall interactions, Atmospheric Meas. Tech., 12, 3453–3461, https://doi.org/10.5194/amt-12-3453-2019, 2019.

Derwent, R. G., Jenkin, M. E., Saunders, S. M., and Pilling, M. J.: Photochemical ozone creation potentials for organic compounds in northwest Europe calculated with a master chemical mechanism, Atmos. Environ., 32, 2429–2441, https://doi.org/10.1016/S1352-2310(98)00053-3, 1998.

Edtbauer, A., Pfannerstill, E. Y., Pires Florentino, A. P., Barbosa, C. G. G., Rodriguez-Caballero, E., Zannoni, N., Alves, R. P., Wolff, S., Tsokankunku, A., Aptroot, A., de Oliveira Sá, M., de Araújo, A. C., Sörgel, M., de Oliveira, S. M., Weber, B., and Williams, J.: Cryptogamic organisms are a substantial source and sink for volatile organic compounds in the Amazon region, Commun. Earth Environ., 2, 1–14, https://doi.org/10.1038/s43247-021-00328-y, 2021.

Ernle, L., Wang, N., Bekö, G., Morrison, G., Wargocki, P., J. Weschler, C., and Williams, J.: Assessment of aldehyde contributions to PTR-MS m / z 69.07 in indoor air measurements, Environ. Sci. Atmospheres, 3, 1286–1295, https://doi.org/10.1039/D3EA00055A, 2023.

Fall, R.: Abundant Oxygenates in the Atmosphere: A Biochemical Perspective, Chem. Rev., 103, 4941–4952, https://doi.org/10.1021/cr0206521, 2003.

Fall, R., Karl, T., Hansel, A., Jordan, A., and Lindinger, W.: Volatile organic compounds emitted after leaf wounding: On-line analysis by proton-transfer-reaction mass spectrometry, J. Geophys. Res. Atmospheres, 104, 15963–15974, https://doi.org/10.1029/1999JD900144, 1999.

Fischer, E. V., Jacob, D. J., Yantosca, R. M., Sulprizio, M. P., Millet, D. B., Mao, J., Paulot, F., Singh, H. B., Roiger, A., Ries, L., Talbot, R. W., Dzepina, K., and Pandey Deolal, S.: Atmospheric peroxyacetyl nitrate (PAN): a global budget and source attribution, Atmospheric Chem. Phys., 14, 2679–2698, https://doi.org/10.5194/acp-14-2679-2014, 2014.

Fruekilde, P., Hjorth, J., Jensen, N. R., Kotzias, D., and Larsen, B.: OZONOLYSIS AT VEGETATION SURFACES: A SOURCE OF ACETONE, 4-OXOPENTANAL, 6-METHYL-5-HEPTEN-2-ONE, AND GERANYL ACETONE IN THE TROPOSPHERE, Atmos. Environ., Vol. 32, No. 11, 1893–1902, 1998.

Fuentes, J. D., Gerken, T., Chamecki, M., Stoy, P., Freire, L., and Ruiz-Plancarte, J.: Turbulent transport and reactions of plant-emitted hydrocarbons in an Amazonian rain forest, Atmos. Environ., 279, 119094, https://doi.org/10.1016/j.atmosenv.2022.119094, 2022.

Gouinguené, S. P. and Turlings, T. C. J.: The Effects of Abiotic Factors on Induced Volatile Emissions in Corn Plants, Plant Physiol., 129, 1296–1307, https://doi.org/10.1104/pp.001941, 2002.

de Gouw, J. and Warneke, C.: Measurements of volatile organic compounds in the earth's atmosphere using proton-transfer-reaction mass spectrometry, Mass Spectrom. Rev., 26, 223–257, https://doi.org/10.1002/mas.20119, 2007.

Guenther, A.: Natural emissions of non-methane volatile organic compounds, carbon monoxide, and oxides of nitrogen from North America, Atmos. Environ., 34, 2205–2230, https://doi.org/10.1016/S1352-2310(99)00465-3, 2000.

Guenther, A.: Biological and Chemical Diversity of Biogenic Volatile Organic Emissions into the Atmosphere, Int. Sch. Res. Not., 2013, e786290, https://doi.org/10.1155/2013/786290, 2013.

Guimbaud, C., Catoire, V., Bergeat, A., Michel, E., Schoon, N., Amelynck, C., Labonnette, D., and Poulet, G.: Kinetics of the reactions of acetone and glyoxal with O2+ and NO+ ions and application to the detection of oxygenated volatile organic compounds in the atmosphere by chemical ionization mass spectrometry, Int. J. Mass Spectrom., 263, 276–288, https://doi.org/10.1016/j.ijms.2007.03.006, 2007.

He, J., Halitschke, R., Schuman, M. C., and Baldwin, I. T.: Light dominates the diurnal emissions of herbivore-induced volatiles in wild tobacco, BMC Plant Biol., 21, 401, https://doi.org/10.1186/s12870-021-03179-z, 2021.

Heiden, A. C., Kobel, K., Komenda, M., Koppmann, R., Shao, M., and Wildt, J.: Toluene emissions from plants, Geophys. Res. Lett., 26, 1283–1286, https://doi.org/10.1029/1999GL900220, 1999.

Hellén, H., Hakola, H., Reissell, A., and Ruuskanen, T. M.: Carbonyl compounds in boreal coniferous forest air in Hyytiälä, Southern Finland, Atmospheric Chem. Phys., 4, 1771–1780, https://doi.org/10.5194/acp-4-1771-2004, 2004.

Holanda, B. A., Pöhlker, M. L., Walter, D., Saturno, J., Sörgel, M., Ditas, J., Ditas, F., Schulz, C., Franco, M. A., Wang, Q., Donth, T., Artaxo, P., Barbosa, H. M. J., Borrmann, S., Braga, R., Brito, J., Cheng, Y., Dollner, M., Kaiser, J. W., Klimach,

T., Knote, C., Krüger, O. O., Fütterer, D., Lavrič, J. V., Ma, N., Machado, L. A. T., Ming, J., Morais, F. G., Paulsen, H., Sauer, D., Schlager, H., Schneider, J., Su, H., Weinzierl, B., Walser, A., Wendisch, M., Ziereis, H., Zöger, M., Pöschl, U., Andreae, M. O., and Pöhlker, C.: Influx of African biomass burning aerosol during the Amazonian dry season through layered transatlantic transport of black carbon-rich smoke, Atmospheric Chem. Phys., 20, 4757–4785, https://doi.org/10.5194/acp-20-4757-2020, 2020.

Holzinger, R., Sandoval-Soto, L., Rottenberger, S., Crutzen, P. J., and Kesselmeier, J.: Emissions of volatile organic compounds from Quercus ilex L. measured by Proton Transfer Reaction Mass Spectrometry under different environmental conditions, J. Geophys. Res. Atmospheres, 105, 20573–20579, https://doi.org/10.1029/2000JD900296, 2000.

Holzinger, R., Lee, A., Paw, K. T., and Goldstein, U. a. H.: Observations of oxidation products above a forest imply biogenic emissions of very reactive compounds, Atmospheric Chem. Phys., 5, 67–75, https://doi.org/10.5194/acp-5-67-2005, 2005.

Hunter, E. P. L. and Lias, S. G.: Evaluated Gas Phase Basicities and Proton Affinities of Molecules: An Update, J. Phys. Chem. Ref. Data, 27, 413–656, https://doi.org/10.1063/1.556018, 1998.

Isidorov, V. A., Zenkevich, I. G., and Ioffe, B. V.: Volatile organic compounds in the atmosphere of forests, Atmospheric Environ. 1967, 19, 1–8, https://doi.org/10.1016/0004-6981(85)90131-3, 1985.

Jacob, D. J., Field, B. D., Jin, E. M., Bey, I., Li, Q., Logan, J. A., Yantosca, R. M., and Singh, H. B.: Atmospheric budget of acetone, J. Geophys. Res. Atmospheres, 107, ACH 5-1-ACH 5-17, https://doi.org/10.1029/2001JD000694, 2002.

Jan, R., Asaf, S., Numan, M., Lubna, and Kim, K.-M.: Plant Secondary Metabolite Biosynthesis and Transcriptional Regulation in Response to Biotic and Abiotic Stress Conditions, Agronomy, 11, 968, https://doi.org/10.3390/agronomy11050968, 2021.

Jardine, K., Barron-Gafford, G. A., Norman, J. P., Abrell, L., Monson, R. K., Meyers, K. T., Pavao-Zuckerman, M., Dontsova, K., Kleist, E., Werner, C., and Huxman, T. E.: Green leaf volatiles and oxygenated metabolite emission bursts from mesquite branches following light–dark transitions, Photosynth. Res., 113, 321–333, https://doi.org/10.1007/s11120-012-9746-5, 2012a.

Jardine, K. J., Monson, R. K., Abrell, L., Saleska, S. R., Arneth, A., Jardine, A., Ishida, F. Y., Serrano, A. M. Y., Artaxo, P., Karl, T., Fares, S., Goldstein, A., Loreto, F., and Huxman, T.: Within-plant isoprene oxidation confirmed by direct emissions of oxidation products methyl vinyl ketone and methacrolein, Glob. Change Biol., 18, 973–984, https://doi.org/10.1111/j.1365-2486.2011.02610.x, 2012b.

Jardine, K. J., Meyers, K., Abrell, L., Alves, E. G., Yanez Serrano, A. M., Kesselmeier, J., Karl, T., Guenther, A., Vickers, C., and Chambers, J. Q.: Emissions of putative isoprene oxidation products from mango branches under abiotic stress, J. Exp. Bot., 64, 3669–3679, https://doi.org/10.1093/jxb/ert202, 2013.

Jardine, K. J., Chambers, J. Q., Holm, J., Jardine, A. B., Fontes, C. G., Zorzanelli, R. F., Meyers, K. T., De Souza, V. F., Garcia, S., Gimenez, B. O., Piva, L. R. de O., Higuchi, N., Artaxo, P., Martin, S., and Manzi, A. O.: Green Leaf Volatile Emissions during High Temperature and Drought Stress in a Central Amazon Rainforest, Plants, 4, 678–690, https://doi.org/10.3390/plants4030678, 2015.

Jiménez, E., Lanza, B., Martínez, E., and Albaladejo, J.: Daytime tropospheric loss of hexanal and <I>trans</I>-2-hexenal: OH kinetics and UV photolysis, Atmospheric Chem. Phys., 7, 1565–1574, https://doi.org/10.5194/acp-7-1565-2007, 2007.

Jordan, A., Haidacher, S., Hanel, G., Hartungen, E., Märk, L., Seehauser, H., Schottkowsky, R., Sulzer, P., and Märk, T. D.: A high resolution and high sensitivity proton-transfer-reaction time-of-flight mass spectrometer (PTR-TOF-MS), Int. J. Mass Spectrom., 286, 122–128, https://doi.org/10.1016/j.ijms.2009.07.005, 2009.

Jordi Vilà-Guerau de Arellano, C. C. van H., Bart J. H. van Stratum, and Kees van den Dries: Atmospheric Boundary Layer, Cambridge University Press, 2015.

Kalalian, C., Abis, L., Depoorter, A., Lunardelli, B., Perrier, S., and George, C.: Influence of indoor chemistry on the emission of mVOCs from Aspergillus niger molds, Sci. Total Environ., 741, 140148, https://doi.org/10.1016/j.scitotenv.2020.140148, 2020.

Karl, T., Guenther, A., Spirig, C., Hansel, A., and Fall, R.: Seasonal variation of biogenic VOC emissions above a mixed hardwood forest in northern Michigan, Geophys. Res. Lett., 30, https://doi.org/10.1029/2003GL018432, 2003.

Karl, T., Potosnak, M., Guenther, A., Clark, D., Walker, J., Herrick, J. D., and Geron, C.: Exchange processes of volatile organic compounds above a tropical rain forest: Implications for modeling tropospheric chemistry above dense vegetation, J. Geophys. Res. Atmospheres, 109, https://doi.org/10.1029/2004JD004738, 2004.

Karl, T., Hansel, A., Cappellin, L., Kaser, L., Herdlinger-Blatt, I., and Jud, W.: Selective measurements of isoprene and 2-methyl-3-buten-2-ol based on NO⁺ ionization mass spectrometry, Atmospheric Chem. Phys., 12, 11877–11884, https://doi.org/10.5194/acp-12-11877-2012, 2012.

Kesselmeier, J.: Exchange of Short-Chain Oxygenated Volatile Organic Compounds (VOCs) between Plants and the Atmosphere: A Compilation of Field and Laboratory Studies, J. Atmospheric Chem., 39, 219–233, https://doi.org/10.1023/A:1010632302076, 2001.

Kesselmeier, J. and Staudt, M.: Biogenic Volatile Organic Compounds (VOC): An Overview on Emission, Physiology and Ecology, J. Atmospheric Chem., 33, 23–88, https://doi.org/10.1023/A:1006127516791, 1999.

Kesselmeier, J., Bode, K., Hofmann, U., Müller, H., Schäfer, L., Wolf, A., Ciccioli, P., Brancaleoni, E., Cecinato, A., Frattoni, M., Foster, P., Ferrari, C., Jacob, V., Fugit, J. L., Dutaur, L., Simon, V., and Torres, L.: Emission of short chained organic acids, aldehydes and monoterpenes from Quercus ilex L. and Pinus pinea L. in relation to physiological activities, carbon budget and emission algorithms, Atmos. Environ., 31, 119–133, https://doi.org/10.1016/S1352-2310(97)00079-4, 1997.

Kesselmeier, J., Kuhn, U., Wolf, A., Andreae, M. O., Ciccioli, P., Brancaleoni, E., Frattoni, M., Guenther, A., Greenberg, J., De Castro Vasconcellos, P., de Oliva, T., Tavares, T., and Artaxo, P.: Atmospheric volatile organic compounds (VOC) at a remote tropical forest site in central Amazonia, Atmos. Environ., 34, 4063–4072, https://doi.org/10.1016/S1352-2310(00)00186-2, 2000.

Khan, M. A. H., Cooke, M. C., Utembe, S. R., Archibald, A. T., Derwent, R. G., Xiao, P., Percival, C. J., Jenkin, M. E., Morris, W. C., and Shallcross, D. E.: Global modeling of the nitrate radical (NO3) for present and pre-industrial scenarios, Atmospheric Res., 164–165, 347–357, https://doi.org/10.1016/j.atmosres.2015.06.006, 2015.

Kirstine, W., Galbally, I., Ye, Y., and Hooper, M.: Emissions of volatile organic compounds (primarily oxygenated species) from pasture, J. Geophys. Res. Atmospheres, 103, 10605–10619, https://doi.org/10.1029/97JD03753, 1998.

Kirstine, W. V. and Galbally, I. E.: The global atmospheric budget of ethanol revisited, Atmospheric Chem. Phys., 12, 545–555, https://doi.org/10.5194/acp-12-545-2012, 2012.

König, G., Brunda, M., Puxbaum, H., Hewitt, C. N., Duckham, S. C., and Rudolph, J.: Relative contribution of oxygenated hydrocarbons to the total biogenic VOC emissions of selected mid-European agricultural and natural plant species, Atmos. Environ., 29, 861–874, https://doi.org/10.1016/1352-2310(95)00026-U, 1995.

Koss, A. R., Warneke, C., Yuan, B., Coggon, M. M., Veres, P. R., and de Gouw, J. A.: Evaluation of NO⁺ reagent ion chemistry for online measurements ofatmospheric volatile organic compounds, Atmospheric Meas. Tech., 9, 2909–2925, https://doi.org/10.5194/amt-9-2909-2016, 2016.

Kreuzwieser, J., Kühnemann, F., Martis, A., Rennenberg, H., and Urban, W.: Diurnal pattern of acetaldehyde emission by flooded poplar trees, Physiol. Plant., 108, 79–86, https://doi.org/10.1034/j.1399-3054.2000.108001079.x, 2000.

Kuhn, U., Rottenberger, S., Biesenthal, T., Wolf, A., Schebeske, G., Ciccioli, P., Brancaleoni, E., Frattoni, M., Tavares, T. M., and Kesselmeier, J.: Seasonal differences in isoprene and light-dependent monoterpene emission by Amazonian tree species, Glob. Change Biol., 10, 663–682, https://doi.org/10.1111/j.1529-8817.2003.00771.x, 2004a.

Kuhn, U., Rottenberger, S., Biesenthal, T., Wolf, A., Schebeske, G., Ciccioli, P., and Kesselmeier, J.: Strong correlation between isoprene emission and gross photosynthetic capacity during leaf phenology of the tropical tree species Hymenaea courbaril with fundamental changes in volatile organic compounds emission composition during early leaf development, Plant Cell Environ., 27, 1469–1485, https://doi.org/10.1111/j.1365-3040.2004.01252.x, 2004b.

Kuhn, U., Andreae, M. O., Ammann, C., Araújo, A. C., Brancaleoni, E., Ciccioli, P., Dindorf, T., Frattoni, M., Gatti, L. V., Ganzeveld, L., Kruijt, B., Lelieveld, J., Lloyd, J., Meixner, F. X., Nobre, A. D., Pöschl, U., Spirig, C., Stefani, P., Thielmann, A., Valentini, R., and Kesselmeier, J.: Isoprene and monoterpene fluxes from Central Amazonian rainforest inferred from tower-based and airborne measurements, and implications on the atmospheric chemistry and the local carbon budget, Atmospheric Chem. Phys., 7, 2855–2879, https://doi.org/10.5194/acp-7-2855-2007, 2007.

Ladino-Orjuela, G., Gomes, E., da Silva, R., Salt, C., and Parsons, J. R.: Metabolic Pathways for Degradation of Aromatic Hydrocarbons by Bacteria, in: Reviews of Environmental Contamination and Toxicology Volume 237, vol. 237, edited by: de Voogt, W. P., Springer International Publishing, Cham, 105–121, https://doi.org/10.1007/978-3-319-23573-8_5, 2016.

Langford, B., Misztal, P. K., Nemitz, E., Davison, B., Helfter, C., Pugh, T. a. M., MacKenzie, A. R., Lim, S. F., and Hewitt, C. N.: Fluxes and concentrations of volatile organic compounds from a South-East Asian tropical rainforest, Atmospheric Chem. Phys., 10, 8391–8412, https://doi.org/10.5194/acp-10-8391-2010, 2010.

Laothawornkitkul, J., Taylor, J. E., Paul, N. D., and Hewitt, C. N.: Biogenic volatile organic compounds in the Earth system, New Phytol., 183, 27–51, https://doi.org/10.1111/j.1469-8137.2009.02859.x, 2009.

Lary, D. J. and Shallcross, D. E.: Central role of carbonyl compounds in atmospheric chemistry, J. Geophys. Res. Atmospheres, 105, 19771–19778, https://doi.org/10.1029/1999JD901184, 2000.

Lelieveld, J., Gromov, S., Pozzer, A., and Taraborrelli, D.: Global tropospheric hydroxyl distribution, budget and reactivity, Atmospheric Chem. Phys., 16, 12477–12493, https://doi.org/10.5194/acp-16-12477-2016, 2016.

Lewis, H. L.: Caproic Acid Metabolism and the Production of 2-Pentanone and Gluconic Acid by Aspergillus niger, Microbiology, 63, 203–210, https://doi.org/10.1099/00221287-63-2-203, 1970.

Li, X.-B., Zhang, C., Liu, A., Yuan, B., Yang, H., Liu, C., Wang, S., Huangfu, Y., Qi, J., Liu, Z., He, X., Song, X., Chen, Y., Peng, Y., Zhang, X., Zheng, E., Yang, L., Yang, Q., Qin, G., Zhou, J., and Shao, M.: Assessment of long tubing in measuring atmospheric trace gases: applications on tall towers, Environ. Sci. Atmospheres, 3, 506–520, https://doi.org/10.1039/D2EA00110A, 2023.

Liu, Q., Gao, Y., Huang, W., Ling, Z., Wang, Z., and Wang, X.: Carbonyl compounds in the atmosphere: A review of abundance, source and their contributions to O3 and SOA formation, Atmospheric Res., 274, 106184, https://doi.org/10.1016/j.atmosres.2022.106184, 2022.

Liu, Y., Brito, J., Dorris, M. R., Rivera-Rios, J. C., Seco, R., Bates, K. H., Artaxo, P., Duvoisin, S., Keutsch, F. N., Kim, S., Goldstein, A. H., Guenther, A. B., Manzi, A. O., Souza, R. A. F., Springston, S. R., Watson, T. B., McKinney, K. A., and Martin, S. T.: Isoprene photochemistry over the Amazon rainforest, Proc. Natl. Acad. Sci., 113, 6125–6130, https://doi.org/10.1073/pnas.1524136113, 2016.

Matsui, K., Sugimoto, K., Kakumyan, P., Khorobrykh, S. A., and Mano, J.: Volatile Oxylipins and Related Compounds Formed Under Stress in Plants, in: Lipidomics: Volume 2: Methods and Protocols, edited by: Armstrong, D., Humana Press, Totowa, NJ, 17–28, https://doi.org/10.1007/978-1-60761-325-1_2, 2010.

Mellouki, A., Wallington, T. J., and Chen, J.: Atmospheric Chemistry of Oxygenated Volatile Organic Compounds: Impacts on Air Quality and Climate, Chem. Rev., 115, 3984–4014, https://doi.org/10.1021/cr500549n, 2015.

Mumm, R. and Dicke, M.: Variation in natural plant products and the attraction of bodyguards involved in indirect plant defense, Can. J. Zool., 88, 628–667, https://doi.org/10.1139/Z10-032, 2010.

Nguyen, T. B., Crounse, J. D., Teng, A. P., St. Clair, J. M., Paulot, F., Wolfe, G. M., and Wennberg, P. O.: Rapid deposition of oxidized biogenic compounds to a temperate forest, Proc. Natl. Acad. Sci., 112, E392–E401, https://doi.org/10.1073/pnas.1418702112, 2015.

Niinemets, Ü., Fares, S., Harley, P., and Jardine, K. J.: Bidirectional exchange of biogenic volatiles with vegetation: emission sources, reactions, breakdown and deposition, Plant Cell Environ., 37, 1790–1809, https://doi.org/10.1111/pce.12322, 2014.

Orzechowska, G. E., Nguyen, H. T., and Paulson, S. E.: Photochemical Sources of Organic Acids. 2. Formation of C5−C9 Carboxylic Acids from Alkene Ozonolysis under Dry and Humid Conditions, J. Phys. Chem. A, 109, 5366–5375, https://doi.org/10.1021/jp050167k, 2005.

Pagonis, D., Krechmer, J. E., de Gouw, J., Jimenez, J. L., and Ziemann, P. J.: Effects of gas–wall partitioning in Teflon tubing and instrumentation on time-resolved measurements of gas-phase organic compounds, Atmospheric Meas. Tech., 10, 4687–4696, https://doi.org/10.5194/amt-10-4687-2017, 2017.

Parolin, P., De Simone, O., Haase, K., Waldhoff, D., Rottenberger, S., Kuhn, U., Kesselmeier, J., Kleiss, B., Schmidt, W., Pledade, M. T. F., and Junk, W. J.: Central Amazonian floodplain forests: Tree adaptations in a pulsing system, Bot. Rev., 70, 357–380, https://doi.org/10.1663/0006-8101(2004)070[0357:CAFFTA]2.0.CO;2, 2004.

Pfannerstill, E. Y., Reijrink, N. G., Edtbauer, A., Ringsdorf, A., Zannoni, N., Araújo, A., Ditas, F., Holanda, B. A., Sá, M. O., Tsokankunku, A., Walter, D., Wolff, S., Lavrič, J. V., Pöhlker, C., Sörgel, M., and Williams, J.: Total OH reactivity over the Amazon rainforest: variability with temperature, wind, rain, altitude, time of day, season, and an overall budget closure, Atmospheric Chem. Phys., 21, 6231–6256, https://doi.org/10.5194/acp-21-6231-2021, 2021.

Pöhlker, C., Walter, D., Paulsen, H., Könemann, T., Rodríguez-Caballero, E., Moran-Zuloaga, D., Brito, J., Carbone, S., Degrendele, C., Després, V. R., Ditas, F., Holanda, B. A., Kaiser, J. W., Lammel, G., Lavrič, J. V., Jing, M., Pickersgill, D., Pöhlker, M. L., Praß, M., Löbs, N., Saturno, J., Sörgel, M., Wang, Q., Weber, B., Wolff, S., Artaxo, P., Pöschl, U., and Andreae, M. O.: Land cover and its transformation in the backward trajectory footprint region of the Amazon Tall Tower Observatory, Atmospheric Chem. Phys., 19, 8425–8470, https://doi.org/10.5194/acp-19-8425-2019, 2019.

Prather, M. J. and Jacob, D. J.: A persistent imbalance in HOx and NOx photochemistry of the upper troposphere driven by deep tropical convection, Geophys. Res. Lett., 24, 3189–3192, https://doi.org/10.1029/97GL03027, 1997.

Restrepo-Coupe, N., da Rocha, H. R., Hutyra, L. R., da Araujo, A. C., Borma, L. S., Christoffersen, B., Cabral, O. M. R., de Camargo, P. B., Cardoso, F. L., da Costa, A. C. L., Fitzjarrald, D. R., Goulden, M. L., Kruijt, B., Maia, J. M. F., Malhi, Y. S., Manzi, A. O., Miller, S. D., Nobre, A. D., von Randow, C., Sá, L. D. A., Sakai, R. K., Tota, J., Wofsy, S. C., Zanchi, F. B., and Saleska, S. R.: What drives the seasonality of photosynthesis across the Amazon basin? A cross-site analysis of eddy flux tower measurements from the Brasil flux network, Agric. For. Meteorol., 182–183, 128–144, https://doi.org/10.1016/j.agrformet.2013.04.031, 2013.

Ringsdorf, A., Edtbauer, A., Vilà-Guerau de Arellano, J., Pfannerstill, E. Y., Gromov, S., Kumar, V., Pozzer, A., Wolff, S., Tsokankunku, A., Soergel, M., Sá, M. O., Araújo, A., Ditas, F., Poehlker, C., Lelieveld, J., and Williams, J.: Inferring the diurnal variability of OH radical concentrations over the Amazon from BVOC measurements, Sci. Rep., 13, 14900, https://doi.org/10.1038/s41598-023-41748-4, 2023.

Rivera-Rios, J. C., Nguyen, T. B., Crounse, J. D., Jud, W., St. Clair, J. M., Mikoviny, T., Gilman, J. B., Lerner, B. M., Kaiser, J. B., Gouw, J., Wisthaler, A., Hansel, A., Wennberg, P. O., Seinfeld, J. H., and Keutsch, F. N.: Conversion of hydroperoxides to carbonyls in field and laboratory instrumentation: Observational bias in diagnosing pristine versus anthropogenically controlled atmospheric chemistry, Geophys. Res. Lett., 41, 8645–8651, https://doi.org/10.1002/2014GL061919, 2014.

Roberts, J. M: PAN and Related Compounds, in: Volatile Organic Compounds in the Atmosphere, Blackwell Publishing Ltd, 2007.

Romano, A. and Hanna, G. B.: Identification and quantification of VOCs by proton transfer reaction time of flight mass spectrometry: An experimental workflow for the optimization of specificity, sensitivity, and accuracy, J. Mass Spectrom., 53, 287–295, https://doi.org/10.1002/jms.4063, 2018.

Rottenberger, S., Kuhn, U., Wolf, A., Schebeske, G., Oliva, S. T., Tavares, T. M., and Kesselmeier, J.: Exchange of Short-Chain Aldehydes Between Amazonian Vegetation and the Atmosphere, Ecol. Appl., 14, 247–262, https://doi.org/10.1890/01-6027, 2004.

Rottenberger, S., Kleiss, B., Kuhn, U., Wolf, A., Piedade, M. T. F., Junk, W., and Kesselmeier, J.: The effect of flooding on the exchange of the volatile C_2-compounds ethanol, acetaldehyde and acetic acid between leaves of Amazonian floodplain tree species and the atmosphere, Biogeosciences, 5, 1085–1100, https://doi.org/10.5194/bg-5-1085-2008, 2008.

Rummel, U., Ammann, C., Gut, A., Meixner, F. X., and Andreae, M. O.: Eddy covariance measurements of nitric oxide flux within an Amazonian rain forest, J. Geophys. Res. Atmospheres, 107, LBA 17-1-LBA 17-9, https://doi.org/10.1029/2001JD000520, 2002.

Scala, A., Allmann, S., Mirabella, R., Haring, M. A., and Schuurink, R. C.: Green Leaf Volatiles: A Plant's Multifunctional Weapon against Herbivores and Pathogens, Int. J. Mol. Sci., 14, 17781–17811, https://doi.org/10.3390/ijms140917781, 2013.

Schade, G. W. and Goldstein, A. H.: Fluxes of oxygenated volatile organic compounds from a ponderosa pine plantation, J. Geophys. Res. Atmospheres, 106, 3111–3123, https://doi.org/10.1029/2000JD900592, 2001.

Sebbar, N., Bozzelli, J. W., and Bockhorn, H.: Thermochemistry and Reaction Paths in the Oxidation Reaction of Benzoyl Radical: C6H5C•(═O), J. Phys. Chem. A, 115, 11897–11914, https://doi.org/10.1021/jp2078067, 2011.

Seco, R., Peñuelas, J., and Filella, I.: Short-chain oxygenated VOCs: Emission and uptake by plants and atmospheric sources, sinks, and concentrations, Atmos. Environ., 41, 2477–2499, https://doi.org/10.1016/j.atmosenv.2006.11.029, 2007.

Singh, H. B., Herlth, D., O'Hara, D., Salas, L., Torres, A. L., Gregory, G. L., Sachse, G. W., and Kasting, J. F.: Atmospheric peroxyacetyl nitrate measurements over the Brazilian Amazon Basin during the wet season: Relationships with nitrogen oxides and ozone, J. Geophys. Res. Atmospheres, 95, 16945–16954, https://doi.org/10.1029/JD095iD10p16945, 1990.

Singh, H. B., Salas, L. J., Chatfield, R. B., Czech, E., Fried, A., Walega, J., Evans, M. J., Field, B. D., Jacob, D. J., Blake, D., Heikes, B., Talbot, R., Sachse, G., Crawford, J. H., Avery, M. A., Sandholm, S., and Fuelberg, H.: Analysis of the atmospheric distribution, sources, and sinks of oxygenated volatile organic chemicals based on measurements over the Pacific during TRACE-P, J. Geophys. Res. Atmospheres, 109, https://doi.org/10.1029/2003JD003883, 2004.

Smith, D., Wang, T., and Španěl, P.: Analysis of ketones by selected ion flow tube mass spectrometry, Rapid Commun. Mass Spectrom., 17, 2655–2660, https://doi.org/10.1002/rcm.1244, 2003.

Smith, D., Chippendale, T. W. E., and Španěl, P.: Selected ion flow tube, SIFT, studies of the reactions of H3O+, NO+ and O2+ with some biologically active isobaric compounds in preparation for SIFT-MS analyses, Int. J. Mass Spectrom., 303, 81–89, https://doi.org/10.1016/j.ijms.2011.01.005, 2011.

Ŝpaněl, P. and Smith, D.: SIFT studies of the reactions of H3O+, NO+ and O+2 with a series of volatile carboxylic acids and esters, Int. J. Mass Spectrom. Ion Process., 172, 137–147, https://doi.org/10.1016/S0168-1176(97)00246-2, 1998.

Španěl, P. and Smith, D.: SIFT studies of the reactions of H3O+, NO+ and O2+ with several ethers, Int. J. Mass Spectrom. Ion Process., 172, 239–247, https://doi.org/10.1016/S0168-1176(97)00277-2, 1998.

Španěl, P., Ji, Y., and Smith, D.: SIFT studies of the reactions of H3O+, NO+ and O2+ with a series of aldehydes and ketones, Int. J. Mass Spectrom. Ion Process., 165–166, 25–37, https://doi.org/10.1016/S0168-1176(97)00166-3, 1997.

Španěl, P., Wang, T., and Smith, D.: A selected ion flow tube, SIFT, study of the reactions of H3O+, NO+ and O2+ ions with a series of diols, Int. J. Mass Spectrom., 218, 227–236, https://doi.org/10.1016/S1387-3806(02)00724-8, 2002.

Tani, A. and Hewitt, C. N.: Uptake of Aldehydes and Ketones at Typical Indoor Concentrations by Houseplants, Environ. Sci. Technol., 43, 8338–8343, https://doi.org/10.1021/es9020316, 2009.

Tani, A., Tobe, S., and Shimizu, S.: Uptake of Methacrolein and Methyl Vinyl Ketone by Tree Saplings and Implications for Forest Atmosphere, Environ. Sci. Technol., 44, 7096–7101, https://doi.org/10.1021/es1017569, 2010.

Trebs, I., Mayol-Bracero, O. L., Pauliquevis, T., Kuhn, U., Sander, R., Ganzeveld, L., Meixner, F. X., Kesselmeier, J., Artaxo, P., and Andreae, M. O.: Impact of the Manaus urban plume on trace gas mixing ratios near the surface in the Amazon Basin: Implications for the NO-NO2-O3 photostationary state and peroxy radical levels, J. Geophys. Res. Atmospheres, 117, https://doi.org/10.1029/2011JD016386, 2012.

Villanueva, F., Tapia, A., Notario, A., Albaladejo, J., and Martínez, E.: Ambient levels and temporal trends of VOCs, including carbonyl compounds, and ozone at Cabañeros National Park border, Spain, Atmos. Environ., 85, 256–265, https://doi.org/10.1016/j.atmosenv.2013.12.015, 2014.

Villanueva-Fierro, I., Popp, C. J., and Martin, R. S.: Biogenic emissions and ambient concentrations of hydrocarbons, carbonyl compounds and organic acids from ponderosa pine and cottonwood trees at rural and forested sites in Central New Mexico, Atmos. Environ., 38, 249–260, https://doi.org/10.1016/j.atmosenv.2003.09.051, 2004.

Wang, C., Yuan, B., Wu, C., Wang, S., Qi, J., Wang, B., Wang, Z., Hu, W., Chen, W., Ye, C., Wang, W., Sun, Y., Wang, C., Huang, S., Song, W., Wang, X., Yang, S., Zhang, S., Xu, W., Ma, N., Zhang, Z., Jiang, B., Su, H., Cheng, Y., Wang, X., and Shao, M.: Measurements of higher alkanes using NO⁺ chemical ionization in PTR-ToF-MS:

important contributions of higher alkanes to secondary organic aerosols in China, Atmospheric Chem. Phys., 20, 14123–14138, https://doi.org/10.5194/acp-20-14123-2020, 2020a.

Wang, M., Zhang, L., Boo, K. H., Park, E., Drakakaki, G., and Zakharov, F.: PDC1, a pyruvate/α-ketoacid decarboxylase, is involved in acetaldehyde, propanal and pentanal biosynthesis in melon (Cucumis melo L.) fruit, Plant J., 98, 112–125, https://doi.org/10.1111/tpj.14204, 2019.

Wang, N., Edtbauer, A., Stönner, C., Pozzer, A., Bourtsoukidis, E., Ernle, L., Dienhart, D., Hottmann, B., Fischer, H., Schuladen, J., Crowley, J. N., Paris, J.-D., Lelieveld, J., and Williams, J.: Measurements of carbonyl compounds around the Arabian Peninsula indicate large missing sources of acetaldehyde, Gases/Field Measurements/Troposphere/Chemistry (chemical composition and reactions), https://doi.org/10.5194/acp-2020-135, 2020b.

Warneck, P.; Williams, J.: The Atmospheric Chemists Companion, 1., Springer Verlag GmbH, 2012.

Warneke, C., Karl, T., Judmaier, H., Hansel, A., Jordan, A., Lindinger, W., and Crutzen, P. J.: Acetone, methanol, and other partially oxidized volatile organic emissions from dead plant matter by abiological processes: Significance for atmospheric HOx chemistry, Glob. Biogeochem. Cycles, 13, 9–17, https://doi.org/10.1029/98GB02428, 1999.

Williams, J., Fischer, H., Harris, G. W., Crutzen, P. J., Hoor, P., Hansel, A., Holzinger, R., Warneke, C., Lindinger, W., Scheeren, B., and Lelieveld, J.: Variability-lifetime relationship for organic trace gases: A novel aid to compound identification and estimation of HO concentrations, J. Geophys. Res. Atmospheres, 105, 20473–20486, https://doi.org/10.1029/2000JD900203, 2000.

Williams, J., Pöschl, U., Crutzen, P. J., Hansel, A., Holzinger, R., Warneke, C., Lindinger, W., and Lelieveld, J.: An Atmospheric Chemistry Interpretation of Mass Scans Obtained from a Proton Transfer Mass Spectrometer Flown over the Tropical Rainforest of Surinam, 2001.

Wolfe, G. M., Thornton, J. A., McKay, M., and Goldstein, A. H.: Forest-atmosphere exchange of ozone: sensitivity to very reactive biogenic VOC emissions and implications for in-canopy photochemistry, Atmospheric Chem. Phys., 11, 7875–7891, https://doi.org/10.5194/acp-11-7875-2011, 2011.

Xing, J.-H., Ono, M., Kuroda, A., Obi, K., Sato, K., and Imamura, T.: Kinetic Study of the Daytime Atmospheric Fate of (Z)-3-Hexenal, J. Phys. Chem. A, 116, 8523–8529, https://doi.org/10.1021/jp303202h, 2012.

Yamauchi, Y., Kunishima, M., Mizutani, M., and Sugimoto, Y.: Reactive short-chain leaf volatiles act as powerful inducers of abiotic stress-related gene expression, Sci. Rep., 5, 8030, https://doi.org/10.1038/srep08030, 2015.

Yáñez-Serrano, A. M., Nölscher, A. C., Williams, J., Wolff, S., Alves, E., Martins, G. A., Bourtsoukidis, E., Brito, J., Jardine, K., Artaxo, P., and Kesselmeier, J.: Diel and seasonal changes of biogenic volatile organic compounds within and above an Amazonian rainforest, Atmospheric Chem. Phys., 15, 3359–3378, https://doi.org/10.5194/acp-15-3359-2015, 2015.

Yáñez-Serrano, A. M., Nölscher, A. C., Bourtsoukidis, E., Derstroff, B., Zannoni, N., Gros, V., Lanza, M., Brito, J., Noe, S. M., House, E., Hewitt, C. N., Langford, B., Nemitz, E., Behrendt, T., Williams, J., Artaxo, P., Andreae, M. O., and Kesselmeier, J.: Atmospheric mixing ratios of methyl ethyl ketone (2-butanone) in tropical, boreal, temperate and marine environments, Atmospheric Chem. Phys., 16, 10965–10984, https://doi.org/10.5194/acp-16-10965-2016, 2016.

Yee, L. D., Goldstein, A. H., and Kreisberg, N. M.: Investigating Secondary Aerosol Processes in the Amazon through Molecular-level Characterization of Semi-Volatile Organics, Univ. of California, Berkeley, CA (United States), https://doi.org/10.2172/1673764, 2020.

Zannoni, N., Wikelski, M., Gagliardo, A., Raza, A., Kramer, S., Seghetti, C., Wang, N., Edtbauer, A., and Williams, J.: Identifying volatile organic compounds used for olfactory navigation by homing pigeons, Sci. Rep., 10, 15879, https://doi.org/10.1038/s41598-020-72525-2, 2020a.

Zannoni, N., Leppla, D., Lembo Silveira de Assis, P. I., Hoffmann, T., Sá, M., Araújo, A., and Williams, J.: Surprising chiral composition changes over the Amazon rainforest with height, time and season, Commun. Earth Environ., 1, 1–11, https://doi.org/10.1038/s43247-020-0007-9, 2020b.

3.8 Supplementary material

Table S 3.1: *The product ion distributions for the ionization with NO^+. The values were obtained by the single compound headspace analysis conducted with the PTR-ToF-8000. Values in bold represent the main m/z used for the measurements in the Amazon rainforest.*

	E/N 70 Td				E/N 120 Td			
Carbonyl species	Peaking masses	Max. ncps	Relative counts	Formular	Peaking masses	Max. ncps	Relative counts	Formular
Acetone	**88.0393**	13609	0.76	$C_3H_6NO_2^+$	**88.0393**	585	0.40	$C_3H_6NO_2^+$
	59.0461	3016	0.17	$C_3H_7O^+$	59.0491	461	0.32	$C_3H_7O^+$
	77.0597	745	0.04	$C_3H_9O_2^+$	43.0178	405	0.28	$C_2H_3O^+$
	43.0178	507	0.03	$C_2H_3O^+$				
Hexanal	**99.0804**	1989	0.79	$C_6H_{11}O^+$	**71.0855**	572	0.38	$C_5H_{11}^+$
	117.091	157	0.06	$C_6H_{13}O_2^+$	99.0804	526	0.35	$C_6H_{11}O^+$
	100.076	152	0.06	$C_5H_{10}NO^+$	43.0542	309	0.21	$C_3H_7^+$
	71.0855	81	0.03	$C_5H_{11}^+$	81.0699	52	0.03	
	101.0961	80	0.03	$C_6H_{13}O^+$	41.0383	45	0.03	
	135.114	72	0.03					
Benzaldehyde	**105.033**	114	0.93	$C_7H_5O^+$	**105.033**	91	0.91	$C_7H_5O^+$
	99.0804	8	0.07		99.0804	9	0.09	
Pentanal	**85.0648**	2704	0.84	$C_5H_9O^+$	57.0699	1048	0.64	$C_4H_9^+$
	86.0726	159	0.05	$C_5H_{10}O^+$	**85.0648**	451	0.28	$C_5H_9O^+$
	103.075	154	0.05	$C_5H_{11}O_2^+$	58.076	53	0.03	
	57.0699	106	0.03	$C_4H_9^+$	41.038	43	0.03	$C_3H_5^+$
	87.0804	99	0.03	$C_5H_{11}O^+$	69.0699	45	0.03	
Nonanal	85.0648	218	0.78	$C_5H_9O^+$	57.0699	40	0.51	$C_4H_9^+$
	88.0393	19	0.07	$C_3H_6NO_2^+$	85.0648	29	0.37	$C_5H_9O^+$
	103.075	14	0.05	$C_5H_{11}O_2^+$	**141.1274**	6	0.08	$C_9H_{17}O^+$
	57.0699	11	0.04	$C_4H_9^+$	86.07262	4	0.05	$C_5H_{10}O^+$
	141.1274	8	0.03	$C_9H_{17}O^+$				
	121.0968	8	0.03					
Octanal	**127.1117**	79	0.65	$C_8H_{15}O^+$	**127.1117**	58	0.56	$C_8H_{15}O^+$
	85.0648	42	0.35	$C_5H_9O^+$	57.0699	39	0.38	$C_4H_9^+$
					85.0648	7	0.07	$C_5H_9O^+$
Trans-2-hexenal	**97.0672**	354	0.73	$C_6H_9O^+$	**97.0672**	1134	0.76	$C_6H_9O^+$
	128.0768	87	0.18	$C_6H_{10}NO_2^+$	55.039	203	0.14	
	99.0804	27	0.06	$C_6H_{11}O^+$	98.060	124	0.08	$C_6H_{10}O^+$
	85.0648	14	0.03	$C_5H_9O^+$	99.0804	40	0.03	$C_6H_{11}O^+$

Table S3.1 *continued*

	E/N 70 Td				E/N 120 Td			
Carbonyl species	Peaking masses	Max. ncps	Relative counts	Formular	Peaking masses	Max. ncps	Relative counts	Formular
Pentanone	**116.0706**	2125	0.95	$C_5H_{10}NO_2^+$	**116.0706**	578	0.57	$C_5H_{10}NO_2^+$
	87.08044	101	0.05	$C_5H_{11}O^+$	86.07262	109	0.11	$C_5H_{10}O^+$
					43.01784	89	0.09	$C_2H_3O^+$
					58.04132	87	0.09	$C_3H_6O^+$
					87.08044	82	0.08	$C_5H_{11}O^+$
					71.04914	70	0.07	$C_4H_7O^+$
Methacrolein	**69.03349**	3114	0.58	$C_4H_5O^+$	**69.03349**	586	0.45	$C_4H_5O^+$
	100.039	1528	0.29	$C_4H_6NO_2^+$	41.0383	562	0.43	$C_3H_5^+$
	57.03349	527	0.10	$C_3H_5O^+$	71.04914	66	0.05	$C_4H_7O^+$
	71.04914	179	0.03	$C_4H_7O^+$	57.03349	54	0.04	$C_3H_5O^+$
					100.039	48	0.04	$C_4H_6NO2^+$
MVK	**100.039**	3067	0.91	$C_4H_6NO_2^+$	**100.039**	240	0.69	$C_4H_6NO_2^+$
	71.04914	319	0.09	$C_4H_7O^+$	71.04914	94	0.27	$C_4H_7O^+$
					43.01784	16	0.05	$C_2H_3O^+$
MEK	**102.055**	7073	0.90	$C_4H_8NO_2^+$	**102.055**	985	0.64	$C_4H_8NO_2^+$
	73.069	531	0.07	$C_4H_9O^+$	73.069	181	0.12	$C_4H_9O^+$
	57.03349	232	0.03	C_3H_5O+	57.03349	158	0.10	$C_3H_5O^+$
					43.01784	155	0.10	$C_2H_3O^+$
					72.05697	71	0.05	$C_4H_8O^+$
Butanal	**71.04914**	2453	0.89	$C_4H_7O^+$	43.05423	434	0.63	$C_3H_7^+$
	72.05697	139	0.05	$C_4H_8O^+$	**71.04914**	200	0.29	$C_4H_7O^+$
	89.05971	90	0.03		41.0383	58	0.08	$C_3H_5^+$
	43.05423	83	0.03	$C_3H_7^+$				
Propanal	**57.03349**	7606	0.85	$C_3H_5O^+$	**57.03349**	3388	0.74	$C_3H_5O^+$
	88.0393	692	0.08	$C_3H_6NO_2^+$	37.0284	782	0.17	
	75.04405	370	0.04	$C_3H_7O_2^+$	59.04914	401	0.09	$C_3H_7O^+$
	59.04914	288	0.03	$C_3H_7O^+$				

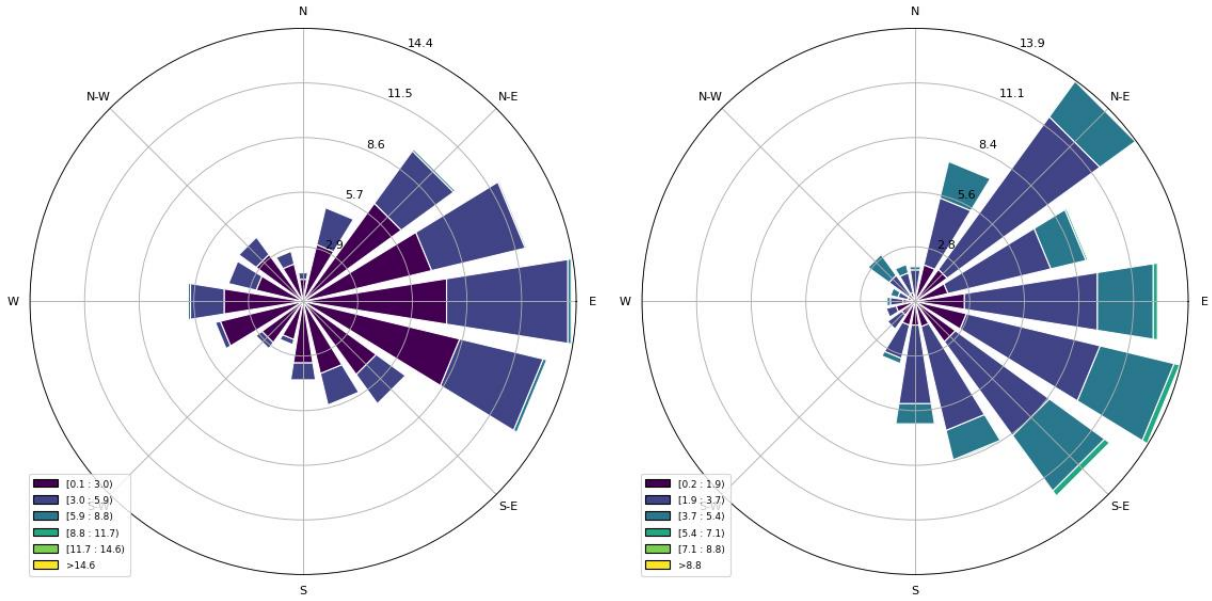

Figure S 3.1: *Wind rose for the measurement period in the dry season (left) and the wet-to-dry transition (right) of 2019.*

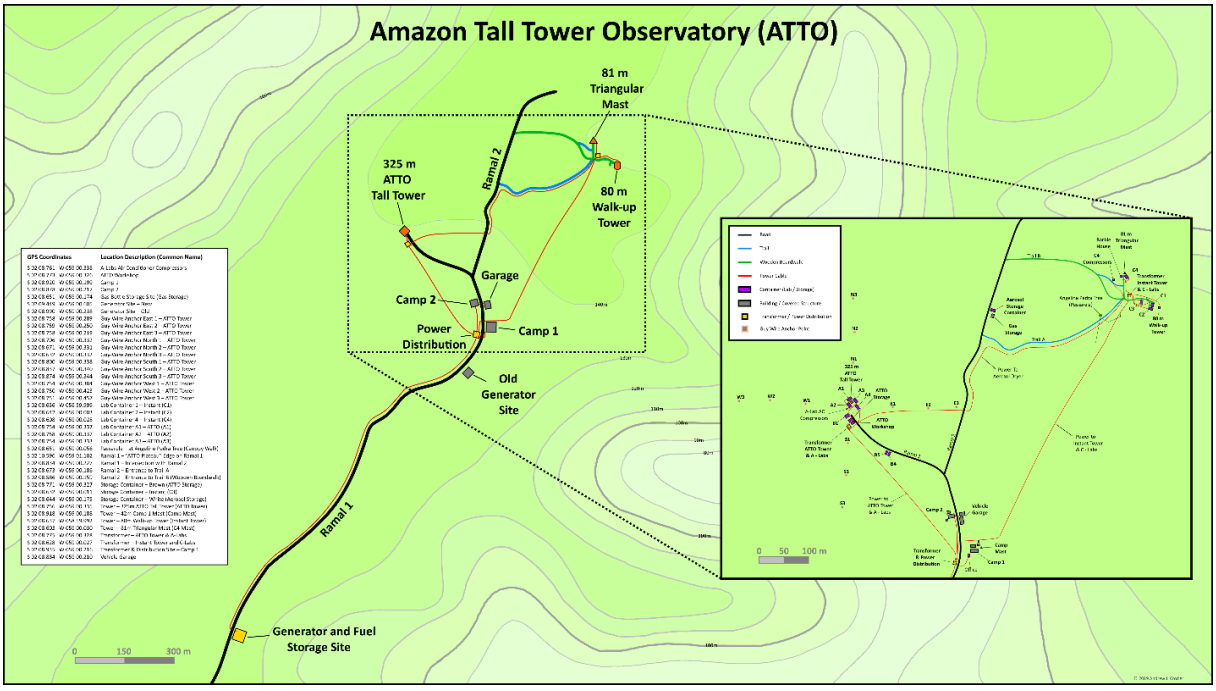

Figure S 3.2: *A map of the ATTO site created and provided by Andrew Crozier.*

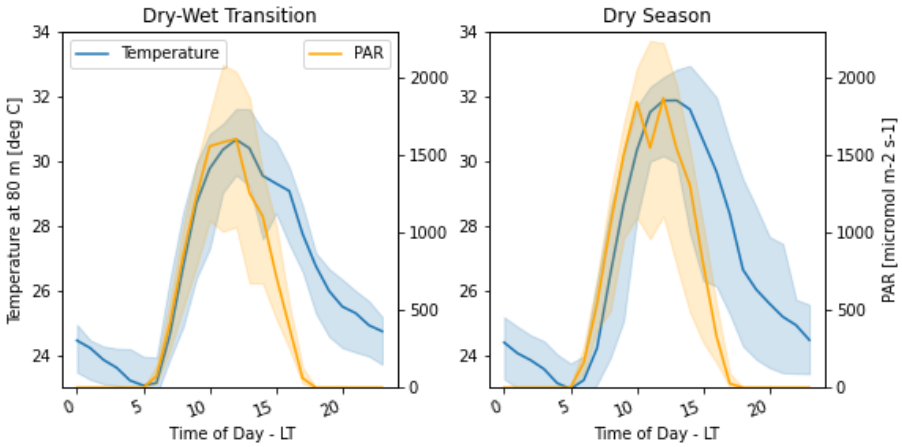

Figure S 3.3: *Median averaged time series of meteorological parameters. Temperatures were measured inside the canopy at 26 m and PAR at 80 m on the 80 m walk-up tower. The shadings indicate the quartiles (25th and 75th).*

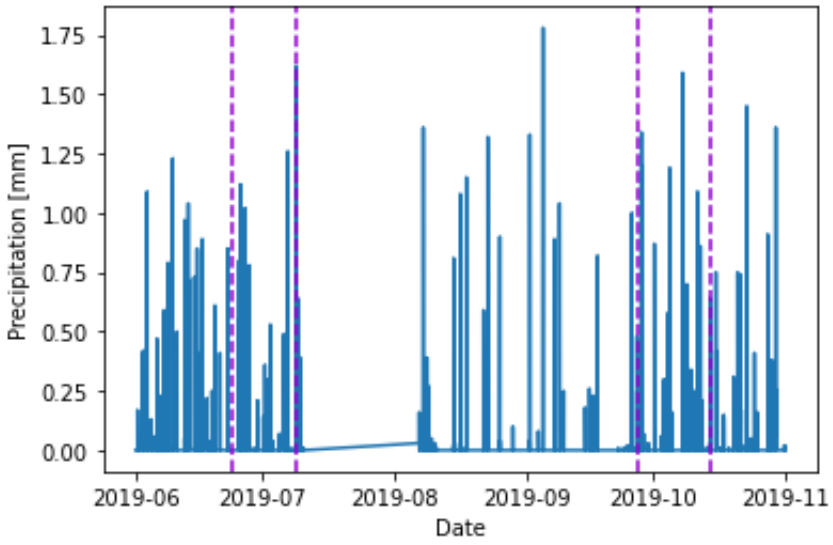

Figure S 3.4: *Precipitation before and during the measurement periods marked with purple dashed lines. Precipitation was measured on the 325 m tall tower.*

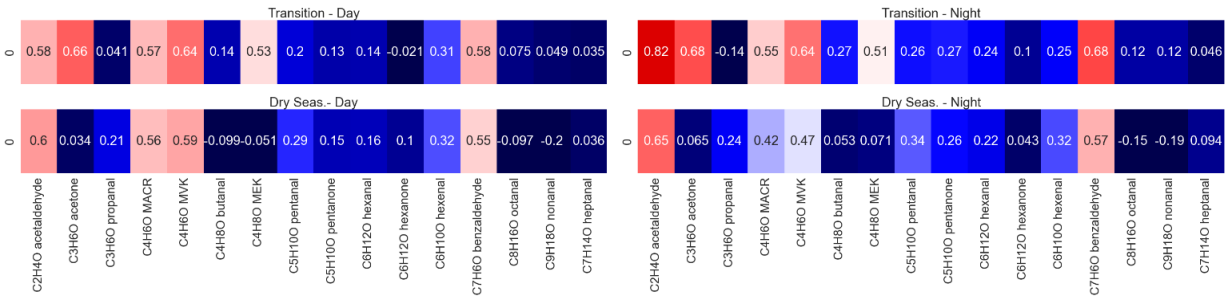

Figure S 3.5: *Pearson correlation coefficients for the observed carbonyl compounds with black carbon measured at 325 m on the tall tower.*

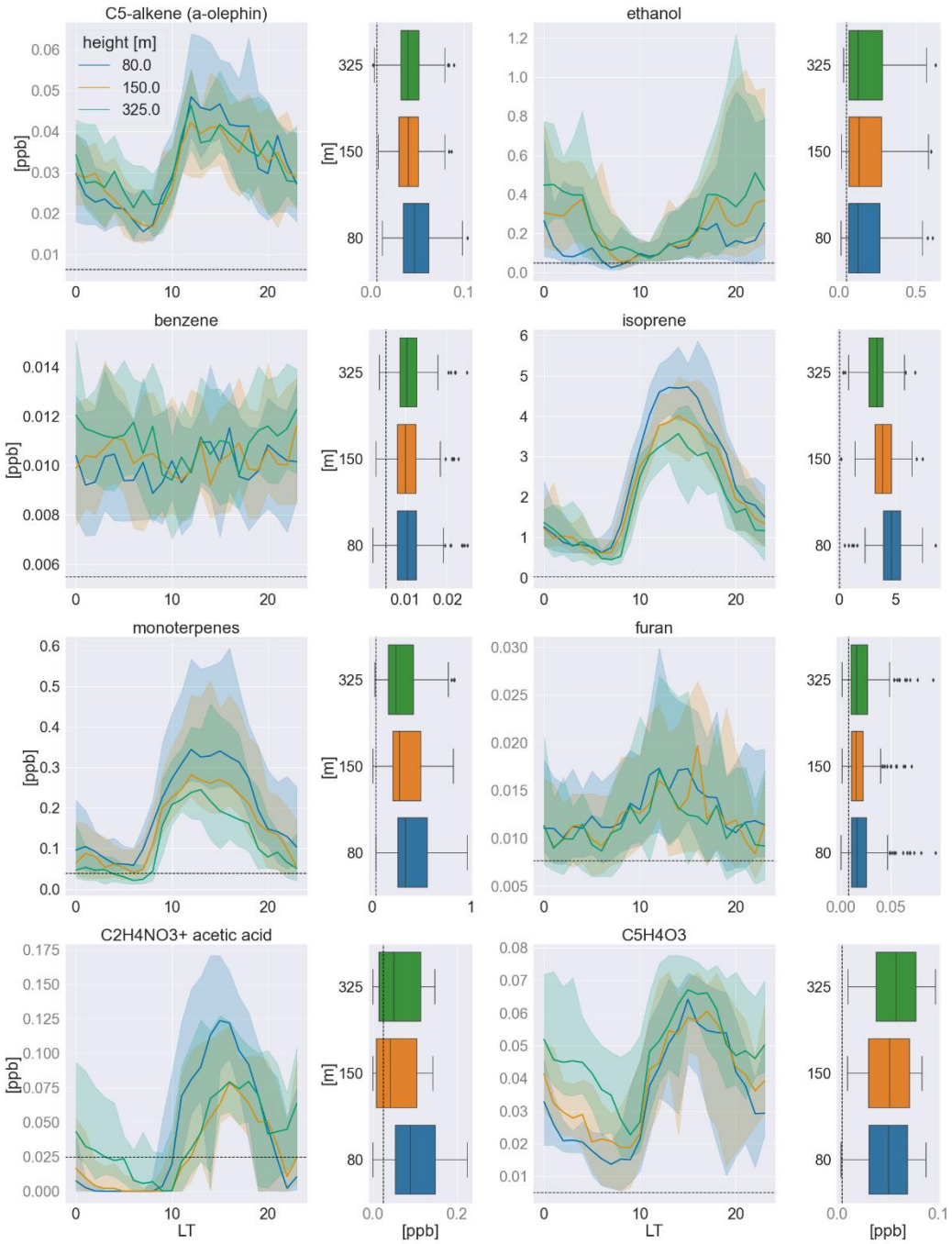

Figure S 3.6: *Median averaged timeseries in the wet-to-dry transition season (June/July) of 2019 measured at all sampling heights for each hydrocarbon and its respective vertical profile at noon (12:00-15:00 LT) to the right. The shadings indicate the quartiles (25th and 75th). In the box-and-whisker plots, the boxes also represent the quartiles, while the residual data except outliers are included in the whiskers. The mixing ratios stated in gray font were calculated based on k-rate.*

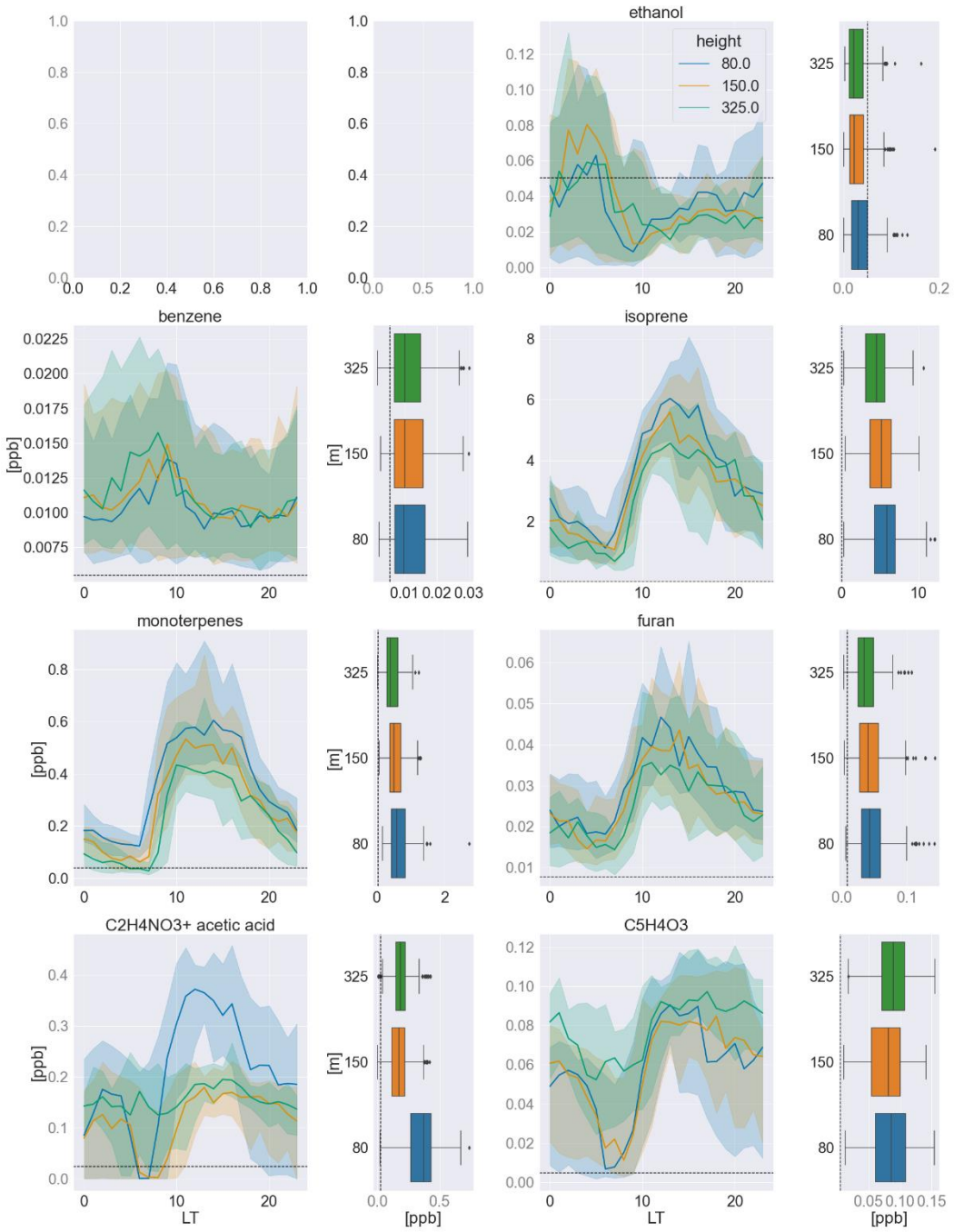

Figure S 3.7: *Median averaged timeseries in the dry season (September/October) of 2019 measured at all sampling heights for each hydrocarbon and its respective vertical profile at noon (12:00-15:00 LT) to the right. The shadings indicate the quartiles (25th and 75th). In the box-and-whisker plots, the boxes also represent the quartiles, while the residual data except outliers are included in the whiskers. The mixing ratios stated in gray font were calculated based on k-rate.*

Chapter 4

This chapter has been published as: Ernle, L., Ringsdorf, M. A., and Williams, J.: Influence of ozone and humidity on PTR-MS and GC-MS VOC measurements with and without a $Na_2S_2O_3$ ozone scrubber, Atmos. Meas. Tech., 16, 1179–1194, https://doi.org/10.5194/amt-16-1179-2023, 2023.

Contribution to this paper: Akima Ringsdorf designed the setup of the experiment together with Lisa Ernle. Moreover, Akima Ringsdorf performed the measurements and data analysis for the PTR-ToF-MS and reviewed the manuscript.

Influence of ozone on VOC measurements

4.1 Abstract

The measurement of volatile organic compounds (VOCs) can be influenced by ozone (O_3), resulting in sampling artefacts that corrupt the data obtained. Published literature reports both positive (false enhancements of signal) and negative (loss of signal) interference in VOC data due to ozonolysis occurring in the sample gas. To assure good data quality it is essential to be aware of such interfering processes, to characterize them and to try to minimize the impact with a suitable sampling setup. Here we present results from experiments with a sodium thiosulfate ozone scrubber ($Na_2S_2O_3$), which is a cost-effective and easily applied option for O_3 scavenging during gas-phase sampling. Simultaneous measurement of selected organic trace gases using gas chromatography–mass spectrometry and proton transfer reaction–mass spectrometry was performed at different ozone levels (0–1 ppm) and different relative humidities (0 %–80 %). In this way both tropospheric and stratospheric conditions were examined. The measured data show that several carbonyl compounds including acetaldehyde, acetone and propanal show artificial signal enhancement when ozone is present at higher concentrations (> 150 ppb) in dry air, while analytes with double bonds like isoprene (measured with GC-MS) and terpenes show lower signals due to reaction with ozone. Both effects can be eliminated or in the case of sesquiterpenes substantially reduced by using $Na_2S_2O_3$ impregnated quartz filters in the inlet line. With the chosen scrubbing material, relative humidity (RH) substantially improves the scrubbing efficiency. Under surface conditions between 50 %–80 % RH, the filter allows for accurate measurement of all species examined.

4.2 Introduction

Volatile organic compounds (VOCs) are trace atmospheric constituents usually present at mixing ratios of parts per billion (ppb) or lower in the earth's atmosphere. Nevertheless, they can have a considerable impact on the global air chemistry and climate and can influence the health of living organisms on the earth's surface (Crutzen and Lelieveld, 2001; Williams, 2004). Organic trace gases can act as greenhouse gases, contribute to particle formation and take part in photochemical oxidation processes that influence ozone. Additionally many VOCs are also considered to be contaminants of the indoor environment where human exposure to such chemicals can be high (Weschler and Carslaw, 2018). VOC sources can be of natural (plants, phytoplankton, volcanoes, etc.) or anthropogenic origin (e.g. fossil fuel combustion, agriculture, industry) (Koppmann, 2008; McDonald et al., 2018; Weschler and Shields, 1997). To understand the chemical reactions and processes in outdoor, as well as indoor environments, it is essential to accurately quantify the VOCs in the air.

Common analytical techniques for sampling organic trace gases are proton transfer reaction–mass spectrometry (PTRMS) and gas chromatography–mass spectrometry (GCMS). With these measurement techniques a wide range of volatile organic compounds can be measured including aliphatic and aromatic hydrocarbons and oxygenated and halogen-containing species (Koppmann, 2008; Warneck and Williams, 2012). However, research has shown that due to the reactivity of some analytes to ozone, measurements can be rendered inaccurate, as already reported by Helmig (1997) more than 20 years ago.

Ozone can influence VOC measurements either due to reaction with the target analytes during sampling, which particularly affects techniques with pre-concentration steps prior to analysis (Helmig, 1997; Koppmann et al., 1995; Pollmann et al., 2005), or by generating sampling artefacts in the inlet of an online instrument. Northway et al. (2004) and Apel et al. (2003) reported for example increased mixing ratios for

acetaldehyde in their systems for measurements in the lower stratosphere where ozone levels are high and humidity is low. Ozone and water are omnipresent in the troposphere with mixing ratios between 10 and 200 ppb (ozone) and humidities (10 %–100 %). Stratospheric O_3 is essential for life on planet Earth, as it absorbs high-energy solar UV radiation. It is formed in the stratosphere through the photolysis of oxygen, which generates mixing ratios between 1–10 ppm. While such processes generate the protective ozone layer in the stratosphere, at ground level this oxidative gas is considered to be a pollutant, as it is detrimental to the human respiratory tract and damages plants (Pandis and Seinfeld, 2006). Being present in both the troposphere and stratosphere, albeit at different concentrations, ozone can potentially affect VOC measurements made at the ground and from high-flying aircraft. The two instruments examined in this study are regularly installed on an aircraft capable of reaching ca. 15 km which at mid-latitudes gives access to the lower stratosphere. Also in indoor environments where ozone is typically 3– 5 times less than outside ambient levels, it may affect the measurement fidelity.

Sodium thiosulfate ($Na_2S_2O_3$) has been reported to have a good ozone scrubbing efficiency for VOC measurements (Lehmpuhl and Birks, 1996; Pollmann et al., 2005) and was therefore chosen as the best test material for O_3 removal in the experiments described here. Like ozone, humidity varies strongly between the dry stratosphere and much more humid conditions of the earth's surface. Humidity is considered an important variable here, as it can strongly influence chemistry occurring at surfaces. Measurement conditions that reflect the conditions likely to be met in these two environments were therefore examined. The aim of this study was to investigate the influence of different ozone levels and different relative humidity (RH) on two specific VOC measurement instruments, namely the fast GC-MS SOFIA described by Bourtsoukidis et al. (2017) and a PTR-ToF-MS described in Wang et al. (2022). We report on the effect of using the sodium thiosulfate impregnated quartz filters for multiple VOC species including carbonyls, alcohols and non-methane hydrocarbons. Additionally, the lifetime of the scrubber with respect to ozone exposure was determined under tropospheric and stratospheric conditions. This is essential to assure that the scrubber is working correctly when applied in the field, to determine optimum exchange times, and to avoid unnecessary exchange and waste. These results will define operational expectations of using a $Na_2S_2O_3$ filter in field conditions to improve organic trace gas measurement techniques, assure good data quality for smaller VOCs and therefore improve the data comparability between different studies.

4.3 Materials and methods

The influence of ozone on measurements from an online VOC instrument (PTR-ToF-MS 8000, IONICON Analytik, Austria) and a custom-built quasi-online fast gas chromatograph–mass spectrometer (GC-MS) (Bourtsoukidis et al., 2017), which collects, concentrates and measures within 3 min, was investigated. Additionally, the effect of an implemented sodium thiosulfate ozone scrubber on those systems, as well as the scrubber lifetime, was examined at different relative humidity. A list with the measured species is shown in Table 4.2. It includes saturated and unsaturated halocarbons, non-methane hydrocarbons (NMHCs), small oxygenated VOCs (OVOCs), siloxanes, and some nitrogenand sulfur-containing molecules. Some species could be detected with both instruments simultaneously, while other species could only be measured by one. The majority of the tubing used in this study was fluorinated ethylene propylene (FEP) Teflon which was found by Deming et al. (2019) to perform well in a comparison of inlet materials (including polyetheretherketone (PEEK) and stainless steel), as adsorption on FEP was found to be

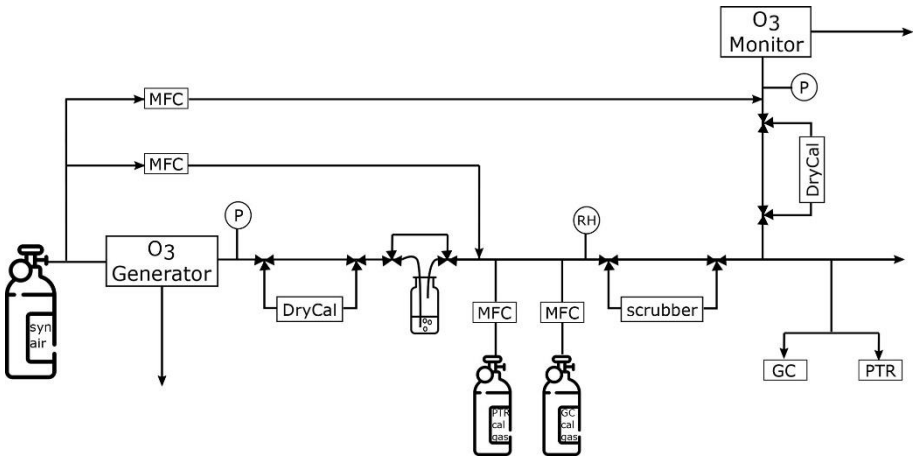

Figure 4.1: *Experimental setup. MFC – mass flow controller, RH – relative humidity sensor, P – pressure gauge, and DryCal – flow metre.*

independent of humidity, concentration and functionality. The tubing was not new but was used previously for airborne measurements aboard a research aircraft. It was flushed with synthetic air for at least 1 h prior to when the experiments were performed. When considering the ozone in the instrument inlet, one could consider passivating the inlet surfaces prior to measurement by the introduction of high (500 ppb) ozone mixing ratios. Northway et al. (2004) tested this possibility and noted a passivation that disappeared during further field measurements. As this will in effect generate a shifting background to the subsequent measurements, and as 6 h flushing is impractical prior to flight measurements, we chose not to follow this procedure.

4.3.1 Experimental setup

The experimental setup includes both PTR-ToF-MS and fast GC-MS as shown in Fig. 4.1. Synthetic air from a gas cylinder (synthetic air, hydrocarbon free, T50, Westfalen, Germany) was connected to the ozone generator which was set to generate O_3 at levels between 25 and 1000 ppb. This corresponds to tropospheric and lower stratospheric levels, similar to those encountered by the *HALO* aircraft on which the instruments are certified to fly. Thereafter, the air stream was led through ultra-pure water for humidification. Ozone as a non-polar molecule has a very low solubility in water and will therefore not be lost during the humidification process. Two different calibration gas cylinders (40 L, Apel Riemer, USA) were connected through a junction (T-piece) to the sampling line. These cylinders contained a gravimetrically prepared mixture of VOCs at known mixing ratios, which could be added to the system air. The VOC-enriched synthetic air could then be directed through the ozone scrubber or directly to the two mass spectrometers, which both drew ca. 200 sccm air from the sampling line. At the end of the Teflon tubing inlet line the ozone monitor was connected to measure the O_3 concentration after the scrubber. Several exhaust lines and pressure gauges were installed in the setup to ensure a system pressure close to ambient pressure (ca. 1000 hPa). This is required for the operation of the ozone instruments. To make sure that the monitor was always operated within the required flow range, a dilution flow could be added shortly before the instrument. Gas flows were checked regularly with a flow metre (DryCal, MesaLabs, USA) after the ozone generator and monitor. All the lines were made of FEP and heated to approximately

45 °C to avoid condensation in the tubing. This simulates conditions on the research aircraft aboard which the measurement devices have been installed. The total tubing length between the ozone generator and scrubber was approximately 2 m; the outer diameter was 1/4 in. (0.635 cm), again equivalent to the aircraft setup.

During the ozone experiment series various tests were performed (see Table 4.1): VOC mixtures were measured at several levels, adding 0, 50 and 1000 ppb ozone to investigate the measurement performance at ambient background ozone levels on the ground and in the lower stratosphere. Additionally, one VOC level was measured at seven different ozone levels up to 1000 ppb (0, 25, 50, 150, 400, 750, 1000 ppb). The tests also included experiments without added VOCs to see if any of the analytes are produced in the pre-used inlet line. Note that during the very first experiment performed, flows were measured every time the VOC level was adjusted. It turned out that some compounds were emitted from the flow metre, resulting in elevated terpene masses. When switching to a new calibration gas level, as well as in the first hour of the experiment, there were spikes in the VOC signal. These were judged to be mechanical flow-related anomalies and therefore removed to assure better visibility of the mixing ratio in the plots. To investigate the influence of sodium thiosulfate impregnated quartz filters as an ozone scrubber, VOC levels at 0.5 and 2 ppb were measured at different ozone levels (0, 50 and 150 ppb) and different relative humidities (0 %, 50 % and 80 % RH) with and without scrubber in the flow path. For scrubber endurance tests, another exhaust line was installed after the ozone generator to reduce the flow through the sodium thiosulfate impregnated quartz filter in order to simulate field conditions. The flow through the filter was set to 200–600 sccm to replicate either typical field measurement conditions or the experiments focusing on the influence on the VOC measurements. For those experiments the flow through the scrubber was higher to provide enough air for both of the instruments. Before each single longevity experiment the $Na_2S_2O_3$ impregnated filter was exchanged and left in the flow path until an abrupt increase in ozone concentration was detected with the O_3 monitor. This rise marks the end of the scrubber lifetime. Further details on the preparation of the filter scrubber can be found in Sect. 4.3.3. Scrubber performance was tested under three different ozone concentrations: 50, 150 and 1000 ppb at 0 % RH. These are the same ozone levels used for the experiment focused on the effect of O_3 on the VOC measurements, which correspond to ambient ground and lower stratospheric ozone levels. Additionally, the influence of 80 % relative humidity on the scrubber lifetime was tested. This RH level was chosen as an extreme to see whether or not it changes the scrubber performance. Relative humidity was measured with a humidity sensor that includes a temperature sensor (MSR145, MSR, Switzerland; indicated with RH in Fig. 4.1).

4.3.2 Instrumentation

4.3.2.1 Ozone instruments

An ozone generator, as well as an ozone monitor (49iQPS and 49iQ, both Thermo Fisher Scientific, USA), were installed in the experimental setup. Each instrument's supply air stream is divided into a reference and a sample gas channel. In the generator the sample gas flows through an ozonator, while the reference gas of the monitor flows through a scrubber to eliminate existing ambient ozone. Both instruments use a spectroscopic approach to determine the mixing ratio: as the O_3 molecule absorbs UV light of 254 nm the

Table 4.1: *Conditions of the different experiments performed in this study.*

Condition	O3 levels (ppb)	CalGas MR (ppb)	RH (%)
Effect of O3 on VOCs	0, 50, 1000	0, 0.5, 1, 2, 4	0
Effect of O3 on tubing	0, 25, 50, 100, 150, 400, 750, 1000	0, 0.5	0
Effect of RH on VOCs with and without scrubber	0, 50, 150	0, 0.5, 2	0, 50, 80
Scrubber endurance	50, 150, 1000	0	0, 80

difference of light intensity of this wavelength in both channels is used to calculate the ozone concentration in the sample stream based on Beer's law (ThermoFisherScientific, 2020a, b).

4.3.2.2 PTR-MS

An IONICON PTR-ToF-MS with a drift tube pressure of 2.2 hPa, drift temperature of 60 °C and E/N 137 Td was operated with H_3O^+ as primary ions. It is a soft ionization technique and therefore causes little fragmentation of the analytes during the detection process. This is the case for most analytes in this study. However, some species (e.g. terpenes, siloxanes) do fragment during ionization (Pagonis et al., 2019). Fragments can impact the measurement of target species such as isoprene if they have exactly the same mass. Identification of the analytes was performed using the exact mass of the most abundant fragment, usually the protonated molecular mass, which does not exclude simultaneous measurement of isomeric compounds. The mass range of the system was 0–500 amu and the mass resolution approximately 3500. The PTR used a FEP inlet tubing (o.d. 1/4 in. (0.635 cm), inner diameter (i.d.) 1⁄8 in. (0.3175 cm)) with an inlet flow of 200 sccm. The distance between the ozone scrubber and PTR was 1.85 m, resulting in an inlet residence time t_{res} of ca. 4 s. In order to regulate the pressure in the drift tube during flight measurements, the sample air passes an adjustable O-ring (fluorinated propylene monomer (FPM) or nitrile butadiene rubber (NBR), t_{res} ≤30 ms). The influence of the O-ring on VOC measurements was found to be zero without O_3 present but has not been tested separately under ozone exposure. Inside the instrument, a 1 m line (i.d. 0.1 cm) made of polyetheretherketone (PEEK) is used (ca. 70 sccm, t_{res} ≤1 s, depending on the flow rate). Limits of detection (LODs) were <0.05 ppb, with a total uncertainty of 15 %–20 %. Measured species included alkenes, siloxanes and OVOCs. For measurements at RH > 0 a humid calibration was applied: the calibration was performed at the same relative humidity as the corresponding experiment.

4.3.2.3 GC-MS

The fast GC-MS system has been described in detail by Bourtsoukidis et al. (2017). In this study it was used to measure halocarbons, small NMHCs and OVOCS, as well as some sulfur-containing compounds and small organic nitrates. Due to its chromatographic column it is capable of separating isomeric compounds prior to detection (e.g. acetone and propanal). The custom-built instrument uses a cryogenic three-step pre-concentration to collect air samples, followed by gas chromatographic separation in a custom-built oven and detection with a quadrupole mass spectrometer which was operated in selected ion monitoring mode (SIM). With a time resolution of 3 min it is currently not possible to measure high molecular mass compounds (e.g. sesquiterpenes), as those would need more time to elute from the GC column. Bromoform is the largest analyte detected with the currently applied method. The system's inlet flow was 200 sccm, and the tubing length between the GC inlet and the ozone scrubber was 2 m (o.d. 1/4 in.

(0.635 cm), i.d. 1⁄8 in. (0.3175 cm)), which results in an inlet residence time of ca. 5 s. Inside the system, the sample air is exposed to silicosteel tubing (o.d. 1⁄16 in. (0.1588 cm), i.d. 0.02 in. (0.0508 cm), 40 sccm, t_{res} < 1 s) and stainless steel surfaces in the traps (t_{res} 1.5 min). LODs were typically < 0.03 ppb (acetaldehyde, acetone and acrolein < 0.2 ppb), and the total measurement uncertainty was approximately 10 %.

4.3.3 Ozone scrubbing

Various materials have been tested to eliminate interferences from ozone on VOC measurements. Helmig (1997) compiled an overview of widely used O_3 scrubbing techniques for the sampling of atmospheric organic compounds. Several groups have reported satisfactory results of sodium thiosulfate as an ozone scavenger for VOC analysis (Helmig, 1997; Lehmpuhl and Birks, 1996; Pollmann et al., 2005; Strömvall and Petersson, 1992). In this study the scrubbers were prepared by soaking quartz fibre filters (37 mm, GE HealthCare Life Sciences, USA) in a 10 % (*w/w*) aqueous solution for 1 h followed by drying under a nitrogen flow of approximately 100 sccm at room temperature. This quartz filter was placed under a 47 mm PTFE filter (Sartorius, Germany) in a Teflon filter holder. The smaller quartz filter was selected to avoid leaks at the filter holder (i.d. 47 mm, Reichelt Chemietechnik, Germany) previously caused due to the thickness of the quartz filter. The volume of the filter housing is ca. 55 mL, resulting in a residence time of ca. 6 s with a flow rate of ∼600 sccm.

4.3.4 Scrubber lifetime calculation

The time that the scrubber remains effective at removing ozone, here termed the scrubber lifetime, is important information for field measurement practitioners. In order to improve data quality and to keep cost and workload low, the ozone scrubbers need to be exchanged before their efficiency is compromised, while still using them as long as possible. Assuming that the scrubber lifetime is a function of ozone mixing ratio and flow, the data from the scrubber lifetime experiment were plotted and fitted with a power function. Additionally the influence of relative humidity on the scrubber lifetime was tested

4.3.5 Potential effects causing interference

VOC measurements performed by the PTR-ToF-MS and the fast GC-MS may in the presence of ozone suffer interference through various effects. Surface reactions on the inner walls of the tubing can lead to ozonolysis of compounds previously absorbed on the FEP inlet tubing. The ozonolysis of alkenes, which are either present on the tubing surface or in the gas phase (sample air), can lead to production of carbonyl compounds which cause positive artefacts on the carbonyl masses. Another potential source of interference is fragmentation during the ionization process in the PTR-MS. Several groups reported for example fragments on PTR *m/z* 69.07 from C_5–C_{10} aldehydes (Buhr et al., 2002; Ruzsanyi et al., 2013; Wang et al., 2022). The instrument-internal fragmentation process itself is independent of ozone, but the presence of the aldehyde species in the sample air is likely to be caused by the release of those species from the sample line surface due to ozonolysis reaction. Not only the PTR but also the GC-MS can suffer interference caused by ozone inside the instrument. It has been reported previously that O_3-induced

Table 4.2: *Measured species and effect of ozone. X: no effect, ↓: negative interference and ↑: positive interference.*

Analytes and effect of O3 on measured MR					
X	Dichlorodifluoromethane	X	Trichloroethene	X	Hydroxyacetone
X	Trichlorofluoromethane (CFC-11)	X	Chlorobenzene	X	Isopropyl nitrate
X	Tetrachloromethane	X	Benzene	X	Acetonitrile
X	1,1,2-Trichloro-1,2,2-Trifluoroethane (CFC-113)	X	m-Xylene	X	Acrylonitrile
X	Bromomethane	X	1,2,4-Trimethylbenzene	X	Carbon disulfide
X	Bromoform	X	3-Methylfuran	X	DMS
X	Chloromethane	X	2-methyl-3-buten-1-ol	X	D3
X	Dichloromethane	↑	Acetaldehyde	X	D4
X	Chloroform	↑	Propanal	X	D5
X	Iodomethane	↑	Acetone	X	n-butane, i-butane
X	Bromodichloromethane	↑	Butanal	X	Propene
X	1,1,1-Trichloroethane	X	MEK	↓	Isoprene
X	1,1,2-Trichloroethane	X	MTBE	↓	Monoterpenes
X	Vinylchloride	X	Acrolein	↓	Sesquiterpenes
X	Tetrachloroethene	↓	Methacrolein		

emission from rotor material of multiposition valves can lead to positive artefacts when measuring C_2–C_4 aldehydes (Apel et al., 2003).

4.4 Results and discussion

4.4.1 Influence of ozone on VOC measurements

For most of the analytes, mainly saturated NMHCs and halocarbons, no ozone interference of the measurement through reactive loss due to ozone was expected. This is because such species do not contain a double bond with which ozone can react, nor do they contain oxygen atoms, so they are unlikely to be produced by surface oxidation processes. However, due to the different molecular structures and physical properties of some analytes, it was potentially possible to obtain negative interference for some unsaturated species like isoprene and terpenes, as well as artificial signal enhancement on the aldehyde masses. Table 4.2 shows whether ozone had an effect on the measured mixing ratio of the VOCs.

4.4.1.1 No effect on VOC measurements

In accordance with the expectations no interference from reactions with ozone were observed for most of the measured species, namely saturated and unsaturated halocarbons, alkanes, aromatics, nitriles, methyl tert butyl ether (MTBE), ethanol, hydroxyacetone, methyl ethyl ketone (MEK), isopropyl nitrate, and the two sulfur-containing species carbon disulfide and dimethyl sulfide (DMS), as well as siloxanes. As an example of the VOCs where ozone did not influence the measurements Fig. 4.2 shows the mixing ratios of chlorobenzene applied and measured by GC- and PTR-MS, as well as the ozone mixing ratio. In this experiment no ozone scrubber was applied. While the instruments observe slightly different mixing

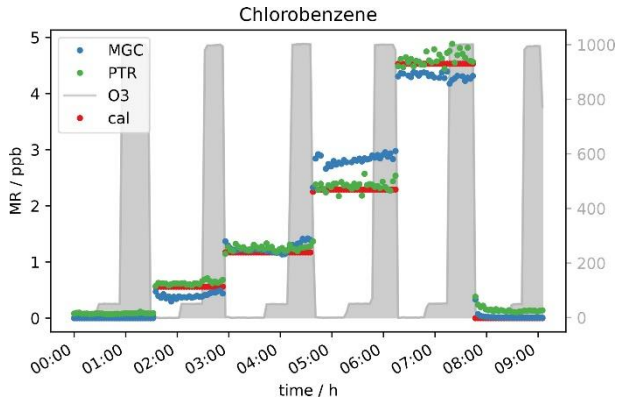

Figure 4.2: *Effect of ozone (0, 50, 1000 ppb) on GC- and PTR-MS measurements of chlorobenzene under different standard gas levels (0–4 ppb).*

ratios owing to differences in sensitivity, the relative change in chlorobenzene mixing ratios remain unchanged when ozone is present.

4.4.1.2 Ozone causing positive interference

Based on current literature, some carbonyl compounds such as aldehydes and ketones do have the potential to show higher mixing ratios when ozone is present. Northway et al. (2004) and Apel et al. (2003) observed positive artefacts under ozone presence for acetaldehyde. Additionally, Apel et al. (2003) observed artefact formation for propanal, acetone and butanal in their fast GC-MS system, which were emitted by parts of their system when ozone was present. Lehmpuhl and Birks (1996) found positive interference also for larger carbonyl compounds. Acetaldehyde measurements in this study under dry conditions agree with the results reported by Northway et al. (2004), Apel et al. (2003) and others. The VOC signal increases with ozone concentration. Both the PTR- and GC-MS measured higher acetaldehyde mixing ratios when O_3 was above 150 ppb (see Fig. 4.3). This indicates that the interference is not instrument-specific but more likely a function of the common inlet tubing exposure to ozone. Note that the inlet lengths to GC and PTR were roughly the same. The higher enhancement of the GC acetaldehyde could be due to emission of oxidation products from the material of multiposition valves as described by Apel et al. (2003). In contrast to the PTR data, the ozoneinduced enhancement of the GC signal increases with acetaldehyde concentration. This effect can be due to the different materials used for the tubing inside the instruments: Deming et al. (2019) showed that in glass and metal tubing competitive adsorption occurs, which depends on humidity and concentration and functionality of the analyte, while polymer tubing shows independent absorption. Our fast GC instrument is equipped with heated silicosteel tubing, which allows for competitive adsorption, while the PTR is equipped with perfluoroalkoxy alkane (PFA) tubing. Additionally, with increasing O_3 mixing ratios ozonolysis reactions during trapping are gaining importance. It seems that the interferences on the VOC measurements caused by high ozone exposure are an effect of both the inlet line and the instrument's surfaces. The higher GC signals at 2 ppb calibration gas are again assigned to the difference in sensitivity (due to filament degradation) already mentioned in the previous section. In Figs. 4.3 and 4.4a, the acetaldehyde signals rise significantly when 1000 ppb ozone was present. For the zero air sample (Fig. 4.4b) the signal rose after increasing ozone from 150 ppb where the effect was negligible to 400ppb. The acetaldehyde signal increased further between 400 and 1000 ppb O_3 to about 0.4 ppb (GC) to 0.5 ppb (PTR). Interestingly, the GC signal in Fig. 4.4b did not drop when the

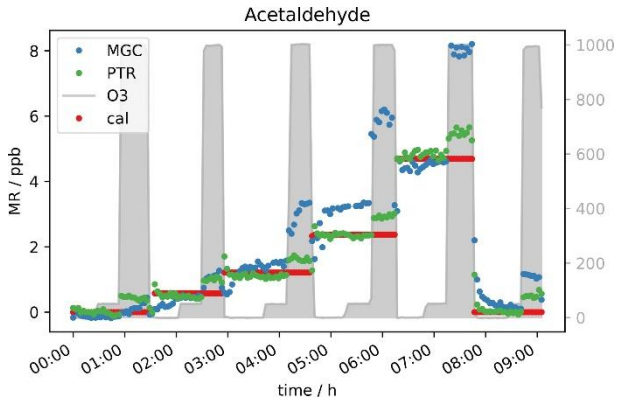

Figure 4.3: *Five different standard gas levels between 0 and approx. 4 ppb at ozone mixing ratios of 0, 50 and 1000 ppb.*

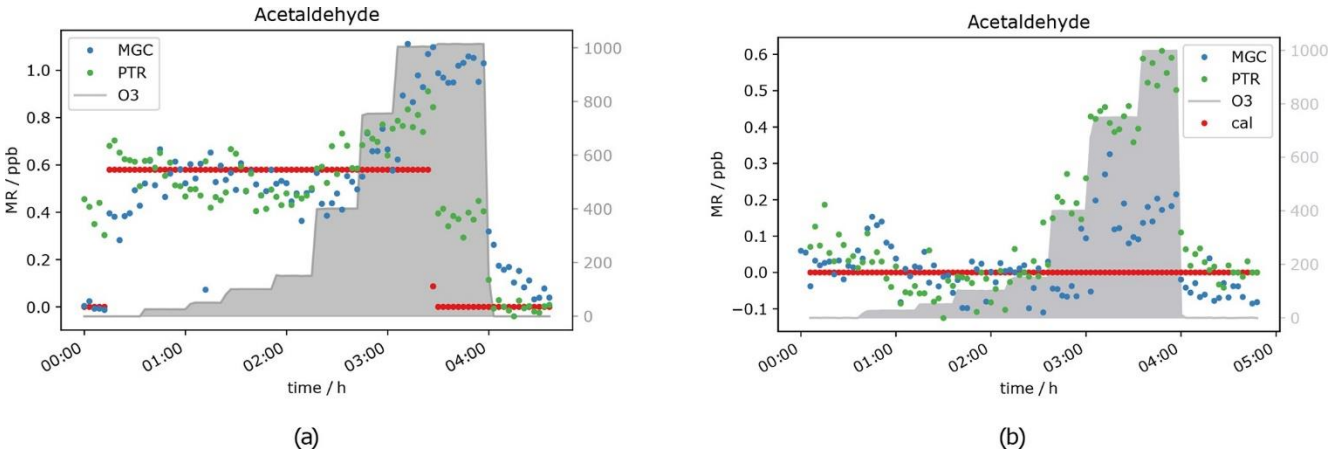

Figure 4.4*: Acetaldehyde mixing ratios at seven different ozone levels between 0 and 1000 ppb and one standard gas level. VOC levels are 0 ppb (a) and 0.5 ppb (b).*

standard gas level dropped to 0 ppb. This is an interesting observation that we currently cannot explain. No abnormal behaviour in the GC-MS could be ascertained at this time, including retention time shifts, tuning anomalies or changes in RH. We conclude that most likely it was an unlogged flow-switching issue. Nevertheless, it does not interfere with our general observation that the acetaldehyde signal is suffering positive interference under high ozone exposure, most likely due to ozonolysis reactions at the tubing surface.

Besides acetaldehyde, C_3 and C_4 aldehydes and ketones have also been measured, namely propanal, acetone, butanal and MEK. Unfortunately, for those compounds the results were not as clear as for the C_2 carbonyl described above. The PTR-ToF-MS in H_3O^+ mode cannot separate the aldehyde from the ketone, as they have exactly the same mass, i.e. the PTR-ToF data presented here always show the sum of propanal and acetone (C_3) and butanal and MEK (C_4) respectively and should therefore be double the GC signals for the separated species. When measuring zero air, ozone increases the signal of the C_3 and C_4 carbonyls (see Fig. 4.5), starting at O_3 mixing ratios of 400 ppb, similar to acetaldehyde. This is most likely due to the reaction of ozone with species attached/adsorbed at the walls of the instrument sampling systems or to unmeasured ozone reactive species in the zero air. While butanal (measured by GC-MS) shows a strong increase, MEK does not show a significant increase in the GC data.

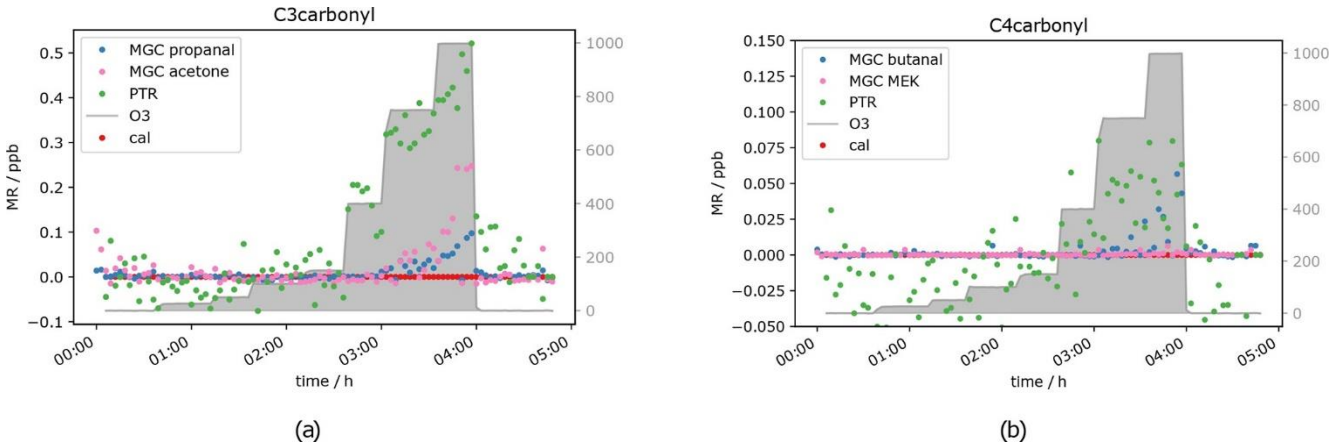

Figure 4.5: *C_3 and C_4 carbonyl mixing ratios of a zero air sample at different ozone levels.*

Interestingly, the aldehyde mixing ratios are relatively stable with a tendency to decrease with ozone when the standard gas was added. Figure 4.6 shows this phenomenon. Propanal and butanal mixing ratios do not show a substantial increase under the same O_3 conditions where they increase in the zero air measurement, while the sum of C_3 carbonyls (PTR signal) and GC acetone again increase (as in the zero air measurement). As propanal slightly decreases and acetone strongly increases with ozone, the PTR measurements show a positive net ozone effect for the C_3 carbonyls. For C_4 carbonyls, the GC quantification during this experiment was compromised (too low mixing ratio) for unknown reasons. However, the qualitative results match the rest of our observations: butanal decreases slightly, while MEK increases slightly, leading to a stable signal for the sum of butanal and MEK, which is shown by the PTR data presented in Fig. 4.6b. Additionally, the qualitative results of butanal and MEK are in line with the qualitative results of C_2–C_3 carbonyls: the signals for the ketones (acetone (C_3), MEK (C_4)) increase with O_3 mixing ratios ≥ 400 ppb, and the signals for the aldehydes (acetaldehyde (C_2), propanal (C_3) and butanal (C_4)) are relatively stable with a tendency to decrease between 200 and 400ppb O_3 and increase as well with O_3 mixing ratios ≥ 400 ppb. Between 3.5 and 4 h after the start of the experiment (see Fig. 4.6), not all signals dropped to background levels. They finally drop once ozone was switched off. This is consistent with the results from the zero air measurement (Fig. 4.5) and the acetaldehyde data (Fig. 4.4b). It shows that exposure of the inlet tubing to high ozone does not rapidly clean the lines of the interfering compounds. Apel et al. reported carbonyl generation in the presence of ozone from the rotor material of VICI valves and a KNF Teflon pump included in their system (Apel et al., 2003). Positive artefacts were reported for acetaldehyde, propanal, acetone and butanal; they did not find any interference for MEK. This matches our results. We assume that C_2–C_4 carbonyl compounds are generated inside the setup inlet tubing and were measured by the GC, as otherwise the signal would have dropped when measuring zero air with 1000 ppb O_3. However, at 0.5 ppb calibration gas we observed a C_3 and C_4 aldehyde loss under high ozone exposure in the GC measurements. A possible explanation for this is the effect is due to OH radicals produced via Criegee intermediates from the ozonolysis reaction of alkenes present in the standard gas. OH radicals react preferentially with aldehydes rather than ketones. Apparently, these reactions are faster than the C_3 and C_4 aldehyde generation within the sampling setup. All the experiments show the same trend: under dry conditions, at tropospheric ozone levels (≤ 150 ppb O_3), no interference from the oxidant can be observed, while under stratospheric conditions (> 400 ppb O_3) there is a strong interference. This leads to the conclusion that both instruments can measure C_2 to C_4 carbonyls in the

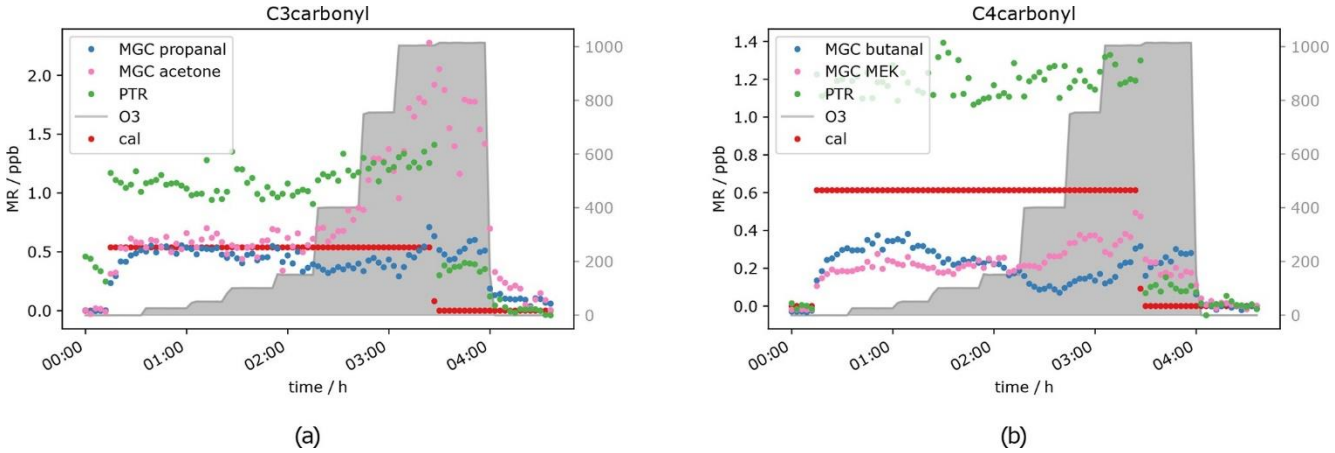

Figure 4.6: *C_3 and C_4 carbonyl mixing ratios at approximately 0.5 ppb per VOC at different ozone levels.*

troposphere without being restricted by the amount of ozone present. No reliable results can be achieved when ozone is above 150 ppb under dry conditions. Hence, the current setup is not suitable for stratospheric measurements of these oxygenated species.

4.4.1.3 Ozone causing negative interference

Due to the presence of reactive double bonds, terpenes (isoprene, alpha-pinene and beta-caryophyllene) were expected to show a decrease in mixing ratio with increasing ozone concentration. This was indeed observed. In Fig. 4.7 it can be seen that the monoterpene signal at 50ppb O_3 is 10 %– 20 % lower for each VOC level compared to the signal without ozone present. The signal drops by almost the same percentage when O_3 is increased to 1000 ppb. For sesquiterpenes the effect is even stronger. With 50 ppb O_3, the signal drops by roughly 80 %, while the signal is close to or below detection limit at an ozone level of 1000 ppb depending on the terpene mixing ratio applied. This behaviour can be explained with reference to the different reaction rate constants *k* of the mono- and sesquiterpenes in the calibration gas with ozone. *α*-pinene, which is the monoterpene included in the standard gas mixture, has a reaction rate constant with ozone of 9.6×10^{-17} cm^3 $molecules^{-1}$ s^{-1}, while *k* for *β*caryophyllene is 1.2×10^{-14} cm^3 $molecules^{-1}$ s^{-1} (IUPAC, 2021). With a reaction rate more than 3 orders of magnitude larger, the reaction is fast enough to remove 1 ppb *β*caryophyllene within the short time the sample air needs to travel through the inlet line (<10 s). Furthermore, it can be seen that the sesquiterpene needs considerable time (more than an hour) to reach a steady-state level in the beginning of the experiment (~3 h in Fig. 4.7), even with lines heated to 45 °C. This could be due to independent absorption of the FEP tubing of these less volatile species (Deming et al., 2019).

Another compound which was expected to show a decreasing mixing ratio with increasing ozone concentration due to its double bonds was isoprene. It was measured simultaneously with PTR- and GC-MS. As can be seen in Fig. 4.8, the signal is not measurably affected by adding 50ppb O_3. At an ozone level of 1000ppb, the GC detects roughly 50% less isoprene. This fits with expectations, as isoprene ozonolysis is rather slow, the reaction rate coefficient being close to the one for *α*-pinene (1.3×10^{-17} cm^3 $molecules^{-1}$ s^{-1}), which results in only partial depletion of the isoprene present. Interestingly the PTR-ToF shows slightly higher mixing ratios of the isoprene mass (*m/z* 69) when ozone is present. The elevated signal on this mass can be caused by carbonyl compounds present in the sample air or in the inlet line.

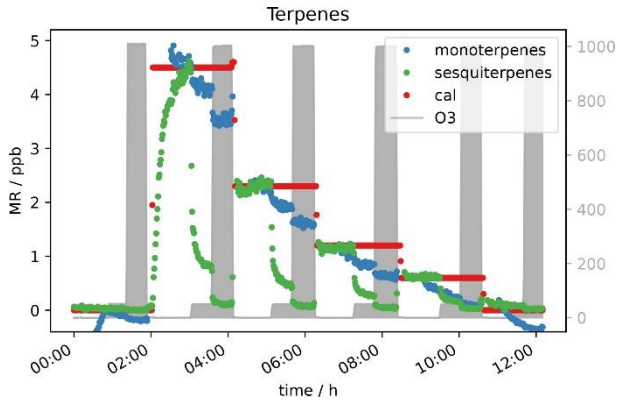

Figure 4.7: *Different terpene levels at 0, 50 and 1000 ppb O_3 measured with PTR-MS.*

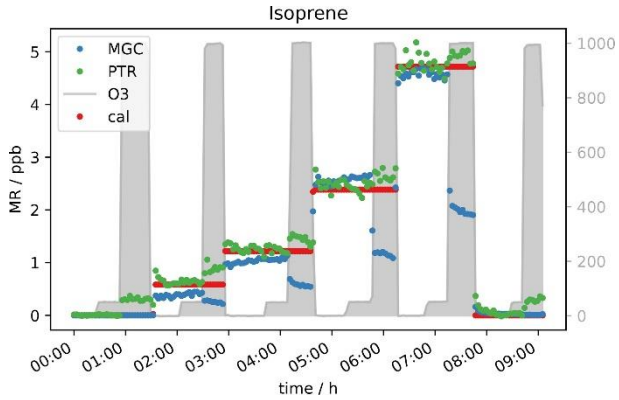

Figure 4.8: *Different isoprene levels at 0, 50 and 1000 ppb O_3.*

Literature reports the same exact mass commonly used for isoprene detection in PTR systems to be a fragment of certain aldehydes (Buhr et al., 2002; Ruzsanyi et al., 2013). Most likely the PTR *m/z* 69 signal in the present study is elevated, because under the experimental conditions the positive offset from the carbonyl compounds is higher than the isoprene depletion. For the GC-MS, aldehydes do not interfere, as the analytes are separated in the chromatographic system prior to detection. The assumption is supported by the measurement of a zero air sample (no standard gas added into the system) at different ozone levels (see Fig. 4.9a). The GC does not detect any isoprene in the zero air sample regardless of the ozone concentration, while the PTR-MS shows an increasing *m/z* 69 signal at O_3 levels between 150 and 1000 ppb. Apparently the PTR-ToF-MS signal correlates with the oxidant's concentration. At 150 ppb O_3 the PTR-MS detects approximately 100 ppt signal at the isoprene mass; at 400 ppb ozone PTR measurements show around 150 ppt and with the highest tested O_3 concentration (1000 ppb) roughly 350 ppt.

Figure 4.9b shows data obtained from the measurement of one isoprene level (~0.6 ppb) at seven different ozone mixing ratios and without ozone. GC-isoprene is stable until 100 ppb O_3. Somewhere between 150 and 400 ppb the isoprene signal starts to decrease until it reaches approximately two-thirds of the real value at 1000 ppb O_3. The two analytical instruments show reverse effects of ozone being present: the PTR-isoprene mass signal is increasing over the same range as the GC signal decreases. This is in line with the measurement of the zero air. The PTR-signal increase is probably due to fragments of

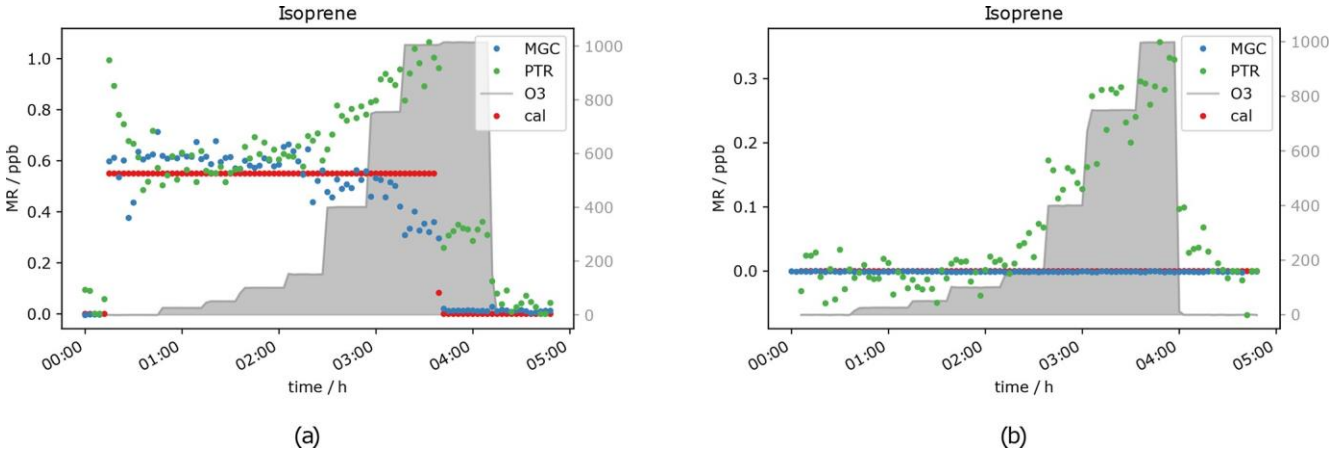

Figure 4.9: *Isoprene mixing ratio at different ozone levels.*

other compounds on the same exact mass. In literature, increased PTR *m/z* 69 signals have been reported in high-ozone environments in indoor and outdoor air studies which could not be attributed to isoprene (Colomb et al., 2006; Wang et al., 2022). Those studies might have been influenced by the same interference we observed.

4.4.1.4 Effect of a sodium thiosulfate scrubber on VOC measurements

Generally, when the sodium thiosulfate impregnated quartz filters were added to the sampling system (see Fig. 4.1), no influence on the VOC measurements was seen for the selected VOCs. The literature also reports that this scrubbing material is suitable for measurement of many VOCs without causing interferences (Helmig, 1997; Pollmann et al., 2005). In Fig. 4.10 the measured terpene mixing ratios 0 and 2 ppb VOC with and without scrubber are shown. It can be seen that the scrubber performed as expected and removed the ozone effectively. *α*-pinene levels reach the same concentration with the scrubber as before ozone was applied. The measurement of this compound is not affected by the sodium thiosulfate filters, and if the scrubber is applied, there is no interference on the measurement with up to 170 ppb ozone. As mentioned before *β*-caryophyllene again needed a long time to reach steady state when 2 ppb VOC was applied to the system (inlet line temperature 45 °C; see Sect. 4.3.1). Steady state is reached after almost 2 h when the scrubber was introduced (~4 h 30 min). For the 30–40 min when the thiosulfate filters were introduced (~4 h 50 min–5 h 30 min) steady state is not even reached. Sesquiterpene adsorption by the tubing material would again explain this effect. The scrubber was connected using Teflon tubing and a filter holder of the same material. The first time when the terpene-rich air was directed through the scrubber (50 ppb O_3, 5 h after the start of the experiment, ~4 h 50 min–5 h 30 min) the sesquiterpene mixing ratio increased within half an hour, while later (170 ppb O_3, ~6 h–7 h 30 min) this was not the case. In other words, in the first half hour the sesquiterpenes appeared to be absorbed by the tubing (~4 h 50 min–5 h 30 min), while afterwards the material was conditioned, and the concentration could reach steady state (~6 h–7 h 30 min). Steady-state mixing ratios decrease with

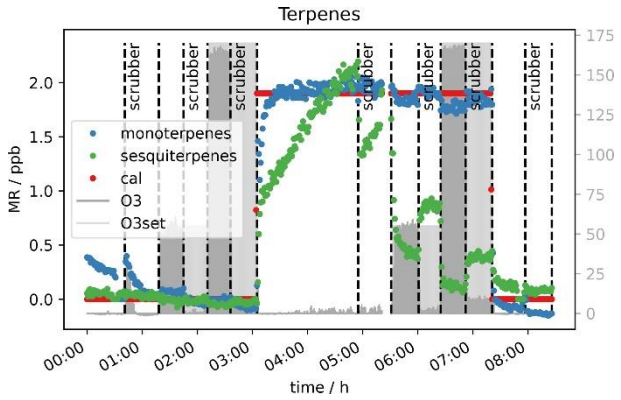

Figure 4.10: *Terpene mixing ratios measured by PTR-MS with and without scrubber at 50 and 170 ppb O_3.*

increasing O_3 mixing ratio, as the scrubber was installed roughly halfway between the junction where the standard gas was connected and the analytical instruments. On their way to the scrubber, the sesquiterpenes are depleted by ozonolysis. Furthermore, at the applied flow rate of approximately 650 sccm, there is already about 10 ppb ozone passing the scrubber (see Sect. 4.4.2), which allows the oxidant to further react with *β*-caryophyllene on the way between the scrubber and the detector. An improved filter assembly or several scrubbing filters as suggested by Pollmann et al. (2005) could improve the sesquiterpene sampling. For all other compounds including isoprene no interference from the scrubber itself could be observed. Furthermore, interferences from ozone on the measurements of analytes like isoprene or acetaldehyde could be eliminated with the filter scrubber in line. The effect on sesquiterpenes could probably also be eliminated if the scrubber was placed at the inlet's front end and the flow through the scrubber was lower. However, it cannot be excluded that the sesquiterpene signal is affected by the scrubber material. Therefore, a longer time span with the scrubber in the sampling line would be required for the signal to reach steady state, and the instrument would be unresponsive to rapid changes.

4.4.2 Scrubber endurance

Figure 4.11 shows the O_3 mixing ratio measured with the ozone monitor behind the sodium thiosulfate scrubber under the dry condition at approximately 200 sccm. Results from the experiment at 1000 ppb O_3 can be seen in Fig. 4.11a. The ozone concentration behind the filter never reached 0 ppb, already at the beginning 100 ppb oxidant could pass the scrubber. That means 1000 ppb ozone results in an overload of the scrubber capacity, and it was not suitable to remove the oxidant completely from the dry sample air – not even for short time periods. The concentration increases slightly in the beginning, while after 15 h a sudden signal rise can be observed where the mixing ratio increases from roughly 200 to 500 ppb. After 55 h no ozone was scavenged anymore; the concentration before the scrubber is the same as after. Despite inefficient scrubbing under these conditions, the scrubber lifetime would be 15 h, as after this time period a strong increase in the signal of the ozone monitor can be observed. In total it can be concluded that the sodium thiosulfate impregnated quartz filters made in the way described in the method section are not suitable for measurements at these flow rates and such high ozone levels as

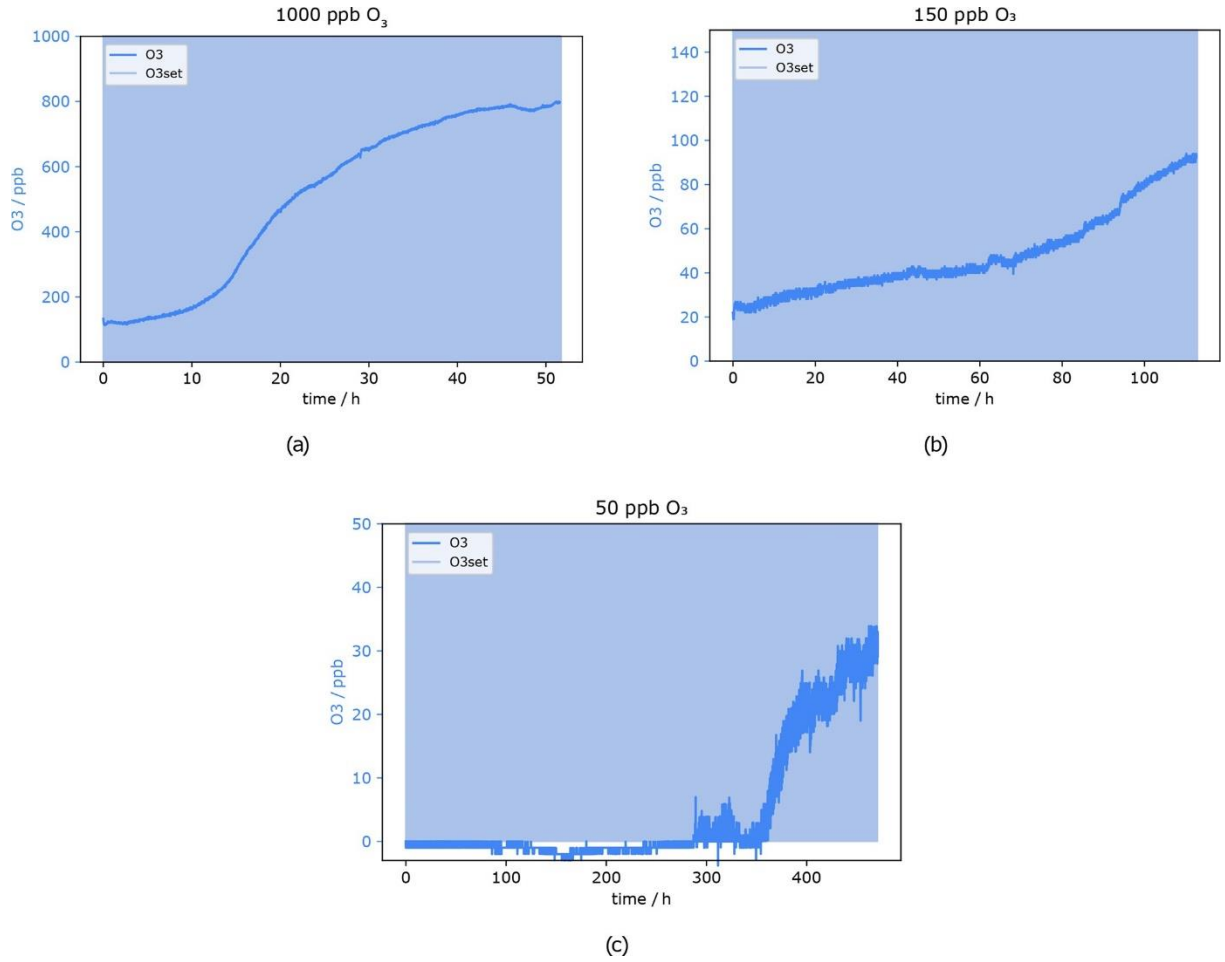

***Figure 4.11**: O_3 mixing ratios after $Na_2S_2O_3$ scrubber at 0 % RH. Flows and O_3 levels before scrubber: (a) 220 sccm, 1000 ppb; (b) 225 sccm, 150 ppb; and (c) 230 sccm, 50 ppb.*

encountered in the lower stratosphere due to insufficient O_3 removal and relatively fast depletion of the scrubbing material. However, at lower flow rates it might be more efficient and effective.

Figure 4.11b presents the result from a similar experiment but with 150 ppb ozone applied, which corresponds to high ozone levels at ground level and is typical for the upper troposphere. In the very beginning, the O_3 concentration was already 20 ppb. It can be excluded that the filter is not able to remove the O_3 completely, as the experiment was started twice under these conditions. The first time the ozone mixing ratio was zero at the beginning, but unfortunately the experiment had to be stopped after 50 h. There was no sudden signal increase visible within that time. This 20 ppb offset during the second experiment might be caused by the filter not being perfectly centred in the filter holder. It is possible that a tiny stream of air bypassed the filter inside the filter holder, as the 37 mm quartz filter was placed under a 47 mm Teflon filter as described in Sect. 4.3.3. With 150 ppb ozone applied, the measured mixing ratio increased by 20 ppb within 40 h and up to 50 ppb within 80 h. As previously shown even isoprene was not affected by 50 ppb ozone. The only compounds affected by such low O_3 levels were mono- and sesquiterpenes. Therefore, it is concluded that the ozone scrubber can be used for up to 80 h (3.3 d) at a flow of 255 sccm. The scrubber lifetime test for the lowest ozone concentration used here (50 ppb) took in total more than 20 d. During the first 300 h (12.5 d) the signal did not change and was below or close

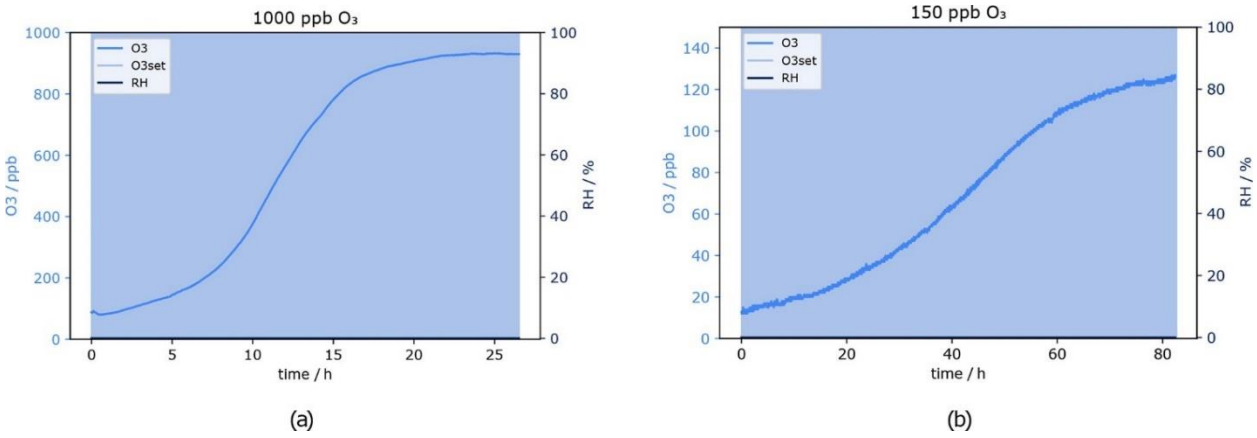

Figure 4.12: *O3 mixing ratio after $Na_2S_2O_3$ scrubber at 0 % RH. Flows and O_3 levels before scrubber: (a) 550 sccm, 1000 ppb and (b) 620 sccm, 150 ppb.*

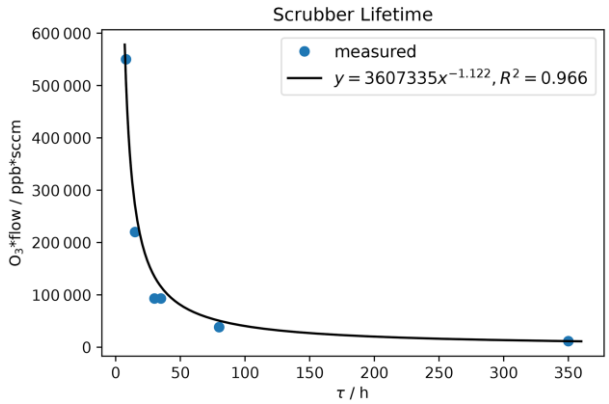

Figure 4.13*: Measured data from the scrubber endurance test.*

to the limit of detection of 0.5 ppb. Around 300 h the measured mixing ratio started to be above detection limit but still below 5 ppb O_3. A sudden increase occurred after approximately 350 h (14.5 d), where the mixing ratio climbed up to 20 ppb within 1.5 d. After the total time of 477 h (almost 20 d) the experiment was stopped; the mixing ratio after the scrubber reached more than 30 ppb. The breakthrough point of the $Na_2S_2O_3$ impregnated filter after 350 h was determined as the end of the scrubber lifetime i.e. at background O_3 mixing ratios of 50 ppb the scrubber lasts more than 14 d.

Results of the test at a flow of 550 sccm, which corresponds approximately to the flow used for the experiments to investigate the effect of ozone on the VOC measurements (Sect. 4.4.1), are presented in Fig. 4.12. Please note that for the average and minimum scrubber lifetimes only measurements at O_3 levels 150 and 1000 ppb have been included, as for 50 ppb there was no measurement at approximately 550 sccm. For quality assurance it is considered important to have a real measurement which can be compared with the calculated results.

The scrubber lifetime is 8 h at 550 sccm and 1000 ppb O_3 according to Fig. 4.12a. At the lower ozone level (150 ppb), the actual flow was 620 sccm. From the plot a lifetime of 30 h has been determined.

Table 4.3: *Ozone mixing ratio and corresponding flows through the scrubber during scrubber endurance tests, as well as resulting lifetimes τ.*

	Measured		
O3 (ppb)	flow (sccm)	*τ* (h)	*τ* (days)
1000	220	15	0.6
150	255	80	3.3
50	230	350	14.6
1000	550	8	0.3
150	620	35	1.5

Table 4.4: *Calculated scrubber lifetimes τ at exactly 200 and 550 sccm.*

	Calculated		
O3 (ppb)	flow (sccm)	*τ* (h)	*τ* (days)
1000	200	18	0.7
150	200	117	4.9
50	200	350	14.6
1000	550	6	0.3
150	550	42	1.8

Scrubber lifetime τ highly depends on ozone concentration and flow rate. In Table 4.3 measured flows and lifetimes can be found. The data were fitted with a power function ($y = ax^b$; see Fig. 4.13) being the best fit with R^2 close to 1. Additionally, the lifetimes for exactly 200 and 550 sccm were calculated with Eq. (E4.1) and can be found in Table 4.4. The factors a and b obtained from the fit were rounded to 3500000 and −1 respectively, as small changes are attributed to measurement uncertainties.

$$\tau = \frac{3500000}{O_3 \times \text{flow}} \qquad \text{(E4.1)}$$

The ozone levels were chosen to correspond to those experienced in the troposphere (50 and 150 ppb O_3) and stratosphere (1000 ppb O_3) so that replacement times of the scrubber under field conditions could be determined. Flows correspond to the inlet flows of the mass spectrometers (200 sccm) and to the flow used for the experiments described in Sect. 4.4.1.

The calculated lifetime at 200 sccm and 1000 ppb ozone is 18 h. Hence, this is the time after which the filter should be exchanged under these conditions if reducing ozone to 100– 200 ppb is enough for the compounds of interest. If the background ozone mixing ratio does not exceed 150 ppb and the flow is the same as used for the here applied mass spectrometers (200 sccm), the scrubber needs to be replaced after 117 h to avoid interference from ozone for analysis of most VOCs except terpenes. However, on

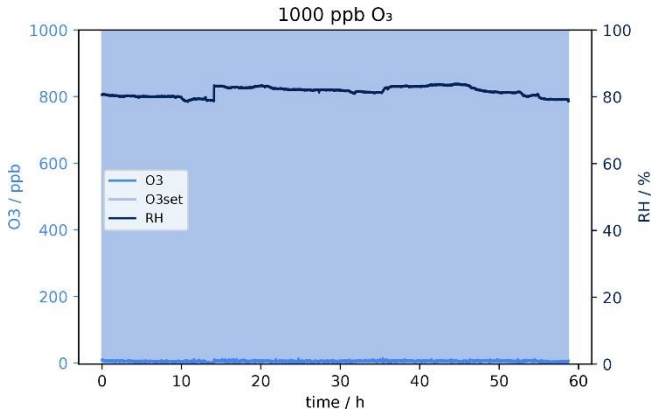

***Figure 4.14**: O_3 mixing ratio after $Na_2S_2O_3$ scrubber at 80 % RH, 230 sccm.*

many ground-based measurement sites in the troposphere the ozone mixing ratio rarely exceeds 50 ppb, which would result in a scrubber exchange every 14 d to assure efficient ozone removal. The lifetime calculation at 550 sccm and stratospheric ozone concentration results in a scrubber lifetime of 6 d and is slightly lower than the measured lifetime (8 d; see Fig. 4.12a). With 150 ppb O_3 and the same flow τ would be 42 h and filter replacement would be due in less than 2 d. The determination of the lifetime is approximate, as we use the time at which a sudden increase in ozone concentration after the scrubber was observed. Exchanging the filter earlier does not affect the data quality and is therefore recommended. The filter assembly could be improved by using a filter housing which fits perfectly to the filter diameter in order to avoid any small air stream bypassing the filter. In this study, we did not examine the effect of several filters placed in series in the line, as it was done by Pollmann et al. (2005). They found that with additional filters the scrubbing efficiency and scrubber endurance could be improved, but we adopted single filters to test their efficacy and endurance while minimizing potential uptake losses.

However, in Sect. 4.4.1 the presented experiments were all performed in less than 1 d, and the maximum ozone concentration (1000 ppb) was applied for only several hours. Thus, the ozone concentration was stable throughout each experiment.

4.4.3 Effect of humidity

Field measurements can take place in various locations and environmental conditions. Relative humidity may influence the analysis of water soluble compounds. However, the presence of water may also affect the behaviour of VOC molecules when interacting with surfaces. The scrubber material used here is inorganic and water soluble and has therefore been tested under dry and humid conditions. For the measurements performed within this study, humidity did not have any influence on the GC-MS and PTR-ToF-MS instrument measurement capability, as these dried the air before detection (GC-MS) or used humid calibrations (PTR-ToFMS). Thus any effects observed can be ascribed to the inlet system. Interestingly, the scrubber lifetime increased dramatically at 80 % relative humidity. The test was done twice to double-check the results obtained. Figure 4.14 shows the ozone mixing ratio and relative humidity measured at 1000 ppb O_3 and a flow of 230 sccm. RH was relatively stable throughout the whole experiment. As mentioned in Sect. 4.4.2, under similar dry conditions the sodium thiosulfate scrubber was able to remove only 90 % of the ozone, and filter performance dropped drastically after 15 h. In contrast,

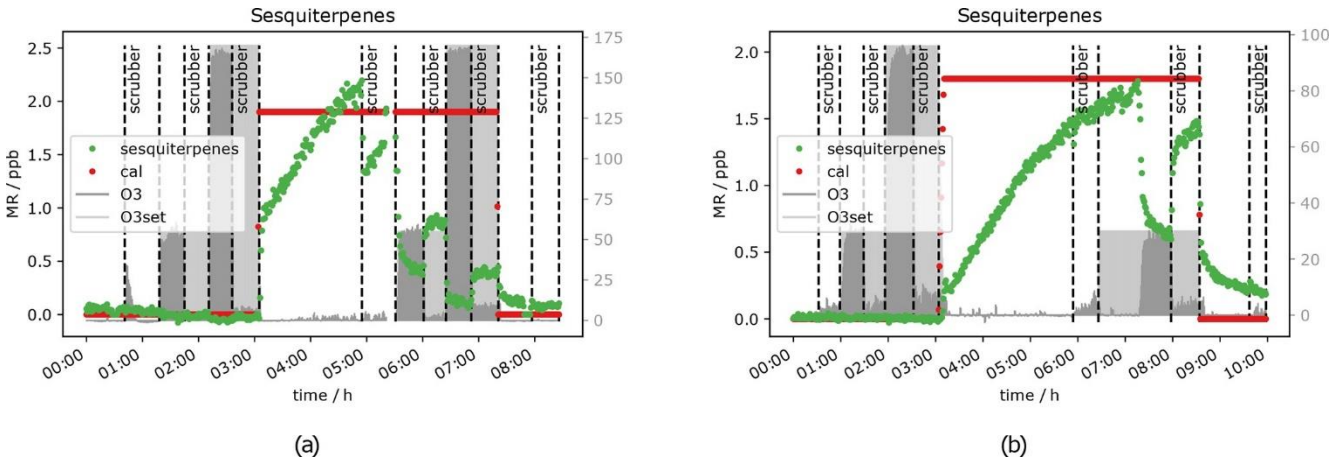

Figure 4.15: *Sesquiterpene mixing ratio with and without scrubber at different O_3 mixing ratios when 2 ppb sesquiterpenes were introduced to the system: (a) 0 % RH and (b) 50 % RH.*

at 80 % RH the ozone could be removed completely from the sample air. The O_3 mixing ratio did not change over 65 h of experiment; it was always below 10 ppb. After 65 h the experiment was stopped.

The only signal that was still influenced by ozone when the filter scrubber was in the sample line was the sesquiterpene signal. Consequently the corresponding mixing ratio can be used to investigate whether or not relative humidity changes the results compared to the dry condition. Figure 4.15 shows the sesquiterpene mixing ratio under dry (Fig. 4.15a) and humid (Fig. 4.15b) conditions when ca. 2 ppb standardgas was introduced to the system. In the first plot the signal with scrubber at 50 ppb ozone (approx. 6 h–6 h 30 min) comes back to 50 % of the original signal, while in the second plot it comes back to approx. 80 % (approx. 8–9 h) of the original height. This is consistent with the results from the scrubber lifetime tests at 80 % RH and suggests that scrubber performance benefits from increased humidity.

Sodium thiosulfate reacts with ozone to tetrathionate, water and oxygen:

$$2S_2O_3^{2-} + O_3 + 2H^+ \leftrightharpoons S_4O_6^{2-} + O_2 + H_2O \qquad (4.1)$$

As it is an equilibrium reaction, the equilibrium will shift to the left if there is an excess of water, recovering the thiosulfate from the $S_4O^2{}_6^-$ produced. This could explain why the ozone level during the scrubber performance test at a relative humidity of 80 % was relatively stable throughout the whole measurement time, which was almost 3 d, and why all the oxidant can be scavenged at an O_3 level of 1000 ppb.

4.5 Conclusions

Most species tested were not affected by ozone being present. Nevertheless, higher mixing ratios were observed for carbonyl compounds, indicating an ozone interference. Signals for acetaldehyde, propanal, acetone and butanal increased with ozone levels above 150 ppb in zero air measurements with GC, as well as PTR. Thus, it can be concluded that there are positive artefacts generated in the experimental

setup, i.e. in the tubing, inside the ozone generator or within both of the mass spectrometers. As we observed the same during stratospheric measurements before, the ozone generator cannot be the only source. Apel et al. (2003) originally conducted ozone sensitivity tests on their airborne GCMS system due to anomalous acetaldehyde observations in the stratosphere. Our experiments also show acetaldehyde to be the species most affected by ozone interference. When our PTR encountered a stratospheric intrusion in flight as on 2 June 2020 we found 0.88 ppb acetaldehyde (altitude 13000 m, O_3 465 ppb), extremely suspect for such a shortlived molecule under otherwise clean conditions. Unfortunately, the fast GC-MS did not measure acetaldehyde during this flight campaign. When 0.5 ppb VOC standard gas was measured, the signals for propanal and butanal decreased due to the reaction with the OH radical, generated from ozonolysis of terpenes. For MEK no ozone interference could be observed. Decreasing signals were found for monoterpenes (α-pinene), sesquiterpenes (β-caryophyllene) and GC-isoprene as expected due to the direct reaction with ozone. The PTRToF-MS measured increasing "isoprene" mixing ratios on *m/z* 69 with increasing ozone concentration due to aldehyde fragments on the same exact mass. Those fragments are most likely ozonolysis products from some adsorbed species inside the FEP tubing or the instrument itself from some former measurements. Therefore caution should be applied when interpreting the isoprene mixing ratios provided by PTR-ToF-MS in high-ozone environments. Generally the scrubber lifetime under tropospheric conditions (O_3 mixing ratios between 50 and 150 ppb) and a flow of 200 sccm is between 5 and 14 d. The inlet flow of both instruments is the same (200 sccm); therefore the result can directly be used for ground-based field measurements with the here employed PTR-ToF-MS and fast GC-MS systems. Sodium thiosulfate impregnated quartz filters are a very convenient means of ozone scavenging, as the filters can be prepared in advance easily and at a low cost and can be stored in a dry, dark and clean place. The preparation, as well as the application, are simple, and the usage time for the filters is with several days long enough to allow measurement of complete diel cycles without stopping the measurements in between to open the inlet line for scrubber exchange. Nevertheless, the scrubbing technique as applied here is not suitable for sesquiterpene measurement. The observed loss of these analytes could be reduced with a $Na_2S_2O_3$ scrubber in line, but it could not be eliminated completely. Similar results have been reported earlier. Pollmann et al. (2005) found ozone concentrations in the sampling air reduced to 0.4 % when using a thiosulfate scrubber at an ozone mixing ratio of 100 ppb and 255 sccm. Unfortunately they did not report how long these conditions were measured. Nevertheless, their finding is comparable to that reported here; at 150 ppb O_3 and at the same flow the scrubber could reduce ozone to almost zero, while at 50 ppb the oxidant's mixing ratio was below the limit of detection for more than 14 d. The tests have shown that the scrubbing technique used in this study performs well for most groundbased operations of the VOC instruments, as inlet flows and ozone levels are usually low enough to stay within range of good performance of the sodium thiosulfate filter scrubber. Nonetheless, it is not possible to completely avoid sesquiterpene loss due to reaction with ozone during sampling. The current setup is not suitable for measuring highly ozonereactive compounds such as sesquiterpenes or under high ozone conditions like in the lower stratosphere. Fortunately, since sesquiterpenes are emitted from the surface, they are extremely unlikely to be present in the stratosphere. In general it can be concluded that higher humidity has a positive influence on the VOC measurements performed here with a sodium thiosulfate filter scrubber, when ozone was present and no interference from the humidity on the gas analysis itself could be observed. Still, the O_3 removal is not sufficient to measure sesquiterpenes when ozone is present, not even at a low mixing ratio such as 50 ppb. Implementing a stable humidification to the measurement system is non-trivial, and additional effects for other analytes could

develop. It is important to continue the development and characterization of reliable techniques which are cheap and easy to implement for lab, as well as field, experiments.

In summary we can say that insertion of the ozone scrubber resulted in the removal of most of the interferences observed. This implies that most of the effects observed were initiated in the inlet, and any residual effects were produced within the instruments being therefore different and specific for each instrument. It is important to note that these improvements apply to the suite of gases tested here and presumably also to those with comparable vapour pressures and ozone reactivities. The filter system could be further improved with a low dead volume filter housing to avoid any tiny air streams bypassing the filter inside the assembly and by the installation of multiple scrubbing filters in series as was tested by Pollmann et al. (2005). However, it is important to consider that the introduction of a filter into the system can also induce some negative effects. For example, highly oxygenated low volatility species are likely to suffer losses on such a filter assembly. Such compounds may need entirely different approaches such as inlet-less collection onto adsorbent filled cartridges or ozone removal at the inlet entrance by the addition of nitric oxide (NO). Furthermore, the filter itself can introduce flow rate limits to the inlet due to its physical restriction of flow. Generally, for field studies, our current recommended strategy is to use a high-volume, constant temperature flow from the inlet tip to close to the instrument and then subsample that flow, through the ozone scrubber, into the instrument at a lower rate. The inlet material should be Teflon in agreement with the findings of Deming et al. (2019). VOC-emitting materials such as silicone should be avoided, and during high local pollution events (such as in an aircraft taxiing on the ground) inlets should be stoppered or back flushed to avoid strong contamination.

Data availability

The data are published at https://doi.org/10. 5281/zenodo.7576413 (Ernle and Ringsdorf, 2022).

Competing interests

The contact author has declared that none of the authors has any competing interests.

Acknowledgements

We would like to acknowledge our lab technicians Thomas Klüpfel and Rolf Hofmann for exchanging gas bottles during long experiments.

Financial support

The article processing charges for this openaccess publication were covered by the Max Planck Society.

Review statement

This paper was edited by Daniela Famulari and reviewed by two anonymous referees.

4.6 References

Apel, E., Hills, A., Lueb, R., Zindel, S., Eisele, S., and Riemer, D.: A fast-GC/MS system to measure C2 to C4 carbonyls and methanol aboard aircraft, J. Geophys. Res.-Atmos., 108, 8794, https://doi.org/10.1029/2002JD003199, 2003.

Bourtsoukidis, E., Helleis, F., Tomsche, L., Fischer, H., Hofmann, R., Lelieveld, J., and Williams, J.: An aircraft gas chromatograph–mass spectrometer System for Organic Fast Identification Analysis (SOFIA): design, performance and a case study of Asian monsoon pollution outflow, Atmos. Meas. Tech., 10, 5089–5105, https://doi.org/10.5194/amt-105089-2017, 2017.

Buhr, K., van Ruth, S., and Delahunty, C.: Analysis of volatile flavour compounds by Proton Transfer Reaction-Mass Spectrometry: fragmentation patterns and discrimination between isobaric and isomeric compounds, Int. J. Mass Spectrom., 221, 1–7, 2002.

Colomb, A., Williams, J., Crowley, J., Gros, V., Hofmann, R., Salisbury, G., Klüpfel, T., Kormann, R., Stickler, A., Forster, C., and Lelieveld, J.: Airborne measurements of trace organic species in the upper troposphere over Europe: the impact of deep convection, Environ. Chem., 3, 244–259, 2006.

Crutzen, P. J. and Lelieveld, J.: Human impacts on atmospheric chemistry, Annu. Rev. Earth Pl. Sc., 29, 17–45, 2001.

Deming, B. L., Pagonis, D., Liu, X., Day, D. A., Talukdar, R., Krechmer, J. E., de Gouw, J. A., Jimenez, J. L., and Ziemann, P. J.: Measurements of delays of gas-phase compounds in a wide variety of tubing materials due to gas–wall interactions, Atmos. Meas. Tech., 12, 3453–3461, https://doi.org/10.5194/amt12-3453-2019, 2019.

Ernle, L. and Ringsdorf, M. A.: VOCdata_O3_Na2S2O3scrubber (1.1), Zenodo [data set], https://doi.org/10.5281/zenodo.7576413, 2022.

Helmig, D.: Ozone removal techniques in the sampling of atmospheric volatile organic trace gases, Atmos. Environ., 31, 3635– 3651, 1997.

IUPAC: Atmospheric Chemical Kinetic Data Evaluation, https:// iupac-aeris.ipsl.fr/, last access: 2 October 2021. Koppmann, R.: Volatile organic compounds in the atmosphere, John Wiley & Sons, ISBN 978-1-405-13115-5, 2008.

Koppmann, R., Johnen, F., Khedim, A., Rudolph, J., Wedel, A., and Wiards, B.: The influence of ozone on light nonmethane hydrocarbons during cryogenic preconcentration, J. Geophys. Res.Atmos., 100, 11383–11391, 1995.

Lehmpuhl, D. W. and Birks, J. W.: New gas chromatographicelectron-capture detection method for the determination of atmospheric aldehydes and ketones based on cartridge sampling and derivatization with 2, 4, 6-trichlorophenylhydrazine, J. Chromatogr. A, 740, 71–81, 1996.

McDonald, B. C., De Gouw, J. A., Gilman, J. B., Jathar, S. H., Akherati, A., Cappa, C. D., Jimenez, J. L., Lee-Taylor, J., Hayes, P. L., McKeen, S. A., and Cui, Y. Y.: Volatile chemical products emerging as largest petrochemical source of urban organic emissions, Science, 359, 760–764, 2018.

Northway, M., De Gouw, J., Fahey, D., Gao, R., Warneke, C., Roberts, J., and Flocke, F.: Evaluation of the role of heterogeneous oxidation of alkenes in the detection of atmospheric acetaldehyde, Atmos. Environ., 38, 6017–6028, 2004.

Pagonis, D., Sekimoto, K., and de Gouw, J.: A library of protontransfer reactions of $H3O^+$ ions used for trace gas detection, J. Am. Soc. Mass Spectr., 30, 1330–1335, 2019.

Pandis, S. N. and Seinfeld, J. H.: Atmospheric chemistry and physics: From air pollution to climate change, Wiley, ISBN 9781-118-94740-1, 2006.

Pollmann, J., Ortega, J., and Helmig, D.: Analysis of atmospheric sesquiterpenes: Sampling losses and mitigation of ozone interferences, Environ. Sci. Technol., 39, 9620–9629, 2005.

Ruzsanyi, V., Fischer, L., Herbig, J., Ager, C., and Amann, A.: Multi-capillary-column proton-transfer-reaction time-of-flight mass spectrometry, J. Chromatogr. A, 1316, 112–118, 2013.

Strömvall, A.-M. and Petersson, G.: Protection of terpenes against oxidative and acid decomposition on adsorbent cartridges, J. Chromatogr. A, 589, 385–389, 1992.

ThermoFisherScientific: 49iQ Instruction Manual, Ozone Analyzer, 2020a.

ThermoFisherScientific: 49iQPS Instruction Manual, Ozone Primary Standard, 2020b.

Wang, N., Ernle, L., Beko¨, G., Wargocki, P., and Williams, J.: Emission Rates of Volatile Organic Compounds from Humans, Environ. Sci. Technol., 56, 4838–4848, 2022.

Warneck, P. and Williams, J.: The atmospheric Chemist's companion: numerical data for use in the atmospheric sciences, Springer Science & Business Media, https://doi.org/10.1007/978-94-0072275-0, 2012.

Weschler, C. J. and Carslaw, N.: Indoor chemistry, Environ. Sci. Technol., 52, 2419–2428, 2018.

Weschler, C. J. and Shields, H. C.: Potential reactions among indoor pollutants, Atmos. Environ., 31, 3487–3495, 1997.

Williams, J.: Organic trace gases in the atmosphere: an overview, Environ. Chem., 1, 125–136, 2004.

Chapter 5

Conclusions and future perspectives

5.1 Conclusions

In this doctoral project, biogenic volatile organic compounds (BVOC) were measured on a tower in the Amazon rainforest at three heights, 80, 150, and 325 m using a proton transfer reaction time-of-flight mass spectrometer (PTR-ToF-MS). Two studies investigated vertical BVOC profiles and their temporal variability in the interface region between the rainforest and the atmosphere. The first study focused on the vertical distribution of isoprene and its reaction products and aimed to infer the diurnal variability of the OH radical concentration from the observed isoprene gradient. Secondly, aldehydes and ketones were detected individually by applying NO^+ chemical ionization, revealing differences in their relative abundance and vertical distributions.

Through this thesis, it was shown that BVOC mixing ratios at the rainforest-atmosphere interface were affected by various interdisciplinary processes. The bidirectional exchange of BVOC between the atmosphere and several ecosystem compartments, driven by metabolic processes, plant communication, BVOC chemical properties, abiotic factors, and atmospheric concentrations determined their emission and uptake rates. Atmospheric oxidative chemistry and photolysis presented a source and sink for BVOC, with the most important oxidant being the OH radical. Moreover, turbulent motions within and above the canopy drove the mixing of BVOC emissions, atmospheric oxidants, and the resulting oxidation products. In the case of isoprene, which only has primary emission sources, the partitioning between turbulent mixing and oxidative chemistry was investigated using a turbulence resolving large eddy simulation (DALES) constrained by observations. It was shown that dilutive mixing is responsible for more than 50 % of the observed isoprene loss between 80 and 325 m. A timescale of mixing was derived based on the observed warming between the two heights. For that, the method of dynamical time warping was applied to quantify the temporal shift between the time series of potential temperature at both heights. The resulting mixing timescale accounts for the up and downward vertical motions and lateral mixing and ranged from about 105 minutes in the morning (7:00-8:00 LT) to 15 minutes in the afternoon (14:00-15:00 LT). Based on these findings the mean diurnal variability of OH radical concentrations was calculated. The OH radical predominantly determines the atmospheric lifetimes of many BVOC, but so far, direct observations in the Amazon have been rare. The diurnal variability and concentrations of OH simulated by the turbulence resolving model DALES, the regional-scale model WRF-chem, and the global model EMAC showed considerable differences between each other and in comparison to the empirically derived diurnal OH variability. At higher altitudes in the boundary layer, the agreement between those models improved, which emphasizes the complex nature of the rainforest-atmosphere interface region.

To individually study isomeric carbonyl compounds, which differ in terms of atmospheric lifetimes and primary and secondary sources, required the adaptation of the PTR-ToF-MS to NO^+ chemical ionization. Favored ionization reactions of ketones were association reactions ($(RNO)^+$) while aldehydes were ionized by hydride abstraction ($(R - H)^+$), leading to the detection of isomeric carbonyls at different m/z ratios. The highest mixing ratios among the observed carbonyl compounds in the rainforest atmosphere were found for the short-chain carbonyls, acetaldehyde and acetone and for the products of isoprene oxidation, methacrolein and methyl vinyl ketone. Butanal and carbonyl compounds higher than C_7 were not found (below the limit of detection). The vertical distributions of the much longer-lived ketones suggested well mixed conditions above and a strong source below 150 m, most likely at canopy level or just above. The observed shorter-lived aldehydes showed distinct vertical distributions, providing indications of their respective sources, in conjunction with correlation analyses. Oxidized BVOC (OVOC) including carbonyl

compounds were taken up by vegetation and efficiently utilized via metabolic pathways. This decreasing mixing ratios observed at 80 m at night most likely reflect the uptake.

Parts of this thesis characterized the measurement interference on the signals of certain VOC, that was found to be initiated by ozone in the inlet tubing or the instrument itself. Ozone is ubiquitous in the troposphere, so a comprehensive experiment conducted with a PTR-ToF-MS and a gas chromatograph mass spectrometer (GC-MS) was performed to investigate the interfering effects of ozone. Furthermore, the effectiveness of a thiosulfate ozone scrubber to inhibit the interference was tested under varying humidity. Overall, the experiment demonstrated that ozone can lead to an artificial decrease or increase of VOC signals, which was successfully inhibited by the installation of the ozone scrubber in the inlet tubing for most species. The ozone scrubber's performance and lifetime improved with increasing humidity. However, the experiment showed that no significant effect is expected for the low ozone mixing ratios found in the Amazon rainforest environment, with the exception of some unsaturated terpenoids. Sesquiterpenes are very reactive towards ozone, which was shown to cause a substantial depletion in the inlet line and the instrument already at ozone levels of 50 ppb. To a lesser degree, this effect was also noticed for monoterpenes, so it requires a careful investigation of their vertical profiles when ozone reaches mixing ratios close to 50 ppb, which is typically not the case.

5.2 Future perspectives

Throughout the period of this doctoral project, the interdisciplinary research at the Amazon Tall Tower Observatory (ATTO) grew. More and more data were accumulated to understand the interactions between the rainforest ecosystem and the atmosphere above and to improve the prediction of how these interactions will be affected by climate changes. The measurements of BVOC are a crucial part of this research. In the past years the methods for BVOC detection improved, a PTR-Quadrupole-MS previously used for the vertical profile measurements was replaced by the PTR-ToF-MS deployed in this doctoral project. Due to its higher mass resolution, it allows for the identification of a wider range of compounds. Limitations in the detection of isomeric compounds were tackled by periodic offline GC sampling, so far mainly for mono- and sesquiterpenes. As demonstrated in this doctoral project the implementation of NO^+ chemical ionization allows for the separate detection of several isomeric aldehydes and ketones. The importance of their individual measurement was shown by their different emission and uptake rates and seasonal variabilities. Thus, the long-term observations of BVOC would profit from periodically switching between H_3O^+ to NO^+ to achieve a better characterization of carbonyl compounds throughout different seasons. Combining this with an extended offline GC sampling would allow for a more detailed speciation of OVOC and BVOC in general.

In December 2022 and January 2023, the aircraft-based measurement of BVOC among many other trace gases, including the OH radical, and sampling of aerosol particles provided a great opportunity to study atmospheric interactions and transport above ATTO (325 m). The vertical BVOC profiles measured at ATTO could be extended throughout the troposphere to investigate the mechanisms of BVOC transport by shallow and deep convection.

Apart from the observations of the vertical distribution of BVOC in the rainforest-atmosphere interface region, flux measurements with a PTR-ToF-MS could strongly improve our understanding of bidirectional canopy exchange. In this doctoral project, the coupling of emissions, oxidative chemistry, and turbulent

mixing was addressed by the application of a turbulence resolving atmospheric model (DALES), while BVOC flux measurements formally consider turbulent flows. Also in this case, the deployment of both H_3O^+ and NO^+ could enable to observe the bidirectional exchange of many OVOC continuously over a long period. However, for a more comprehensive investigation, the bidirectional exchange studied on the canopy level (tower-based) could be extended by measurements on the tree or leaf level, for example by branch enclosure experiments, etc.

The vertical distributions and their temporal and seasonal variabilities provide a good basis to constrain models on biogenic VOC emissions. In this doctoral study, the explicitly resolved turbulence above the canopy was beneficial for the investigation of vertical gradients. Therefore, the further development of models to include the turbulent and bidirectional exchange of BVOC could be advanced hand in hand with PTR-ToF-MS measurements of BVOC concentrations and fluxes above and within the canopy.

Appendices

List of figures

Figure 1.1: Overview of biological and atmospheric processes that involve BVOC. BVOC released to the atmosphere imply feedback to the biosphere by direct (e.g. generation of Ozone) and indirect (e.g. cloud formation) effects. This schematic drawing is taken from Laothawarnkitkull et al., 2009 with permission from the publisher "John Wiley and Sons". 9
Figure 1.2: A schematic setup showing the main components of a PTR-ToF-MS. The two different flight paths towards the detector are indicated by blue and gray beams in the ToF-MS. This figure is taken from Jordan et al. 2009, with permission from the publisher "Elsevier". 13
Figure 2.1: Overview of the processes that govern the vertical distribution of variables observed at ATTO a) Time series of the boundary layer height simulated by DALES b) Schematic sketch of the processes governing the vertical gradient of reactive trace gases, here isoprene, emitted from the Amazon forest. Dynamic processes are marked with yellow arrows while blue arrows indicate chemistry related processes. The Damköhler effect has two arrows since it quantifies the relation between the turbulent and chemistry time scales. The relative vertical gradients of isoprene, the isoprene oxidation products Methyl Vinyl Ketone + Methacrolein + Isoprene Hydroxyhydroperoxides (ISOPOOH), specific humidity q and potential temperature θ observed at ATTO are median averages at 12:00-14:00. The error bars indicate the (0.15, 0.85) quantiles. 31
Figure 2.2: Example of Dynamical Time Warping alignment of the normalized time series of potential temperature θ between zero and one over the course of one day. The dotted lines visualize their alignment pointwise. Convective ABL conditions apply only for the marked alignments, thus the mixing timescale is derived only from this period. This precludes edge effects. The index represents the time steps depending on their resolution. a) θ observed at the measurement heights. The period under analysis includes 23 dry season days. b) θ at two corresponding levels simulated for a representative day with DALES. 33
Figure 2.3: Variations of the mixing time with time of day and height a) The box-whisker plots shows the median and the range of the 75th percentile of the Dynamical Time Warping derived mixing time from ATTO observations. Whiskers include all datapoints. The numbers in the boxes describe the numbers of days used to generate the box and whiskers. The dark red line is the DTW derived mixing time with potential temperature simulated at the corresponding altitude levels of DALES. Timescales calculated from the convective velocity with the ABL height (h) and sampling height (z) are included as dashed lines. The purple line shows the DTW derived mixing time from observed timeseries of q. b) The distribution of the vertical velocity timescale based on turbulent kinetic energy (TKE) by DALES at 12:00 LT. Blue arrows point at the ATTO sampling heights. 34
Figure 2.4: Isoprene profiles above the rainforest canopy under varying OH concentrations simulated with DALES and compared to ATTO observations and the resulting Damköhler Number (Da) a) Relative vertical gradients, median averaged between 12:00-14:00 of isoprene under increasing OH recycling efficiencies calculated with DALES. Inert isoprene represents a non reactive tracer with identical initial profile and emission flux as isoprene. The shadings of the measured isoprene gradient indicate the (0.15, 0.85) quantiles. b) In the box insert the variation of Da for the different recycling efficiencies and over the course of one day is shown. The Dynamical Time Warping based mixing time of DALES is used here. For the Da at ATTO isoprene observations, the mixing time at ATTO (Fig. 2.3) and final OH concentrations (Fig. 2.5) are applied. 35
Figure 2.5: OH concentrations inferred over the course of one day from ATTO observations. The shadings indicate the (0.15, 0.85) quantiles. a) The daily evolution of estimated OH using the gradient and ratio based method corrected for the impact of dynamics on the isoprene gradient using the inert isoprene simulated by DALES. The color code represents the number of median averaged days. The sensitivity of OH towards the composition of IsoO without ISOPOOH is shown in purple. **b)** The plot includes sensitivity of OH from the gradient method towards the Damköhler effect, the reaction time used and the correction for the effect of dynamics with inert isoprene (blue) and q (pink). OH concentrations inferred with the ABL-timescale (grey) have units on the right axis. 38

Figure 2.6: Diurnal variability of OH time series at different heights compared to OH estimate in this study (80 – 325 m) with the gradient method. The shadings indicate the (0.15, 0.85) quantiles for inferred OH and 1 sigma for modeled concentrations. a) DALES results are obtained by including the sensitivity towards OH recycling efficiencies of 0.8 and 1.5 b) WRF-Chem c) EMAC run with halved biogenic emissions at different heights and the full emission for comparison. 42
Figure 2.7: Diurnal variability of simulated Isoprene, O_3 and NO concentration time series compared to ATTO observations under no-rain conditions. The shadings indicate the (0.15, 0.85) quantiles for observations and 1 sigma for modeled data. a) Isoprene mixing ratio measured at ATTO compared to model results. The number of days with isoprene data presented as colored marks decreases after noon as precipitation events are excluded. For DALES simulations with two different recycling efficiencies are included. b) O_3 observed and simulated c) NO observed and simulated 43
Figure 3.1: Median averaged timeseries in the wet-to-dry transition season (June/July) of 2019 measured at all sampling heights for each carbonyl compound and its respective vertical profile at noon (12:00-15:00 LT) to the right. The shadings indicate the quartiles (25^{th} and 75^{th}). In the box-and-whisker plots, the boxes also represent the quartiles, while the residual data except outliers are included in the whiskers. The mixing ratios stated in black font were calibrated to standard, while those in gray font were calculated based on k-rate. 68
Figure 3.2: Median averaged timeseries in the dry season (September/October) of 2019 measured at all sampling heights for each carbonyl compound and its respective vertical profile at noon (12:00-15:00 LT) to the right. The shadings indicate the quartiles (25^{th} and 75^{th}). In the box-and-whisker plots, the boxes also represent the quartiles, while the residual data except outliers are included in the whiskers. The mixing ratios stated in black font were calibrated to standard, while those in gray font were calculated based on k-rate. 69
Figure 3.3: Pearson correlation coefficients from the intercorrelation of the carbonyl species in the wet-to-dry transition season (upper) and in the dry season (lower). 71
Figure 3.4: Pearson correlation coefficients from the correlation of the carbonyl species with selected hydrocarbons in the wet-to-dry transition season (upper) and the dry season (lower). 73
Figure 4.1: Experimental setup. MFC – mass flow controller, RH – relative humidity sensor, P – pressure gauge, and DryCal – flow metre. 108
Figure 4.2: Effect of ozone (0, 50, 1000 ppb) on GC- and PTR-MS measurements of chlorobenzene under different standard gas levels (0–4 ppb). 113
Figure 4.3: Five different standard gas levels between 0 and approx. 4 ppb at ozone mixing ratios of 0, 50 and 1000 ppb. 114
Figure 4.4: Acetaldehyde mixing ratios at seven different ozone levels between 0 and 1000 ppb and one standard gas level. VOC levels are 0 ppb (a) and 0.5 ppb (b). 114
Figure 4.5: C_3 and C_4 carbonyl mixing ratios of a zero air sample at different ozone levels. 115
Figure 4.6: C_3 and C_4 carbonyl mixing ratios at approximately 0.5 ppb per VOC at different ozone levels. 116
Figure 4.7: Different terpene levels at 0, 50 and 1000 ppb O_3 measured with PTR-MS. 117
Figure 4.8: Different isoprene levels at 0, 50 and 1000 ppb O_3. 117
Figure 4.9: Isoprene mixing ratio at different ozone levels. 118
Figure 4.10: Terpene mixing ratios measured by PTR-MS with and without scrubber at 50 and 170 ppb O_3. 119
Figure 4.11: O_3 mixing ratios after $Na_2S_2O_3$ scrubber at 0 % RH. Flows and O_3 levels before scrubber: (a) 220 sccm, 1000 ppb; (b) 225 sccm, 150 ppb; and (c) 230 sccm, 50 ppb. 120
Figure 4.12: O3 mixing ratio after $Na_2S_2O_3$ scrubber at 0 % RH. Flows and O_3 levels before scrubber: (a) 550 sccm, 1000 ppb and (b) 620 sccm, 150 ppb. 121
Figure 4.13: Measured data from the scrubber endurance test. 121
Figure 4.14: O_3 mixing ratio after $Na_2S_2O_3$ scrubber at 80 % RH, 230 sccm. 123
Figure 4.15: Sesquiterpene mixing ratio with and without scrubber at different O_3 mixing ratios when 2 ppb sesquiterpenes were introduced to the system: (a) 0 % RH and (b) 50 % RH. 124

Figure S 3.1: Wind rose for the measurement period in the dry season (left) and the wet-to-dry transition (right) of 2019. 100
Figure S 3.2: A map of the ATTO site created and provided by Andrew Crozier. 100
Figure S 3.3: Median averaged time series of meteorological parameters. Temperatures were measured inside the canopy at 26 m and PAR at 80 m on the 80 m walk-up tower. The shadings indicate the quartiles (25^{th} and 75^{th}). . 101
Figure S 3.4: Precipitation before and during the measurement periods marked with purple dashed lines. Precipitation was measured on the 325 m tall tower. 101
Figure S 3.5: Pearson correlation coefficients for the observed carbonyl compounds with black carbon measured at 325 m on the tall tower. 101
Figure S 3.6: Median averaged timeseries in the wet-to-dry transition season (June/July) of 2019 measured at all sampling heights for each hydrocarbon and its respective vertical profile at noon (12:00-15:00 LT) to the right. The shadings indicate the quartiles (25^{th} and 75^{th}). In the box-and-whisker plots, the boxes also represent the quartiles, while the residual data except outliers are included in the whiskers. The mixing ratios stated in gray font were calculated based on k-rate. 102
Figure S 3.7: Median averaged timeseries in the dry season (September/October) of 2019 measured at all sampling heights for each hydrocarbon and its respective vertical profile at noon (12:00-15:00 LT) to the right. The shadings indicate the quartiles (25^{th} and 75^{th}). In the box-and-whisker plots, the boxes also represent the quartiles, while the residual data except outliers are included in the whiskers. The mixing ratios stated in gray font were calculated based on k-rate. 103

List of tables

Table 2.1: Overview of OH observations conducted in largely remote, forested sites. a) values taken from averaged daily cycles, b) daily mean values, c) box model simulations with MCM v3.3.1, d) mean values 10:00 – 15:00 LT, e) simulated mean values 10:00 – 15:00 40
Table 3.1: List of identified carbonyl compounds and other hydrocarbons and their properties for the detection with NO^+ CIMS (PTR-ToF-MS 4000). The sensitivities are compared to the classical PTR-MS method using H_3O^+ reagent ions. The "product factor" represents the weighting factor for the k-rate obtained from the distribution of product ions as described in section 3.3.3. Compounds given in bold were quantified using a primary standard. 64
Table 3.2: Rate coefficients for the reaction with OH, NO_3, and O_3 and the atmospheric lifetime considering an OH radical concentration of $1x10^6$ molecules cm^{-1}. The rate coefficients and boiling point temperature were taken from the NIST database. Water solubility has been reported by Sander et al.(Sander, 2023).The loss rate is calculated based on the median averaged slopes of the nocturnal (22:00-04:00) carbonyl timeseries. 75
Table 3.3: Median averaged mixing ratios of the observed carbonyl compounds for the measurement periods in the dry-to-wet transition and the dry season 2019. The range presents the lowest mixing ratio included in the 25^{th} and the highest mixing ratio included in the 75^{th} quantile of the median averaged diurnal cycle. Numbers in italics represent the limit of detection. 76
Table 4.1: Conditions of the different experiments performed in this study. 110
Table 4.2: Measured species and effect of ozone. X: no effect, ↓: negative interference and ↑: positive interference. 112
Table 4.3: Ozone mixing ratio and corresponding flows through the scrubber during scrubber endurance tests, as well as resulting lifetimes τ 122
Table 4.4: Calculated scrubber lifetimes τ at exactly 200 and 550 sccm. 122

Abbreviations and acronyms

ABL	Atmospheric boundary layer
ATTO	Amazonia tall tower observatory
BC	Black carbon
BL	Boundary layer
BVOC	Biogenic volatile organic compounds
CAFE	Chemistry of the atmosphere field experiment
CAM-chem	Community atmosphere model with chemistry
CIMS	Chemical ionization mass spectrometer
DALES	Dutch large eddy simulation
DMS	Dimethyl sulfide
DTW	Dynamic time warping
ECHAM	Earth system model with core atmospheric general circulation model - Hamburg
EDGAR	Emission database for global atmospheric research
EMAC	ECHAM/MESSy Atmospheric Chemistry
E/N	Electrical field strength/number density of the neutral molecules
ERA 5	ECMWF Reanalysis 5
FEP	Fluorinated ethylene propylene
FPM	Fluorinated propylene monomer
GC or GC-MS	Gas chromatoraph mass spectrometer
GFAS	Global fire assimilation system
GHG	Greenhouse gas
GLV	Green leaf volatiles
HALO	High altitude and long range research aircraft
HERMESv3	High-elective resolution modelling emission system version 3
Iso	Isoprene
IsoO	Isoprene oxidation products
ISOPOOH	Isprenehydroxyhydroperoxide
LES	Large eddy simulation
LoD or LOD	Limit of detection
LT	Local time
MACR	Methacrolein
MECCA	Module efficiently calculating the chemistry of the atmosphere
MEGAN	Model of emissions of gases and aerosols from nature
MEK	Methyl ethyl ketone
MESSy	Modular earth submodel system
MOM	Mainz oxidation mechanism
MTBE	Methyl tert butyl ether
MVK	Methyl ethyl ketone
NBR	Nitrile butadiene rubber
NMHC	None-methane hydrocarbons
OD	Outer diameter
OVOC	Oxidized volatile organic compounds

PAN	Peroxycarboxylic nitric anhydrides
PAR	Photosynthetically active radiation
ppb	Parts per billion (by volume)
ppm	Parts per million (by volume)
ppt	Parts per trillion (by volume)
PEEK	Polyetheretherketone
PFA	Perfluoroalkoxy alkane
PTR or PTR-ToF-MS	Proton transfer reaction time-of.flight mass spectrometer
RH	Relative humidity
SIFT	Selected ion flow tube
TKE	Turbulent kinetic energy
UTC	Coordinated universal time
UV	Ultraviolet
VOC	Volatile organic compounds
WRF-chem	Weather research and forecasting model coupled with chemistry

CURRICULUM VITAE

List of publications

Keber, T., Bönisch, H., Hartick, C., Hauck, M., Lefrancois, F., Obersteiner, F., **Ringsdorf, A.**, Schohl, N., Schuck, T., Hossaini, R., Graf, P., Jöckel, P., and Engel, A.: Bromine from short-lived source gases in the extratropical northern hemispheric upper troposphere and lower stratosphere (UTLS), Atmospheric Chem. Phys., 20, 4105–4132, https://doi.org/10.5194/acp-20-4105-2020, 2020.

Engel, A., Hartick, C., Hauck, M., Hossaini, R., Joeckel, P., Keber, T., Lefrancois, F., Schohl, N., **Ringsdorf, A.**, and Schuck, T.: Observed and modelled distribution of brominated VSLS species in the extratropical UTLS and implications for the bromine budget of the lowermost stratosphere, Geophys. Res. Abstr., 21, 1–1, 2019.

Williams, J. and **Ringsdorf, A.**: Human odour thresholds are tuned to atmospheric chemical lifetimes, Philos. Trans. R. Soc. B Biol. Sci., 375, 20190274, https://doi.org/10.1098/rstb.2019.0274, 2020.

Pfannerstill, E. Y., Reijrink, N. G., Edtbauer, **A., Ringsdorf**, A., Zannoni, N., Araújo, A., Ditas, F., Holanda, B. A., Sá, M. O., Tsokankunku, A., Walter, D., Wolff, S., Lavrič, J. V., Pöhlker, C., Sörgel, M., and Williams, J.: Total OH reactivity over the Amazon rainforest: variability with temperature, wind, rain, altitude, time of day, season, and an overall budget closure, Atmospheric Chem. Phys., 21, 6231–6256, https://doi.org/10.5194/acp-21-6231-2021, 2021.

Carter, T. S., Heald, C. L., Kroll, J. H., Apel, E. C., Blake, D., Coggon, M., Edtbauer, A., Gkatzelis, G., Hornbrook, R. S., Peischl, J., Pfannerstill, E. Y., Piel, F., Reijrink, N. G., **Ringsdorf, A.**, Warneke, C., Williams, J., Wisthaler, A., and Xu, L.: An improved representation of fire non-methane organic gases (NMOGs) in models: emissions to reactivity, Atmospheric Chem. Phys., 22, 12093–12111, https://doi.org/10.5194/acp-22-12093-2022, 2022.

Dewald, P., Nussbaumer, C. M., Schuladen, J., **Ringsdorf, A**., Edtbauer, A., Fischer, H., Williams, J., Lelieveld, J., and Crowley, J. N.: Fate of the nitrate radical at the summit of a semi-rural mountain site in Germany assessed with direct reactivity measurements, Atmospheric Chem. Phys., 22, 7051–7069, https://doi.org/10.5194/acp-22-7051-2022, 2022.

Sheu, R., Hass-Mitchell, T., **Ringsdorf, A.**, Berkemeier, T., Machesky, J., Edtbauer, A., Klüpfel, T., Filippi, A., Bandowe, B. A. M., Wietzoreck, M., Kukučka, P., Tong, H., Lammel, G., Pöschl, U., Williams, J., and Gentner, D. R.: Emerging investigator series: deposited particles and human lung lining fluid are dynamic, chemically-complex reservoirs leading to thirdhand smoke emissions and exposure, Environ. Sci. Atmospheres, 2, 943–963, https://doi.org/10.1039/D1EA00107H, 2022.

Voigt, C., Lelieveld, J., Schlager, H., Schneider, J., Curtius, J., Meerkötter, R., Sauer, D., Bugliaro, L., Bohn, B., Crowley, J. N., Erbertseder, T., Groß, S., Hahn, V., Li, Q., Mertens, M., Pöhlker, M. L., Pozzer, A., Schumann, U., Tomsche, L., Williams, J., Zahn, A., Andreae, M., Borrmann, S., Bräuer, T., Dörich, R., Dörnbrack, A., Edtbauer, A., Ernle, L., Fischer, H., Giez, A., Granzin, M., Grewe, V., Harder, H., Heinritzi, M., Holanda, B. A., Jöckel, P., Kaiser, K., Krüger, O. O., Lucke, J., Marsing, A., Martin, A., Matthes, S., Pöhlker, C., Pöschl, U., Reifenberg, S., **Ringsdorf, A.**, Scheibe, M., Tadic, I., Zauner-Wieczorek, M., Henke, R., and Rapp, M.: Cleaner Skies during the COVID-19 Lockdown, Bull. Am. Meteorol. Soc., 103, E1796–E1827, https://doi.org/10.1175/BAMS-D-21-0012.1, 2022.

Ernle, L., **Ringsdorf, M. A.**, and Williams, J.: Influence of ozone and humidity on PTR-MS and GC-MS VOC measurements with and without a $Na_2S_2O_3$ ozone scrubber, Atmospheric Meas. Tech., 16, 1179–1194, https://doi.org/10.5194/amt-16-1179-2023, 2023.

Ringsdorf, A., Edtbauer, A., Vilà-Guerau de Arellano, J., Pfannerstill, E. Y., Gromov, S., Kumar, V., Pozzer, A., Wolff, S., Tsokankunku, A., Soergel, M., Sá, M. O., Araújo, A., Ditas, F., Poehlker, C., Lelieveld, J., and Williams, J.: Inferring the diurnal variability of OH radical concentrations over the Amazon from BVOC measurements, Sci. Rep., 13, 14900, https://doi.org/10.1038/s41598-023-41748-4, 2023.

Machado, L. A. T., Kesselmeier, J., Botia, S., Van Asperen, H., de Araújo, A. C., Artaxo, P., Edtbauer, A., Ferreira, R., Harder, H., Jones, S., Dias-Júnior, C. Q., Haytzmann, G. G., Quesada, C. A., Komiya, S., Lavric, J., Lelieveld, J., Levin, I., Nölscher, A., Pfannerstill, E., Pöhlker, M., Pöschl, U., **Ringsdorf, A.,** Rizzo, L., Yáñez-Serrano, A. M., Trumbore, S., Valenti, W. I. D., Vila-Guerau de Arellano, J., Walter, D., Williams, J., Wolff, S., and Pöhlker, C.: How Rainfall Events Modify Trace Gas Concentrations in Central Amazonia, EGUsphere, 1–28, https://doi.org/10.5194/egusphere-2023-2901, 2024.